

A Levelized Comparison of Pulsed and Steady-State Tokamaks

by

Daniel Joseph Segal

B.S. Engineering Physics, University of Wisconsin (2014)

Submitted to the Department of Nuclear Science and Engineering
in partial fulfillment of the requirements for the degree of

Master of Science in Nuclear Science and Engineering

at the

MASSACHUSETTS INSTITUTE OF TECHNOLOGY

February 2018

© Massachusetts Institute of Technology 2018. All rights reserved.

Author

Department of Nuclear Science and Engineering

November 11, 2018

Certified by

Jeffrey P. Freidberg

KEPCO Professor Emeritus

Thesis Supervisor

Certified by

Anne E. White

Cecil and Ida Green Associate Professor

Thesis Reader

Accepted by

Ju Li

Battelle Energy Alliance Professor

Chair, Department Committee on Graduate Students

A Levelized Comparison of Pulsed and Steady-State Tokamaks

by

Daniel Joseph Segal

Submitted to the Department of Nuclear Science and Engineering
on November 11, 2018, in partial fulfillment of the
requirements for the degree of
Master of Science in Nuclear Science and Engineering

Abstract

The goal of fusion energy research is to build an economically competitive reactor. This is difficult due to the complicated system composing a reactor and the nonlinearities it entails. Practically, to even get to the neighborhood of an economic reactor requires hundreds of simulations – which in turn necessitate quick running fusion systems codes. Moving towards these economic reactors then involves finding what design parameters provide the most leverage in lowering reactor costs.

As highlighted by the difference between European and American designs, however, the most important decision for tokamaks is whether to run them as *pulsed* or *steady-state*. This paper aims to fairly compare the two modes of operation using a single, comprehensive model. Benchmarked against other codes, this model actually shows that no fusion reactor is achievable without some technological advancements. This can be seen through every referenced design using nonstandard values of H and N_G .

The interesting result this paper shows is that developing high-temperature superconducting (HTS) tape could actually make both steady-state and pulsed tokamaks economically competitive against solar and coal. Further, this HTS tape actually has different best uses for the two modes of operation, appearing in the magnet structures of: TF coils for steady state and the central solenoid for pulsed. Developments in this technology should produce economic reactors within the coming decade.

Thesis Supervisor: Jeffrey P. Freidberg

Title: Professor of Nuclear Science and Engineering (Emeritus)

Contents

29	1	Introducing Fusion Reactor Design	17
30	1.1	Distinguishing Pulsed from Steady-State	18
31	1.2	Pricing a Fusion Reactor	19
32	1.3	Modeling Fusion Systems	21
33	1.4	Discussing HTS Magnet Technology	22
34	2	Designing a Steady-State Tokamak	25
35	2.1	Defining Plasma Parameters	26
36	2.1.1	Understanding Tokamak Geometry	26
37	2.1.2	Prescribing Plasma Profiles	28
38	2.2	Solving the Steady Current	31
39	2.2.1	Enforcing the Greenwald Density Limit	31
40	2.2.2	Declaring the Bootstrap Current	34
41	2.2.3	Deriving the Fusion Power	35
42	2.2.4	Using Current Drive	37
43	2.2.5	Completing the Steady Current	38
44	2.3	Handling Current Drive Self-Consistently	39
45	3	Formalizing the Systems Model	41
46	3.1	Explaining Static Variables	42
47	3.2	Connecting Dynamic Variables	42
48	3.3	Enforcing Power Balance	46
49	3.3.1	Collecting Power Sources	46
50	3.3.2	Approximating Radiation Losses	48

51	3.3.3	Estimating Heat Conduction Losses	49
52	3.3.4	Writing the Lawson Parameter	51
53	3.3.5	Finalizing the Primary Constraint	53
54	3.4	Collecting Limiting Constraints	56
55	3.4.1	Introducing the Beta Limit	57
56	3.4.2	Giving the Kink Safety Factor	58
57	3.4.3	Working under the Wall Loading Limit	59
58	3.4.4	Setting a Maximum Power Cap	60
59	3.4.5	Listing the Heat Loading Limit	61
60	3.5	Summarizing the Fusion Systems Model	62
61	4	Designing a Pulsed Tokamak	65
62	4.1	Modeling Plasmas as Circuits	66
63	4.1.1	Drawing the Circuit Diagram	66
64	4.1.2	Plotting Pulse Profiles	68
65	4.1.3	Specifying Circuit Variables	72
66	4.1.4	Constructing the Pulse Length	76
67	4.2	Producing Flux Balance	77
68	4.2.1	Rearranging the Circuit Equation	77
69	4.2.2	Adding Poloidal Field Coils	79
70	4.3	Improving Tokamak Geometry	80
71	4.3.1	Defining Central Solenoid Dimensions	81
72	4.3.2	Calculating Component Thicknesses	82
73	4.3.3	Revisiting Central Solenoid Dimensions	84
74	4.4	Piecing Together the Generalized Current	86
75	4.5	Simplifying the Generalized Current	88
76	4.5.1	Recovering the Steady Current	88
77	4.5.2	Extracting the Pulsed Current	89
78	4.5.3	Rationalizing the Generalized Current	90
79	5	Completing the Systems Model	91

80	5.1	Describing a Simple Algebra	91
81	5.2	Generalizing Previous Equations	93
82	5.2.1	Including Limiting Constraints	93
83	5.2.2	Minimizing Intermediate Quantities	95
84	5.2.3	Pinning Dynamic Variables	96
85	5.2.4	Detailing the Equation Solver	96
86	5.3	Wrapping up the Logic	99
87	6	Presenting the Code Results	101
88	6.1	Testing the Code against other Models	102
89	6.1.1	Comparing with the PSFC Arc Reactor	103
90	6.1.2	Contrasting with the Aries Act Studies	104
91	6.1.3	Benchmarking with the Process DEMO Designs	105
92	6.2	Developing Prototype Reactors	113
93	6.2.1	Navigating around Charybdis	118
94	6.2.2	Pinning down Proteus	118
95	6.2.3	Highlighting Operation Differences	118
96	6.3	Learning from the Data	119
97	6.3.1	Picking a Design Point	119
98	6.3.2	Utilizing High Field Magnets	124
99	6.3.3	Looking at Design Alternatives	127
100	7	Planning Future Work for the Model	135
101	7.1	Incorporating Stellarator Technology – Ladon	135
102	7.2	Making a Composite Reactor – Janus	136
103	7.3	Bridging Confinement Scalings – Daedalus	137
104	7.4	Addressing Model Shortcomings	138
105	7.4.1	Integrating Pedestal Temperature Profiles	138
106	7.4.2	Expanding the Radiation Loss Term	139
107	7.4.3	Taking Flux Sources Seriously	139

108	8 Concluding Reactor Discussion	141
109	A Cataloging Static Variables	143
110	B Simulating with Fussy.jl	145
111	B.1 Getting the Code to Work	145
112	B.2 Sorting out the Codebase	146
113	B.2.1 Typing out Structures	147
114	B.2.2 Referencing Input Decks and Solutions	149
115	B.2.3 Acknowledging Utility Functions	149
116	B.2.4 Mentioning Base Level Files	149
117	B.3 Delving into Reactor Methods	150
118	B.4 Demonstrating Code Usage	151
119	B.4.1 Initializing the Workspace	152
120	B.4.2 Running a Study	152
121	B.4.3 Extracting Results	153
122	B.4.4 Plotting Curves	154
123	C Discussing Fusion Power	159
124	C.1 Theoretical Background	159
125	C.2 Bosch-Hale Reactivity	161
126	D Selecting Plasma Profiles	165
127	D.1 Density – n	165
128	D.2 Temperature – T	167
129	D.3 Pressure – p	169
130	D.4 Bootstrap Current – f_{BS}	170
131	D.5 Volume Averaged Powers	172
132	E Determining Plasma Flux Surfaces	175
133	E.1 Flux Surface Coordinates	175
134	E.2 Cross-sectional Area and Volume	177

135	E.3 Surface and Volume Integrals	178
136	F Expanding on the Bootstrap Current	181
137	F.1 Summarized Results	181
138	F.2 Detailed Analysis	183
139	G Compending Code Plots	189
140	G.1 Magnet Strength Scans	190
141	G.2 Cost Sensitivity Studies	211

142 List of Figures

143	1-1	Cut-Away of Tokamak Reactor	18
144	1-2	Comparison of Pulsed and Steady-State Current	19
145	1-3	Steady State Magnet Components	23
146	1-4	Pulsed Magnet Components	23
147	2-1	Geometry of a Tokamak	27
148	2-2	Geometric Parameters	28
149	2-3	Radial Plasma Profiles	29
150	2-4	Greenwald Density Limit	32
151	3-1	Current Balance in a Tokamak	45
152	3-2	Power Balance in a Reactor	52
153	3-3	H-Mode Confinement Time Scaling	54
154	4-1	A Simple Plasma Transformer Description	67
155	4-2	Time Evolution of Circuit Profiles	69
156	4-3	Dimensions of Tokamak Cross-Section	81
157	5-1	Equation Selection for Fusion System	92
158	5-2	Minimize Cost Step II/III – Optimize Reactor	97
159	6-1	Act Studies Cost Dependence on the H Factor	105
160	6-2	Arc Model Comparison	108
161	6-3	Aries Act I Model Comparison	109
162	6-4	Aries Act II Model Comparison	110
163	6-5	Demo Steady Model Comparison	111
164	6-6	Demo Pulsed Model Comparison	112

165	6-7	Designing Reactor Prototypes	115
166	6-8	Steady State Prototype Comparison	116
167	6-9	Pulsed Prototype Comparison	117
168	6-10	Limiting Constraint Regimes	120
169	6-11	Steady State Cost Curves	122
170	6-12	Pulsed Cost Curves	123
171	6-13	Pulsed B_{CS} Sensitivity	125
172	6-14	Pulsed Monte Carlo Sampling	126
173	6-15	Bootstrap Current Monte Carlo Sampling	128
174	6-16	Internal Inductance Sensitivities	129
175	6-17	Pulsed H Sensitivities	131
176	6-18	Steady State Current Drive Efficiency	132
177	6-19	Current Drive Efficiency vs Launch Angle	133
178	7-1	Cut-Away of Stellarator Reactor	136
179	7-2	Current Balance in a Tokamak	137
180	B-1	A Blank Plot	155
181	B-2	An Empty Plot	156
182	B-3	An Unscaled Plot	157
183	B-4	A Scaled Plot	157
184	C-1	Comparing Nuclear Fusion and Fission	160
185	C-2	The D-T Fusion Reaction	161
186	D-1	Radial Plasma Profiles	165
187	E-1	Cut-Away of Tokamak Reactor	175
188	E-2	Dimensions of Tokamak Cross-Section	178
189	G-1	Magnet Scan: \bar{T} vs B_0	191
190	G-2	Magnet Scan: \bar{n} vs B_0	192
191	G-3	Magnet Scan: I_P vs B_0	193

192	G-4 Magnet Scan: R_0 vs B_0	194
193	G-5 Magnet Scan: \bar{p} vs B_0	195
194	G-6 Magnet Scan: τ_E vs B_0	196
195	G-7 Magnet Scan: η_{CD} vs B_0	197
196	G-8 Magnet Scan: f_{BS} vs B_0	198
197	G-9 Magnet Scan: W_M vs B_0	199
198	G-10 Magnet Scan: C_W vs B_0	200
199	G-11 Magnet Scan: q_{DV} vs B_0	201
200	G-12 Magnet Scan: $(\beta_N)_{norm}$ vs B_0	202
201	G-13 Magnet Scan: $(q_{95})_{norm}$ vs B_0	203
202	G-14 Magnet Scan: $(P_W)_{norm}$ vs B_0	204
203	G-15 Magnet Scan: P_F vs B_0	205
204	G-16 Magnet Scan: b vs B_0	206
205	G-17 Magnet Scan: c vs B_0	207
206	G-18 Magnet Scan: d vs B_0	208
207	G-19 Magnet Scan: h_{CS} vs B_0	209
208	G-20 Magnet Scan: R_{CS} vs B_0	210
209	G-21 Cost Sensitivity: H vs. B_0	212
210	G-22 Cost Sensitivity: Q vs. B_0	213
211	G-23 Cost Sensitivity: τ_{FT} vs. B_0	214
212	G-24 Cost Sensitivity: N_G vs. B_0	215
213	G-25 Cost Sensitivity: f_D vs. B_0	216
214	G-26 Cost Sensitivity: Z_{eff} vs. B_0	217
215	G-27 Cost Sensitivity: ϵ vs. B_0	218
216	G-28 Cost Sensitivity: κ_{95} vs. B_0	219
217	G-29 Cost Sensitivity: δ_{95} vs. B_0	220
218	G-30 Cost Sensitivity: ν_n vs. B_0	221
219	G-31 Cost Sensitivity: ν_T vs. B_0	222
220	G-32 Cost Sensitivity: l_i vs. B_0	223
221	G-33 Cost Sensitivity: $(\beta_N)_{max}$ vs. B_0	224

222	G-34 Cost Sensitivity: $(q_{95})_{max}$ vs. B_0	225
223	G-35 Cost Sensitivity: $(P_W)_{max}$ vs. B_0	226

224 List of Tables

225	3.1	Dynamic Variables	42
226	4.1	Piecewise Linear Scheme for Pulsed Operation	69
227	4.2	Example TF Coils and Central Solenoid Critical Values	84
228	5.1	Main Equation Bank	94
229	6.1	Arc Variables	108
230	6.2	Act I Variables	109
231	6.3	Act II Variables	110
232	6.4	Demo Steady Variables	111
233	6.5	Demo Pulsed Variables	112
234	6.6	Charybdis Variables	116
235	6.7	Proteus Variables	117
236	6.8	Proteus and Charybdis Comparison	119
237	A.1	List of Static Variables	143
238	C.1	Bosch-Hale parametrization coefficients for volumetric reaction rates .	163
239	C.2	Tabulated Bosch-Hale reaction rates $[\text{m}^3 \text{ s}^{-1}]$	163

240 List of Equations

241	1.1	Magnetic Energy – W_M	20
242	1.3	Cost per Watt – C_W	21
243	2.1	Minor Radius – a	27
244	2.2	Density Profile – n	29
245	2.4	Temperature Profile – T	30
246	2.5	Current Profile – J	30
247	2.6	Internal Inductance – l_i	31
248	2.7	Normalized Poloidal Magnetic Field – b_p	31
249	2.8	Current Balance – I	31
250	2.11	Greenwald Density – \bar{n}	33
251	2.15	Bootstrap Current – I_{BS}	35
252	2.20	Dilution Factor – f_D	36
253	2.21	Volume Integral – Q_V	36
254	2.23	Fusion Power – P_F	36
255	2.28	Current Drive – I_{CD}	38
256	2.30	Steady Current – I_P	39
257	2.31	Current Drive Efficiency – η_{CD}	40
258	3.1	Scanned Temperature – \bar{T}	43
259	4.75	Generalized Current – I_P	87
260	C.1	Fusion Energy – E_F	159
261	C.3	Neutron Power – P_n	160
262	C.4	Alpha Power – P_α	160

Chapter 1

Introducing Fusion Reactor Design

The central goal of fusion energy research is to build an economically competitive nuclear reactor. It has long been joked, though, that fusion power will always be twenty years away. This is mainly due to the nonlinearities inherent to a reactor system and the high upfront cost of building a new machine. The model developed for this paper uses standard theory and empirical fits to find cost trends from this nonlinear system. An important conclusion is that building an economic reactor using existing technology would be impossible. One solution may be improving magnet technology – as MIT is exploring with high-temperature superconducting (HTS) tape.

As can be seen by comparing the European and American/Asian fusion reactor design efforts, though, one of the most important decisions is whether to run the reactor as pulsed (EU¹) or steady-state (US² and Korea³). The distinction between the two mainly manifests itself in the choice of auxiliary current drive: inductive for pulsed and lower hybrid for steady-state.⁴ With the model built for this thesis, it is possible to perform a direct comparison of these two modes of operations.

Due to the speed and simplicity of the model, hundreds of reactors can be simulated in minutes. Further, the model has been benchmarked against other ones from the literature,^{2,5–7} allowing it to answer several critical questions regarding the comparison of the two modes of operation. A major finding of this is that HTS tape should

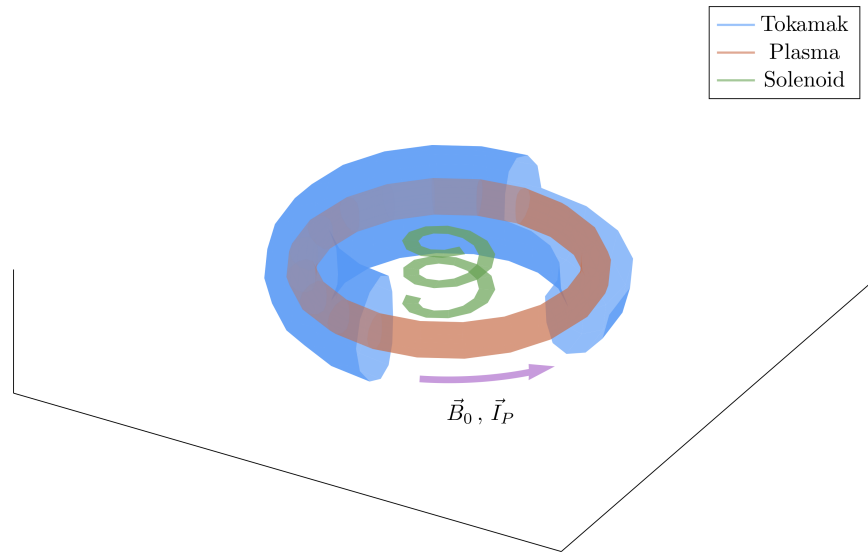


Figure 1-1: Cut-Away of Tokamak Reactor

The three main components of a magnetic fusion reactor are: the tokamak structure, the plasma fuel, and the spring-like solenoid at the center. Here, the directions of the magnetic field (B_0) and plasma current (I_P) variables are shown to be in the toroidal direction.

appear in different places for the two modes of operation: within the central solenoid for pulsed machines and inside the TF coil magnets for steady-state ones.

1.1 Distinguishing Pulsed from Steady-State

The leading candidate for the first economic, power-producing fusion reactor is a tokamak. As shown in ??, tokamaks are doughnut-shaped metal structures that use magnets to confine their fusion-grade plasmas. The challenge in building such a device comes from the various physics and engineering constraints it must satisfy – i.e. not surpassing acceptable levels of neutron damage, plasma pressure, etc.

One of the most contentious points of reactor design, however, is whether to run it as: pulsed (the European effort¹) or steady-state (the American/Asian approach^{2,3}). Here, pulsed operation refers to how a reactor is ramped up and down several times a day. Whereas steady-state implies a machine is functionally kept ramped up the

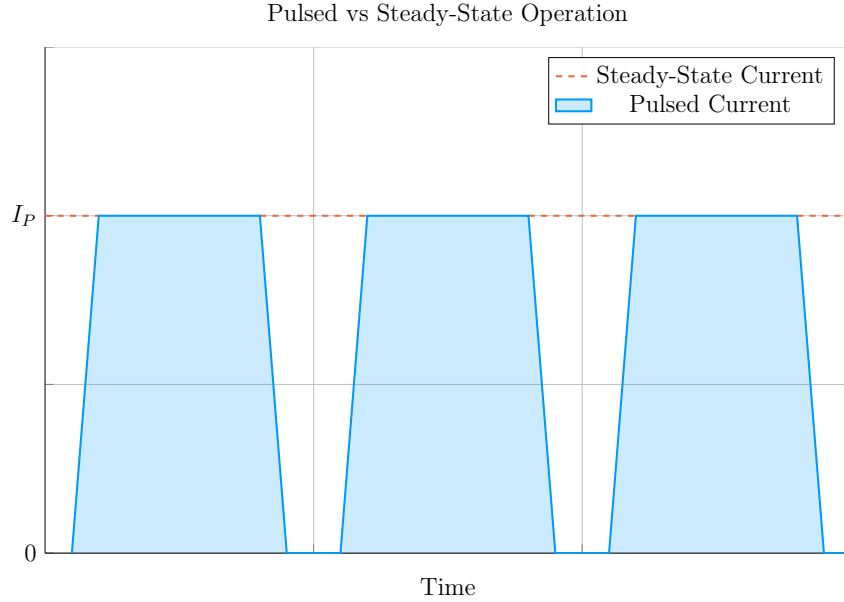


Figure 1-2: Comparison of Pulsed and Steady-State Current

Inside a pulsed reactor, current is ramped up and down several times a day – with downtime in-between. Steady state reactors are meant to remain on for weeks or months.

entirety of its fifty-year campaign. These behaviors are shown in ???. The difficulties
involves with the two modes of operation are then: cyclical stresses for pulsed and
expensive current drive for steady state.⁴

The main way these two modes of operation, *pulsed* and *steady-state*, influence reactor
design, though, is through the current balance equation (derived later). What this
means practically is a tokamak plasma requires some current to stay in equilibrium
and this current has to be partially generated by auxiliary systems: inductively for
pulsed and non-inductively for steady-state. To fairly compare the two modes of
operation thus requires a generalized handling of current balance that can incorporate
both auxiliary systems.

1.2 Pricing a Fusion Reactor

To truly compare tokamaks used as fusion reactors, though, the obvious metrics are
costs. ITER – the most expensive experiment in the world^{8,9} – has a history full of

countries backing out for high construction costs and rejoining only after they finally get lowered.⁴ The problem is \$20B is a lot of money and 20 years is a long time. Moreover, approximating true costs is difficult due to the need to project (or neglect) economies-of-scale for expensive components, such as the superconducting magnets and irradiated materials.

Therefore, this paper adopts stand-ins for the conventional capital cost and cost-per-watt metrics. This is done for simplicity, both in: formulating the relations and conveying the two metrics to physicists. The approximation for the capital cost – how much a tokamak costs to build – is the magnetic energy.¹⁰

$$W_M \propto R^3 B^2 \quad (1.1)$$

In this magnetic energy proportion relation, the tokamak’s major radius – R – is involved in a volumetric term (R^3) and B is the strength (in Teslas) of the toroidal magnetic field. This quantity simply states that the two surefire ways to make a machine more expensive are to build it bigger and to use stronger magnets. As these terms also improve confinement, this cost introduces a trade-off between size and magnet technology. This is why the proposed ARC reactor – designed with HTS tape – could be half the size of ITER, which uses conventional LTS technology.

The next metric, the cost-per-watt, is defined by dividing the capital cost (i.e. the magnetic energy) by the main source of power output. For a tokamak, this source of power is fusion – discussed in more detail in ???. The cost-per-watt thus measures how economically competitive a reactor will be once it is build. This is how to compare the rate of return for different base-load power sources (e.g. fission, coal, and solar).

$$\tilde{C}_W = \frac{W_M}{P_F} \quad (1.2)$$

A final correction can be made on the cost-per-watt to account for reactor downtime,

which is fundamental to pulsed operation. This is handled through the duty factor (f_{Duty}) that is defined as the ratio of a reactor’s quasi-steady-state flattop duration to the entire pulse length of a tokamak. In the context of the cost-per-watt, it scales down the fusion power:

$$C_W = \frac{W_M}{f_{Duty} \cdot P_F} \quad (1.3)$$

For a steady-state reactor, this duty factor is assumed to be held at one. Pulsed machines, on the other hand, can see around thirty minutes of downtime,⁷ which leads to duty factors around 80%. Analysis in ??, however, shows that pulsed reactors may also have duty factors near unity.

Combined, these two cost metrics allow designers to pinpoint economically competitive tokamaks within reactor space. Although not rigorous in an engineering context, these capital cost and cost-per-watt approximations do provide true physics meaning while comparing different machines – whether they run as pulsed or steady-state.

1.3 Modeling Fusion Systems

Before reactors can be priced, though, they have to be modeled. Therefore the first half of this thesis is devoted to the theory behind tokamak design. Emphasis is placed more on a physicist’s intuition than an engineer’s costing rigor. This is justified by the nonlinearities inherent to fusion systems and rationalized by this paper’s results matching more sophisticated models with high fidelity.

Stepping back, a fusion systems model is an approach to designing reactors based on satisfying various physics and engineering constraints. Zero-dimensional (0-D) systems models are then a particular subclass of these that reduce the inherently 3-D problem of design to a collection of scalar, averaged values. This reduction in complexity allows models to be orders of magnitude faster. The natural corollary of this is that hundreds of reactors can be simulated in minutes.

358 Within the context of reactor design, these 0-D systems models serve an important
359 role due to their speed and simplicity. Although not truly self-consistent,* these
360 models are capable of exploring large areas of reactor space. This is especially impor-
361 tant in the early stages of tokamak planning when researchers are selecting a design
362 point. These models also have use in finding general costing trends – as shown in this
363 document.

364 What makes this paper’s systems model different from other ones, though, is its gen-
365 eralized handling of both modes of tokamak operation: pulsed and steady-state. This
366 was necessitated by a desire to fairly compare the two. The most fundamental result
367 of this analysis is that both modes are actually capable of leading to economically
368 competitive reactors – assuming some technological advancements.

369 1.4 Discussing HTS Magnet Technology

370 As mentioned, no economically competitive fusion reactor can be built using existing
371 technology – regardless of whether it runs as pulsed or steady-state. This is why MIT
372 has been exploring HTS magnet technology for their Arc reactor in an effort to nearly
373 double the maximum achievable field strength. What this paper shows is that this
374 logic is indeed correct and HTS may be the final magnet advancement needed for the
375 conventional fusion paradigm (i.e. D-T fuel, H-Mode, etc.)

376 More concretely, this paper shows that new HTS technology is capable of lowering
377 reactor costs – both for pulsed and steady-state operation. Further, this HTS tape has
378 different uses within the two modes of operation – as set by cost concerns (see ???).
379 This analysis shows that HTS should be employed in the TF coils for steady-state
380 reactors *and* in the central solenoid for pulsed ones. This is because pulsed machines
381 require lower toroidal field strengths, which are achievable with less expensive LTS
382 magnets.

*For speed concerns, 0-D fusion systems models often ignore self consistency in quantities like pres-
sure profiles and use empirical fits to estimate values such as the confinement time.

Now that the problem has been thoroughly introduced, we will go over the theory behind steady-state and, then, pulsed tokamaks. A couple detours will be taken along the way to show how the model can be incorporated into a fusion systems code. This code – Fussy.jl – is the topic of ?? and is freely available at:

git.io/tokamak

388

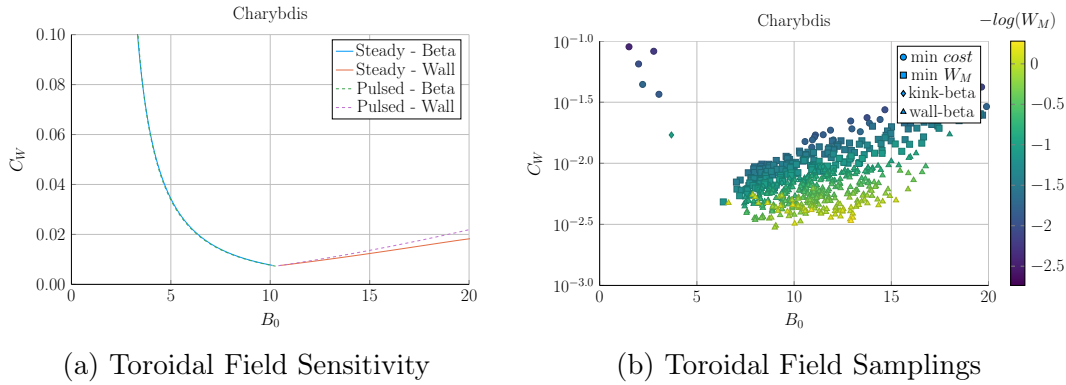


Figure 1-3: Steady State Magnet Components

Steady-state reactors benefit from increased toroidal field strength until neutron wall loading starts to dominate design (at around 10-15 T for Charybdis). This is well within the range accessible to HTS magnets.

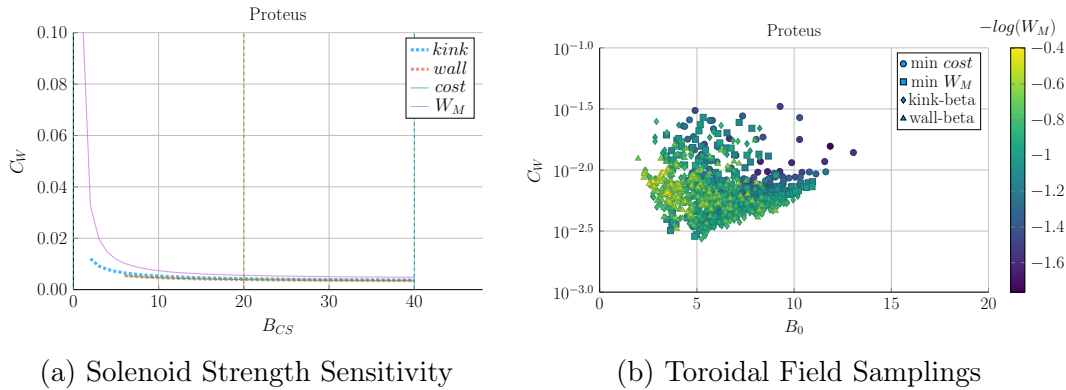


Figure 1-4: Pulsed Magnet Components

Pulsed reactors are shown to receive strong decreases in reactor cost as the central solenoid field strength is increased, until around 20 T. However, the TF coils do not receive the same cost reduction with field strength – as shown by the minimum cost appearing at 5 T.

Chapter 2

Designing a Steady-State Tokamak

This chapter explores a simple model for designing steady-state tokamaks. In the next couple chapters, the model is first formalized for use in a systems code and then generalized to handle pulsed operation. These derivations highlight that the only difference between the two modes of operation is how they generate their auxiliary plasma current: LHCD for steady-state operation and inductive sources for when a reactor is purely pulsed.

Along the way, equations will be derived that get rather complicated. To remedy the situation, a distinction between dynamic and static values is now given, which will allow splitting most equations into static and dynamic parts. Dynamic values – i.e. the tokamak’s major radius (R_0) and magnet strength (B_0), as well as the plasma’s current (I_P), temperature (\overline{T}), and density (\overline{n}) – are first-class variables in the model (see ??). Everything is derived to relate them. Static values, on the other hand, can be treated as code inputs, which remain constant throughout a reactor solve. These most obviously include the various geometric and profile parameters introduced next section.

The overall structure of this chapter, then, is built around developing an equation for plasma current in a steady-state tokamak. It is shown that this value arises from balancing current in a reactor using both a plasma’s own bootstrap current (I_{BS}),

409 as well the tokamak's auxiliary driven current (I_{CD}). These relations necessitate
410 geometric parameters and plasma profiles, which will be given shortly. Along the
411 way, definitions will also be needed for the Greenwald density (N_G) and the fusion
412 power (P_F). What is shown is that the current does not actually depend directly
413 on the major radius (R_0) or magnet strength (B_0) of a tokamak – allowing these
414 variables to be put off until next chapter.

415 2.1 Defining Plasma Parameters

416 As mentioned previously, the zero-dimensional model derived here can closely approx-
417 imate solutions from higher-dimensional codes that might take many hours to run.
418 The essence of boiling down three-dimensional behaviors to one dimensional profiles
419 – and zero-dimensional averaged values – begins with defining the most important
420 plasma parameters. These are the: current density (J), temperature (T), and density
421 (n) of a plasma.

422 Solving this problem most generally usually involves decoupling the geometry of the
423 plasma from the shaping of its nearly parabolic radial-profiles – both of which will be
424 explained shortly.

425 2.1.1 Understanding Tokamak Geometry

426 The first thing people see when they look at a tokamak is its geometry – see ???. How
427 big is it? Is it stretched out like a bicycle tire or compressed to the point of being
428 nearly spherical? Would a slice across the major radius result in two cross-sections
429 that were: circular, elliptic, or triangular?

430 These questions lend themselves to the three important geometric variables – the
431 inverse aspect ratio (ϵ), the elongation (κ), and the triangularity (δ). The inverse

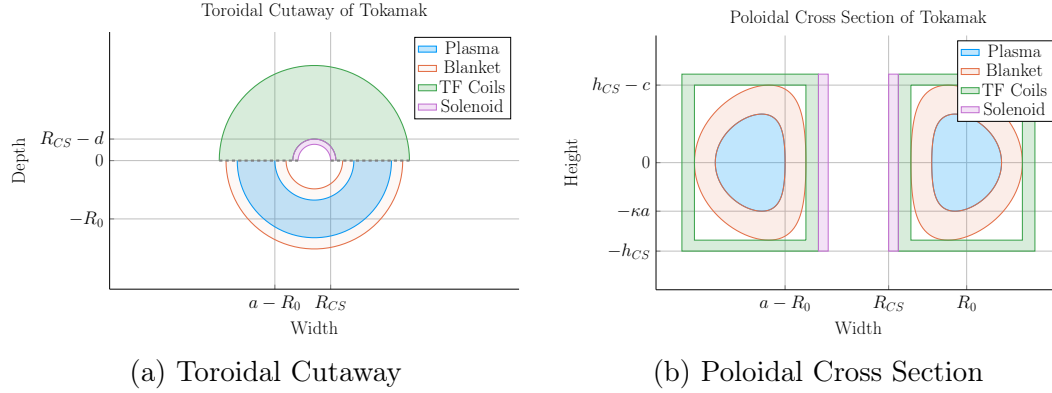


Figure 2-1: Geometry of a Tokamak

This diagram is of a tokamak's toroidal (top) view and the poloidal cross section of a slice across the major axis. Included are the four components of a reactor: the plasma, its metallic blanket, the toroidal field magnets surrounding them, and the central solenoid. These have thicknesses of a , b , c and d , respectively. R_{CS} is where the solenoid starts.

aspect ratio is a measure of how stretched out the device is, or formulaically:

$$a = \epsilon \cdot R_0 \quad (2.1)$$

This says that the minor radius (a), measured in meters, is related to the major radius of the machine (R_0) through ϵ . Or more tangibly, the minor radius is related to the two small cross-sections that result from a slice across the major radius of the machine.

The remaining two geometric parameters – κ and δ – are related to the shape of the torn halves. As the name hints, elongation (κ) is a measure of how stretched out the tokamak is vertically – is the cross-section a circle or an oval? The triangularity (δ) is then how much the cross-sections point outward from the center of the device. All three's effects can be seen in ???. Their exact usage within describing flux surfaces is shown in ???.

These geometric factors allow the volumetric and surface integrals governing fusion power and bootstrap current to be condensed to simple radial ones – see ?????. The only remaining step is to define the radial profiles for: the density, temperature, and

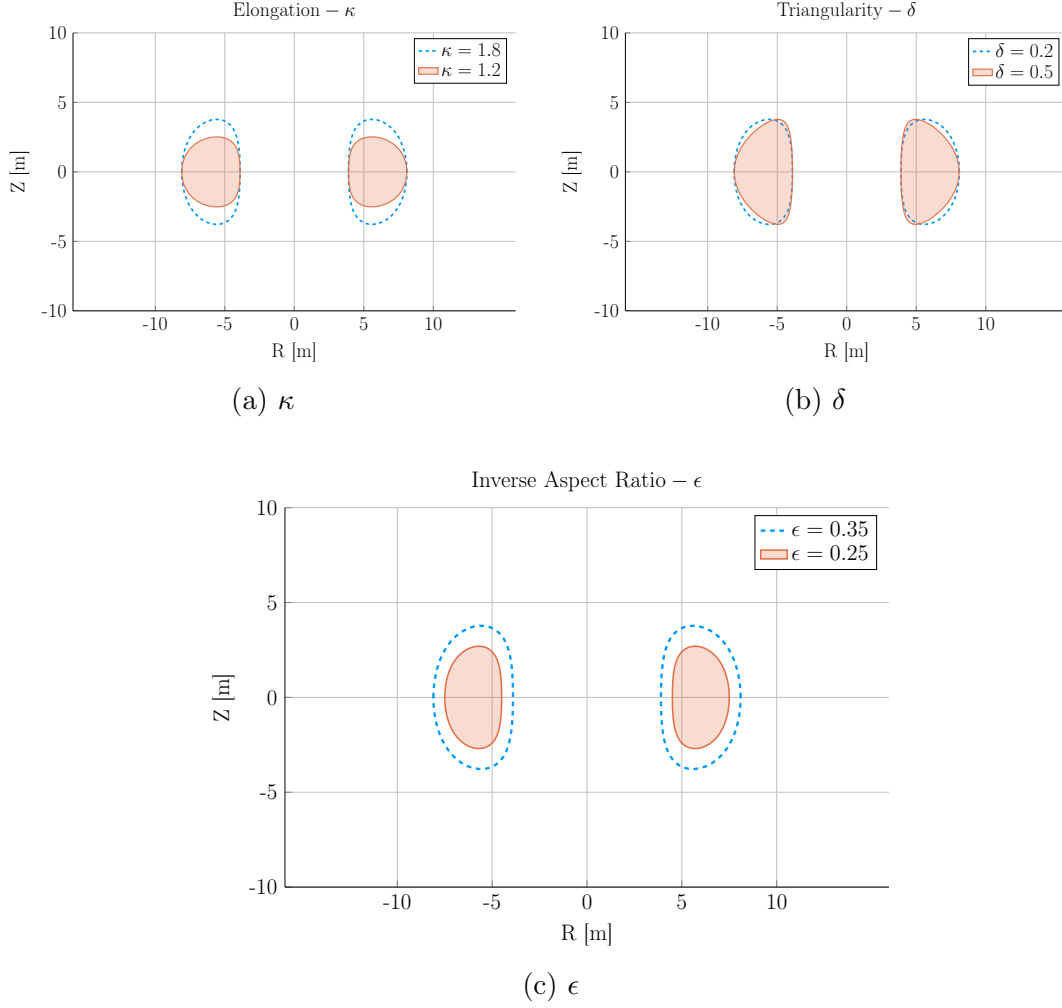


Figure 2-2: Geometric Parameters

These three geometric parameters allow the toroidal cross-sections to scale radially, stretch vertically, and become more triangular – thus improving upon simple circular slices.

current of a plasma.

2.1.2 Prescribing Plasma Profiles

The first step in defining radial profiles is realizing that all three quantities are essentially parabolas – i.e. the temperature, density and current density, shown in ??, are peaked at some radius (usually the center) and then decay to zero somewhere before the walls of the tokamak enclosure.

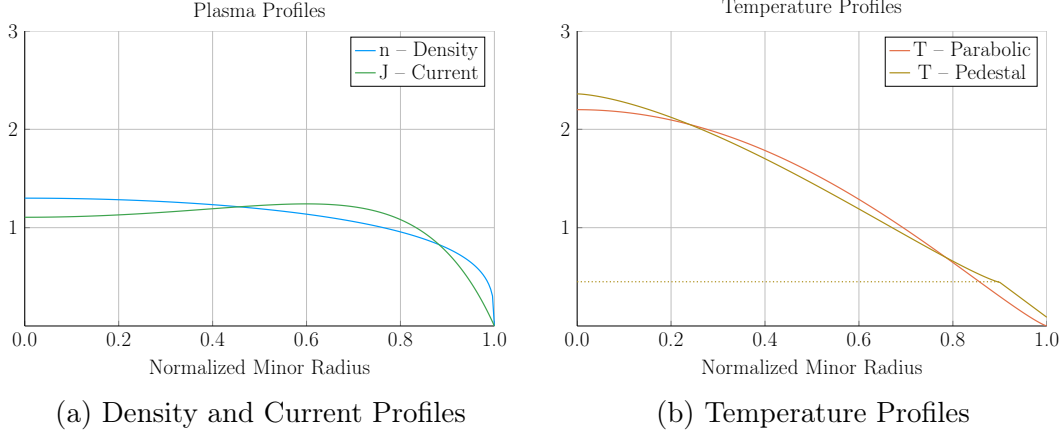


Figure 2-3: Radial Plasma Profiles

The three most fundamental profiles of a fusion plasma are its temperature, density, and current. These allow the model to reduce from three dimensions to just half of one.

Although not self-consistent, these profiles do capture enough of the physics to approximate relevant phenomenon, such as transport and fusion power.¹¹

The Density Profile

To begin, density has the simplest profile. This is because it is relatively flat, remaining near the average value – \bar{n} – throughout the body of the plasma until quickly decaying to zero near the edge of the plasma.* For this reason, a parabolic profile with a very low peaking factor – ν_n – is well suited.

$$n(\rho) = \bar{n} \cdot (1 + \nu_n) \cdot (1 - \rho^2)^{\nu_n} \quad (2.2)$$

The reason \bar{n} is referred to as the volume-averaged density is because using the volume integral – given by ?? – over the density profile results in that value after dividing through by the volume (V):

$$\bar{n} = \frac{\int n(\mathbf{r}) d\mathbf{r}}{V} \quad (2.3)$$

*Even in H-Mode plasmas where density profiles have a pedestal,¹² they usually have much less of a peak than temperatures¹³ – especially so in a reactor setting.¹⁴

462 A final point to make is this parabolic profile allows for a short closed-form relation
 463 for the Greenwald density limit – substantially simplifying this fusion systems model.

464 The Temperature Profile

465 The use of a parabolic profile for the plasma temperature is slightly more dubious.
 466 This is because H-Mode plasmas are actually highly peaked at the center, decaying
 467 to a non-zero pedestal temperature near the edge before finally dropping sharply to
 468 zero. This model chooses to forego this pedestal representation for a simple parabolic
 469 one – although the pedestal approach is discussed in ???. Analogous to the density,
 470 the profile treats \bar{T} as the average value and ν_T as the peaking parameter.

$$T(\rho) = \bar{T} \cdot (1 + \nu_T) \cdot (1 - \rho^2)^{\nu_T} \quad (2.4)$$

471

472 The Current Density Profile

473 The plasma current density is the third profile and cannot safely be represented by a
 474 simple parabola. This is because having an adequate bootstrap current relies heavily
 475 on a profile being peaked off-axis – i.e. at some radius not at the center. This hollow
 476 profile can then be modeled with the commonly given plasma internal inductance (l_i).
 477 Concretely, the current's hollow profile is described by:

$$J(\rho) = \bar{J} \cdot \frac{\gamma^2 \cdot (1 - \rho^2) \cdot e^{\gamma \rho^2}}{e^\gamma - 1 - \gamma} \quad (2.5)$$

478 The intermediate γ quantity can then be numerically solved for from the plasma
 479 internal inductance using the following relations – with b_p representing the normalized
 480 poloidal magnetic field. These are derived in ??.

$$l_i = \frac{4\kappa}{1 + \kappa^2} \int_0^1 b_p^2 \rho d\rho \quad (2.6)$$

481

$$b_p(\rho) = \frac{-e^{\gamma\rho^2}(\gamma\rho^2 - 1 - \gamma) - 1 - \gamma}{\rho(e^\gamma - 1 - \gamma)} \quad (2.7)$$

482 Combined, these three geometric parameters and profiles lay the foundation for this
 483 zero-dimensional fusion systems model.

484 2.2 Solving the Steady Current

485 As suggested, one of the most important equations in a fusion reactor is current
 486 balance. In steady-state operation, all of a plasma's current (I_P) must come from
 487 a combination of its own bootstrap current (I_{BS}), as well as auxiliary current drive
 488 (I_{CD}). This can be represented mathematically as:

$$I_P = I_{BS} + I_{CD} \quad (2.8)$$

489 The goal is then to write equations for bootstrap current and driven current. This will
 490 make heavy use of the Greenwald density limit. The steady current will then be shown
 491 to be only a function of temperature! In other words, this current is independent of
 492 a tokamak's geometry and magnet strength. As will be pointed out then, though, a
 493 subtlety arises that will bring the two back into the picture – self-consistency in the
 494 current drive efficiency (η_{CD}).

495 2.2.1 Enforcing the Greenwald Density Limit

496 The Greenwald density limit is a density limit that applies to all tokamaks. It sets a
 497 hard limit on the density and how it scales with current and reactor size. Although
 498 currently lacking a true first-principles theoretical explanation, it does have a real
 499 meaning within the design context. Operate at too low a density and run the risk of
 500 never entering H-Mode. Run the density too high, and cause the tokamak's plasma
 501 to disrupt. These conclusions can be seen in ??.

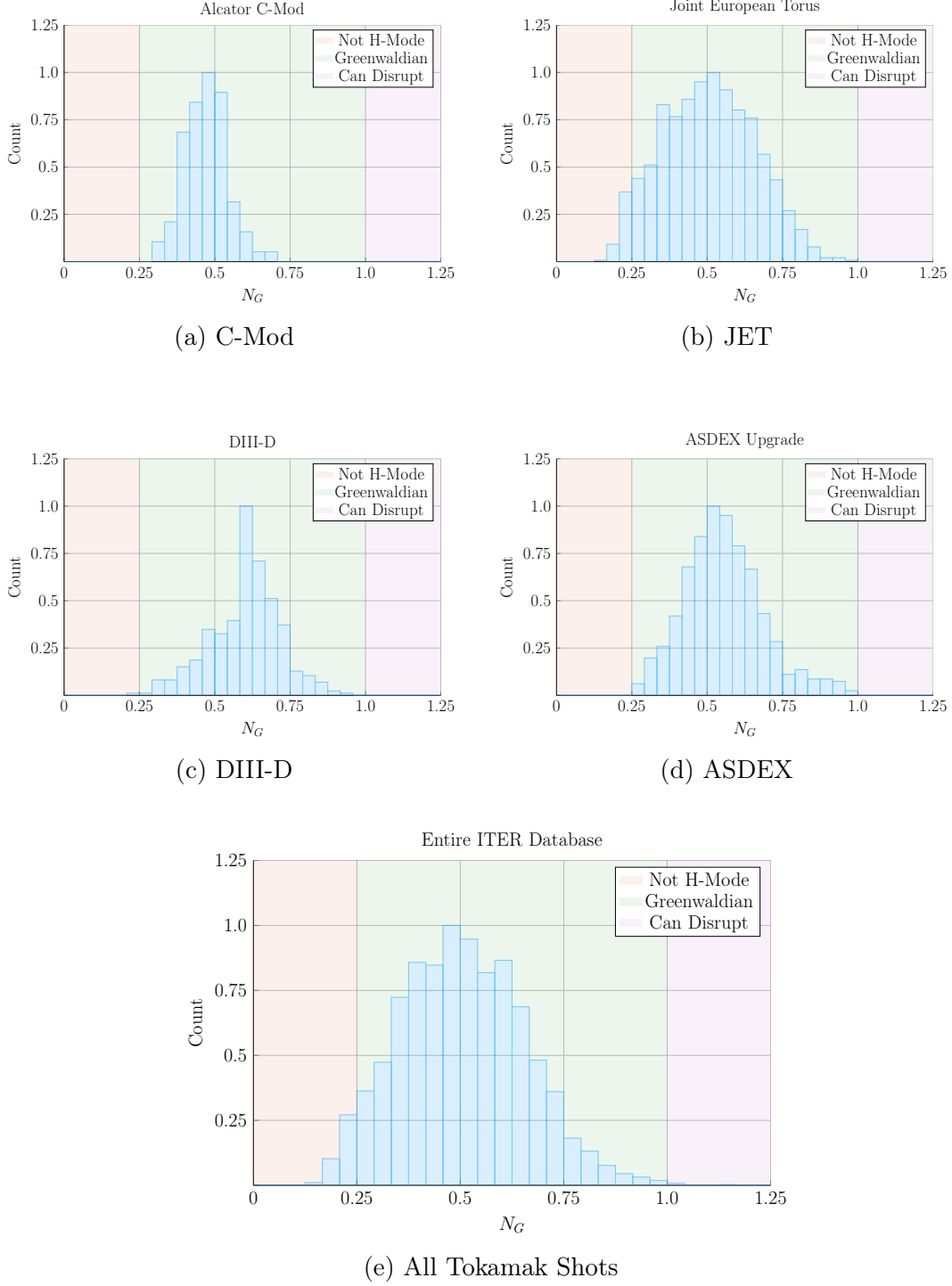


Figure 2-4: Greenwald Density Limit

The Greenwald Density Limit is a robust metric of what densities an H-Mode plasma can attain. Although empirical in nature, it accurately predicts when a tokamak will undergo degraded plasma transport.¹⁵

502 As no theoretical backing exists, the Greenwald density limit can simply be written
 503 (with citation) as:¹⁵

$$\hat{n} = N_G \cdot \left(\frac{I_P}{\pi a^2} \right) \quad (2.9)$$

504 Here, \hat{n} has units of $10^{20} \frac{\text{particles}}{\text{m}^3}$, N_G is the Greenwald density fraction, and I_P is
 505 again the plasma current (measured in mega-amps). The final variable is then the
 506 minor radius – a – which was previously defined through:

$$a = \epsilon \cdot R_0 \quad (??)$$

507 The next step is transforming the *line-averaged* density (\hat{n}) into the *volume-averaged*
 508 version (\bar{n}) used in this model. Harnessing the simplicity of the density's parabolic
 509 profile allows this relation to be written in a closed form as:

$$\hat{n} = \frac{\sqrt{\pi}}{2} \cdot \left(\frac{\Gamma(\nu_n + 2)}{\Gamma(\nu_n + \frac{3}{2})} \right) \cdot \bar{n} \quad (2.10)$$

510 Where $\Gamma(\dots)$ represents the gamma function: the non-integer analogue of the facto-
 511 rial function.

512 Combining these pieces allows the volume-averaged density to be written in standard-
 513 ized units as:

$$\bar{n} = K_n \cdot \left(\frac{I_P}{R_0^2} \right) \quad (2.11)$$

514

$$K_n = \frac{2N_G}{\epsilon^2 \pi^{3/2}} \cdot \left(\frac{\Gamma(\nu_n + \frac{3}{2})}{\Gamma(\nu_n + 2)} \right) \quad (2.12)$$

515 The format of the previous equation pair will be used throughout the remainder of
 516 the paper. The top equation relates dynamic variables (i.e. \bar{n} , I_P , and R_0), while the
 517 static-value coefficient (K_n) lumps together static quantities, such as: N_G , ϵ , 2 , π ,
 518 and ν_n .

519 2.2.2 Declaring the Bootstrap Current

520 The first term to define in current balance, ??, is the bootstrap current. This boot-
 521 strap current is a mechanism of tokamak plasmas that helps supply some of the
 522 current needed to keep a plasma in equilibrium. Its underlying behavior stems from
 523 particles stuck in banana-shaped orbits on the outer edges of the device propelling
 524 the majority species along their helical trajectories around the tokamak.

525 Utilizing the surface integral from ??, the bootstrap current (I_{BS}) can be written in
 526 terms of the temperature and density profiles:

$$I_{BS} = 2\pi a^2 \kappa g \int_0^1 J_{BS} \rho d\rho \quad (2.13)$$

527

$$\begin{aligned} J_{BS} &= f \left(n, T, \frac{dn}{d\rho}, \frac{dT}{d\rho} \right) \\ &\equiv -4.85 \cdot n \cdot T \cdot \frac{R_0 \sqrt{\epsilon} \rho}{d\psi/d\rho} \cdot \left(\frac{1}{n} \frac{dn}{d\rho} + 0.54 \frac{1}{T} \frac{dT}{d\rho} \right) \end{aligned} \quad (2.14)$$

528 The second definition for the bootstrap current density – J_{BS} – comes from using
 529 well known theoretical results plus several simplifying assumptions, including the
 530 large aspect limit. The value of $d\psi/d\rho$ is given in ??.

531 As shown later in the results, bootstrap fractions are often under-predicted by this
 532 model. This is due to parabolic profiles (i.e. for temperature) having much less steep
 533 declines near the edge (i.e. in their derivatives) than characteristic H-Mode profiles
 534 with pedestals. This implies that the area most positively impacted by a pedestal
 535 profile for temperature would be the bootstrap current derivation. The instructions
 536 to do so are given in ??.

537 Finally, summarizing the results of ??, the bootstrap current is found to be only a
 538 function of temperature and static variables! In standardized units, it can be written

539 as:

$$I_{BS} = K_{BS} \cdot \bar{T} \quad (2.15)$$

540

$$K_{BS} = 4.879 \cdot K_n \cdot \left(\frac{1 + \kappa^2}{2} \right) \cdot \epsilon^{5/2} \cdot H_{BS} \quad (2.16)$$

541

$$H_{BS} = (1 + \nu_n)(1 + \nu_T)(\nu_n + 0.054\nu_T) \int_0^1 \frac{\rho^{5/2} (1 - \rho^2)^{\nu_n + \nu_T - 1}}{b_p} d\rho \quad (2.17)$$

542 Quickly noting, this H_{BS} term serves as the analogue of static-value coefficients (e.g.
 543 K_{BS} and K_n) when they contain an integral. And b_p represents the poloidal magnet
 544 strength given by Eq. ??.

545 2.2.3 Deriving the Fusion Power

546 The next segue on our journey to solving for the steady current is deriving the fusion
 547 power (P_F), which appears in current drive. A comprehensive introduction to this is
 548 given in ??. Summarized, though, a formula for fusion power from a D-T reaction –
 549 in megawatts – is given by the following volume integral:[?]

$$P_F = \int E_F n_D n_T \langle \sigma v \rangle d\mathbf{r} \quad (2.18)$$

550

$$E_F = 17.6 \text{ MeV} \quad (2.19)$$

551 The E_F quantity is the energy created from a deuterium-tritium fusion reaction. The
 552 n_D and n_T in this equation then represent the density of the deuterium and tritium
 553 ions, respectively. Assuming a 50-50 mix of the two, they can be related to the
 554 electron density – i.e. the one used in this model – through the dilution factor (f_D).
 555 This dilution factor represents the decrease in available fuel from part of the plasma
 556 actually being composed of non-hydrogen gasses:

$$n_D = n_T = f_D \cdot \left(\frac{n}{2} \right) \quad (2.20)$$

557 The fusion reactivity, $\langle\sigma v\rangle$, is then a nonlinear function of the temperature, T, which
 558 the model approximates using the Bosch-Hale tabulation (described in the appendix).
 559 As this tabulated value appears inside an integral, it seems important to point out
 560 that the temperature is now the most difficult dynamic variable to handle – over R_0 ,
 561 B_0 , \bar{n} , and I_P . This will come into play when the model is formalized next chapter.
 562 The next step in the derivation of fusion power is transforming the three-dimensional
 563 volume integral (see Eq. ??) into a zero-dimension averaged value. First, the volume
 564 analogue of the previously given surface-area integral is:

$$Q_V = 4\pi^2 R_0 a^2 \kappa g \int_0^1 Q(\rho) \rho d\rho \quad (2.21)$$

565 Where again, Q is an arbitrary function of ρ and g is a geometric factor approximately
 566 equal to one. The fusion power can now be rewritten as:

$$P_F = \pi^2 E_F f_D^2 R_0 a^2 \kappa g \int_0^1 n^2 \langle\sigma v\rangle \rho d\rho \quad (2.22)$$

567 In standardized units, this becomes:

$$P_F = K_F \cdot \bar{n}^2 \cdot R_0^3 \cdot (\sigma v) \quad (2.23)$$

568

$$K_F = 278.3 \cdot f_D^2 \cdot (\epsilon^2 \kappa g) \quad (2.24)$$

569 Where the standardized fusion reactivity is now,

$$(\sigma v) = 10^{21} (1 + \nu_n)^2 \int_0^1 (1 - \rho^2)^{2\nu_n} \langle\sigma v\rangle \rho d\rho \quad (2.25)$$

570 At this point, the current drive needed for steady-state can now be defined.

2.2.4 Using Current Drive

As may have been lost along the way, this chapter's mission is to define a formula for steady current – from the current balance equation for steady-state tokamaks:

$$I_P = I_{BS} + I_{CD} \quad (??)$$

In standardized units, the equation for current drive is often given in the literature as:¹⁶

$$I_{CD} = \eta_{CD} \cdot \left(\frac{P_H}{\bar{n}R_0} \right) \quad (2.26)$$

Here, η_{CD} is the current drive efficiency with units $\left(\frac{\text{MA}}{\text{MW}\cdot\text{m}^2} \right)$ and P_H is the heating power in megawatts driven by LHCD (and absorbed by the plasma).

Let it be known, though, that driving current in a plasma is hard! In fact, pulsed reactor designers (i.e. European fusion researchers) think it is so difficult, they may choose to forego it completely – focusing only on inductive sources that necessitate reactor fatigue and downtime.

A common current drive efficiency (η_{CD}) seen in many designs is 0.3 ± 0.1 in the standard units. It is however inherently a function of all the plasma parameters – with subtlety put off until the discussion of self-consistency. For now it assumed to have some constant/static value.

The remaining step in deriving an equation for driven current (I_{CD}) is a formula for the heating power (P_H). The way fusion systems models – like this one – handle the heating power is through the physics gain factor, Q . Sometimes referred to as big Q , this value represents how many times over the heating power (P_H) is amplified as it is transformed into fusion power (P_F):

$$P_H = \frac{P_F}{Q} \quad (2.27)$$

591 Now, utilizing the previously defined Greenwald density and fusion power:

$$\bar{n} = K_n \cdot \left(\frac{I_P}{R_0^2} \right) \quad (??)$$

592

$$P_F = K_F \cdot \bar{n}^2 \cdot R_0^3 \cdot (\sigma v) \quad (??)$$

593 The current from LHCD can be written as:

$$I_{CD} = K_{CD} \cdot I_P \cdot (\sigma v) \quad (2.28)$$

594

$$K_{CD} = (K_F K_n) \cdot \frac{\eta_{CD}}{Q} \quad (2.29)$$

595 As η_{CD} and Q appear within a static coefficient, it is implied that both remain con-
596 stant throughout a solve. This subtlety is lifted when handling η_{CD} self-consistently,
597 which will be discussed shortly. However, even in that context, it proves beneficial to
598 still think of η_{CD} as a sequence of static variables – set by the model rather than the
599 user.

600 2.2.5 Completing the Steady Current

601 The goal of this chapter has been to derive a simple formula for steady current (I_P).

602 The problem started with current balance in a steady-state reactor:

$$I_P = I_{BS} + I_{CD} \quad (??)$$

603 Two equations were then found for the bootstrap (I_{BS}) and driven (I_{CD}) current:

$$I_{BS} = K_{BS} \cdot \bar{T} \quad (??)$$

604

$$I_{CD} = K_{CD} \cdot I_P \cdot (\sigma v) \quad (??)$$

605 Combining these three equations and solving for the total plasma current (I_P) – in
 606 mega-amps – yields:

$$I_P = \frac{K_{BS} \bar{T}}{1 - K_{CD}(\sigma v)} \quad (2.30)$$

607 This is the answer we have been seeking!

608 As mentioned before, this simple formula appears to only depend on temperature!*

609 Apparently, the plasma should have the same current at some temperature (i.e. $\bar{T} =$
 610 15 keV), regardless of the size of the machine or the strength of its magnets. This
 611 has the important corollary that each temperature maps to only one current value.
 612 Further, each temperature would then map to a single magnet strength, capital cost,
 613 etc. (as shown next chapter).

614 As has become a mantra, though, the subtlety of this behavior lies in the self-
 615 consistency of the current-drive efficiency – η_{CD} .

616 2.3 Handling Current Drive Self-Consistently

617 Although a thorough description of the wave theory behind lower-hybrid current
 618 drive (LHCD) is well outside the scope of this text, it does motivate the solving of
 619 a tokamak's major radius (R_0) and field strength (B_0). It also shows how what was
 620 once a simple problem has now transformed into a rather complex one – a common
 621 occurrence with plasmas.

622 The logic behind finding a self-consistent current-drive efficiency is starting at some
 623 plausible value (i.e. $\eta_{CD} = 0.3$), solving for the steady current – i.e. $I_P = f(\bar{T})$ – and
 624 then somehow iteratively creeping towards a value deemed self-consistent. What this

* This dependence only on temperature refers to dynamic variables. The plasma current can still be highly volatile to many of the static variables, such as: ϵ , κ , N_G , f_D , ν_n , l_i , etc.

means is that in addition to the solver described in the last section, there needs to be a black-box function that solutions are sent through to get better guesses at η_{CD} . The black-box function we use is a variation of the Ehst-Karney model.¹⁷

As mentioned, a self-consistent η_{CD} is found once a trip through the Ehst-Karney black-box results in the same η_{CD} as was sent in – to some tolerable level of error. This consistency incorporates an explicit dependence on the tokamak configuration. Mathematically,

$$\tilde{\eta}_{CD} = f(R_0, B_0, \bar{n}, \bar{T}, I_P) \quad (2.31)$$

As such, to recalculate it after every solution of the steady current requires a value for both B_0 and R_0 – the targets of this model’s primary and limiting constraints. These will be the highlight of the next chapter.

Chapter 3

Formalizing the Systems Model

The goal of this chapter is to take a step back from the steady current derivation and see the larger picture behind reactor design. As such, a more in-depth description of static and dynamic variables is given. This discussion of dynamic variables will then lend itself to a description of the framework underpinning the fusion systems model. As such, we will now need formulas for the radius and magnet strength of the tokamak. Moving forward, the current will remain a connecting piece as we redirect focus to pulsed tokamaks and compare the underlying solvers of the two schemes.

The end result of this analysis will then be equations that allow the density (\bar{n}), current (I_P), major radius (R_0), and magnet strength (B_0) to be written as functions of the temperature (\bar{T}) and static variables (e.g. ν_n , N_G , f_D). These formulas are the product of applying constraints required for all tokamak reactors with several other limiting constraints. The constraints relevant to all tokamak reactors are: the Greenwald limit, current balance, and power balance. Limit constraints then include: the Troyon beta limit, the kink safety factor, the wall loading limit, the maximum power constraint, and the heat loading limit.

Actual methodologies for solving for the five dynamic variables simultaneously – i.e. \bar{T} , \bar{n} , I_P , R_0 , B_0 – are put off until ??.

3.1 Explaining Static Variables

In this model, static variables are ones that remain constant while solving for a reactor. These include geometric scalings (i.e. ϵ , δ , κ), profile parameters (i.e. ν_n , ν_T , l_i), and a couple dozen of physics constants related to pulsed and steady-state design (e.g. Q , N_G , f_D). For a complete list of static variables, consult ???. The point to make now is that this model treats static variables as immutable objects. As such they often reside in static coefficients – K_{\square} – which are treated as constants.

3.2 Connecting Dynamic Variables

Dynamic variables – \bar{T} , \bar{n} , I_P , R_0 , B_0 – are the first-class variables of this fusion systems model. They represent the fundamental properties of a plasma and tokamak (which constitute a fusion reactor). As such, they will be reintroduced one at a time, explaining how they fit into the model – and which equations are capable of representing them.

Table 3.1: Dynamic Variables

Symbol	Name	Units
I_P	Plasma Current	MA
\bar{T}	Plasma Temperature	keV
\bar{n}	Electron Density	10^{20} m^{-3}
R_0	Major Radius	m
B_0	Magnetic Field	T

Bluntly, this fusion systems model is a simple algebra problem: solve five equations with five unknowns (i.e. \bar{T} , \bar{n} , I_P , R_0 , B_0). Although this naive approach would work, we can do a little better by collapsing these five equations down to just one. This was already done while deriving the steady current. It just happened that the current was not directly dependent on the tokamak size (R_0) or magnet strength (B_0).

This will prove more challenging for the generalized current needed for pulsed operation. Even so, this equation will still be reduced to one equation with a single

unknown – I_P . A solution to which can be solved much faster than the naive 5
equation approach. This is one reason the model is so fast.

The Plasma Temperature – \bar{T}

The plasma temperature, measured in keV (kilo-electron-volts), is one of the most
nonlinear variables in the fusion systems framework. It first proved troublesome
when it was shown that a pedestal profile – not a parabolic one used here – would
be needed for an accurate calculation of bootstrap current. The black-box tabulation
for reactivity – (σv) – which appeared in fusion power only further exposed this
nonlinearity.

Acknowledging that temperature is the most difficult to handle parameter prompts
its use as the scanned variable. What this means practically is scanning temperatures
is the most straightforward method to produce curves of reactors. By example, a scan
may be run over the average temperatures (\bar{T}): 10, 15, 20, 25, and 30 keV – where
each corresponds to its own reactor with its own field strength (B_0), plasma current
(I_P), etc. In equation form, this becomes:

$$\bar{T} = \text{const.} \tag{3.1}$$

The constant value, here, happens to be 10 keV in one run, 15 keV for the next, and
30 keV in the fifth.

The Plasma Density – \bar{n}

The Greenwald density limit is a constraint with a simple form that applies to all
tokamak reactors. It is for this reason – as well as being a good approximation –
that a parabolic profile was rationalized over a pedestal (H-Mode) one. Repeated,
the Greenwald density limit is:

$$\bar{n} = K_n \cdot \frac{I_P}{R_0^2} \tag{??}$$

696 This is an exceptionally simple relationship and why it guided the model. Unlike the
697 next three variables, it is actually used in their derivations.

698 The Plasma Current – I_P

699 The plasma current is what separates steady-state from pulsed operation. From
700 before, the steady current was found to be:

$$I_P = \frac{K_{BS}\bar{T}}{1 - K_{CD}(\sigma v)} \quad (??)$$

701 This was derived by setting the total current equal to the two sources of current:
702 bootstrap and current drive. Or in fractional form,

$$I_P = I_{BS} + I_{CD} \rightarrow 1 = f_{BS} + f_{CD} \quad (3.2)$$

703 This says that the current fractions of bootstrap and current drive must sum to one.
704 As shown next chapter, inductive sources can be included into this current balance:

$$1 = f_{BS} + f_{CD} + f_{ID} \quad (3.3)$$

705

706 This equation shows how steady-state and pulsed operation can coexist (see ??). The
707 final point to make is reducing the model to being purely pulsed – i.e. neglecting the
708 current drive:

$$1 = f_{BS} + f_{ID} \quad (3.4)$$

709 Therefore, the next chapter will generalize the steady current to allow pulsed oper-
710 ation, and then simplify it to the purely pulsed case. Just as steady current faced
711 self-consistency issues with η_{CD} , this current will also involve its own root solving
712 conundrum – the description of which will be given in the following two chapters.

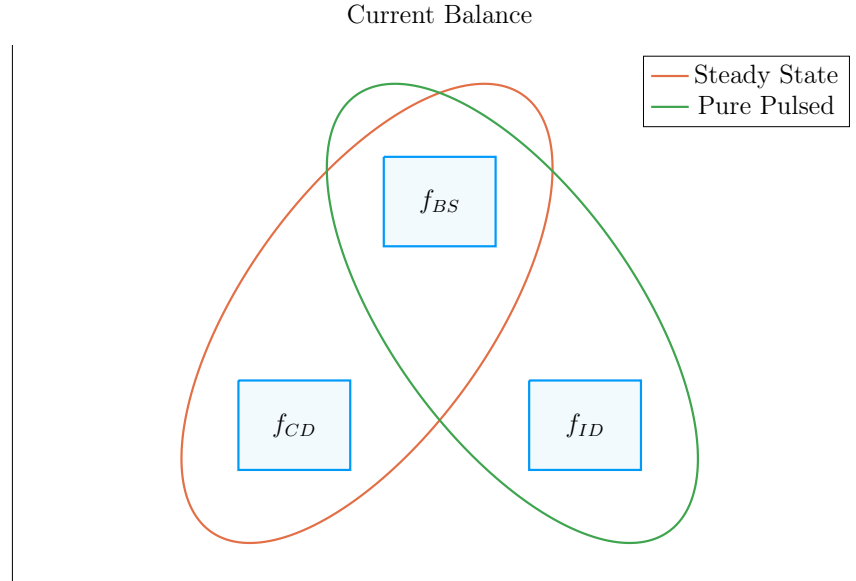


Figure 3-1: Current Balance in a Tokamak

In a tokamak, there needs to be a certain amount of current – and that current has to come from somewhere. All good reactors have an adequate bootstrap current. What provides the remaining current is what distinguishes steady state from pulsed operation.

713 The Tokamak Magnet Strength – B_0

714 The tokamak magnet strength has no unique equation to eliminate it. With foresight,
 715 the one this model uses is the power balance inherent to every reactor. Similar to
 716 current balance, power balance is what separates a reactor from a device incapable
 717 of producing net electricity. As such, it is referred throughout this document as: the
 718 primary constraint. It will be derived later this chapter.

719 The Tokamak Major Radius – R_0

720 Much like the magnet strength, the major radius has no unique relation to express
 721 it. The model therefore uses this equation to handle a reactor's various physical
 722 and engineering-based constraints. This list of requirements further restricts reactor
 723 space to the curves shown in the results section. Collectively, these are referred to
 724 as the limiting constraints – discussed later this chapter. These constraints all just
 725 happen to depend on the size of the reactor – the reason they are chosen to represent

726 the radius.

727 3.3 Enforcing Power Balance

728 What separates a reactor from a device incapable of producing net electricity is power
729 balance. Within a tokamak, it accounts for how the power going into a plasma's
730 core exactly matches the power coming out of it. To approximate this conservation
731 equation, two sets of power will be introduced: the sources and the sinks.

732 The sources have mainly been introduced at this point – they include the alpha
733 power (P_α) from fusion reactions and the heating power (P_H), as well as a new ohmic
734 power term (P_Ω). The remaining two powers – the sinks – then appear through the
735 radiation and heat conduction losses, which will be given shortly. In equation form,
736 power balance becomes:

$$\sum_{sources} P = \sum_{sinks} P \quad (3.5)$$

737 or expanded to fit this model:

$$P_\alpha + P_H + P_\Omega = P_{BR} + P_\kappa \quad (3.6)$$

738 For clarity, the left-hand side of this equality are the sources. Whereas the remaining
739 two are sinks, i.e. Bremsstrahlung radiation (P_{BR}) and heat conduction losses (P_κ).

740 3.3.1 Collecting Power Sources

741 As suggested, the two dominant sources of power in a tokamak are: alpha power
742 (P_α) and auxiliary heating (P_H). From ??, it was determined that alpha particles
743 (i.e. helium nuclei) carry around 20% of the total fusion power; or as we put it
744 mathematically:

$$P_\alpha = \frac{P_F}{5} \quad (3.7)$$

745 Additionally, it was determined that the heating power is what was eventually am-
 746 plified into fusion power – or through equation:

$$P_H = \frac{P_F}{Q} \quad (3.8)$$

747 The final source term then is the ohmic power (P_Ω). This is identical to how copper
 748 wires in a home heat up as current runs through them. From a simple circuits
 749 picture, the power across the plasma is related to its current and resistance – in our
 750 standardized units – through:

$$P_\Omega = 10^6 \cdot I_P^2 \cdot R_P \quad (3.9)$$

751 This fusion systems model handles the plasma resistance (R_P) with the neoclassical
 752 Spitzer resistivity. Through equation,⁴

$$R_P = \frac{K_{RP}}{R_0 \bar{T}^{3/2}} \quad (3.10)$$

753

$$K_{RP} = 5.6e-8 \cdot \left(\frac{Z_{eff}}{\epsilon^2 \kappa} \right) \cdot \left(\frac{1}{1 - 1.31\sqrt{\epsilon} + 0.46\epsilon} \right) \quad (3.11)$$

754 Combined with the Greenwald limit, ohmic power can be written more compactly as,

755

$$P_\Omega = K_\Omega \cdot \left(\frac{\bar{n}^2 R_0^3}{\bar{T}^{3/2}} \right) \quad (3.12)$$

756

$$K_\Omega = 10^6 \cdot \frac{K_{RP}}{K_n^2} \quad (3.13)$$

757 With the sources defined, we are now in a position to discuss the two sink terms used
 758 in this model's power balance.

3.3.2 Approximating Radiation Losses

All nuclear reactors emit radiation. From a power balance perspective, this means some power has to always be reserved to recoup from its losses – measured in megawatts. In a fusion reactor, the three most important types of radiation are: Bremsstrahlung radiation, line radiation, and synchrotron radiation.

This model chooses to only model Bremsstrahlung radiation – as it usually dominates within the plasma’s core. Within most designs, Bremsstrahlung radiation outweighs the other two’s contribution, to core power balance, two-to-one.^{2,7} However, adding the effects of line-radiation and synchrotron radiation would drive results closer to real-world experiments. For example, line-radiation would better account for the effects of heavy impurities that are emitted from the divertor plate and first wall

For clarity, Bremsstrahlung – or breaking – radiation is what occurs when a charged particle (e.g. an electron) is accelerated by some means. In a tokamak, this happens all the time as electrons collide with the ion species.¹⁸ This term can be described by the volume integral:⁴

$$P_{BR} = \int S_{BR} d\mathbf{r} \quad (3.14)$$

Where the radiation power density (S_{BR}) is given by:

$$S_{BR} = \left(\frac{\sqrt{2}}{3\sqrt{\pi^5}} \cdot \frac{e^6}{\epsilon_0^2 c^3 h m_e^{3/2}} \right) \cdot (Z_{eff} n^2 T^{1/2}) \quad (3.15)$$

The constants in the left set of parentheses all have their usual physics meanings (i.e. c is the speed of light and m_e is the mass of an electron). What is new is the effective charge: Z_{eff} .

The effective charge is a scheme for reducing the charge each ion has to a single representative value. Fundamental charge, here, is what: neutrons lack, electrons and hydrogen have one of, and helium has two. As such, a plasma with a purely deuterium and tritium fuel would have an effective charge of one. This value would

then quickly rise if a Tungsten tile – with 74 units of charge – were to fall into the plasma core from the walls of the tokamak.

Using the volume integral – seen in the derivation of fusion power – allows the Bremsstrahlung power to be written in standardized units as:

$$P_{BR} = K_{BR} \bar{n}^2 \bar{T}^{1/2} R_0^3 \quad (3.16)$$

786

$$K_{BR} = 0.1056 \frac{(1 + \nu_n)^2 (1 + \nu_T)^{1/2}}{1 + 2\nu_n + 0.5\nu_T} Z_{eff} \epsilon^2 \kappa g \quad (3.17)$$

This power term represents the radiation power losses involved in power balance. All that is needed now is a formula for heat conduction losses – one of the most difficult plasma behaviors to model to date.

3.3.3 Estimating Heat Conduction Losses

Heat is energy that moves about randomly on a microscopic level. Macroscopically, it generally moves from hotter areas to colder ones. As hinted by the plasma profile for temperature, heat emanates from the center of a plasma and migrates towards the walls of its tokamak enclosure. It therefore is a critical quantity to calculate when balancing power in a plasma's core.

The difficulty of estimating heat conduction, though, lies in the nonlinear behaviors of plasmas – no theory or quick-running code can properly model it. As such, reactor designers have turned towards experimentalists for empirical scaling laws based on the dozen or so strongest tokamaks in the world. These are collectively referred to as confinement time scalings, i.e. the ELMy H-Mode Scaling Law.

The derivation of this heat conduction loss term (P_κ) starts in a manner similar to the previous powers. To begin, an equation for P_κ can be found using the following volume integral:⁴

$$P_\kappa = \frac{1}{\tau_E} \int U d\mathbf{r} \quad (3.18)$$

804 This volume integral includes two new terms: the confinement time (τ_E) and the
805 internal energy (U). Before explaining these terms, a qualitative description is in
806 order. As mentioned previously, the heat – or microscopically random – energy is
807 captured by the internal energy (U). Then the confinement time (τ_E) is how long it
808 would take for the heat to undergo an e-folding if the device were suddenly turned
809 off.

810 A formula for confinement time will be delayed till the end of this section, when it is
811 needed to solve for the magnetic field (B_0). The internal energy (U), however, can be
812 given now as it has its typical physics meaning. This assumes that all three plasma
813 species are held nearly at the same temperature (T) as the electrons:

$$U = \frac{3}{2} (n + n_D + n_T) T \quad (3.19)$$

814 Here again, n_D and n_T – the density of deuterium and tritium, respectively – are
815 related to the electron density (used in this model) through the dilution factor, which
816 assumes a 50-50 mix of D-T fuel:

$$n_D = n_T = f_D \cdot \left(\frac{n}{2} \right) \quad (3.20)$$

817 After several substitutions, the equations here can be combined to form an equation
818 for P_κ – the heat conduction losses – in standardized units:

$$P_\kappa = K_\kappa \frac{R_0^3 \bar{n} \bar{T}}{\tau_E} \quad (3.21)$$

819

$$K_\kappa = 0.4744 (1 + f_D) \frac{(1 + \nu_n)(1 + \nu_T)}{1 + \nu_n + \nu_T} (\epsilon^2 \kappa g) \quad (3.22)$$

820 Now that all five terms have been defined in power balance, the next step is expanding
821 it and solving for the tokamak's toroidal magnetic field strength: B_0 .

822 3.3.4 Writing the Lawson Parameter

823 Before arriving at a formula for the magnet strength (B_0) using power balance, – it
824 seems appropriate to take a detour and explain an intermediate solution: the Lawson
825 Parameter. Within the fusion community, the Lawson Parameter is the cornerstone
826 in any argument on the possibility of a tokamak ever being used as a reactor.

827 An equation for the Lawson Parameter – sometimes referred to as the *triple product*
828 – is easily found in the literature as:

$$n \cdot T \cdot \tau_E = \frac{60}{E_F} \cdot \frac{T^2}{\langle \sigma v \rangle} \quad (3.23)$$

829 Similar to the steady current derived earlier, the right-hand side is only dependent
830 on temperature. Further, as the left-hand side is a measure of difficult to achieve
831 parameters, the goal is to minimize both sides. As shown in ??, this occurs when the
832 plasma temperature is around 15 keV – a fact well known to many fusion engineers.
833 As will be seen, this is a simplified result of our model. This is why $\bar{T} = 15$ keV is
834 not always the optimum temperature – but usually is in the right neighborhood for
835 reasonable reactor designs.

836 As all the terms in power balance have already been defined, the starting point will
837 be simply repeating the standardized equations for all five included powers.

$$P_\alpha = \frac{P_F}{5} \quad (??)$$

838

$$P_H = \frac{P_F}{Q} \quad (??)$$

839

$$P_\Omega = K_\Omega \cdot \left(\frac{\bar{n}^2 R_0^3}{\bar{T}^{3/2}} \right) \quad (??)$$

840

$$P_{BR} = K_{BR} \bar{n}^2 \bar{T}^{1/2} R_0^3 \quad (??)$$

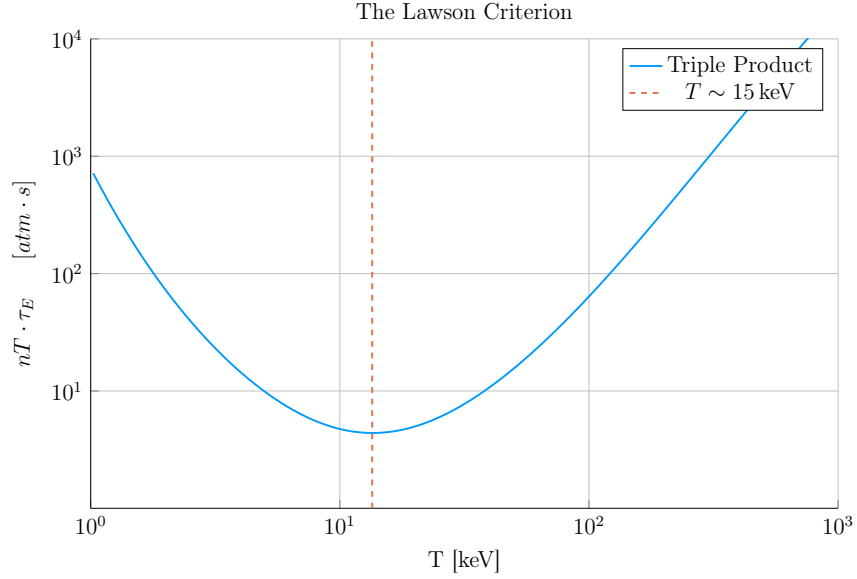


Figure 3-2: Power Balance in a Reactor

Power balance is what differentiates a reactor from a radiator. When cast as the Lawson Parameter for fusion, it explains why D-T plasmas often have a temperature around 15 keV.

841

$$P_{\kappa} = K_{\kappa} \frac{R_0^3 \bar{n} \bar{T}}{\tau_E} \quad (??)$$

842 With the fusion power again being,

$$P_F = K_F \cdot \bar{n}^2 \cdot R_0^3 \cdot (\sigma v) \quad (??)$$

843 These can then be substituted into power balance:

$$P_{\alpha} + P_H + P_{\Omega} = P_{BR} + P_{\kappa} \quad (??)$$

844 After a couple lines of algebra, power balance can be rewritten in a form analogous
845 to the triple product:

$$\bar{n} \cdot \bar{T} \cdot \tau_E = \frac{K_{\kappa} \bar{T}^2}{\left(K_P (\sigma v) + K_{OH} \bar{T}^{-3/2} \right) - K_{BR} \bar{T}^{1/2}} \quad (3.24)$$

$$K_P = K_F \cdot \left(\frac{5 + Q}{5 \times Q} \right) \quad (3.25)$$

847 As expected, this shares a form similar to the simple Lawson Parameter:

$$n \cdot T \cdot \tau_E = \frac{60}{E_F} \cdot \frac{T^2}{\langle \sigma v \rangle} \quad (??)$$

848 The main difference is this model does not ignore ohmic power and radiation losses
 849 completely. The inclusion of radiation for example sometimes bars a range of temper-
 850 atures from being physically realizable.* With this intermediate relation in place, the
 851 goal is now to give a formula for the confinement time and solve it for the magnetic
 852 field strength (B_0) – thus giving the Primary Constraint.

853 3.3.5 Finalizing the Primary Constraint

854 The goal now is to transform the Lawson Parameter into an equation for magnet
 855 strength (B_0). This choice to solve the equation for B_0 was motivated by the goals
 856 of analysis and how it will fit into the fusion systems model. To solve the primary
 857 constraint, the confinement time scaling law will need to be introduced. At the end,
 858 a convoluted – albeit highly useful – relation will be the reward.

859 The energy confinement time – τ_E – is one of the most difficult to obtain terms in all
 860 of fusion energy. It is an attempt to reduce all the nonlinear behaviors of plasmas into
 861 a simple measure of how fast its internal energy would be ejected from the tokamak
 862 if the device was instantaneously shut down. As such, reactor designers have turned
 863 toward experimentalists for empirical scalings based on the world’s tokamaks (see
 864 ??). These all share a form similar to:

$$\tau_E = K_\tau H \frac{I_P^{\alpha_I} R_0^{\alpha_R} a^{\alpha_a} \kappa^{\alpha_\kappa} \bar{n}^{\alpha_n} B_0^{\alpha_B} A^{\alpha_A}}{P_{src}^{\alpha_P}} \quad (3.26)$$

* The denominator of Eq ?? has discontinuities when the $K_{BR} \bar{T}^{1/2}$ term exactly equals the parenthesised one. Therefore, valid reactors only exist outside the discontinuities, when the entire triple product is finite and positive.

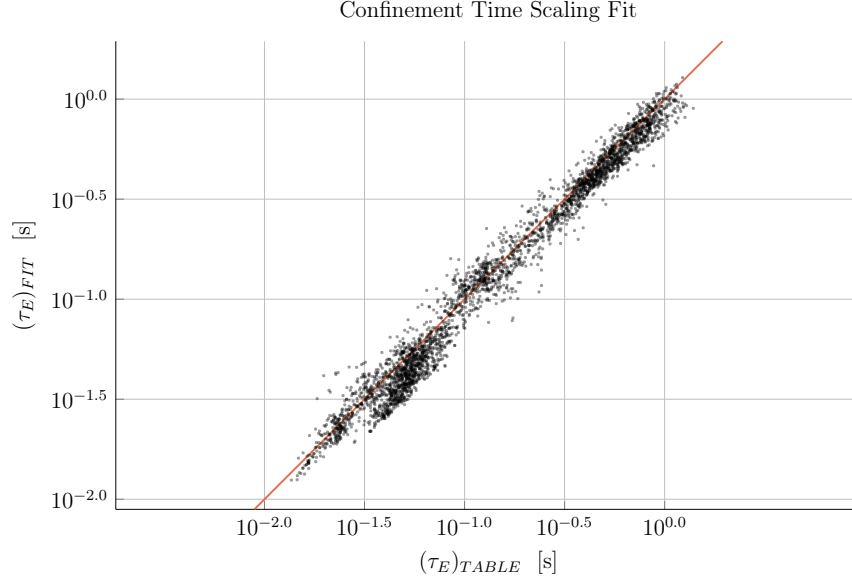


Figure 3-3: H-Mode Confinement Time Scaling

This plot shows how well the ELMy H-Mode Scaling Law does for fitting τ_E to the ITER98 database of global tokamaks. For most values, the fit is at least 80% accurate with the measured value.

865 This regressional fit is how the field actually designs machines (i.e. ITER). Let it be
 866 known, though, that fits of this kind often do remarkable well, having relative errors
 867 less than 20% on interpolated data. The new terms in this equation are: P_{src} , K_τ , H,
 868 A, and the α_\square factors.

869 First, the loss power is a metric used in the engineering community to quantify the
 870 power being transported out of the “core” of the plasma by charged particles (i.e. not
 871 the neutrons).⁶ To optimize fits, experimentalists have defined this as a combination
 872 of the source power terms:

$$P_{src} = P_\alpha + P_H + P_\Omega \quad (3.27)$$

873 Moving on, K_τ is simply a constant fit-makers use in their scalings. Whereas H is
 874 the enhancement factor over the empirical fit. Next, A is the average mass number of
 875 the fuel source, in atomic mass units. For a 50-50 D-T fuel, this is 2.5, as deuterium
 876 weighs two amus and tritium weighs three. Lastly, the alpha factors (e.g. α_n , α_a ,

α_P) are fitting parameters that represent each variable's relative importance in the scaling.

For ELMy H-Mode, this confinement scaling law can be written as:

$$\tau_E = 0.145 H \frac{I_P^{0.93} R_0^{1.39} a^{0.58} \kappa^{0.78} \bar{n}^{0.41} B_0^{0.15} A^{0.19}}{P_{src}^{0.69}} \quad (3.28)$$

However, similar scaling laws can be written for L-Mode, I-Mode, etc. One final remark to make before moving on is that even these fits have subtleties. The value of κ , for example, may have a slightly different geometric meaning from tokamak to tokamak. And the exact definition of loss power – P_{src} – introduces an even larger area of discrepancy.

Returning to the problem at hand, though, this model's Lawson Parameter (eq. ??) can be simplified after expanding the left-hand side using the Greenwald density and substituting in a confinement time scaling law. After a few lines of algebra, this can be transformed into a formula for B_0 !

$$B_0 = \left(\frac{G_{PB}}{K_{PB}} \cdot \left(I_P^{\alpha_I^*} R_0^{\alpha_R^*} \right)^{-1} \right)^{\frac{1}{\alpha_B}} \quad (3.29)$$

$$G_{PB} = \frac{\bar{T} \cdot \left(K_P(\sigma v) + K_\Omega \bar{T}^{-3/2} \right)^{\alpha_P}}{\left(K_P(\sigma v) + K_\Omega \bar{T}^{-3/2} - K_{BR} \bar{T}^{1/2} \right)} \quad (3.30)$$

$$K_{PB} = H \cdot \left(\frac{K_\tau K_n^{\alpha_n^*}}{K_\kappa} \right) \cdot (\epsilon^{\alpha_a} \kappa^{\alpha_\kappa} A^{\alpha_A}) \quad (3.31)$$

Where we have added new starred alpha values for the density, current, and major radius:

$$\alpha_n^* = 1 + \alpha_n - 2\alpha_P \quad (3.32)$$

$$\alpha_I^* = \alpha_I + \alpha_n^* \quad (3.33)$$

$$\alpha_R^* = \alpha_R + \alpha_a - 2\alpha_n^* - 3\alpha_p \quad (3.34)$$

895 This equation for B_0 – derived from power balance – is thus the primary constraint
 896 for reactor designs. It is the first step in connecting the plasma (i.e. \bar{n} , \bar{T} , and I_P) to
 897 its tokamak enclosure (i.e. B_0 and R_0). The remaining step is finding an equation –
 898 or in this case, equations – for the major radius of the device. These radius equations
 899 will collectively be referred to as: the limiting constraints.

900 3.4 Collecting Limiting Constraints

901 As of now, the only missing equation within our list of static variables – i.e. R_0 , B_0 ,
 902 \bar{T} , \bar{n} , and I_P – is for the major radius of the tokamak. This equation will come from
 903 around five potential limits, each either physical or engineering-based. These limits
 904 will then correspond to different curves through reactor space. As will be shown,
 905 many of these reactors will be invalid (as they violate at least one of the other limits).
 906 Our analysis is always based on selecting the most stringent criterion.

907 Before tackling the subject of finding reactors that exist on the fine line of satisfying
 908 every limiting constraints, though, it is essential to collect them one-by-one. These
 909 are: the Troyon Beta Limit, the Kink Safety Factor, the Wall Loading Limit, the
 910 Power Cap Constraint, and the Heat Loading Limit.

911 The goal of this section is to solve for each of these constraints on the major radius.
 912 As with the primary constraint, this choice of solving for R_0 was not completely
 913 unique, just motivated by physics and engineering concerns. It just so happens that
 914 each limit described here depends on the size of a reactor – which is not true for the
 915 magnetic field strength.

3.4.1 Introducing the Beta Limit

The Beta Limit is the most important limiting constraint – especially for steady-state reactors. It sets a maximum on the amount of pressure a plasma is willing to tolerate. As with future limiting constraints, literature-based equations will be transformed into formulas for R_0 . Each will then contain some limiting quantity that can be handled by a static variable – as β_N will be used shortly.

The starting point for the beta limit is to define the important plasma physics quantity: β – the plasma beta. This value is a ratio between a plasma’s internal pressure and the pressure exerted on it by the tokamak’s magnetic configuration. Mathematically,⁴

$$\beta = \frac{\text{plasma pressure}}{\text{magnetic pressure}} = \frac{\bar{p}}{\left(\frac{B_0^2}{2\mu_0}\right)} \quad (3.35)$$

Using this model’s temperature and density profiles, the volume-averaged pressure (\bar{p}) can be written in units of atmospheres (i.e. atm) as:

$$\bar{p} = 0.1581 (1 + f_D) \frac{(1 + \nu_n)(1 + \nu_T)}{1 + \nu_n + \nu_T} \bar{n} \bar{T} \quad (3.36)$$

Moving forward, the final step is plugging this definition for plasma beta into the Troyon Beta Limit derived using standard MHD stability analysis. This equation can be written in the following form, where β_N is the normalized plasma beta – i.e. a static variable usually set between 2% and 4%.¹⁹

$$\beta = \beta_N \frac{I_P}{aB_0} \quad (3.37)$$

Substituting the plasma β from eq. ??, into this relation results in the model’s first equation for tokamak radius:

$$R_0 = \frac{K_{TB}\bar{T}}{B_0} \quad (3.38)$$

934

$$K_{TB} = 4.027 \times 10^{-2} \cdot \left(\frac{K_n \epsilon}{\beta_N} \right) \cdot (1 + f_D) \cdot \frac{(1 + \nu_n)(1 + \nu_T)}{1 + \nu_n + \nu_T} \quad (3.39)$$

935 As mentioned, this is often the dominating constraint in a steady-state reactor. The
 936 often dominating constraint for pulsed designs – the kink safety factor – will be the
 937 focus of the next subsection.

938 3.4.2 Giving the Kink Safety Factor

939 Just like how the Troyon Beta Limit set a fluids-based maximum on plasma pressure,
 940 the Kink Safety Factor sets one on the plasma’s current. This constraint usually
 941 only appears in pulsed designs, as it is assumed that getting to this high a current in
 942 steady-state (with only LHCD) would prove extremely impractical.

943 The starting point, again, is an equation from the literature for the kink condition:^{6,20}

944

$$q_* = 5\epsilon^2 \cdot \frac{R_0 B_0}{I_P} \cdot \left(\frac{1 + \kappa^2 \cdot (1 + 2\delta^2 - 1.2\delta^3)}{2} \right) \quad (3.40)$$

945 Here the safety factor – q_* – typically has values around 3.

946 Combined, the kink safety factor can now be written in standardized units as:

$$R_0 = \frac{K_{SF} I_P}{B_0} \quad (3.41)$$

947

$$K_{SF} = \frac{q_*}{5\epsilon^2} \cdot \left(\frac{2}{1 + \kappa^2 \cdot (1 + 2\delta^2 - 1.2\delta^3)} \right) \quad (3.42)$$

948 This relation is the limiting constraint important for most pulsed reactor designs. As
 949 with the Beta Limit, the two are derived through plasma physics alone. The remaining
 950 limiting constraints, however, are engineering-based in origin – these include: the Wall
 951 Loading Limit, the Power Cap Constraint, and the Heat Loading Limit. Each will be
 952 defined shortly.

3.4.3 Working under the Wall Loading Limit

The first engineering-based limiting constraint – the wall loading limit – will prove to be an important quantity when determining the magnet strength at which reactor costs begin to increase. As hinted, its definition originates from nuclear engineering concerns: it is a measure of the maximum neutron damage a tokamak’s walls can take over the lifetime of the machine.*

The first step in deriving a limiting constraint for wall loading is a description of the problem it models. In a reactor, fusion reactions typically make high-energy neutrons – with around 14.1 MeV of kinetic energy – that collide with the tokamak enclosure. Therefore a simple metric would be limiting the amount of neutron power that can be unloaded on the surface area of a tokamak. This can be written as:²¹

$$P_W = \frac{P_n}{S_P} \quad (3.43)$$

$$S_P = 4\pi^2 a R_0 \cdot \frac{\left(1 + \frac{2}{\pi} (\kappa^2 - 1)\right)}{\kappa} \quad (3.44)$$

Here, S_P is the surface area of the tokamak’s inner wall and P_n is the neutron power derived in the subsection on fusion power. The quantity, P_W , then serves a role analogous to β_N for the beta limit and q_* for the kink safety factor – it is a static variable representing the maximum allowed wall loading. For fusion reactors, P_W is assumed to be around 2-4 $\frac{\text{MW}}{\text{m}^2}$. It will be shown that the wall loading limit is important in any tokamak – regardless of operating mode (i.e. steady-state or pulsed).

Finishing this limiting constraint, the Wall Loading limit can be written in standardized units as:

$$R_0 = K_{WL} \cdot I_P^{\frac{2}{3}} \cdot (\sigma v)^{\frac{1}{3}} \quad (3.45)$$

*For clarity, the wall loading limit should actually be a energy fluence limit. It is converted to an instantaneous power limit for ease of design purposes.

973

$$K_{WL} = \left(\frac{K_F K_n^2}{5\pi^2 P_W} \cdot \frac{\kappa}{\epsilon} \cdot \frac{1}{1 + \frac{2}{\pi} \cdot (\kappa^2 - 1)} \right)^{\frac{1}{3}} \quad (3.46)$$

974 3.4.4 Setting a Maximum Power Cap

975 As opposed to the previous three limiting constraints, the maximum power cap is
 976 more of a constraint set by economic competitiveness. Because no reactor – coal,
 977 solar, or otherwise – has a 4000 MW reactor, neither should fusion.* It makes sense
 978 from a practical position after realizing the long history of tokamaks being delayed,
 979 underfunded, or completely canceled. Mathematically, this has the simple form:

$$P_E \leq P_{CAP} \quad (3.47)$$

980 Here, P_{CAP} is the maximum allowed power output of the reactor. Similar to the
 981 other limiting quantities, P_{CAP} is treated as a static variable (i.e. set to 4000 MW).
 982 The electrical power output of the reactor (P_E) is then related to the fusion power
 983 through:⁴

$$P_E = 1.273 \eta_T \cdot P_F \quad (3.48)$$

984 The variable η_T is the thermal efficiency of the reactor – which is usually found to
 985 be around 40%. And the constant in front (i.e. 1.273) represents some extra power
 986 the reactor makes as fuel is bred by the fusion neutrons passing through a tokamak's
 987 lithium-filled blanket. Explicitly this results from including the energy released by
 988 lithium-6 as it undergoes neutron capture (E_{Li}).

$$1.273 = \frac{E_F + E_{Li}}{E_F} \quad (3.49)$$

989

$$E_{Li} = 4.8 \text{ MeV} \quad (3.50)$$

*Note that this 4000 MW (electric) is a maximum. A 1000 MW reactor would obviously not violate this constraint. Instead it would likely be pressing on either the kink or beta limit.

990 Substituting in fusion power and solving for the major radius results in:

$$R_0 = K_{PC} \cdot I_P^2 \cdot (\sigma v) \quad (3.51)$$

991

$$K_{PC} = K_F K_n^2 \cdot \left(\frac{1.273 \eta_I}{P_{max}} \right) \quad (3.52)$$

992 This limiting constraint can be used to create curves of reactors, although it is mainly
 993 used as a stopping point for designs – i.e. if you get to the power-cap regime, you
 994 have gone too far. This is different than the next constraint, which is fundamentally
 995 an unsolved problem within the modern tokamak design paradigm.²²

996 3.4.5 Listing the Heat Loading Limit

997 Fusion plasmas are hot. The commonly given relation is one electron volt is around
 998 20,000 °F – which makes 15 keV around a quarter-billion Fahrenheit. Although slightly
 999 deceptive, heat damage to a tokamak is an all too real concern. The problem is there
 1000 is currently no solution to the problem. Although researchers have explored various
 1001 types of heat divertors, none have been shown to withstand the gigawatts-per-square-
 1002 meter of heat emitted from a reactor-size tokamak.²²

1003 As such, this model takes an approach similar to the research community, calculating
 1004 it at the end as a manual check on the difficulty of building such a device – but not
 1005 using it to explicitly guide design. For completeness though, a limiting constraint will
 1006 still be derived. The first step is giving the heat load limit commonly found in the
 1007 literature.²¹

$$q_{DV} = \frac{K_{DV}}{K_F} \cdot \frac{P_F I_P^{1.2}}{R_0^{2.2}} \quad (3.53)$$

1008

$$K_{DV} = \frac{18.31 \times 10^{-3}}{\epsilon^{1.2}} \cdot K_P \cdot \left(\frac{2}{1 + \kappa^2} \right)^{0.6} \quad (3.54)$$

1009 This is the heat load that impinges on an extended leg, double null divertor – primarily

1010 from the outer midplane of the plasma core. After a simple rearrangement and
 1011 substitution for fusion power, this becomes:

$$R_0 = K_{DH} \cdot I_P \cdot (\sigma v)^{\frac{1}{3.2}} \quad (3.55)$$

1012

$$K_{DH} = \left(\frac{K_{DV} K_n^2}{q_{DV}} \right)^{\frac{1}{3.2}} \quad (3.56)$$

1013 At this point all the limiting constraints have been defined. The next step is taking
 1014 a step back and motivating the derivation of a current equation suitable for pulsed
 1015 tokamaks.

1016 3.5 Summarizing the Fusion Systems Model

1017 Stepping back, this chapter focused on the bigger picture behind designing a zero-
 1018 dimension fusion systems model. It started with a description of various design pa-
 1019 rameters and then moved onto explaining the five relations needed to close the model
 1020 – i.e. for \bar{T} , \bar{n} , I_P , B_0 , and R_0 .

1021 Before generalizing the steady current to allow modeling pulsed reactors, though, a
 1022 quick recap of the equations will prove beneficial. The first variable described was
 1023 temperature – i.e. scan five evenly-spaced \bar{T} values between 10 and 30 keV. This was
 1024 then quickly followed by the Greenwald density limit – the a simple relation assumed
 1025 to apply to all fusion reactors. Through equations, these two were written as:

$$\bar{T} = \text{const.} \quad (??)$$

1026

$$\bar{n} = K_n \cdot \frac{I_P}{R_0^2} \quad (??)$$

1027 The next variable handled was the steady current:

$$I_P = \frac{K_{BS}\overline{T}}{1 - K_{CD}(\sigma v)} \quad (??)$$

1028 As was mentioned then, this only directly depends on temperature, but is strongly af-
 1029 fected by a tokamak's configuration – R_0 and B_0 - through the current drive efficiency
 1030 (η_{CD}). For pulsed reactors, this equation proves too simple as it ignores inductive
 1031 current. To remedy the situation, current balance will be revisited next chapter. The
 1032 main point to make now, though, is that the R_0 and B_0 dependence will be made
 1033 explicit.

1034 Moving on, the remaining equations were the primary and limiting constraints for B_0
 1035 and R_0 , respectively. It was through these relations that a tokamak's configuration
 1036 was brought back into the fold. The choice of solving the two constraints for their
 1037 respective variables was not completely unique – motivated only by the foresight of
 1038 how they fit into the model. Repeated below, they served as the proper vehicles for
 1039 closing the system of equations.

$$B_0 = \left(\frac{G_{PB}}{K_{PB}} \cdot \left(I_P^{\alpha_I^*} R_0^{\alpha_R^*} \right)^{-1} \right)^{\frac{1}{\alpha_B}} \quad (??)$$

$$R_0 = \frac{K_{TB}\overline{T}}{B_0} \quad (??)$$

1040

$$R_0 = \frac{K_{SF}I_P}{B_0} \quad (??)$$

$$R_0 = K_{WL} \cdot I_P^{\frac{2}{3}} \cdot (\sigma v)^{\frac{1}{3}} \quad (??)$$

1041

$$R_0 = K_{PC} \cdot I_P^2 \cdot (\sigma v) \quad (??)$$

1042

$$R_0 = K_{DH} \cdot I_P \cdot (\sigma v)^{\frac{1}{3.2}} \quad (??)$$

1043 The next step now is to learn how to generalize the current formula and design a pulsed
1044 tokamak reactor (see ??). After this is done, ?? will pick up where this chapter leaves
1045 off – transforming this fusion systems model into a simple reactor solver.

1046 Chapter 4

1047 Designing a Pulsed Tokamak

1048 Pulsed tokamaks are the flagship of the European fusion reactor design effort. As such,
1049 this paper's model will now be generalized to accommodate this mode of operation.
1050 Fundamentally, this involves transforming current balance into flux balance – adding
1051 inductive (pulsed) sources to stand alongside the LHCD (steady-state) ones.

1052 The first step in generalizing current balance will be understanding the problem from
1053 a basic electrical engineering perspective – i.e. with circuit analysis. The resulting
1054 equation will then be transformed into the flux balance seen in other models from
1055 the literature. All that will need to be done then is solving the problem for plasma
1056 current (I_P) and simplifying it for various situations – e.g. steady-state operation.

1057 This generalized plasma current will then be found to be a function of the other
1058 dynamic variables (i.e. R_0 , B_0 , and \bar{T}). This, of course, is more difficult to handle
1059 computationally than the steady current, which only directly depended on tempera-
1060 ture (\bar{T}). Discussion about solving this new root solving problem will be the topic of
1061 the next chapter.

1062 4.1 Modeling Plasmas as Circuits

1063 Although it may have been lost along the way, what makes plasmas so interesting and
1064 versatile – in comparison to gases – is their ability to respond to electric and magnetic
1065 fields. It seems natural then to model plasma current from a circuits perspective (i.e.
1066 with resistors, voltage sources, and inductors). By name, this circuit is referred to as
1067 a transformer where: the plasma is the secondary and the yet-to-be discussed central
1068 solenoid (of the tokamak) is the primary.

1069 The first step in deriving a current equation is to determine the circuit equations
1070 that govern pulsed operation in a tokamak. This will be done in two steps. First, we
1071 will draw a circuit diagram and write the equations that describe it. Next, we will
1072 use a simple schematic for how current evolves in a transformer to boil the resulting
1073 differential equations into simple algebraic ones – as is the hallmark of our model.

1074 4.1.1 Drawing the Circuit Diagram

1075 Understanding a circuit always starts with drawing a simple diagram, see ???. This
1076 figure depicts the transformer governing pulsed reactor. The left sub-circuit is the
1077 transformer’s primary – the central solenoid component of the tokamak that provides
1078 most of the inductive current. Whereas, the right sub-circuit is the plasma acting as
1079 the transformer’s secondary. The central solenoid, here, is then a helically-spiraled
1080 metal coil that fits within the inner ring of the doughnut. For now, every other flux
1081 source (besides this central solenoid) is neglected.

1082 This is described by the standard circuits involving voltage sources, resistors, and
1083 inductors:

$$V_i = \sum_j^n \frac{d}{dt} (M_{ij} I_j) + I_i R_i, \quad \forall i = 1, 2, \dots, n \quad (4.1)$$

1084 Without going into the inductances (M) and resistances (R), the variable n is the
1085 number of sub-circuits, here being 2. Whereas, the variables i and j are the indices
1086 of sub-circuits (i.e. 1 for the primary, 2 for the secondary). For illustrative purposes,

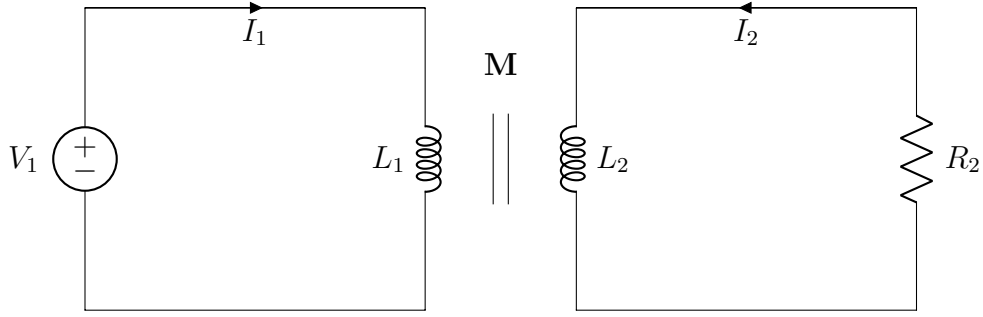


Figure 4-1: A Simple Plasma Transformer Description

A plasma transformer consists of a solenoid primary (left) and a plasma secondary (right). They are connected by their mutual inductance, M . Note that the two currents – I_1 and I_2 – travel in opposite directions.

1087 this would boil down to the following relation for a battery attached to a lightbulb:

$$V = IR \quad (4.2)$$

1088 Back to the transformer diagram, the equations for the two subcircuits can be ex-
 1089 panded and greatly simplified. Besides ignoring every inductive source other than the
 1090 central solenoid, the next powerful assumption is treating the solenoid as a supercon-
 1091 ductor (i.e. with negligible resistance). Lastly, the inductances between components
 1092 and themselves are held constant – independent of time. This allows the coupled
 1093 transformer equations to be written as:

$$V_1 = L_1 \dot{I}_1 - M \dot{I}_2 \quad (4.3)$$

$$-I_2 R_P = L_2 \dot{I}_2 - M \dot{I}_1 \quad (4.4)$$

1094 With I_1 and I_2 going in opposite directions. Note, here, that the subscript on M
 1095 has been dropped, as there are only two components. This was done in conjunction
 1096 to adding internal (self-)inductance terms. Mathematically, the mapping between
 1097 variables is:

$$M = M_{12} = M_{21} \quad (4.5)$$

1098

$$L_1 = M_{11} \quad (4.6)$$

1099

$$L_2 = M_{22} \quad (4.7)$$

1100 Repeated, the one subscript represents the primary – the central solenoid – and the
 1101 two stands for the plasma as the transformer’s secondary. Exact definitions for the
 1102 inductances will be put off till the end of the next subsection.

1103 4.1.2 Plotting Pulse Profiles

1104 Up until now, little has been discussed that has a time dependence. For steady-state
 1105 tokamaks, this did not occur because it is an extreme case where pulses could last
 1106 weeks or months. By definition, though, a pulsed machine has pulses – with around
 1107 ten scheduled per day. For this reason, a fusion pulse is now investigated in detail.

1108 Transformer pulses between the central solenoid and the plasma occur on the timescale
 1109 of hours. During this time, a plasma is brought up to some quasi-steady-state cur-
 1110 rent (I_P^*) for several hour and then ramped back down using the available flux in
 1111 the solenoid (measured in volt-seconds). For clarity, each pulse is subdivided into
 1112 four phases: ramp-up, flattop, ramp-down, and dwell. Pictorially represented in ??,
 1113 these divisions allow a simple scheme for transforming the coupled circuit differential
 1114 equations – from ????? – into simple algebraic formulas.

1115 Along the way, we will approximate derivatives with linear piecewise functions. Using
 1116 t_i to represent the initial time and t_f as the final one, these can be written as:

$$\dot{I} = \frac{I(t_f) - I(t_i)}{t_f - t_i} \quad (4.8)$$

1117 In tabular form, the data from ?? can be written in this piecewise fashion as:

1118 The exact definitions for the plasma’s inductive current (I_P^*) and the maximum volt-
 1119 age in the central solenoid (V_{max}) will be put off until the end of the section.

Tokamak Circuit Profiles

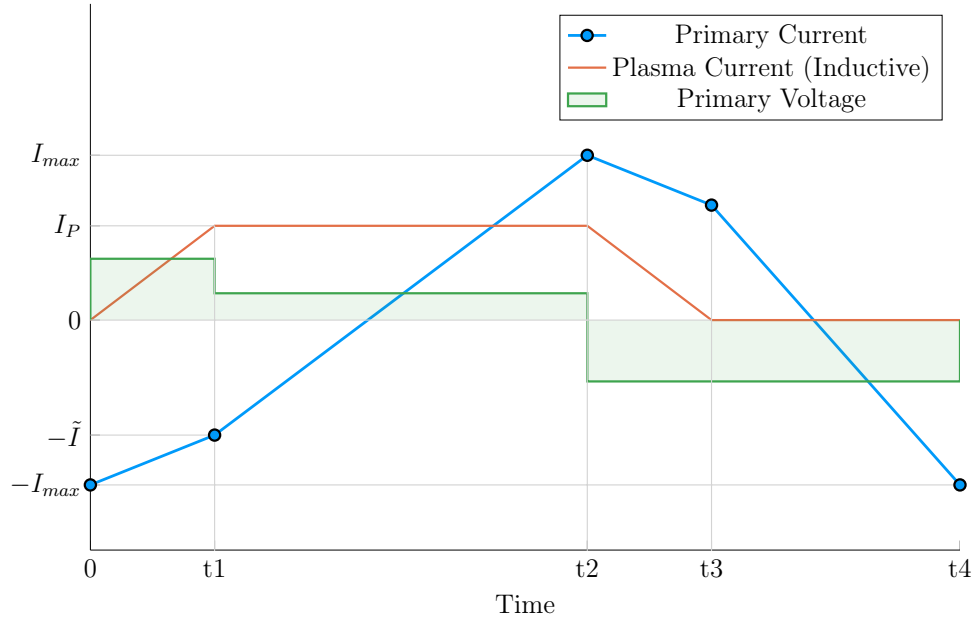


Figure 4-2: Time Evolution of Circuit Profiles

A circuit pulse involves four phases: (1) Ramp-Up, (2) Flattop, (3) Ramp-Down, and (4) Dwell. In reality, flattop can last more than 90% of the pulse.⁷ This makes the slope of the primary current during this phase much shallower than shown.

Table 4.1: Piecewise Linear Scheme for Pulsed Operation

(a) Currents			(b) Voltage			
Time	I_1	I_2	Phase	t_i	t_f	V_1
0	$-I_{max}$	0	Ramp-Up	0	t_1	$+V_{max}$
t_1	$-\tilde{I}$	I_P^*	Flattop	t_1	t_2	$+\tilde{V}$
t_2	$+I_{max}$	I_P^*	Ramp-Down	t_2	t_3	$-V_{max}$
t_3	$+\tilde{I}$	0	Dwell	t_3	t_4	$-V_{max}$
t_4	$-I_{max}$	0				

1120 The Ramp-Up Phase – RU

1121 The first phase in every plasma pulse is the ramp-up. During ramp-up, the central
 1122 solenoid starts discharging from its fully charged values, as the plasma is brought to
 1123 its quasi-steady-state current. As this occurs on the timescale of minutes – not hours
 1124 – resistive effects of the plasma can safely be ignored. This results in the ramp-up
 1125 equations becoming:

$$V_{max} = \frac{1}{\tau_{RU}} \cdot \left(L_1 \cdot (I_{max} - \tilde{I}) - M \cdot I_{ID} \right) \quad (4.9)$$

$$0 = \frac{1}{\tau_{RU}} \cdot \left(M \cdot (I_{max} - \tilde{I}) - L_2 \cdot I_{ID} \right) \quad (4.10)$$

1126 Simplifying these equations will be done shortly, for now the new terms are what
 1127 is important. The maximum voltage of the solenoid is V_{max} – usually measured in
 1128 kilovolts. Next, I_{max} is the solenoid’s current at the beginning of ramp-up. Whereas
 1129 \tilde{I} is the magnitude of the current once the plasma is at its flattop inductive-drive
 1130 current – I_{ID} . The τ_{RU} quantity, then, is the duration of time it takes to ramp-
 1131 up (i.e. RU). Again, L_1 and L_2 are the microhenry-scale internal inductances of the
 1132 solenoid and plasma, respectively, and M is the mutual inductance between them.

1133 The last step in discussing ramp-up is giving the two important formulas that come
 1134 from it:

$$\tilde{I} = I_{max} - I_{ID} \cdot \left(\frac{L_2}{M} \right) \quad (4.11)$$

1135

$$\tau_{RU} = \frac{I_{ID}}{V_{max}} \cdot \left(\frac{L_1 L_2 - M^2}{M} \right) \quad (4.12)$$

1136 The Flattop Phase – FT

1137 The most important phase in any reactor’s pulse is flattop – the quasi-steady-state
 1138 time when the tokamak is making electricity. Flattops are assumed to last a couple
 1139 of hours for a profitable machine, during which the central solenoid completely dis-
 1140 charges to overcome a plasma’s resistive losses – keeping it in a quasi-steady-state
 1141 mode of operation. In a steady-state reactor, this phases constitutes the entirety of
 1142 the pulse.

1143 Although the resistance cannot be safely neglected for flattop – as it was for ramp-up –
 1144 the plasma’s inductive current (I_{ID}) is assumed constant. This leads to its derivative
 1145 in equations cancelling out! Mathematically,

$$\tilde{V} = \frac{L_1}{\tau_{FT}} \cdot (I_{max} + \tilde{I}) \quad (4.13)$$

$$I_{ID}R_P = \frac{M}{\tau_{FT}} \cdot (I_{max} + \tilde{I}) \quad (4.14)$$

1146 As with ramp-up, the simplifications will be given shortly. The new terms here,
 1147 however, are an intermediate voltage for the central solenoid (\tilde{V}), and the duration of
 1148 the flattop (τ_{FT}). The resistance term was given in ???. Solutions can then be found
 1149 by substituting \tilde{I} – from ??? – into the flattop equations:

$$\tilde{V} = I_{ID}R_P \cdot \left(\frac{L_1}{M} \right) \quad (4.15)$$

1150

$$\tau_{FT} = \frac{I_{max} \cdot 2M - I_{ID} \cdot L_2}{I_{ID}R_P} \quad (4.16)$$

1151 The Ramp-Down Phase – RD

1152 Due to the simplicity – and symmetry – of this model’s reactor pulse, ramp-down is
 1153 the exact mirror of ramp-up. It takes the same amount of time and results in the
 1154 same algebraic equations. For brevity, this will just be represented as:

$$\tau_{RD} = \tau_{RU} \quad (4.17)$$

1155 For clarity, this is the time when a plasma’s current is brought down from its flattop
 1156 value to zero.

1157 The Dwell Phase – DW

1158 Where the first three phases had little ambiguity, the dwell phase changes definition
 1159 from model to model. For now, it is assumed to be the time it takes the central
 1160 solenoid to reset after a plasma has been completely ramped-down to an off-mode.

1161 To get a more realistic duty factor for cost estimates, it could include an evacuation
 1162 time, set to last around thirty minutes. During this evacuation, a plasma is vacuumed
 1163 out of a device as it undergoes some inter-pulse maintenance.

1164 Ignoring evacuation for now, the dwell phase involves resetting the central solenoid
 1165 when the plasma's current is negligible. This means the secondary of the transformer
 1166 is an open circuit – fundamentally the central solenoid is the only component. In
 1167 equation form,

$$V_{max} = \frac{L_1}{\tau_{DW}} \cdot (I_{max} + \tilde{I}) \quad (4.18)$$

1168 Or substituting in \tilde{I} and solving for τ_{DW} ,

$$\tau_{DW} = \frac{L_1}{M} \cdot \frac{(I_{max} \cdot 2M - I_{ID} \cdot L_2)}{V_{max}} \quad (4.19)$$

1169 4.1.3 Specifying Circuit Variables

1170 The goal now is to collect the results from the four phases and introduce the induc-
 1171 tance, resistance, voltage, and current terms relevant to our model. This will motivate
 1172 recasting the problem as flux balance in a reactor – the form commonly used in the
 1173 literature (and discussed next section).

1174 First, collecting the phase durations in one place:

$$\tau_{RU} = \frac{I_{ID}}{V_{max}} \cdot \left(\frac{L_1 L_2 - M^2}{M} \right) \quad (??)$$

$$\tau_{FT} = \frac{I_{max} \cdot 2M - I_{ID} \cdot L_2}{I_{ID} R_P} \quad (??)$$

$$\tau_{RD} = \tau_{RU} \quad (??)$$

$$\tau_{DW} = \frac{L_1}{M} \cdot \frac{(I_{max} \cdot 2M - I_{ID} \cdot L_2)}{V_{max}} \quad (??)$$

1175 These can be used in the definition of the duty-factor: the fraction of time a reactor

1176 is putting electricity on the grid. Formulaically,

$$f_{duty} = \frac{\tau_{FT}}{\tau_{pulse}} \quad (4.20)$$

1177

$$\tau_{pulse} = \tau_{RU} + \tau_{FT} + \tau_{RD} + \tau_{DW} \quad (4.21)$$

1178 As will turn out, the solving of pulsed current actually only involves ???. What is
 1179 interesting about this, is that there is no explicit dependence on ramp-down or dwell!
 1180 Whereas ramp-up passes \tilde{I} to the flattop phase, the other two are just involved in
 1181 calculating the duty factor.

1182 The remainder of this subsection will then be defining the following circuit variables:
 1183 I_{ID} , I_{max} , V_{max} , L_1 , L_2 , and M . Again, the resistance was defined last chapter as:

$$R_P = \frac{K_{RP}}{R_0 \bar{T}^{3/2}} \quad (??)$$

1184 **The Inductive Current – I_{ID}**

1185 The inductive current is the source of current that separates pulsed from steady-state
 1186 operation. Quickly fitting it into the previous definitions of current balance – see ??:
 1187

$$I_{ID} = I_P - (I_{BS} + I_{CD}) \quad (4.22)$$

1188 As before, I_P is the total plasma current in mega-amperes, I_{BS} is the bootstrap current,
 1189 and I_{CD} is the current from LHCD (i.e. lower hybrid current drive). For this model,
 1190 the relation can be rewritten as:

$$I_{ID} = I_P \cdot \left(1 - K_{CD}(\sigma v)\right) - K_{BS} \bar{T} \quad (4.23)$$

1191 The Central Solenoid Maximums – V_{max} and I_{max}

1192 For this simple model, the central solenoid has two maximum values: the voltage and
1193 current. The voltage is the easier to give value. Literature values have this around:⁵

$$V_{max} \approx 5 \text{ kV} \quad (4.24)$$

1194 The maximum current, on the other hand, can be defined through Ampere's Law on
1195 a helically-shaped central solenoid:¹⁰

$$I_{max} = \frac{B_{CS} h_{CS}}{N \mu_0} \quad (4.25)$$

1196 Here, B_{CS} is a magnetic field strength the central solenoid is assumed to operate at
1197 (i.e. 12 T), h_{CS} is the height of the solenoid, N is the number of loops, and μ_0 has
1198 its usual physics meaning (i.e. $40 \pi \frac{\mu\text{H}}{\text{m}}$). As will be seen, the value of N does not
1199 directly affect the model, as it cancels out in the final flux balance. The height of
1200 the central solenoid will be the focus of an upcoming section on improving tokamak
1201 geometry.

1202 The Central Solenoid Inductance – L_1

1203 For a central solenoid with circular cross-sections of finite thickness (d), the inductance
1204 can be written as:¹⁹

$$L_1 = G_{LT} \cdot \left(\frac{\mu_0 \pi N^2}{h_{CS}} \right) \quad (4.26)$$

1205

$$G_{LT} = \frac{R_{CS}^2 + R_{CS} \cdot (R_{CS} + d) + (R_{CS} + d)^2}{3} \quad (4.27)$$

1206 Note that R_{CS} is the inner radius of the central solenoid and $(R_{CS} + d)$ is the outer
1207 one. In the limit where d is negligible, this says that the inductance is quadratically

1208 dependent on the radius of the central solenoid:

$$\lim_{d \rightarrow 0} G_{LT} = G_{LT}^\dagger = R_{CS}^2 \quad (4.28)$$

1209 The formulas for both R_{CS} and d will be defined in a few sections.

1210 The Plasma Inductance – L_2

1211 The plasma inductance is a composite of several different terms, but overall scales
1212 with radius. Through equation,

$$L_2 = K_{LP} R_0 \quad (4.29)$$

1213 This static coefficient – K_{LP} – then combines three inductive behaviors of the plasma.
1214 The first is its own self inductance (through l_i).⁴ The next is a resistive component
1215 through the Ejima coefficient, C_{ejima} , which is usually set to $\sim \frac{1}{3}$.⁶ And lastly, a
1216 geometric component – involving ϵ and κ – is given by the Hirshman-Neilson model.²³
1217 Mathematically,

$$K_{LP} = \mu_0 \cdot \left(\frac{l_i}{2} + C_{ejima} + \frac{(b_{HN} - a_{HN})(1 - \epsilon)}{(1 - \epsilon) + \kappa d_{HN}} \right) \quad (4.30)$$

1218 Here the HN values come from the 1985 Hirshman-Neilson paper:

$$a_{HN}(\epsilon) = 2.0 + 9.25\sqrt{\epsilon} - 1.21 \epsilon \quad (4.31)$$

1219

$$b_{HN}(\epsilon) = \ln(8/\epsilon) \cdot (1 + 1.81\sqrt{\epsilon} + 2.05 \epsilon) \quad (4.32)$$

1220

$$d_{HN}(\epsilon) = 0.73\sqrt{\epsilon} \cdot (1 + 2\epsilon^4 - 6\epsilon^5 + 3.7\epsilon^6) \quad (4.33)$$

1221 **The Mutual Inductance – M**

1222 The mutual inductance – M – represents the coupling between the solenoid primary
1223 and the plasma secondary. A common method for treating this mutual inductance is
1224 through a coupling coefficient, k , that links the two self-inductances. Formulaically,

$$M = k\sqrt{L_1 L_2} \quad (4.34)$$

1225 The value of the coupling coefficient, k , is always less than (or equal to) 1, but usually
1226 has a value around one-third. With all the equations defined, we are now at a position
1227 to explain one of the larger nuances of this fusion systems framework: declaring the
1228 pulse length of a tokamak.

1229 **4.1.4 Constructing the Pulse Length**

1230 This subsection focuses on a quantitative estimate for how to select a pulse length.
1231 As no fusion reactor exists in the world today, the writers believe this is an acceptable
1232 calculation. Further, the resulting length of two hours matches the durations of other
1233 studies in the literature.

1234 Starting at the end, our goal is to find the pulse length of a tokamak reactor in
1235 seconds – as dictated by cyclical stress concerns. The first piece of information is
1236 the expected lifetime of the central solenoid, $N \approx 10$ years. The next is the desired
1237 number of pulses the central solenoid will have to last: $M \approx 50,000$ pulses.* This
1238 gives the rough estimate of around 10 pulses a day – or a flattop pulse length of two
1239 hours.

1240 With the pulse length defined, we are now in a position to justify neglecting the
1241 duty factor for pulsed reactors in this model. Using expected reactor values – while
1242 assuming the central solenoid has around 4000 turns – leads to the following scalings:

*This 50,000 pulses is based on the values from the ITER design specifications.²⁴

1243

$$\tau_{FT} \sim \tau_{pulse} \sim \text{O}(\text{hours}) \quad (4.35)$$

1244

$$\tau_{RU} \sim \tau_{RD} \sim \tau_{DW} \sim \text{O}(\text{mins}) \quad (4.36)$$

1245 As such, even pulsed tokamak reactors should have a duty factor of around unity:

$$f_{duty} \approx 1 \quad (4.37)$$

1246 This analysis of course would change if the central solenoid became an inexpensive
1247 component to replace. For example, if a tokamak had a new one installed annually,
1248 the pulse length could shorten to be on the order of minutes.

1249 Now that all the terms in a pulsed circuit have been explored, we will move on to
1250 rearranging the flattop equation to reproduce flux balance. This will then naturally
1251 lead to a generalized current equation – which is the main result of the chapter.

1252 4.2 Producing Flux Balance

1253 The goal of this section is to arrive at a conservation equation for flux balance that
1254 mirrors the ones in the literature. The fusion systems model this one attempts to
1255 follow most is the PROCESS code.⁶ In a manner similar to power balance, flux
1256 balance can be written as:

$$\sum_{sources} \Phi = \sum_{sinks} \Phi \quad (4.38)$$

1257 4.2.1 Rearranging the Circuit Equation

1258 The way to arrive at flux balance from the circuit equation is to rearrange the flattop
1259 phase's duration equation:

$$\tau_{FT} = \frac{I_{max} \cdot 2M - I_{ID} \cdot L_2}{I_{ID} R_P} \quad (??)$$

1260 Multiplying by the right-hand side's denominator and moving the negative term over
 1261 yields:

$$2MI_{max} = I_{ID} \cdot (L_2 + R_P\tau_{FT}) \quad (4.39)$$

1262 This equation is flux balance, where the left-hand side are the sources (e.g. the central
 1263 solenoid), and the other terms are the sinks (i.e. ramp-up and flattop). The source
 1264 term can currently be encapsulated in:

$$\Phi_{CS} = 2MI_{max} \quad (4.40)$$

1265 The sinks, namely the ramp-up inductive losses (Φ_{RU}) and the flattop resistive losses
 1266 (Φ_{FT}), are what drain up the flux. Again, ramp-down and dwell are not included as
 1267 sinks because flux balance only tracks till the end of flattop. They come into play
 1268 when measuring the cost of electricity – through the duty factor from ??.

1269 Relabeling terms, flux balance can now be rewritten as:

$$\Phi_{CS} = \Phi_{RU} + \Phi_{FT} \quad (4.41)$$

1270 With the ramp-up and flattop flux given respectively by:

$$\Phi_{RU} = L_2 \cdot I_{ID} \quad (4.42)$$

1271

$$\Phi_{FT} = (R_P\tau_{FT}) \cdot I_{ID} \quad (4.43)$$

1272 On comparing these quantities to the ones from the PROCESS team, Φ_{RU} and Φ_{FT}
 1273 are exactly the same. The source terms, on the other hand, are off for two reasons
 1274 – both related to the central solenoid being the only source term in flux balance.
 1275 This can partially be remedied by adding the second most dominant source of flux
 1276 a posteriori – i.e. the PF coils. The second, and inherently limiting factor, is the
 1277 simplicity of the current model. All that can be shown to this regard is that the Φ_{CS}
 1278 terms does reasonably predict the values from the PROCESS code.

1279 4.2.2 Adding Poloidal Field Coils

1280 Adding the effect of PF coils – belts of current driving plates on the outer edges of
 1281 the tokamak – leads to as much as a 50% improvement^{6,7} over relying solely on the
 1282 central solenoid for flux generation. From the literature, this can be modeled as:¹⁹

$$\Phi_{PF} = \pi B_V \cdot (R_0^2 - (R_{CS} + d)^2) \quad (4.44)$$

1283 Where again R_{CS} and d are the inner radius and thickness of the central solenoid,
 1284 respectively. These will be the topic of the next section.

1285 Moving forward, the vertical field – B_V – is a magnetic field oriented up-and-down
 1286 with the ground. It is needed to prevent a tokamak plasma from drifting radially out
 1287 of the machine. From the literature, the magnitude of this vertical field (valid for a
 1288 circular plasma) is given by:⁶

$$|B_V| = \frac{\mu_0 I_P}{4\pi R_0} \cdot \left(\ln \left(\frac{8}{\epsilon} \right) + \beta_p + \frac{l_i}{2} - \frac{3}{2} \right) \quad (4.45)$$

1289 Analogous to the previously covered plasma beta, the poloidal beta can be represented
 1290 by:²⁵

$$\beta_p = \frac{\bar{p}}{\left(\frac{B_p}{2\mu_0} \right)^2} \quad (4.46)$$

1291 Where the average poloidal magnetic field comes from a simple application of Am-
 1292 pere's law:

$$\bar{B}_p = \frac{\mu_0 I_P}{l_p} \quad (4.47)$$

1293 The variable l_p is then the perimeter of the tokamak's cross-sectional halves:

$$l_p = 2\pi a \cdot \sqrt{g_p} \quad (4.48)$$

1294 Here, g_p is another geometric scaling factor,

$$g_p = \frac{1 + \kappa^2(1 + 2\delta^2 - 1.2\delta^3)}{2} \quad (4.49)$$

1295 After a few lines of algebra, this relation for the magnitude of the vertical magnetic
 1296 field can be written in standardized units as:

$$|B_V| = \left(\frac{1}{10 \cdot R_0} \right) \cdot (K_{VI} I_P + K_{VT} \bar{T}) \quad (4.50)$$

1297

$$K_{VT} = K_n \cdot (\epsilon^2 g_P) \cdot (1 + f_D) \frac{(1 + \nu_n)(1 + \nu_T)}{1 + \nu_n + \nu_T} \quad (4.51)$$

1298

$$K_{VI} = \ln \left(\frac{8}{\epsilon} \right) + \frac{l_i}{2} - \frac{3}{2} \quad (4.52)$$

1299 For clarity, this will be plugged into the new PF coil flux contribution (Φ_{PF}):

$$\Phi_{PF} = \pi B_V \cdot (R_0^2 - (R_{CS} + d)^2) \quad (??)$$

1300 Which then gets plugged into a more complete flux balance:

$$\Phi_{CS} + \Phi_{PF} = \Phi_{RU} + \Phi_{FT} \quad (4.53)$$

1301 The R_{CS} and d terms found in Φ_{PF} will now be discussed as they are needed for this
 1302 more sophisticated tokamak geometry.

1303 4.3 Improving Tokamak Geometry

1304 From before, this fusion systems model has been said to depend on the major and
 1305 minor radius – R_0 and a , respectively – and along the way, various geometric param-
 1306 eters have been defined (e.g. ϵ , κ , δ) to describe the geometry further. Now three
 1307 more thicknesses will be added: b , c , and d . Additionally, two fundamental dimension
 1308 corresponding to the solenoid will be given: the radius (R_{CS}) and height (h_{CS}). These
 1309 are the topics of this section.

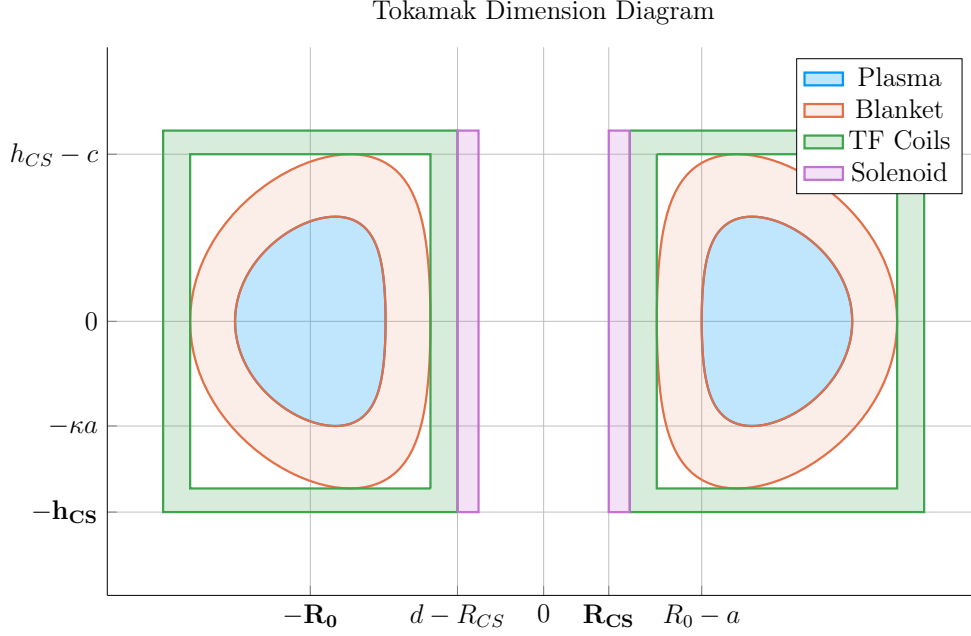


Figure 4-3: Dimensions of Tokamak Cross-Section

1310 4.3.1 Defining Central Solenoid Dimensions

1311 The best way to conceptualize tokamak geometry is through cartoon – see ???. What
 1312 this says is there is a gap at the very center of a tokamak. This gap extends radially
 1313 outwards to R_{CS} meters where the spiraled central solenoid – of thickness d – begins.
 1314 Between the outer edge of the solenoid and the wall of the torus (i.e. the doughnut)
 1315 are the blanket and toroidal field (TF) coils.

1316 The blanket and TF coils have thicknesses of b and c , respectively. Before defining
 1317 b , c , and d , though, it proves fruitful to relate all the quantities in equations for the
 1318 inner radius (R_{CS}) and height (h_{CS}) of the central solenoid.

$$R_{CS} = R_0 - (a + b + c + d) \quad (4.54)$$

1319

$$h_{CS} = 2 \cdot (\kappa a + b + c) \quad (4.55)$$

1320 Again, this relation is pictorially represented in ??. The next step is defining: b , c ,
 1321 and d – to close the variable loop.

1322 4.3.2 Calculating Component Thicknesses

1323 In between the inner surface of the central solenoid and the major radius of the
1324 tokamak are four thicknesses: a , b , c , and d . This subsection will go over them
1325 one-by-one.

1326 The Minor Radius – a

1327 The minor radius was the first of these thicknesses we encountered. To calculate it,
1328 we introduced the inverse aspect ratio (ϵ) to relate it to the major radius (R_0):

$$a = \epsilon \cdot R_0 \quad (??)$$

1329 The Blanket Thickness – b

1330 The blanket is an area between the TF coils and the torus that is composed mainly
1331 of lithium steel. It serves to both: protect the superconducting magnet structures
1332 from neutron damage, as well as breed more tritium fuel from stray fusion neutrons.
1333 In equation form, the blanket thickness is given by:²¹

$$b = 1.23 + 0.074 \ln P_W \quad (4.56)$$

1334 Here, P_W is a correction to account for extra wall loading (as discussed in ??).

1335 Moving forward, the remaining two thicknesses – c and d – are handled differently,
1336 estimating structural steel portions as well as magnetic current-carrying ones.

1337 The Toroidal Field Coil Thickness – c

1338 The thickness of the TF coils – c – is a little beyond the scope of this paper. It does,
1339 however, have a form that combines a structural steel component with a magnetic

1340 portion. From a previous model, this can be given as:²¹

$$c = G_{CI}R_0 + G_{CO} \quad (4.57)$$

1341

$$G_{CI} = \frac{B_0^2}{4\mu_0\sigma_{TF}} \cdot \frac{1}{(1 - \epsilon_b)} \cdot \left(\frac{4\epsilon_b}{1 + \epsilon_b} + \ln \left(\frac{1 + \epsilon_b}{1 - \epsilon_b} \right) \right) \quad (4.58)$$

1342

$$G_{CO} = \frac{B_0}{\mu_0 J_{TF}} \cdot \frac{1}{(1 - \epsilon_b)} \quad (4.59)$$

1343 The critical stress – σ_{TF} in G_{CI} implies it depends on the structural component,
 1344 whereas the maximum current density – J_{TF} – implies a magnetic predisposition
 1345 in G_{CO} . The use of G_{\square} in these quantities, instead of K_{\square} is because they include
 1346 the toroidal magnetic field strength – B_0 . For this reason, they are referred to as
 1347 dynamic coefficients. Lastly, the term ϵ_b represents the blanket inverse aspect ratio
 1348 that combines the minor radius with the blanket thickness:

$$\epsilon_b = \frac{a + b}{R_0} \quad (4.60)$$

1349 **The Central Solenoid Thickness – d**

1350 Finishing this discussion where we started, the central solenoid's thickness – d – has
 1351 a form similar to the TF coil's (i.e. c). In mathematical form, this can be represented
 1352 as:²¹

$$d = K_{DR}R_{CS} + K_{DO} \quad (4.61)$$

1353

$$K_{DR} = \frac{3B_{CS}^2}{6\mu_0\sigma_{CS} - B_{CS}^2} \quad (4.62)$$

1354

$$K_{DO} = \frac{6B_{CS}\sigma_{CS}}{6\mu_0\sigma_{CS} - B_{CS}^2} \cdot \left(\frac{1}{J_{OH}} \right) \quad (4.63)$$

Here, the use of K_{\square} for the coefficients signifies their use as static coefficients. Therefore, B_{CS} must be treated as a static variable representing the magnetic field strength in the central solenoid. For prospective solenoids using high temperature superconducting (HTS) tape, B_{CS} may be around 20 T. The values of σ_{CS} and J_{CS} have similar meanings to the ones for TF coils. These are collected in a table below with example values representative of our model.

Table 4.2: Example TF Coils and Central Solenoid Critical Values

(a) Stresses [MPa]			(b) Current Densities [MA/m ²]		
Item	Symbol	Limit	Item	Symbol	Limit
Solenoid	σ_{CS}	600	Solenoid	J_{CS}	100
TF Coils	σ_{TF}	600	TF Coils	J_{TF}	200

Before moving on, it seems important to say that although K_{DI} and K_{DO} do not depend on dynamic variables, R_{CS} most definitely does. This is what makes the central solenoid's thickness difficult.

4.3.3 Revisiting Central Solenoid Dimensions

Now that the various thicknesses have been defined (i.e. a , b , c , and d), the equations for the solenoid's dimensions (i.e. R_{CS} and h_{CS}), can now be revisited and simplified. From before,

$$R_{CS} = R_0 - (a + b + c + d) \quad (??)$$

$$h_{CS} = 2 \cdot (\kappa a + b + c) \quad (??)$$

Utilizing the four thicknesses from before, these can now be expanded to simple formulas. Repeating the thicknesses:

$$a = \epsilon \cdot R_0 \quad (??)$$

$$b = 1.23 + 0.074 \ln P_W \quad (??)$$

$$c = G_{CI}R_0 + G_{CO} \quad (??)$$

$$d = K_{DR}R_{CS} + K_{DO} \quad (??)$$

Plugging these into the central solenoid's dimensions results in:

$$h_{CS} = 2 \cdot (R_0 \cdot (\epsilon\kappa + G_{CI}) + (b + G_{CO})) \quad (4.64)$$

$$R_{CS} = \frac{1}{1 + K_{DR}} \cdot (R_0 \cdot (1 - \epsilon - G_{CI}) - (K_{DO} + b + G_{CO})) \quad (4.65)$$

1369 These are the complete central solenoid dimension formulas. To make them more
1370 tractable to the reader, they will now be simplified one step at a time. (The same
1371 simplification exercise will be done again after the generalized current is derived later
1372 this chapter.)

1373 The first simplification to make while estimating central solenoid dimensions is to
1374 neglect the magnetic current-carrying portions of the central solenoid and TF coils.

1375 This results in:

$$\lim_{\substack{G_{CO} \rightarrow 0 \\ K_{DO} \rightarrow 0}} h_{CS} = h_{CS}^{\dagger} = 2R_0 \cdot (K_{EK} + \epsilon_b + G_{CI}) \quad (4.66)$$

1376

$$\lim_{\substack{G_{CO} \rightarrow 0 \\ K_{DO} \rightarrow 0}} R_{CS} = R_{CS}^{\dagger} = \frac{R_0}{1 + K_{DR}} \cdot (1 - \epsilon_b - G_{CI}) \quad (4.67)$$

1377 The new static coefficient, here, is:

$$K_{EK} = \epsilon \cdot (\kappa - 1) \quad (4.68)$$

1378 The next simplification is ignoring the TF coil thickness – and thus magnetic field
 1379 dependence – altogether:

$$\lim_{G_{CI} \rightarrow 0} h_{CS}^{\dagger} = h_{CS}^{\ddagger} = 2R_0 \cdot (K_{EK} + \epsilon_b) \quad (4.69)$$

1380

$$\lim_{G_{CI} \rightarrow 0} R_{CS}^{\dagger} = R_{CS}^{\ddagger} = \frac{R_0}{1 + K_{DR}} \cdot (1 - \epsilon_b) \quad (4.70)$$

1381 These oversimplifications will be used later this chapter while simplifying the gener-
 1382 alized current equation to something more tractable. For now, they highlight how the
 1383 dimensions change as different components are neglected. The next step is bringing
 1384 plasma physics back into the flux balance equation and solving for the generalized
 1385 current.

1386 4.4 Piecing Together the Generalized Current

1387 The goal of this section is to quickly expand flux balance using all the defined quan-
 1388 tities and then massage it into an equation for plasma current – which is suitable for
 1389 root solving. This starts with a restatement of flux balance in a reactor:

$$\Phi_{CS} + \Phi_{PF} = \Phi_{RU} + \Phi_{FT} \quad (??)$$

1390

$$\Phi_{CS} = 2MI_{max} \quad (??)$$

1391

$$\Phi_{PF} = \pi B_V \cdot (R_0^2 - (R_{CS} + d)^2) \quad (??)$$

1392

$$\Phi_{RU} = L_2 \cdot I_{ID} \quad (??)$$

1393

$$\Phi_{FT} = (R_P \tau_{FT}) \cdot I_{ID} \quad (??)$$

1394 The first step is realizing that the central solenoid flux can now be rewritten using
1395 the new geometry in a standardized form:

$$\Phi_{CS} = K_{CS} \cdot \sqrt{R_0 G_{LT} h_{CS}} \quad (4.71)$$

1396

$$K_{CS} = 2k B_{CS} \cdot \sqrt{\frac{\pi K_{LP}}{\mu_0}} \quad (4.72)$$

1397 Next, we will slightly simplify the PF coil flux using a dynamic variable coefficient:

$$\Phi_{PF} = G_V \cdot \frac{K_{VI} I_P + K_{VT} \bar{T}}{R_0} \quad (4.73)$$

1398

$$G_V = \frac{\pi}{10} \cdot (R_0^2 - (R_{CS} + d)^2) \quad (4.74)$$

1399 This allows us to rewrite the generalized current as:

$$I_P = \frac{(K_{BS} + G_{IV}/G_{IP}) \cdot \bar{T}}{1 - K_{CD}(\sigma v) - G_{ID}/G_{IP}} \quad (4.75)$$

1400

$$G_{IV} = K_{VT} G_V + K_{CS} R_0^{3/2} \cdot \frac{\sqrt{h_{CS} G_{LT}}}{\bar{T}} \quad (4.76)$$

1401

$$G_{ID} = K_{VI} G_V \quad (4.77)$$

1402

$$G_{IP} = K_{LP} R_0^2 + \frac{K_{RP} \tau_{FT}}{\bar{T}^{3/2}} \quad (4.78)$$

1403 As we will show in the next section, this form not only has a form remarkably similar
1404 to the steady current – it reduces to it in the limit of infinitely long pulses!

1405 4.5 Simplifying the Generalized Current

1406 This section focuses on making various simplifications to the generalized current:

$$I_P = \frac{(K_{BS} + G_{IU}/G_{IP}) \cdot \bar{T}}{1 - K_{CD}(\sigma v) - G_{ID}/G_{IP}} \quad (??)$$

1407 As promised, this will start with the trivial simplification of the generalized current
 1408 into steady state. Next it will move on to a basic simplification for the purely pulsed
 1409 case. These two activities should shed some light on how to interpret the equation in
 1410 the more complicated hybrid case.

1411 4.5.1 Recovering the Steady Current

1412 The place to start with the steady current is the dynamic coefficient, G_{IP} :

$$G_{IP} = K_{LP}R_0^2 + \frac{K_{RP} \tau_{FT}}{\bar{T}^{3/2}} \quad (??)$$

1413 As can be seen, as $\tau_{FT} \rightarrow \infty$, so does the coefficient,

$$\lim_{\tau_{FT} \rightarrow \infty} G_{IP} = \infty \quad (4.79)$$

1414 Because G_{IU} and G_{ID} remain constant, their contribution to plasma current becomes
 1415 insignificant in this limit. Concretely,

$$\lim_{\tau_{FT} \rightarrow \infty} I_P = \frac{K_{BS} \bar{T}}{1 - K_{CD}(\sigma v)} \quad (4.80)$$

1416 This is precisely the steady current given by ??! The generalized current automati-
 1417 cally works when modeling steady-state tokamaks.*

* It should be noted that this is much harder when setting τ_{FT} to a large, but finite number – as η_{CD} still needs to be solved self-consistently.

1418 4.5.2 Extracting the Pulsed Current

1419 For pulsed reactors, we have to resolve a similar problem – except now τ_{FT} is expected
1420 to be a reasonably sized number (i.e. 2 hours).

1421 With an aim at intuition, the reactor is first treated as purely pulsed – having no
1422 current drive assistance:

$$\lim_{\eta_{CD} \rightarrow 0} I_P = \frac{(K_{BS} + G_{IU}/G_{IP}) \cdot \bar{T}}{1 - (G_{ID}/G_{IP})} \quad (4.81)$$

1423 Next, for simplicity-sake, the PF coil contribution to flux balance is assumed negligi-
1424 ble, as it was always just a correction term:

$$\lim_{\Phi_{PF} \ll \Phi_{CS}} G_{IU} = K_{CS} R_0^{3/2} \cdot \frac{\sqrt{h_{CS} G_{LT}}}{\bar{T}} \quad (4.82)$$

1425

$$\lim_{\Phi_{PF} \ll \Phi_{CS}} G_{ID} = 0 \quad (4.83)$$

1426 Piecing this altogether, we can write a new current for this highly simplified case,

$$I_P^\dagger = K_{BS} \bar{T} + \frac{K_{CS} R_0^{3/2} \cdot \sqrt{h_{CS} G_{LT}}}{K_{LP} R_0^2 + K_{RP} \tau_{FT} \bar{T}^{-3/2}} \quad (4.84)$$

1427 As this is not quite simple enough, these previous simplifications will be incorporated:

1428

$$G_{LT}^\dagger = R_{CS}^2 \quad (??)$$

1429

$$h_{CS}^\dagger = 2R_0 \cdot (K_{EK} + \epsilon_b) \quad (??)$$

1430

$$R_{CS}^\dagger = \frac{R_0}{1 + K_{DR}} \cdot (1 - \epsilon_b) \quad (??)$$

1431 Taking these into consideration results in the following current formula:

$$I_P^\dagger = K_{BS} \bar{T} + \left(\frac{K_{CS} R_0^3}{K_{LP} R_0^2 + K_{RP} \tau_{FT} \bar{T}^{-3/2}} \cdot \frac{(1 - \epsilon_b) \cdot \sqrt{2(K_{EK} + \epsilon_b)}}{1 + K_{DR}} \right) \quad (4.85)$$

1432 In the limit that the pulse length drops to zero (and bootstrap current is negligible),

$$\lim_{\tau_{FT} \rightarrow 0} I_P^\dagger = R_0 \cdot \left(\frac{K_{CS}}{K_{LP}} \cdot \frac{(1 - \epsilon_b) \cdot \sqrt{2(K_{EK} + \epsilon_b)}}{1 + K_{DR}} \right) \quad (4.86)$$

1433 This implies that a purely pulsed current scales with major radius to leading order.

1434 4.5.3 Rationalizing the Generalized Current

1435 From the previous two subsections, we arrived at equations for infinitely large and
1436 infinitely small pulse lengths:

$$\lim_{\tau_{FT} \rightarrow \infty} I_P = \frac{K_{BS} \bar{T}}{1 - K_{CD}(\sigma v)} \quad (??)$$

1437

$$\lim_{\tau_{FT} \rightarrow 0} I_P^\dagger = R_0 \cdot \left(\frac{K_{CS}}{K_{LP}} \cdot \frac{(1 - \epsilon_b) \cdot \sqrt{2(K_{EK} + \epsilon_b)}}{1 + K_{DR}} \right) \quad (??)$$

1438 What these imply at an intuitive level is that at small pulses, current scales with the
1439 major radius. While for long pulses, current scales with plasma temperature. In the
1440 general case, of course, the problem becomes much harder to predict. – as shown by
1441 the code's results using ??.

Chapter 5

Completing the Systems Model

As opposed to previous chapters, this one will focus on the numerics behind the fusion systems model. A simple algebra will lead to a generalized solver for exploring reactor space for low cost and interesting machines. This will then naturally segue into a discussion of how plots are made and should be interpreted. The remaining chapters will then decouple the presentation of results from their analytic conclusions.

5.1 Describing a Simple Algebra

In essence, the systems model used here is a simple algebra problem – given five equations, solve for five unknowns. The goal is then to pick the five equations that best represent modern fusion reactor design (as shown in ??). This selection should also be done in such a way that actually reduces the system of equations to a simple univariate root solving equation (i.e. one equation with one unknown). As will be shown in the results, this model does reasonably well: matching other modeling campaigns in seconds.

The logical place to start in a discussion of this algebra problem is with the three equations fundamental to all reactor-grade tokamaks – both in steady-state and pulsed operation. These are: the Greenwald density limit, power balance, and current bal-

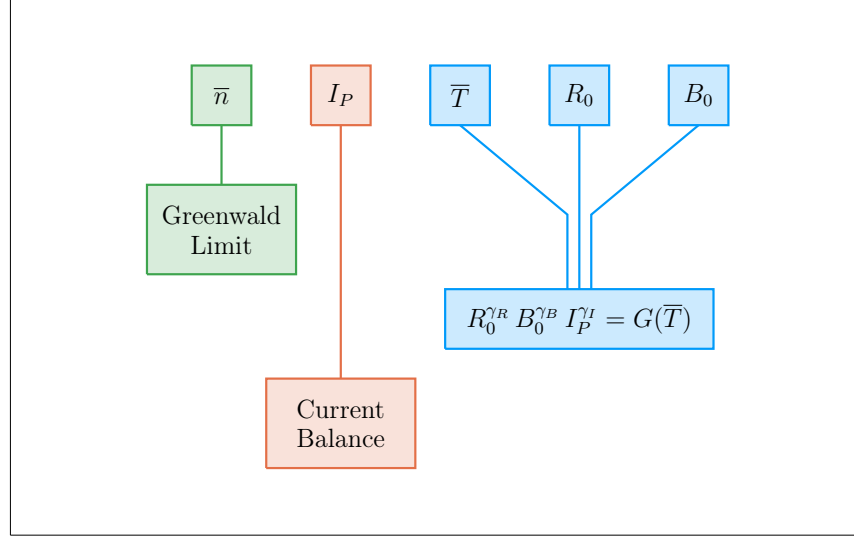


Figure 5-1: Equation Selection for Fusion System

The goal of this fusion system is to create a set of equations that model the five dynamic variables. These are the Greenwald limit for density, current balance for the plasma current, and three generalized formulas for the temperature, major radius, and toroidal field strength.

1460 ance. The Greenwald density's importance was hinted early on when it was used to
 1461 simplify every equation derived thereafter.

$$\bar{n} = K_n \cdot \frac{I_P}{R_0^2} \quad (??)$$

1462 The two balance equations proved to be slightly more complicated. As was shown,
 1463 current balance was the more difficult of the two – bringing forth the notion of self-
 1464 consistency for steady-state machines and a highly-coupled multi-root equation for
 1465 pulsed ones. As such, current balance stands as the equation everything is substituted
 1466 into to do a final univariate root solve.

$$I_P = \frac{(K_{BS} + G_{IV}/G_{IP}) \cdot \bar{T}}{1 - K_{CD}(\sigma v) - G_{ID}/G_{IP}} \quad (??)$$

1467 Although slightly buried in ??, the right-hand side actually depends on all the quan-
 1468 tities (including I_P through the wall loading term in blanket thickness). Through

1469 equation,

$$I_P = f(I_P, \bar{T}, R_0, B_0) \quad (5.1)$$

1470 The remaining equation common to all reactor-grade tokamaks is power balance –
1471 the relation that quantifies its net electricity production capabilities. Due to the use
1472 of the ELMy H-Mode scaling law for modeling the diffusion coefficient, this had the
1473 complicated form of:

$$R_0^{\alpha_R^*} \cdot B_0^{\alpha_B} \cdot I_P^{\alpha_I^*} = \frac{G_{PB}}{K_{PB}} \quad (5.2)$$

1474 Although being rather cumbersome, this equation actually remains relatively simple
1475 in that all three quantities on the left-hand side are separable. To close the system,
1476 two more equations of this form are needed. These have the following form and will
1477 be described next.

$$R_0^{\gamma_R} \cdot B_0^{\gamma_B} \cdot I_P^{\gamma_I} = G(\bar{T}) \quad (5.3)$$

1478 5.2 Generalizing Previous Equations

1479 Where the equations defined up to this point in the chapter are shared among all
1480 fusion reactors, the remaining two equations – needed to close the system – must
1481 be partially chosen by the user. These equations come in three varieties: limits,
1482 intermediate quantities, and dynamic variables. By convention, we enforce that at
1483 least one limit must be used. The other constraint can then come from any of the
1484 three defined collections, which we will refer to as the closure equation.

1485 5.2.1 Including Limiting Constraints

1486 The limits category is composed of the limiting constraints given in ???. These include
1487 the physics derived limits from MHD theory – i.e. the beta limit (β_N) and the kink
1488 safety factor (q_*) – which for clarity, set maximums on the allowed plasma pressure
1489 and current, respectively. Additionally, there were several engineering limits also
1490 described: wall loading, heat loading, and maximum power capacity. For this paper,

1491 wall loading from neutrons (P_W) is assumed to be important, whereas the other two
1492 engineering limits are not allowed to explicitly guide designs.

1493 Combined all these limits, as well as the yet to be defined dynamic and intermediate
1494 equations, are given in ???. These share a remarkably similar form to power balance
1495 when put into a generalized, separable state. This hints at why the major radius (R_0),
1496 the toroidal field strength (B_0), and the plasma current (I_P) can easily be separated
1497 and substituted out of the current balance equation.

1498 Before moving on, it proves useful to explain the two limits not used to explicitly guide

Table 5.1: Main Equation Bank

To close the system of equations for potential reactors, different equations can be used to lock down tokamak designs. These include physics and engineering limits (L), as well as ways to set dynamic (D) or intermediate (I) variables to constant values.

Variable	Category	$G(\bar{T})$	γ_R	γ_B	γ_I
Power Balance	-	G_{PB}/K_{PB}	α_R^*	α_B	α_I^*
Beta (β_N)	L	$K_{TB}\bar{T}$	1	1	0
Kink (q_*)	L	K_{KF}	1	1	-1
Wall Loading (P_W)	L	$K_{WL}(\sigma v)^{1/3}$	1	0	-2/3
Power Cap (P_E)	L	$K_{PC}(\sigma v)$	1	0	-2
Heat Loading (q_{DV})	L	$K_{DV}(\sigma v)^{1/3.2}$	1	0	-1
Major Radius (R_0)	D	$(R_0)_{const}$	1	0	0
Magnet Strength (B_0)	D	$(B_0)_{const}$	0	1	0
Plasma Current (I_P)	D	$(I_P)_{const}$	0	0	1
Plasma Temperature (\bar{T})	D	$(\bar{T})_{const}/\bar{T}$	0	0	0
Electron Density (\bar{n})	D	$(\bar{n})_{const}/K_n$	-2	0	1
Plasma Pressure (\bar{p})	I	$(\bar{p})_{const}/K_n K_{nT} \bar{T}$	-2	0	1
Bootstrap Current (f_{BS})	I	$(f_{BS})_{const}/K_{BS} \bar{T}$	0	0	-1
Fusion Power (P_F)	I	$(P_F)_{const}/K_F K_n^2(\sigma v)$	-1	0	2
Magnetic Energy (W_M)	I	$(W_M)_{const}/K_{WM}$	3	2	0
Cost per Watt (C_W)	I	$(C_W)_{const} \cdot (K_F K_n^2(\sigma v)/K_{WM})$	4	2	-2

1499 reactor design – divertor heat loading and the maximum power capacity. The simpler
 1500 of the two to reason is the heat loading limit. Although removing the gigawatts-per-
 1501 square-meter of heat is extremely difficult, it remains an unsolved problem worthy of
 1502 its own research machine.²² As such, it is only kept to provide a human-interpreted
 1503 measure of difficulty. The power cap, on the other hand, is just handled informally.
 1504 If a reactor surpasses it (i.e. $P_E > 4000MW$), it is considered invalid.

1505 While the maximum power cap informally sets a maximum major radius for a ma-
 1506 chine, there also exists an implicit minimum major radius. This minimum occurs due
 1507 to the hole-size constraint – i.e. at some point there is no longer enough room on the
 1508 inside of the machine to store the central solenoid, blanket, and TF coils.

1509 At this point, we can now explain how various quantities in the systems model can
 1510 be set to user-given constant values. This basically allows users to treat one dynamic
 1511 variable as a static one (e.g. the temperature and bootstrap fraction).

1512 5.2.2 Minimizing Intermediate Quantities

1513 Whereas the limits from the previous section represented constraints with real physics
 1514 and engineering repercussions, the intermediate quantities here are just used to find
 1515 when reactors reach certain user-supplied values. Most notable are the capital cost
 1516 (through the magnetic energy – W_M) and the cost-per-watt (C_W). The model also,
 1517 however, allows easily setting values for the bootstrap fraction, plasma pressure, and
 1518 fusion power. As mentioned previously, they are given in ?? through a generalized
 1519 representation of the form:

$$R_0^{\gamma_R} \cdot B_0^{\gamma_B} \cdot I_P^{\gamma_I} = G(\overline{T}) \quad (??)$$

1520 What this collection of variables is really useful for, though, is finding minimum cost
 1521 reactors – both in a capital context as well as a cost-per-watt one. This is done in
 1522 a three stage process. The first of which is to find a valid reactor – i.e. one that
 1523 satisfies every limiting constraint. Practically, this is done by searching over a range

1524 of scanned temperatures.

1525 After a valid reactor is found, its cost is recorded leading to a drill-down stage. In
1526 this step, the cost is continuously halved until a valid reactor cannot be found. Once
1527 this invalid reactor is reached, it sets a bound on the minimum cost reactor. As such,
1528 the final stage is a simple bisection step where the minimum cost is honed down to
1529 some acceptable margin of error – see ??.

1530 5.2.3 Pinning Dynamic Variables

1531 The remaining collection of closure equations is for the five dynamic variables in the
1532 systems model: R_0 , B_0 , \bar{n} , \bar{T} , and I_P . As we are making equations of the following
1533 form, the formulas for R_0 , B_0 , and I_P are trivial.

$$R_0^{\gamma_R} \cdot B_0^{\gamma_B} \cdot I_P^{\gamma_I} = G(\bar{T}) \quad (??)$$

1534 Next, the equation for \bar{n} – shown in ?? – is just a simple undoing of the Greenwald
1535 density limit. The remaining equation is then from the original temperature equation:

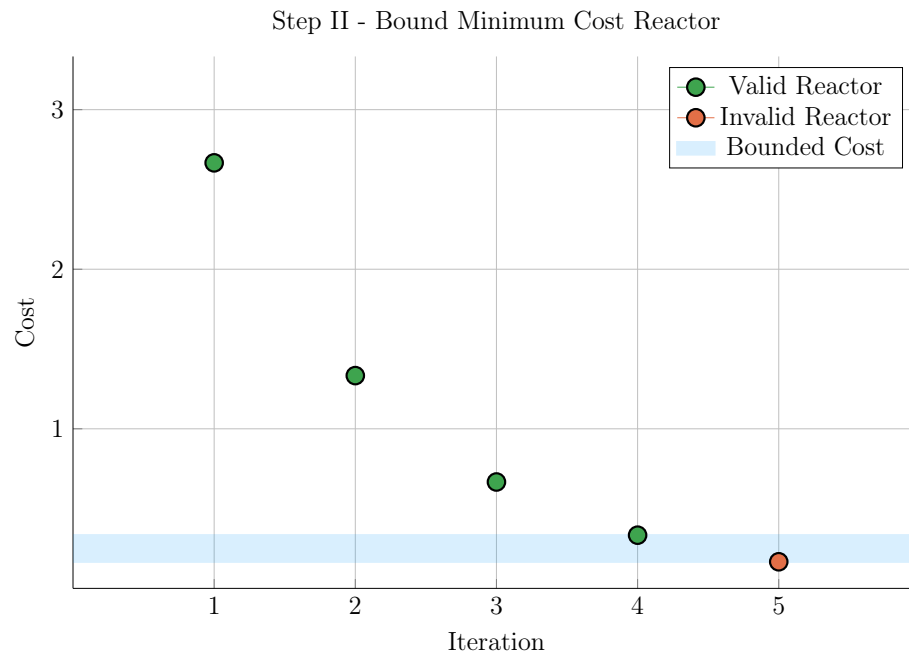
1536

$$\bar{T} = \text{const.} \quad (??)$$

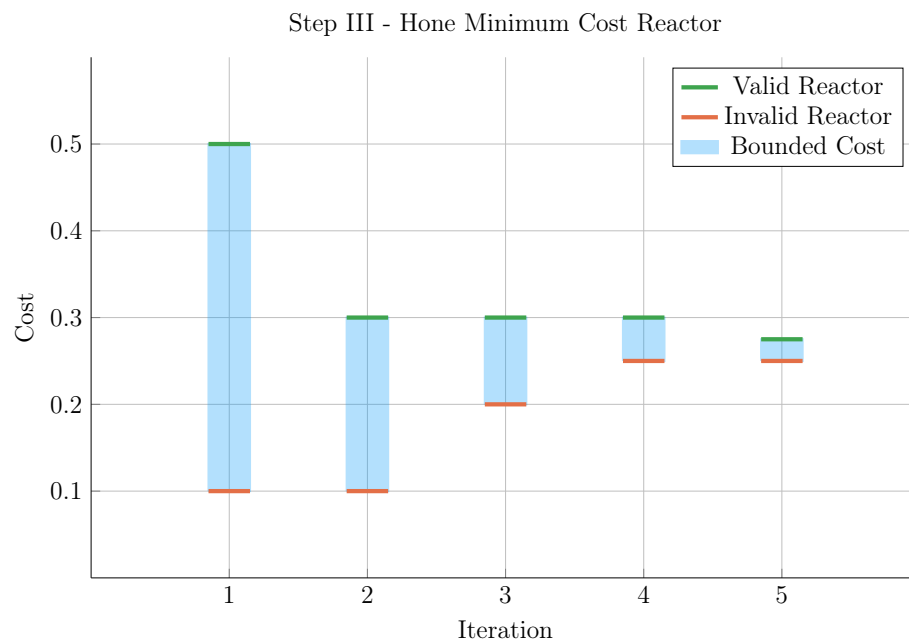
1537 As was assumed earlier, this is sort of a default equation for the systems model. By
1538 this, we mean reactor curves can be created by scanning over temperatures, i.e. set
1539 $\bar{T} = 5$ keV in one run, 10 in the next, etc. This temperature equation also brings
1540 up a difficulty for the algebraic solver, as it does not depend on: current, radius, or
1541 magnet strength. Overcoming this difficulty is discussed next subsection.

1542 5.2.4 Detailing the Equation Solver

1543 The algorithm that motivated this generalized equation approach most notably bi-
1544 furcates in the situation where the closure equation does not depend on R_0 , B_0 , or I_P
1545 (i.e. for the temperature equation). The two scenarios are given in ????????????????



(a) Minimize Step II



(b) Minimize Step III

Figure 5-2: Minimize Cost Step II/III – Optimize Reactor

1546 – where at least R_0 and B_0 are substituted out of the system. In the temperature
 1547 case, I_P is not needed to be explicitly removed.

1548 Concretely, the root solve for the temperature scenario is for the current, whereas it
 1549 is for the temperature in all other cases. The nomenclature in the code is a *match*
 1550 for Scenario I (i.e. root solving for plasma temperature), and a *solve* for Scenario II
 1551 (i.e. root solving for plasma current).

1552 **Scenario I – Match for \bar{T}**

$$R_0(\bar{T}) = \left(G_1^{(\gamma_{B,2} \gamma_{I,3} - \gamma_{B,3} \gamma_{I,2})} \cdot G_2^{(\gamma_{B,3} \gamma_{I,1} - \gamma_{B,1} \gamma_{I,3})} \cdot G_3^{(\gamma_{B,1} \gamma_{I,2} - \gamma_{B,2} \gamma_{I,1})} \right)^{\frac{1}{\gamma_{RBI}}} \quad (5.4)$$

1553

$$B_0(\bar{T}) = \left(G_1^{(\gamma_{I,2} \gamma_{R,3} - \gamma_{I,3} \gamma_{R,2})} \cdot G_2^{(\gamma_{I,3} \gamma_{R,1} - \gamma_{I,1} \gamma_{R,3})} \cdot G_3^{(\gamma_{I,1} \gamma_{R,2} - \gamma_{I,2} \gamma_{R,1})} \right)^{\frac{1}{\gamma_{RBI}}} \quad (5.5)$$

1554

$$I_P(\bar{T}) = \left(G_1^{(\gamma_{R,2} \gamma_{B,3} - \gamma_{R,3} \gamma_{B,2})} \cdot G_2^{(\gamma_{R,3} \gamma_{B,1} - \gamma_{R,1} \gamma_{B,3})} \cdot G_3^{(\gamma_{R,1} \gamma_{B,2} - \gamma_{R,2} \gamma_{B,1})} \right)^{\frac{1}{\gamma_{RBI}}} \quad (5.6)$$

$$\begin{aligned} \gamma_{RBI} = & (\gamma_{R,1} \gamma_{B,2} \gamma_{I,3} + \gamma_{R,2} \gamma_{B,3} \gamma_{I,1} + \gamma_{R,3} \gamma_{B,1} \gamma_{I,2}) - \\ & (\gamma_{R,1} \gamma_{B,3} \gamma_{I,2} + \gamma_{R,2} \gamma_{B,1} \gamma_{I,3} + \gamma_{R,3} \gamma_{B,2} \gamma_{I,1}) \end{aligned} \quad (5.7)$$

1555 **Scenario II – Solve for I_P**

$$R_0(\bar{T}) = \left(G_1^{\gamma_{B,2}} \cdot G_2^{-\gamma_{B,1}} \cdot I_P^{(\gamma_{B,1} \gamma_{I,2} - \gamma_{B,2} \gamma_{I,1})} \right)^{\frac{1}{\gamma_{RBT}}} \quad (5.8)$$

1556

$$B_0(\bar{T}) = \left(G_1^{-\gamma_{R,2}} \cdot G_2^{\gamma_{R,1}} \cdot I_P^{(\gamma_{I,1} \gamma_{R,2} - \gamma_{I,2} \gamma_{R,1})} \right)^{\frac{1}{\gamma_{RBT}}} \quad (5.9)$$

1557

$$\gamma_{RBT} = \gamma_{R,1} \gamma_{B,2} - \gamma_{R,2} \gamma_{B,1} \quad (5.10)$$

1558 5.3 Wrapping up the Logic

1559 As stated at the beginning of the chapter, this systems model basically reduces to a
1560 simple 5 equation/5 unknown algebra problem. The Greenwald density was implicitly
1561 used in the initial derive to simplify the logic. The current balance was then delegated
1562 to be the root solve equation. Lastly, three equations were needed to remove the major
1563 radius and magnet strength, as well as either the current or temperature. These 16
1564 equations were given in ?? with the generalized solution given in ???????????????.

1565 This now sets the stage for the most interesting part of the document – the results.
1566 These will come in several forms. The first result type will be temperature scans
1567 that allow us to validate the model against other designs from the literature. These
1568 are created using the Scenario II solver.

1569 The Scenario I matcher will then be used to create sensitivity studies and Monte
1570 Carlo samplings. The simple one variable sensitivities will reveal local trends from
1571 sweeping various static (i.e. input) variables – namely H , κ , B_{CS} , etc. – one at a time.
1572 Whereas the samplings will highlight global trends as many static/input variables are
1573 allowed to vary simultaneously.

1574 These Scenario I matchers are further subdivided in regards to the nature of their
1575 closure equation. The first type comes from finding so called two limit solutions,
1576 which live at the point where the beta and kink (or wall) limits are just marginally
1577 satisfied. The second main type is then minimum cost reactors – measured in either
1578 a capital cost or cost-per-watt context. These will be used in depth next chapter.

1579 Chapter 6

1580 Presenting the Code Results

1581 Now that our fusion systems model has been formulated and completed, the next
1582 logical step is to build a codebase and explore reactor space. To this, the code
1583 encompassing this document’s model – Fussy.jl – is available at git.io/tokamak (with
1584 a short guide given in ??). The results from this chapter will be divided into three
1585 sections. The first is an attempt to test how accurate the model is by comparing it
1586 with other codes in the field.^{1,5,6} The next will be two prototypes developed to fairly
1587 compare pulsed and steady state reactors, the initial motivation for this project.

1588 This chapter will then conclude with a discussion on how best to lower reactor costs.
1589 In line with the MIT mission, this will highlight how using stronger magnets leads
1590 to more compact, economic machines. The new piece of insight, then, is how to
1591 optimally incorporate high-temperature superconducting (HTS) tape technology –
1592 the assumed technological advancement found in the ARC design family.

1593 Succinctly, we will show that HTS tape should be used in the TF coils for steady-state
1594 tokamaks (i.e. B_0), whereas it should only be appear in the central solenoid (i.e. B_{CS})
1595 for pulsed ones. This is a fundamentally new result!

1596 6.1 Testing the Code against other Models

1597 After developing a new model, the first next step is to make sure its results are sensical.
1598 The goal, however, is to not go too far, i.e. by: comparing it with too many models
1599 or requiring perfect matches with their results. To this, we will compare Fussy.jl with
1600 five designs from the literature – hopefully casting a wide enough net through reactor-
1601 space to prove sufficient. It should be noted that for how simple this model is, it does
1602 a remarkable job matching the other group’s more sophisticated frameworks. It also
1603 highlights how discrepancies arise in this highly non-linear computational problem.

1604 The first reactor design that will provide a basis for comparison is the ARC reactor.⁵
1605 As it was also designed by MIT researchers, the fit is shown to be almost exact. This
1606 of course probably involves a fair amount of inherent biases stemming from shared
1607 scientific philosophies and knowledge base.

1608 The next set of reactor designs come from the ARIES four-act study.² This ARIES
1609 team is a United States effort to reevaluate the problem of designing a fusion reactor
1610 around once a decade. The most recent study focused on how tokamaks would look as
1611 you assume optimistic and conservative values for physics and engineering parameters.
1612 Although our model recovers their results, it does highlight one peculiarity of their
1613 algorithm – reliance on the minimum achievable value of H .

1614 The final series of reactors comes from the major codebase used among European
1615 fusion systems experts: PROCESS.⁶ As such, this group actually gives an example for
1616 pulsed vs. steady-state tokamaks. Although these designs have the most discrepancies
1617 with our model, discussion will be given that remedy some of the shortcomings. These
1618 basically amount to: alternative definitions for heat loss appearing in the ELMy H-
1619 Mode Scaling, as well as the simplified nature of our flux balance equation – which
1620 only accounts for central solenoid and PF coil source terms.

1621 The most important detail to take from the comparisons done in ????????, however,
1622 is that each steady state design from the literature has H factors and Greenwald
1623 densities (N_G) that violate standard values (i.e. 1.0). What this means, practically,

1624 is steady-state reactors are not possible in the current tokamak paradigm – some
1625 technological advancement is needed.

1626 6.1.1 Comparing with the PSFC Arc Reactor

1627 As mentioned, this model matches the results from the ARC design almost perfectly
1628 – see ?????. This probably stems from how both models were developed within the
1629 MIT community. Two notable discrepancies between the models, however, are in the
1630 fusion power (P_F) and bootstrap current fraction (f_{BS}). These discrepancies likely
1631 arise from the use of simple parabolic profiles for temperature and, thus, can be seen
1632 in the subsequent model comparisons.

1633 Before moving on, though, it is important to explain how the plots and table used
1634 for this comparison are made. First, a list of temperatures between 1 and 40 keV is
1635 scanned to produce a set of reactors – each with their own size (R_0), magnet strength
1636 (B_0), etc. These reactors are then turned into the two curves shown in ?? by mapping
1637 to their respective values. Note that R_0 vs. B_0 is then a measure of the accuracy in
1638 the tokamak’s engineering, while I_P vs \bar{T} is a measure on its plasma’s physics.

1639 Once these curves are created, a design point is chosen on them that has the least
1640 distance to the marked point (from the original model’s paper). These two points – or
1641 reactors – are then compared in detail in ??. Note that the input variables are shared
1642 between the original model and this model’s input file. The output between the two
1643 is what is different. For clarity, V is the volume of a tokamak in cubic meters, and
1644 the dash on the inductive current fraction f_{ID} implies it makes up 0% of the current.

1645 The use of a dash for β_N brings up the final piece of information needed to understand
1646 the plots and table creation process – limiting constraints. Note that in ??, the solid
1647 curve has two portions: **beta** and **wall**. These are the portions where the beta limit
1648 and the wall loading limit are the driving constraints, respectively. For example at B_0
1649 = 5T, the wall loading (P_W) will be much less than the maximum allowed 2.5 MW/m².
1650 This is why the dash is next to β_N in ??, as it is held at the maximum allowed value

1651 (i.e. $\beta_N = 0.026$.)

1652 Finally, the reason there is a dashed **pulsed** curve and a solid **steady** one is because
1653 this reactor was run in both modes of operation. The pulsed label is actually a slight
1654 misnomer as it implies the generalized current balance formula is used (over the simple
1655 steady current from ??). Because pulses are set to 50 years, they are functionally
1656 steady-state regardless. The real reason the two curves diverge is because the steady
1657 current has a self-consistent current drive efficiency (η_{CD}).

1658 **6.1.2 Contrasting with the Aries Act Studies**

1659 Moving on, the Aries Act study focuses on how steady-state reactors would look under
1660 both a conservative and optimistic perspective. This is highlighted in ??, which shows
1661 how costs decreases as the H factor is allowed to increase. Notice that for every value
1662 of H, the ACT I study (i.e. the optimistic act) has a lower cost than the design from
1663 ACT II (i.e. the conservative one).

1664 This figure also highlights another peculiarity of the ARIES study – a reliance on the
1665 minimum possible value of H. Note that just left of the reactor point on both plots
1666 is a highly erratic portion of the curve. As such, if even a slightly smaller value of H
1667 were used in either case, a quite distinct reactor would occur. This is not a robust
1668 way to design machines. A better approach would be to build with some safety factor
1669 – i.e at a slightly more optimistic value of H. This can be seen in ARC’s H-Sweep.

1670 **Act I – Advanced Physics and Engineering**

1671 Act 1 is the ARIES study that assumes advanced physics and engineering design
1672 parameters. Although this paper’s model does a fair job recovering the results from
1673 their paper, it does show what optimistic design really means. As can be seen, this
1674 design actually only surpasses the minimum possible toroidal field strength by as less
1675 than a Tesla! Practically, this means their reactor is barely realizable. Trying to build
1676 a 5T device would not be possible using their stated reactor input parameters.

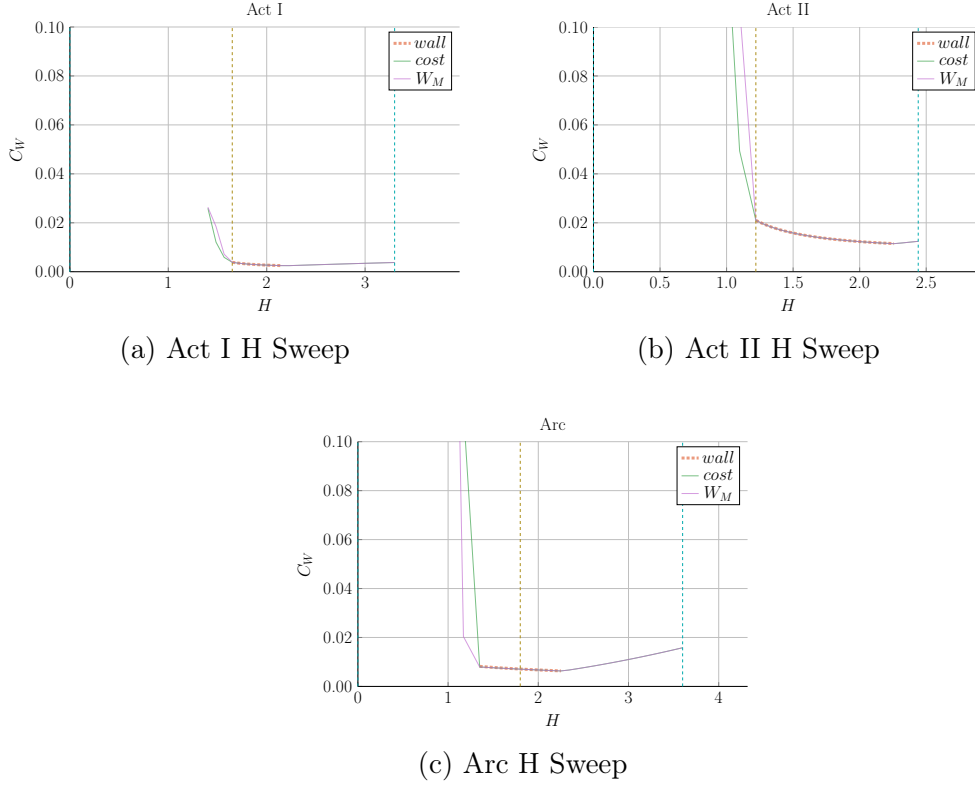


Figure 6-1: Act Studies Cost Dependence on the H Factor

1677 Act II – Conservative Physics and Engineering

1678 ARIES more conservative design – Act II – is much more like ARC in nature. From
 1679 the plots, it is obvious the paper’s model is basically right on top of the reactor curve
 1680 made using Fussy.jl. Much like ARC, too, it shows how the model overestimates fusion
 1681 power and underestimates bootstrap fraction due to their selection of a pedestal profile
 1682 for plasma temperature.

1683 6.1.3 Benchmarking with the Process DEMO Designs

1684 The PROCESS team’s prospective designs for successors to ITER constitute the final
 1685 set of model comparisons: the steady-state and pulsed DEMO reactors. As this paper
 1686 is designed to compare these modes of operation, this study proves most informative.
 1687 It also highlights how common model decisions can dramatically alter what reactors

1688 come out of the solvers.

1689 The first discrepancy is how the PROCESS team defines the loss term in the ELMy H-
1690 Mode scaling law. As shown in their paper, they actually subtract out a Bremsstrahlung
1691 component, while leaving the fitting coefficients the same.⁶ After modifying Fussy.jl
1692 to incorporate this definition, the steady-state reactor is easily reproducible in $R_0 -$
1693 B_0 slice of reactor space.

$$P_L^{DEMO} = P_{src} - P_{BR} \quad (6.1)$$

1694 Unlike the steady-state case, however, the modified power loss term does not fix the
1695 pulsed case, as it actually draws the reactor curves further from the design in their
1696 paper. As such, it is flux balance that is now the main culprit for discrepancies
1697 between the two models. This makes sense, as this model uses highly simplified
1698 source terms – namely neglecting anything but the central solenoid and PF coils (as
1699 well as ignoring crucial physics for these two components). Even acknowledging the
1700 differences between the two models, Fussy.jl still does reasonably well at reproducing
1701 their much more sophisticated coding framework.

1702 The final point to make is about selecting optimum points to build as the dynamic
1703 variables are allowed to make curves through reactor space. Up to this point, only
1704 steady-state tokamak designs have been explored. In every single one of these, though,
1705 the paper values have been very close to the point where the beta curves and wall
1706 loading curves cross. This is because they all result in the minimum cost-per-watt.

1707 For pulsed designs, on the other hand, kink curves start to appear for low magnetic
1708 field strengths. Just as beta-wall intersections were optimum places to design for low
1709 cost-per-watt (C_W) reactors, these beta-kink intersections will prove to be the place
1710 where minimum capital cost (W_M) reactors usually occur. This is discussed in more
1711 detail in ??.

1712 DEMO Steady – A Steady-State ITER Successor

1713 As shown in ????, the DEMO steady reactor is the design captured worst by the
1714 Fussy.jl model. Some discrepancy, however can be removed by using the PROCESS
1715 team’s modified version of heat loss, as given by ??.⁶ Although not supported by the
1716 official ITER database fit,²⁶ the PROCESS team reduces the absorbed power by the
1717 Bremsstrahlung power²⁷ – which can lengthen τ_E by more than 25%.⁷

1718 With this correction, the $R_0 - B_0$ curve is drawn to be right on top of their model’s
1719 design. The same cannot be said for the $I_P - \bar{T}$ curve as steady current was shown to
1720 have little dependence on tokamak configuration (R_0 and B_0) and, correspondingly,
1721 the limiting constraint (e.g. `beta` and `wall`).

1722 Note that the labels of `modified` and `pulsed` are slightly obscure in this context.
1723 Pulsed, for starters, is actually the generalized solver that does not rely on self-
1724 consistent current drive (i.e. in η_{CD}). The modified label is then when the pulsed
1725 solver uses the P_L^{DEMO} value in approximating heat conductive losses.

1726 DEMO Pulsed – A Pulsed ITER Successor

1727 This pulsed version of DEMO is the only reactor in our collection that is not run in
1728 steady-state. As such, it may be the most important one (i.e. it is the only pulsed
1729 reactor). The first observation from ?? is that this design actually has no valid wall
1730 loading portion – only a kink and beta curve exist! Even so, the results match pretty
1731 well. It should be noted, though, that this current drive is treated as an input and
1732 not solved self-consistently.

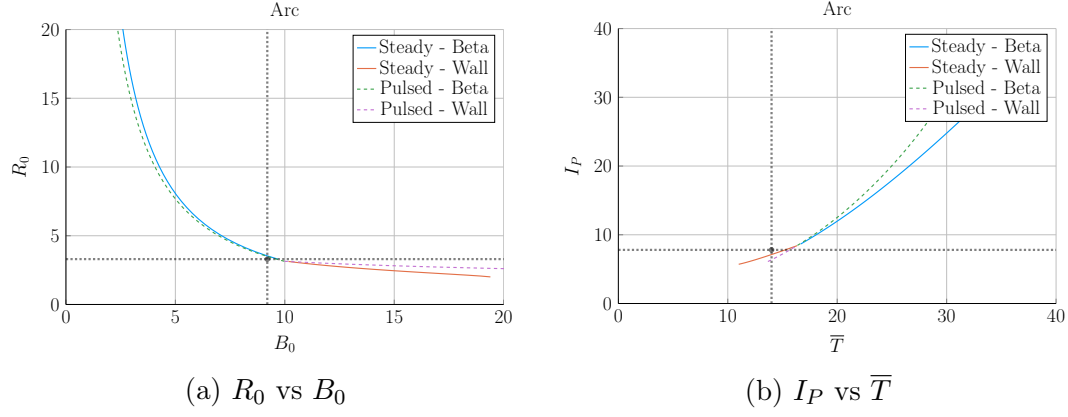


Figure 6-2: Arc Model Comparison

Table 6.1: Arc Variables

(a) Input Variables

Input	Value
H	1.8
Q	13.6
N_G	0.67
ϵ	0.333
κ_{95}	1.84
δ_{95}	0.333
ν_n	0.385
ν_T	0.929
l_i	0.670
A	2.5
Z_{eff}	1.2
f_D	0.9
τ_{FT}	1.6e9
B_{CS}	12.77

(b) Output Variables

Output	Original	Fussy.jl
R_0	3.3	3.4
B_0	9.2	9.5
I_P	7.8	8.8
\bar{n}	1.3	1.3
\bar{T}	14.0	16.8
β_N	0.026	-
q_{95}	7.2	6.1
P_W	2.5	2.2
f_{BS}	0.63	0.56
f_{CD}	0.37	0.44
f_{ID}	-	-
V	141	157
P_F	525	726
η_{CD}	0.321	0.316

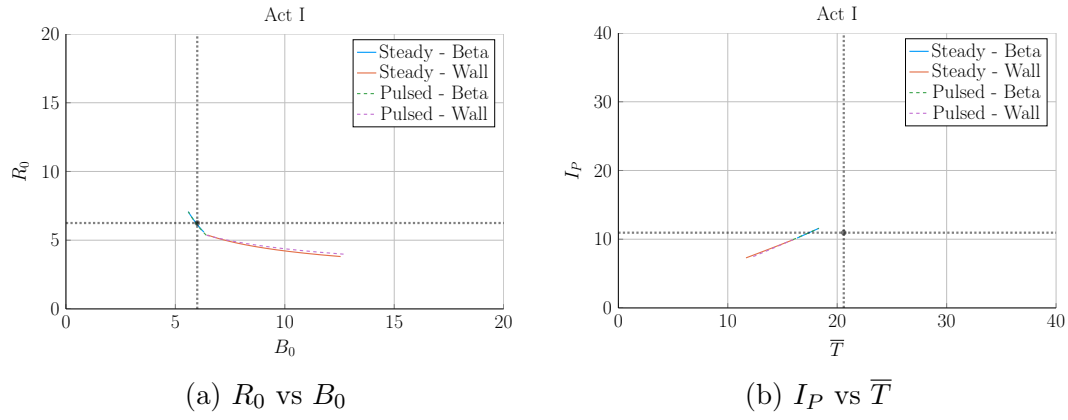


Figure 6-3: Aries Act I Model Comparison

Table 6.2: Act I Variables

(a) Input Variables

Input	Value
H	1.65
Q	42.5
N_G	1.0
ϵ	0.25
κ_{95}	2.1
δ_{95}	0.4
ν_n	0.27
ν_T	1.15
l_i	0.359
A	2.5
Z_{eff}	2.11
f_D	0.75
τ_{FT}	1.6e9
B_{CS}	12.77

(b) Output Variables

Output	Original	Fussy.jl
R_0	6.25	6.23
B_0	6.0	6.0
I_P	10.95	10.78
\bar{n}	1.3	1.3
\bar{T}	20.6	17.2
β_N	0.0427	-
q_{95}	4.5	4.0
P_W	2.45	2.00
f_{BS}	0.91	0.91
f_{CD}	0.09	0.09
f_{ID}	-	-
V	582.0	621.4
P_F	1813	1865
η_{CD}	0.188	0.185

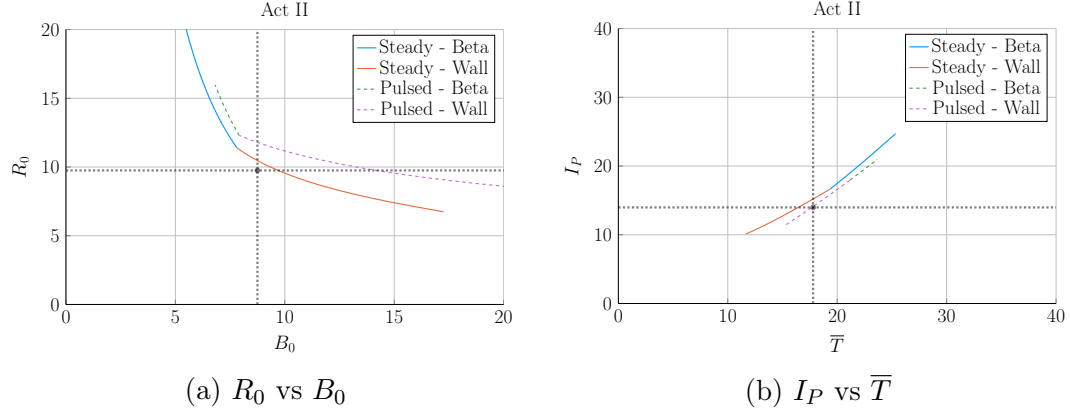


Figure 6-4: Aries Act II Model Comparison

Table 6.3: Act II Variables

(a) Input Variables

Input	Value
H	1.22
Q	25.0
N_G	1.3
ϵ	0.25
κ_{95}	1.964
δ_{95}	0.42
ν_n	0.41
ν_T	1.15
l_i	0.603
A	2.5
Z_{eff}	2.12
f_D	0.74
τ_{FT}	1.6e9
B_{CS}	12.77

(b) Output Variables

Output	Original	Fussy.jl
R_0	9.75	10.22
B_0	8.75	9.05
I_P	13.98	14.84
\bar{n}	0.86	0.82
\bar{T}	17.8	17.4
β_N	0.026	0.023
q_{95}	8.0	6.6
P_W	1.46	-
f_{BS}	0.77	0.66
f_{CD}	0.23	0.34
f_{ID}	-	-
V	2209	2559
P_F	2637	3460
η_{CD}	0.256	0.307

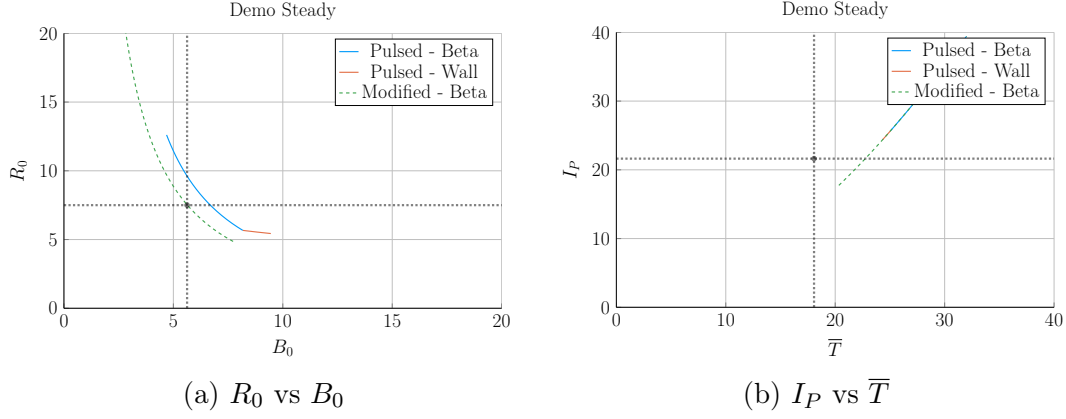


Figure 6-5: Demo Steady Model Comparison

Table 6.4: Demo Steady Variables

(a) Input Variables

Input	Value
H	1.4
Q	24.46
N_G	1.2
ϵ	0.385
κ_{95}	1.8
δ_{95}	0.333
ν_n	0.3972
ν_T	0.9187
l_i	0.900
A	2.856
Z_{eff}	4.708
f_D	0.7366
τ_{FT}	1.6e9
B_{CS}	12.85

(b) Output Variables

Output	Original	Fussy.jl	Modified
R_0	7.5	8.2	7.6
B_0	5.627	6.307	5.577
I_P	21.63	30.93	22.05
\bar{n}	0.875	1.048	0.855
\bar{T}	18.07	27.83	23.00
β_N	0.038	-	-
q_{95}	4.405	3.761	4.360
P_W	1.911	4.151	2.281
f_{BS}	0.611	0.424	0.492
f_{CD}	0.389	0.576	0.508
f_{ID}	-	-	-
V	2217	2879	2351
P_F	3255	8971	4306
η_{CD}	0.4152	-	-

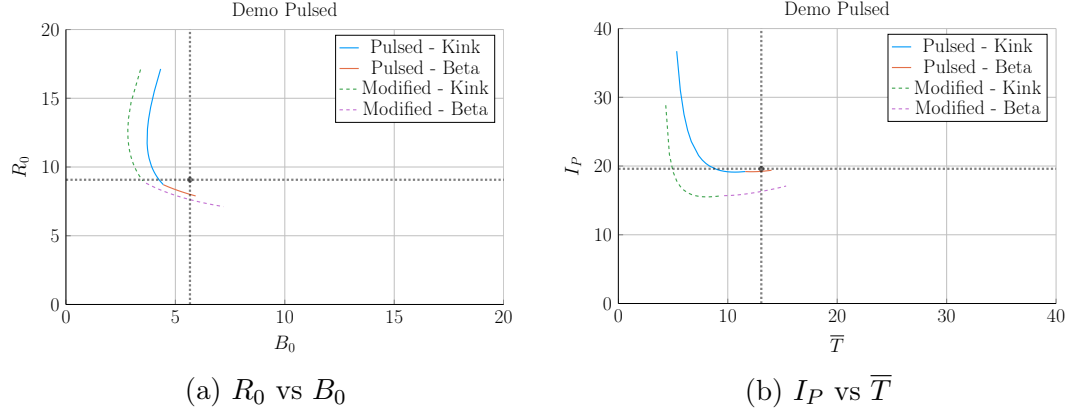


Figure 6-6: Demo Pulsed Model Comparison

Table 6.5: Demo Pulsed Variables

(a) Input Variables

Input	Value
H	1.1
Q	39.86
N_G	1.2
ϵ	0.3226
κ_{95}	1.59
δ_{95}	0.333
ν_n	0.27
ν_T	1.094
l_i	1.155
A	2.735
Z_{eff}	2.584
f_D	0.7753
τ_{FT}	7273
B_{CS}	12.77

(b) Output Variables

Output	Original	Fussy.jl	Modified
R_0	9.07	8.10	7.61
B_0	5.67	5.48	5.71
I_P	19.6	19.3	16.3
\bar{n}	0.7983	0.9795	0.9384
\bar{T}	13.06	13.28	13.00
β_N	0.0259	-	-
q_{95}	3.247	2.853	3.303
P_W	1.05	1.47	1.23
f_{BS}	0.348	0.164	0.190
f_{CD}	0.096	0.106	0.103
f_{ID}	0.557	0.730	0.707
V	2502	1751	1452
P_F	2037	2376	1756
η_{CD}	0.2721	-	-

1733 6.2 Developing Prototype Reactors

1734 Now that the model used in Fussy.jl has been tested against other fusion systems codes
1735 in the field, we will develop our own prototype reactors. Because this paper is about
1736 making a levelized comparison of pulsed and steady-state tokamaks, we will develop
1737 middle-of-the-road reactors that only differ by operating mode. The parameters for
1738 these two designs are captured in ????.

1739 To compare the two modes of operation, the steady-state prototype, Charybdis, is
1740 the obvious choice to start with – as the model was tested against four of these typed
1741 reactors. It was also pointed out that the model did remarkably well when recreating
1742 ARC. As the authors share many of the ARC team’s philosophies, Charybdis uses
1743 static parameters very similar to them.⁵

1744 Next, although led to believe Charybdis’ pulsed twin reactor – Proteus – would be
1745 created by a simple flip of the switch, it was a slight oversimplification. The first
1746 difference is that the pulsed twin, Proteus, is assumed to be purely pulsed: $\eta_{CD} = 0$.
1747 Further, the bootstrap current is much less important than it was for steady-state
1748 tokamaks. This corresponds to a current profile peaked at the origin – i.e. a parabola.
1749 Numerically, this is done by raising l_i from around 0.55 to 0.6.

1750 The final difference creates the largest change in the twin reactors: the choice of
1751 necessary technological advancement. As mentioned several times before, the H factor
1752 is a common way designers artificially boost the confinement of their machines. This
1753 H value will thus be the technological advancement needed for Charybdis, the steady-
1754 state prototype. Next, as the main conclusion of this paper is to state the advantages
1755 of high magnetic field, an inexpensive way to strengthen the central solenoid – through
1756 B_{CS} – will be employed using HTS coils.

1757 The goal now is to impose a constraint on a reactor’s economic competitiveness by
1758 setting the fusion power to a relatively low value for both designs – i.e. 1250 MW.
1759 As ?? shows, this results in Charybdis having an H factor of 1.7 and Proteus having
1760 a B_{CS} of around 20T. As shown in the Proteus cost curve, this was at a point where

1761 the ratio between the minimum capital cost and the minimum cost-per-watt leveled
1762 off.

1763 Note that these technological advancements (in H and B_{CS}) are necessary to get
1764 economic – or even physically realizable – reactors. This is the same reason why all
1765 the literature reactors used values for H and N_G that violate standard values.

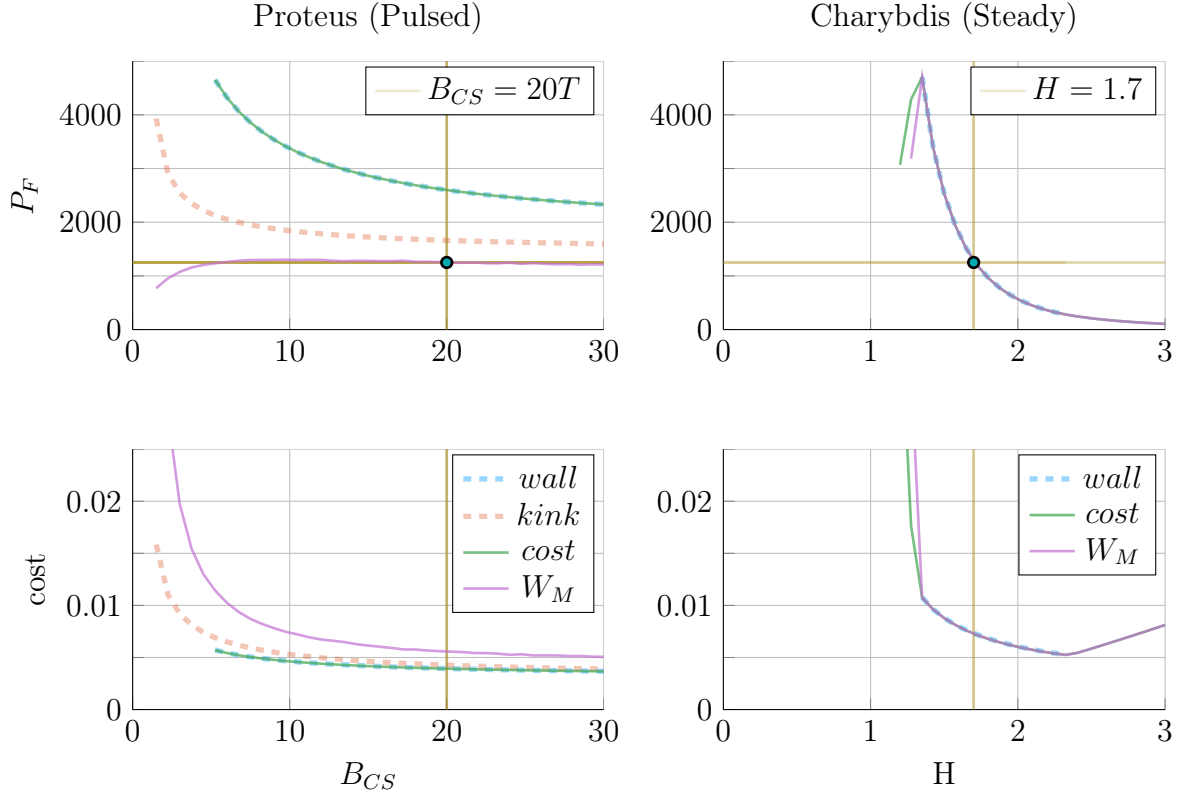


Figure 6-7: Designing Reactor Prototypes

As is convention in fusion engineering, designs are built using one assumed technological advancement. For steady-state reactors, we assume a method for improving confinement – by increasing H . While in the pulsed case, the advancement is inexpensive magnet technology for stronger fields in the central solenoid – B_{CS} .

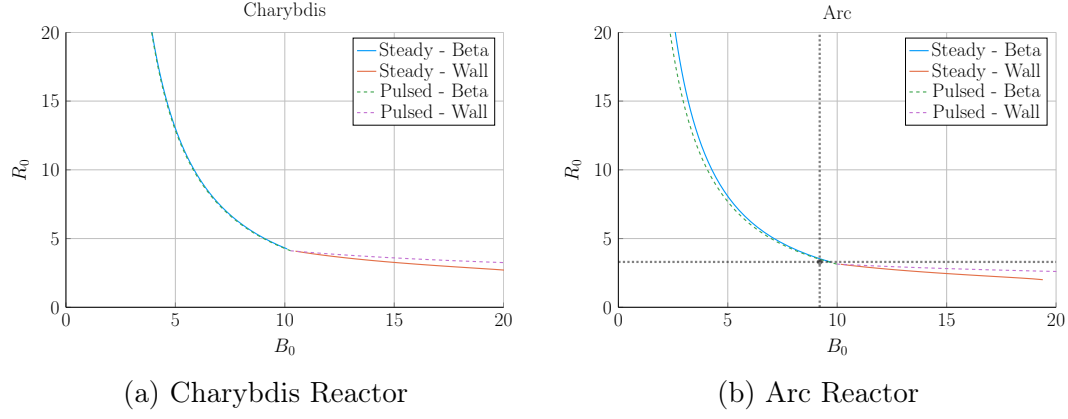


Figure 6-8: Steady State Prototype Comparison

Table 6.6: Charybdis Variables

(a) Input Variables

Input	Value
H	1.7
Q	25.0
N_G	0.9
ϵ	0.3
κ_{95}	1.8
δ_{95}	0.35
ν_n	0.4
ν_T	1.1
l_i	0.558
A	2.5
Z_{eff}	1.75
f_D	0.9
τ_{FT}	1.6e9
B_{CS}	12.0

(b) Output Variables

Output	Value
R_0	4.13
B_0	10.28
I_P	8.98
\bar{n}	1.47
\bar{T}	15.81
β_N	0.028
q_{95}	6.089
P_W	3.003
f_{BS}	0.723
f_{CD}	0.277
f_{ID}	0.0
V	225.5
P_F	1294
η_{CD}	0.291

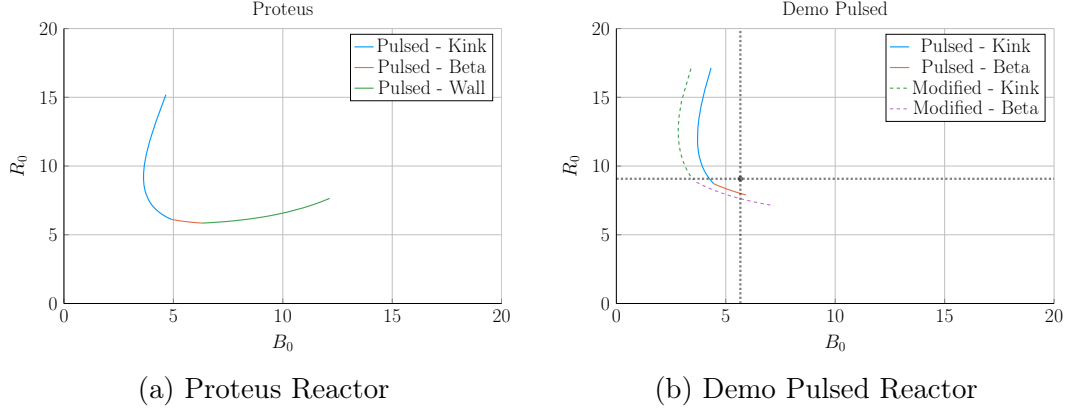


Figure 6-9: Pulsed Prototype Comparison

Table 6.7: Proteus Variables

(a) Input Variables

Input	Value
H	1.0
Q	25.0
N_G	0.9
ϵ	0.3
κ_{95}	1.8
δ_{95}	0.35
ν_n	0.4
ν_T	1.1
l_i	0.633
A	2.5
Z_{eff}	1.75
f_D	0.9
τ_{FT}	7200
B_{CS}	20.0

(b) Output Variables

Output	Value
R_0	6.11
B_0	4.93
I_P	15.54
\bar{n}	1.16
\bar{T}	11.25
β_N	0.028
q_{95}	2.5
P_W	1.763
f_{BS}	0.2675
f_{CD}	0.0
f_{ID}	0.7325
V	732.6
P_F	1667
η_{CD}	0.0

1766 6.2.1 Navigating around Charybdis

1767 The Charybdis reactor is the steady-state twin developed for this paper. As men-
1768 tioned, its parameters are similar to the ARC design. This is shown in ??, where the
1769 two $R_0 - B_0$ curves are almost interchangeable. Before moving on, it proves useful
1770 to note that the optimum place to build on these curves is where the two portions
1771 intersect – as it minimizes costs. These cost curves are shown in ??.

1772 6.2.2 Pinning down Proteus

1773 The pulsed twin reactor, Proteus, highlights the effects of a high field central solenoid.
1774 When compared to the Pulsed Demo design, the $R_0 - B_0$ curve looks far more favor-
1775 able – i.e. each machine built at a certain magnet strength would be more compact
1776 (and cheaper). An interesting facet of Proteus is that it exhibits all three used limits:
1777 kink safety factor, Troyon beta, and wall loading. Cost curves are shown in ??.

1778 6.2.3 Highlighting Operation Differences

1779 Before moving onto general conclusions taken from the data, a quick investigation
1780 into the pulsed vs steady-state twin results is in order. A comparison between the
1781 two is best abridged in ??.

1782 Most apparently, pulsed reactors are typically larger than steady-state ones and are
1783 meant to be run at higher plasma currents. The former behavior was seen with
1784 the DEMO designs,^{6,7} whereas the latter was already mentioned in discussing how
1785 steady-state reactors never saw a kink (current limiting) regime. Additionally pulsed
1786 machines can be run at much lower temperatures because their higher current im-
1787 proves confinement.

1788 These combined effects lead to the minimum cost reactors for steady-state operation
1789 having much higher toroidal field strengths than their pulsed counterparts. This is
1790 discussed in ?? when explaining optimum use of HTS tape.

Table 6.8: Proteus and Charybdis Comparison

(a) Charybdis		(b) Proteus	
Output	Value	Output	Value
R_0	4.13	R_0	6.11
B_0	10.28	B_0	4.93
I_P	8.98	I_P	15.54
\bar{n}	1.47	\bar{n}	1.16
\bar{T}	15.81	\bar{T}	11.25
f_{BS}	0.72	f_{BS}	0.27
f_{CD}	0.28	f_{ID}	0.73
P_F	1300	P_F	1650
W_M	9.48	W_M	7.09
C_W	0.007	C_W	0.004

1791 6.3 Learning from the Data

1792 Now that the model has been properly vetted and prototypes designed, we can ex-
 1793 plore how pulsed and steady-state tokamaks scale. This will lead to three mostly
 1794 independent results. The first result will explore how to minimize costs for a reactor
 1795 by choosing optimum design points. The next will be an argument for how to prop-
 1796 erly utilize the HTS magnet technology in component design. Lastly, we will take a
 1797 cursory look at the other parameters capable of lowering machine costs.

1798 6.3.1 Picking a Design Point

1799 With more than twenty design parameters, finding the most economic reactor is com-
 1800 putationally intractable. Intuition building aside, finding optimum reactors becomes
 1801 much more feasible when only focusing on dynamic variables – i.e. when keeping static
 1802 variables constant. This method, for example, is how all the $R_0 - B_0$ curves have
 1803 been produced this chapter. Once these curves are produced, it is up to the user to
 1804 choose which reactor on them to build. However, the guiding metric usually involves
 1805 lowering some cost, either: capital cost or cost-per-watt.

1806 Regardless of reactor type, most economic tokamaks operate near the beta limit –
 1807 where plasma pressure is greatest. Besides being a regime highly sensitive to magnetic

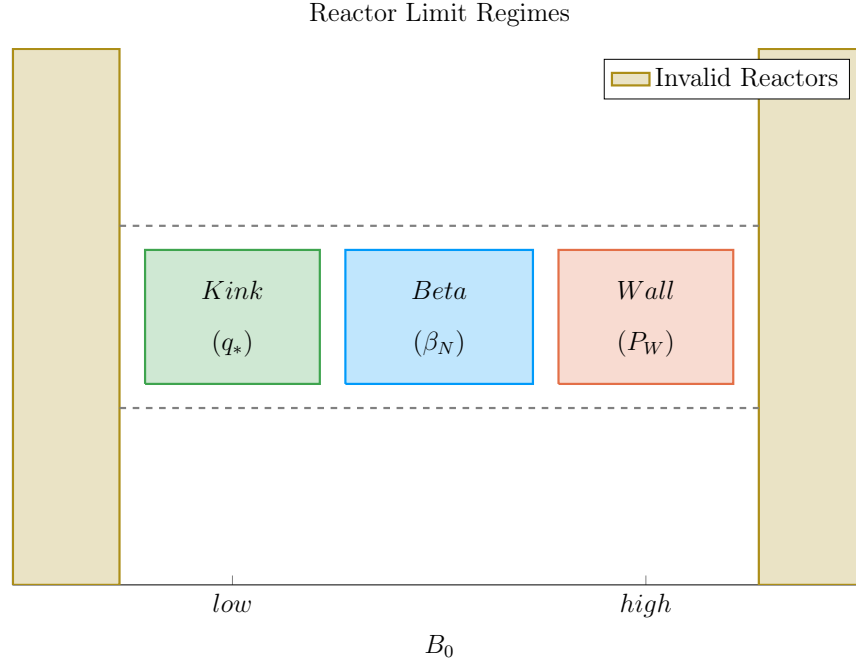


Figure 6-10: Limiting Constraint Regimes

At a simple level, a reactor has around three regimes of design limiting constraints. At low fields, the kink safety factor – through q_* and ?? – drives design. Then at high fields, wall loading – through P_W and ?? – guide reactors. And between the two, the beta limit – through β_N and ?? – are the limiting constraint.

1808 field strength, the beta limit is a constraint that occurs on every reactor (seen by the
 1809 authors). This beta limit (β_N) is usually nested between the kink limit (q_*) to lower
 1810 B_0 values and wall loading (P_W) to higher ones. Understanding these regimes is the
 1811 first step towards building an intuition favoring economic machines – see ??.

1812 Now that the beta limit curve has been designated as the most economic regime to
 1813 operate in (usually), the goal is to select which reactor on it is the best one to build.
 1814 Starting with the easier of the two, the optimum design point for steady-state reactors
 1815 is the point where wall loading first starts to dominate the design. Due to the wall
 1816 loading relation (see ??), this causes the reactor to start increasing in size and cost –
 1817 which is bad. This conclusion is justified by the cost curves for all five reactors in ??.
 1818 As these show, it is also where these reactor designers pinned down their tokamaks.*

* Simply stated, the optimum reactor for steady-state tokamaks is one that just barely satisfies the beta and wall loading limit simultaneously – i.e. where the two curves intersect.

1819 The problem of selecting an optimum design is more difficult for the pulsed case.
1820 This is mainly due to there being a regime where the kink safety factor can actually
1821 be a guiding limiting constraint. Following the conclusion from steady-state reactors
1822 would be an oversimplification because there are actually two costs relevant to a
1823 reactor: capital cost and cost-per-watt. These beta-wall reactors are actually the
1824 points often best for minimizing cost-per-watt (i.e. your rate of return). The new
1825 beta-kink reactors, then, lead to cheap to build machines – as they minimize capital
1826 cost. These conclusions are shown in ??.

1827 Summarizing the conclusions of this subsection, the beta limit is usually the best
1828 constraint to operate at. For lowering the cost-per-watt, a reactor should always be
1829 run at the highest magnetic field strength (B_0) that has the beta limit at its maximum
1830 allowed value. This most often occurs when wall loading takes over (for steady-state
1831 reactors) or reactors start being physically unrealizable (for pulsed ones). Building
1832 cheap to build reactors – i.e. minimizing capital cost – then actually proved to make
1833 pulsed design one of trade-offs. This is because the beta-kink curve intersection
1834 produces a low capital cost reactor, but at the price of operating at a subpar cost-
1835 per-watt. Designers should therefore balance the two cost metrics when pinning down
1836 a pulsed reactor.

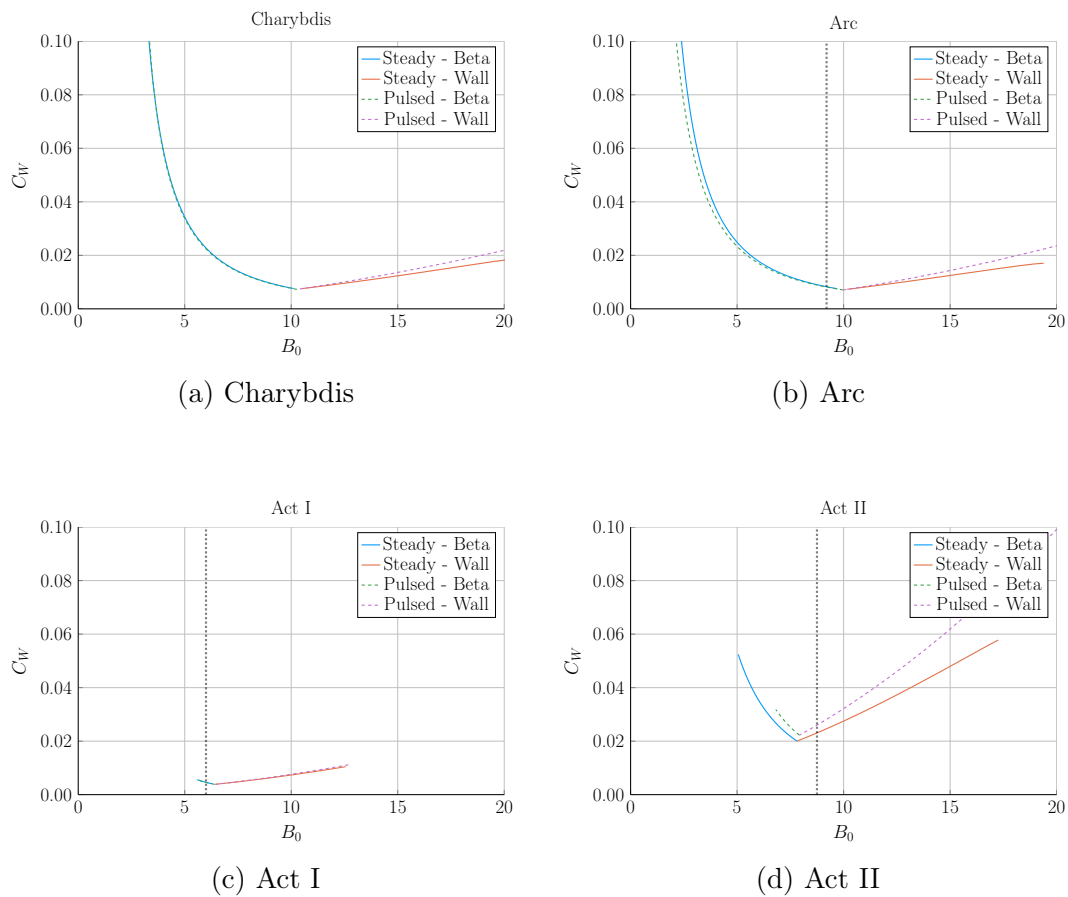
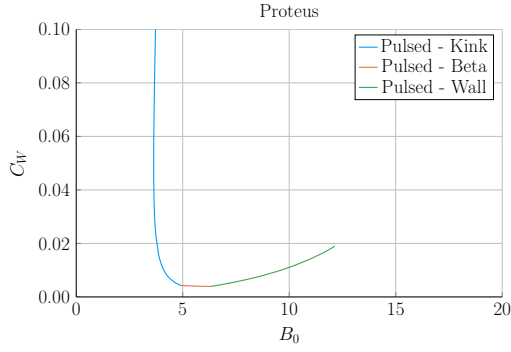
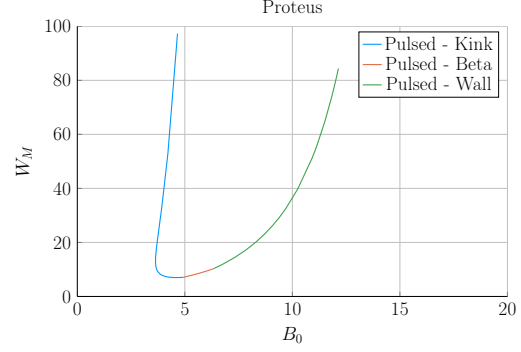


Figure 6-11: Steady State Cost Curves

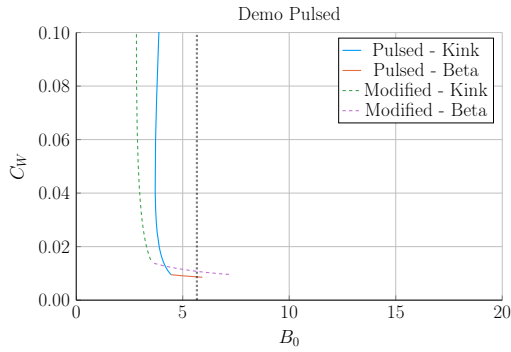
Steady state reactors typically have two regimes – a lower magnet strength **beta** limiting one and a high field **wall** loading one. As shown, each steady state scan produces a minimum cost reactor at the point where the two regimes meet.



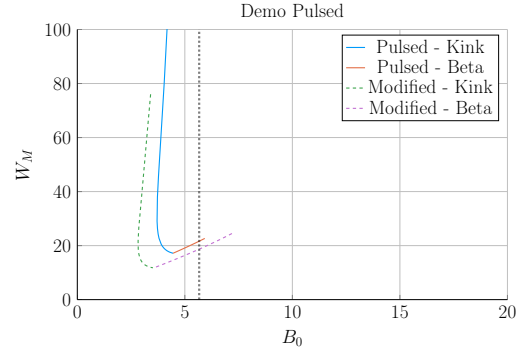
(a) Proteus Cost-per-Watt



(b) Proteus Capital Cost



(c) Demo Pulsed Cost-per-Watt



(d) Demo Pulsed Capital Cost

Figure 6-12: Pulsed Cost Curves

Pulsed reactor design is slightly more ambiguous than steady-state in terms of selecting an operating point. These plots show that the cost-per-watt is reduced at the highest field strength available to **beta** regime reactors. The minimum capital cost then occurs when the **beta** and **kink** limit are both just marginally satisfied.

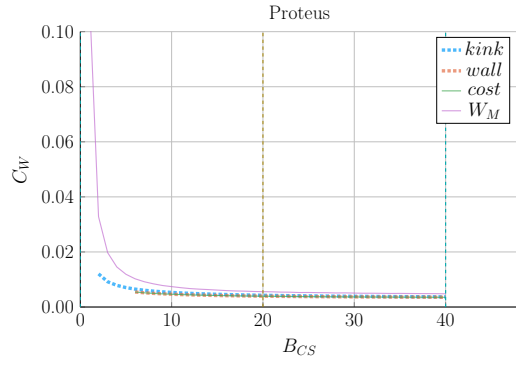
1837 6.3.2 Utilizing High Field Magnets

1838 The main conclusion for this paper is that high field magnets are the way to go to
1839 build an economic, compact fusion reactor. In line with the MIT ARC effort, these
1840 high fields will be built with high-temperature superconducting (HTS) tape. This
1841 innovation is set to nearly double the strength of conventional magnets. The real
1842 question is how best to use this technology.

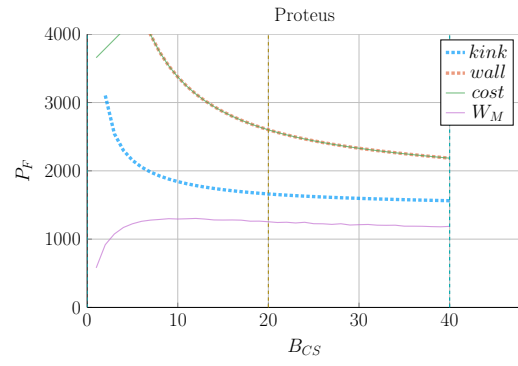
1843 At a very simple level, there are two main places strong magnets can be employed:
1844 the toroidal fields (B_0) and the central solenoid (B_{CS}). The easier mode of operation
1845 to start with is steady-state. This is because steady-state tokamaks do not rely on
1846 a central solenoid to run their functionally infinite length pulses. Further, the cost
1847 curves in ?? show that all these designs would benefit from toroidal fields (B_0) not
1848 achievable with conventional magnets – which can only reach around 13 T.

1849 The more interesting result is that pulsed reactors gain no real benefit from using
1850 HTS toroidal field magnets – as mentioned previously in ?. Within the modern
1851 paradigm (i.e. D-T fuel, H-Mode, etc), pulsed reactors never have to exceed the
1852 limits of less expensive LTS magnets. The place HTS can really help is with the
1853 central solenoid, which governs how long a pulse can last. Further, improvements
1854 to the central solenoid have diminishing returns past the range accessible to HTS
1855 tape. Again, HTS would be more than adequate for the modern paradigm. These
1856 conclusions are shown in ????.

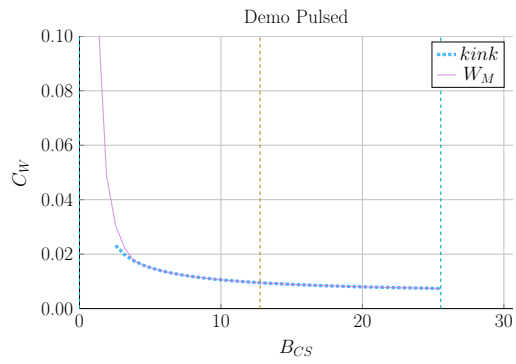
1857 Summarizing this subsection, HTS tape is one of the best ways to lower the cost of
1858 fusion reactors at a commercial scale. For steady-state reactors, HTS works best in
1859 the toroidal field coils (B_0), while the tape would fare better in the central solenoid
1860 (B_{CS}) of pulsed reactors. Further, both effects saturate within the range of this HTS
1861 tape, rendering more sophisticated magnetic technology unnecessary. HTS is thus
1862 one technological advancement that could help usher in an era of affordable fusion
1863 energy.



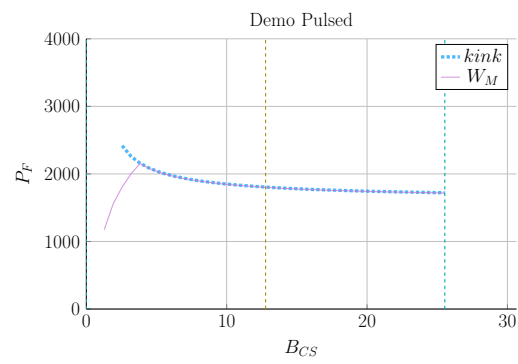
(a) Proteus Cost-per-Watt



(b) Proteus Fusion Power

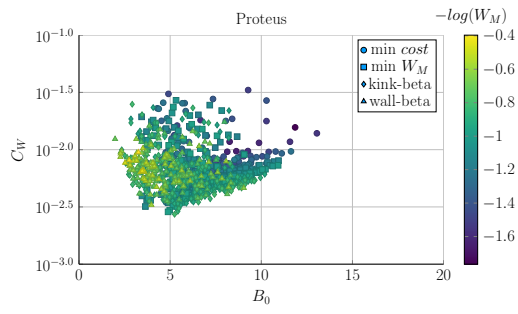


(c) Demo Pulsed Cost-per-Watt

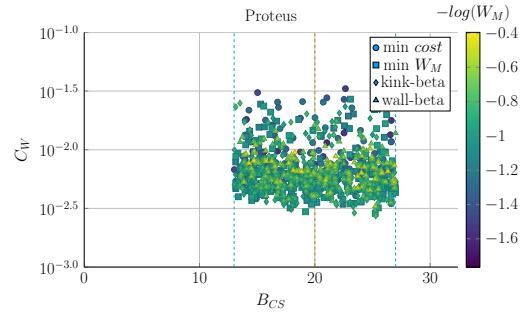


(d) Demo Pulsed Fusion Power

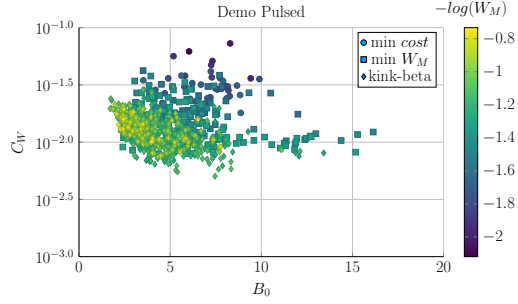
Figure 6-13: Pulsed B_{CS} Sensitivity



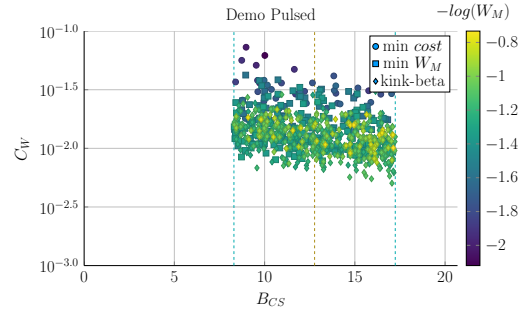
(a) Proteus B_0 Sampling



(b) Proteus B_{CS} Sampling



(c) Demo Pulsed B_0 Sampling



(d) Demo Pulsed B_{CS} Sampling

Figure 6-14: Pulsed Monte Carlo Sampling

1864 6.3.3 Looking at Design Alternatives

1865 Even in this relatively simple fusion model, there are more than twenty static/in-
1866 put variable knobs a designer can tune to improve reactor feasibility. Many have
1867 practical limits, such as being physically realizable or fitting within the ELMy H-
1868 Mode database. Thus, the goal of this subsection is to investigate some of the more
1869 interesting results. Although many more plots are available in the appendix.

1870 Capitalizing the Bootstrap Current

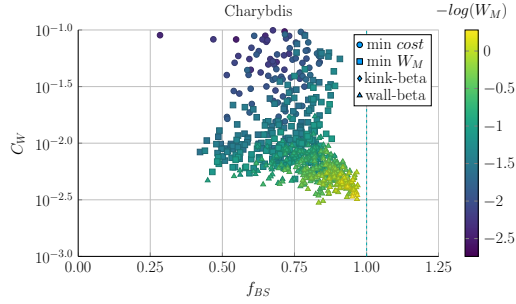
1871 Besides artificially enhancing a plasmas confinement with the H-factor, steady-state
1872 reactor designers may also heavily rely on high bootstrap currents. This is because
1873 bootstrap current is the portion of current you do not have to pay for. The research
1874 groups most focused on this technological advancement are General Atomic's DIII-
1875 D in San Diego and PPPL's NSTX-U in New Jersey. This advancement relies on
1876 tailoring current profiles to be much more hollow.

1877 Quickly reasoning this thought process are two sets of plots. The first plot (??)
1878 highlights how the cheapest possible steady-state designs have bootstrap fractions
1879 approaching unity – they use almost no current drive. This makes sense as current
1880 drive is extremely cost prohibitive (i.e. why people consider pulsed tokamaks).

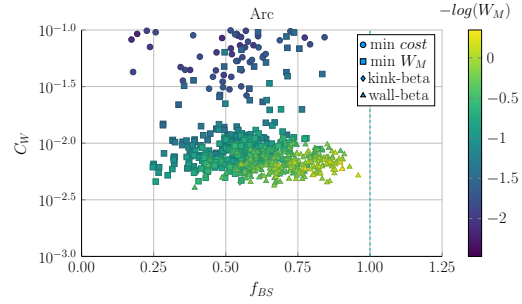
1881 The next plot (??) is the parameter that determines a current profile's peak radius:
1882 l_i . As can be seen, the current peak approaches the outer edge of the plasma as
1883 l_i decreases. This in turn boosts the bootstrap fraction closer to one – leading to
1884 inexpensive reactors.

1885 Contextualizing the H-Factor

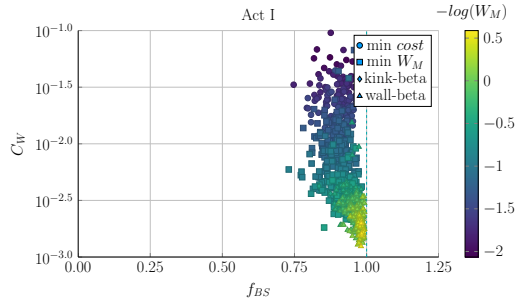
1886 From before, increasing the H-factor always led to more cost effective steady-state
1887 reactors. This is because the enhanced confinement allows for smaller machines.
1888 This was already heavily explored in ??. These plots also show that steady state



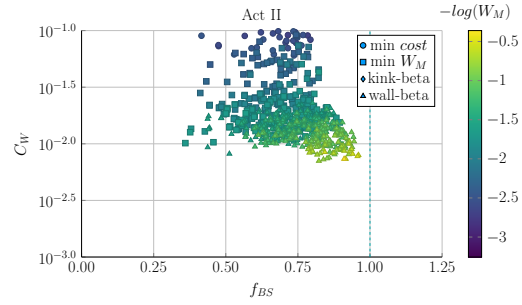
(a) Charybdis l_i Sampling



(b) Arc l_i Sampling



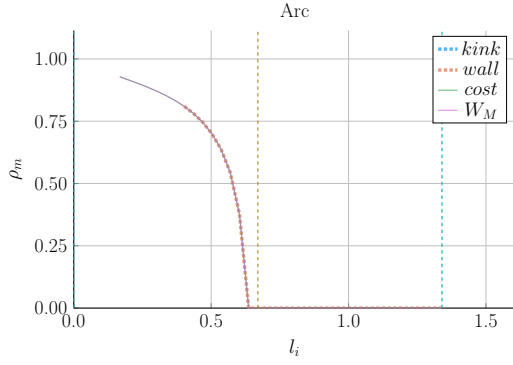
(c) Act I l_i Sampling



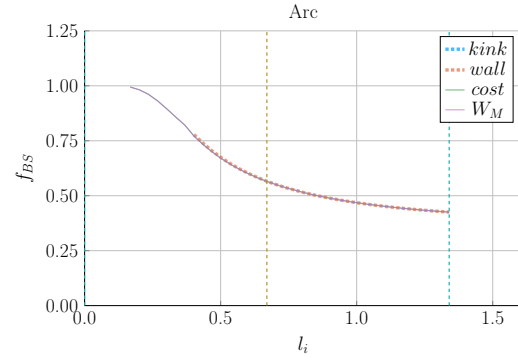
(d) Act II l_i Sampling

Figure 6-15: Bootstrap Current Monte Carlo Sampling

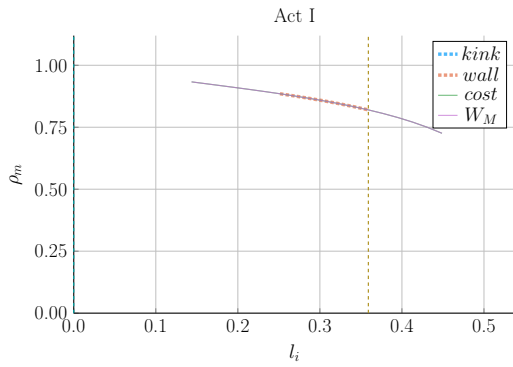
The purpose of these plots is to show that a high bootstrap current always reduces the cost of a steady state reactor – highly independent of actual input quantities (i.e. ϵ , l_i , etc.)



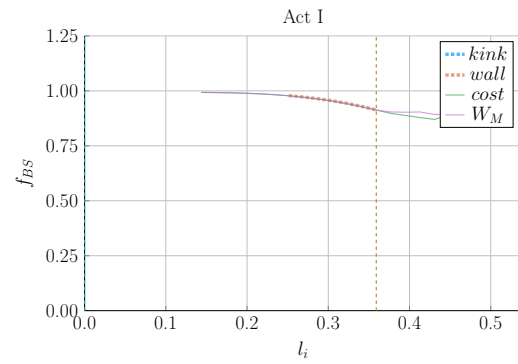
(a) Arc Peak Radius



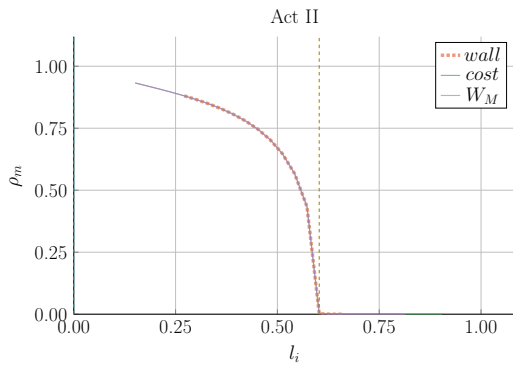
(b) Arc Bootstrap Fraction



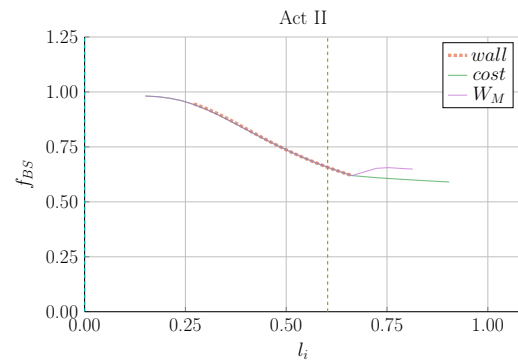
(c) Act I Peak Radius



(d) Act I Bootstrap Fraction



(e) Act II Peak Radius



(f) Act II Bootstrap Fraction

Figure 6-16: Internal Inductance Sensitivities

The internal inductance has a strong influence on the peaking radius (ρ_m) of the hollow profile and the bootstrap current fraction (f_{BS}). Lowering the internal inductance thus makes a profile more hollow, which in turn increases the bootstrap fraction.

1889 reactors would not be physically possible using a default H factor of one! In other
1890 words, steady-state tokamaks require some technical advancement before they can
1891 ever be used as fusion reactors. The same cannot be said for pulsed machines.

1892 For pulsed reactors, increasing H always reduces capital cost, but may actually in-
1893 crease the cost-per-watt. This is because the fusion power can decrease at a faster
1894 rate than the capital cost in a pulsed tokamak – both of which appear in ?? defin-
1895 ing the cost-per-watt. This interesting result demonstrates the unusual behaviors of
1896 highly non-linear systems: masterclass intuition may not match model results.

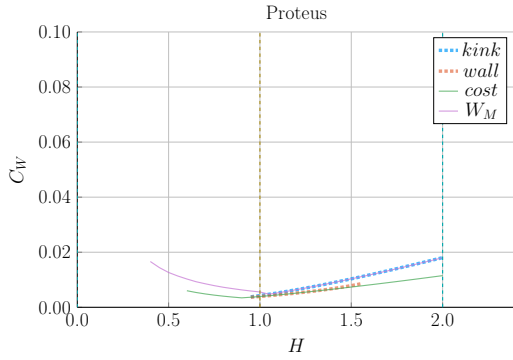
1897 **Showcasing the Current Drive Efficiency**

1898 The last exploration is less about building an economic machine and more about
1899 understanding the self-consistent current drive efficiency in steady-state tokamaks.
1900 Using the Ehst-Karney model¹⁷ coupled with standard analysis⁴ leads to a remarkably
1901 simple and accurate solver. As shown in ??, the model captures the physics almost
1902 exactly for the different designs.*

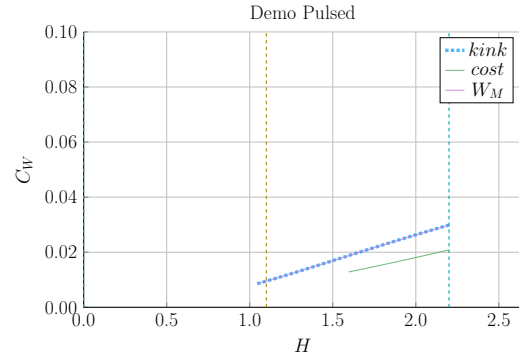
1903 In a similar fashion as the bootstrap fraction results, the variable that most captures
1904 how to directly maximize η_{CD} is the LHCD wave launch angle, θ_{wave} . When below
1905 90° it is considered outside launch, whereas up to 135° it is considered inside launch.
1906 Notably, these curves are not monotonic, there is an optimum launching angle – as
1907 shown in ??.

1908 It should be noted that the launch angle was not found to have a major impact. This
1909 may be a due to an oversimplification of the model, as sources suggest inside launch
1910 is preferable for multiple reasons./citeadx

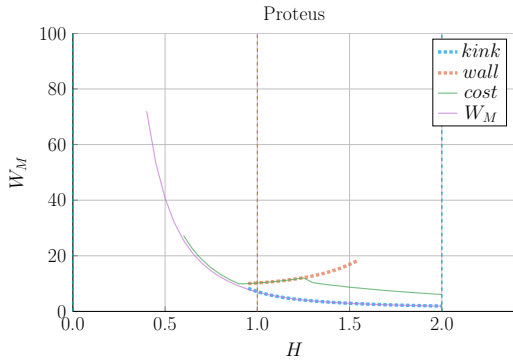
* It did, however, not converge for the DEMO steady reactor. This is probably due to lack of self-consistency for η_{CD} in their systems framework.



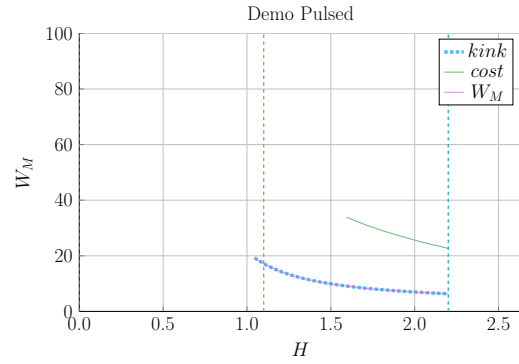
(a) Proteus Cost-per-Watt



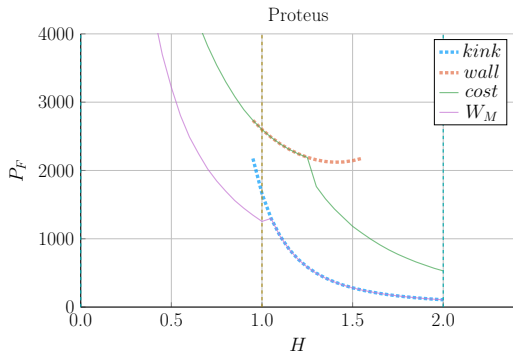
(b) Demo Pulsed Cost-per-Watt



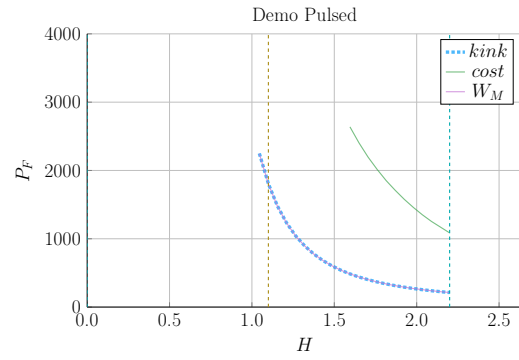
(c) Proteus Capital Cost



(d) Demo Pulsed Capital Cost

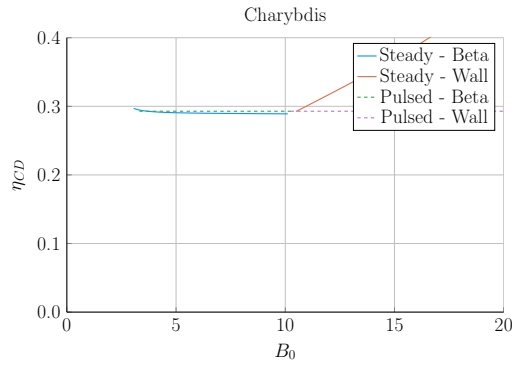


(e) Proteus Fusion Power

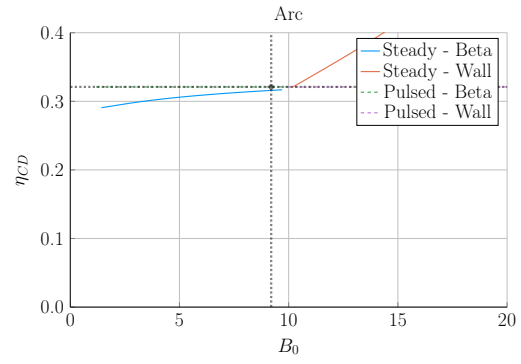


(f) Demo Pulsed Fusion Power

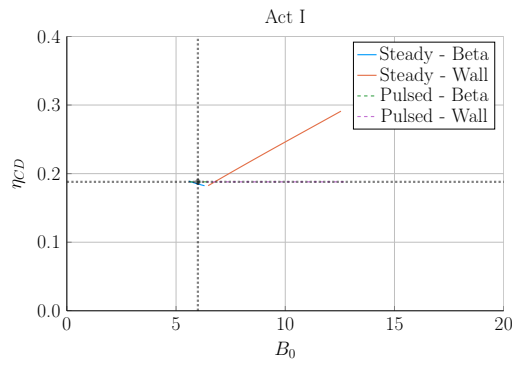
Figure 6-17: Pulsed H Sensitivities



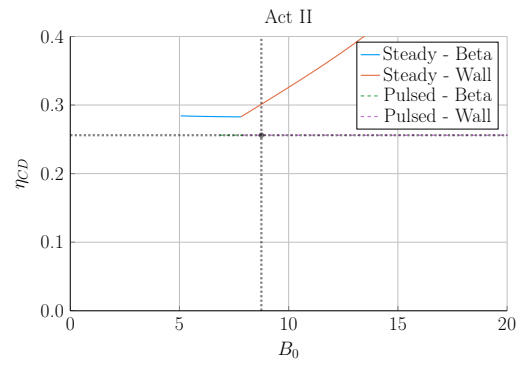
(a) Charybdis



(b) Arc

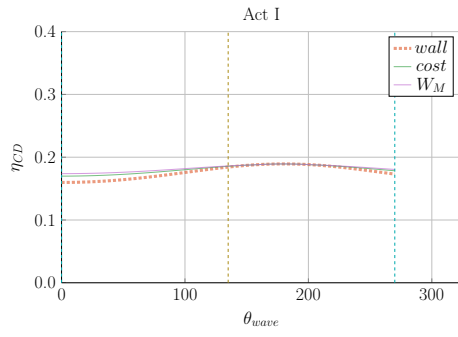


(c) Act I

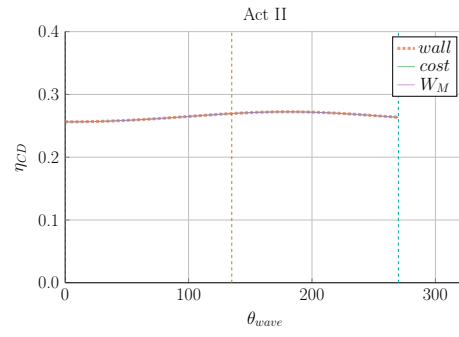


(d) Act II

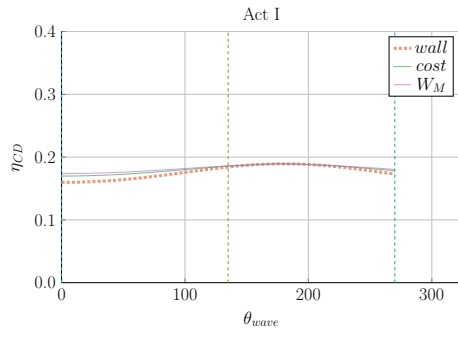
Figure 6-18: Steady State Current Drive Efficiency



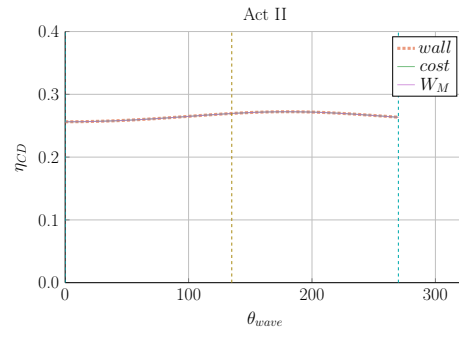
(a) Charybdis



(b) Arc



(c) Act I



(d) Act II

Figure 6-19: Current Drive Efficiency vs Launch Angle

Chapter 7

Planning Future Work for the Model

This model may run and produce interesting results, but there is always more to be done. This chapter explores three potential fusion reactors that could help guide real world designs. These are: a stellarator (Ladon), a steady-state/pulsed composite (Janus), and a tokamak capable of reaching H, L, and I modes (Daedalus). The chapter then concludes by describing several possible model improvements, including: adding radiation sources, using pedestal profiles, and improving flux balance.

7.1 Incorporating Stellarator Technology – Ladon

A stellarator is, at a basic level, a tokamak helically twisted along the length of its major circle. For a long time they were dismissed because of their poor transport properties. Recent technological improvements, though, have eased this situation – as seen with the Wendelstein 7-X device in Germany. The problem now is engrained in the underdeveloped scaling laws stemming from a lack of machines and, more fundamentally, data points.

To model Ladon, this paper’s proposed stellarator, one would need to replace at least: the Greenwald density limit and the confinement time scaling law. In place of the Greenwald density will likely be some other density or current limit, possibly the

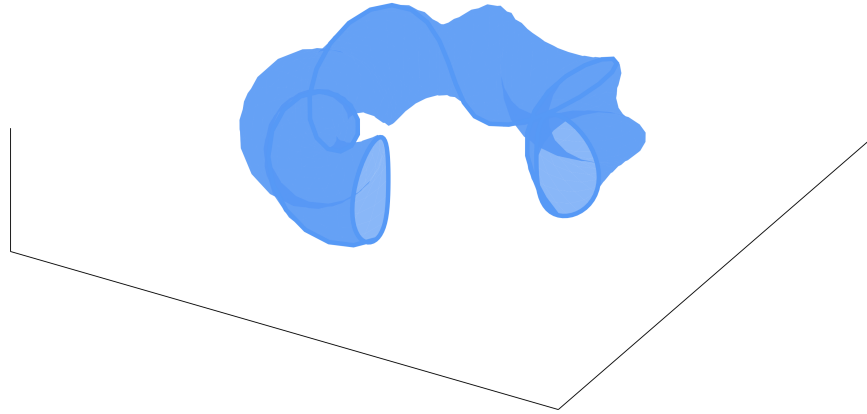


Figure 7-1: Cut-Away of Stellarator Reactor

1929 Bremsstrahlung density limit.²⁸ This may require the density to be carried throughout
 1930 analysis – thus appearing explicitly in one column of ??.

1931 7.2 Making a Composite Reactor – Janus

1932 The next interesting reactor would be a composite tokamak incorporating pulsed and
 1933 steady-state operation: Janus. Fundamentally, this would involve current coming
 1934 from both LHCD (steady-state), as well as inductive (pulsed) sources. This was
 1935 actually used in Demo Pulsed, but the current drive was not handled self-consistently.
 1936 Coupling these two current sources could reduce reliance on bootstrap current and
 1937 lead to much more compact machines.

1938 The arguments against this are mainly technical: why build two difficult auxiliary
 1939 systems when one is needed – especially when they probably work against each other.
 1940 Although rational, it may turn out that the larger current achievable with two sources
 1941 leads to a smaller, more economic machine.

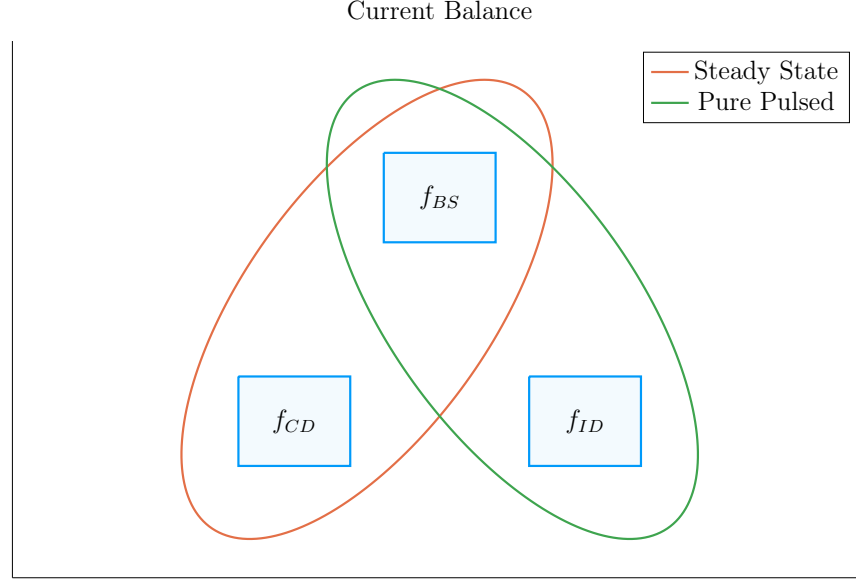


Figure 7-2: Current Balance in a Tokamak

In a tokamak, there needs to be a certain amount of current – and that current has to come from somewhere. All good reactors have an adequate bootstrap current. What provides the remaining current is what distinguishes steady state from pulsed operation.

7.3 Bridging Confinement Scalings – Daedalus

The final potential reactor – Daedalus – is designed so that it can be run in H-Mode, L-Mode, and I-Mode. Because L-Mode is available on any machine, the first step is actually building under H-Mode. The goal then is to find reactors that can also reach I-Mode – simultaneously improving the scaling law’s fit and possibly making the actual reactor more economic.

Presented below are the three confinement scaling laws, as well as the generalized formula. As should be noted, the I-Mode scaling currently lacks a true radial dependence – as it has only been found on two machines. This is one reason Daedalus would be so valuable.

$$\tau_E^G = K_\tau H \frac{I_P^{\alpha_I} R_0^{\alpha_R} a^{\alpha_a} \kappa^{\alpha_\kappa} \bar{n}^{\alpha_n} B_0^{\alpha_B} A^{\alpha_A}}{P_{src}^{\alpha_P}} \quad (??)$$

$$\tau_E^H = 0.145 H \frac{I_P^{0.93} R_0^{1.39} a^{0.58} \kappa^{0.78} \bar{n}^{0.41} B_0^{0.15} A^{0.19}}{P_{src}^{0.69}} \quad (??)$$

1952

$$\tau_E^L = 0.048 H \frac{I_P^{0.85} R_0^{1.2} a^{0.3} \kappa^{0.5} \bar{n}^{0.1} B_0^{0.2} A^{0.5}}{P_{src}^{0.5}} \quad (7.1)$$

1953

$$\tau_E^I = \frac{0.014 H}{0.68^{\lambda_R} \cdot 0.22^{\lambda_a}} \cdot \frac{I_P^{0.69} R_0^{\lambda_R} a^{\lambda_a} \kappa^{0.0} \bar{n}^{0.17} B_0^{0.77} A^{0.0}}{P_{src}^{0.29}} \quad (7.2)$$

1954

$$\lambda_R + \lambda_a = 2.2 \quad (7.3)$$

1955 A final point to make is reemphasizing that the I-Mode scaling law is significantly
1956 underdeveloped It is the target of ongoing research at the MIT PSFC.

1957 7.4 Addressing Model Shortcomings

1958 Before moving on to the final conclusions, we will give a quick recap of several of the
1959 more overly simplified phenomena in this fusion systems framework. These include:
1960 approximating temperature profiles as simple parabolas, neglecting all radiation ex-
1961 cept Bremsstrahlung, and handling flux sources at too basic a level. This list is
1962 non-comprehensive, as more sophisticated analysis would also help: the divertor heat
1963 load, the neutron wall loading, etc.

1964 7.4.1 Integrating Pedestal Temperature Profiles

1965 One of the biggest shortcomings of this model is not handling plasma profiles self-
1966 consistently – instead replacing them with simple parabolas. Although these parab-
1967 olas work for densities and L-Mode plasma temperatures, the same cannot be said
1968 about H-Mode temperatures. This is because they have a distinct pedestal region on
1969 the outer edge of the plasma.

1970 The usage of pedestal temperatures – discussed in the appendix – improves two as-
1971 pects of the model: the fusion power and the bootstrap current. These were shown in
1972 the results to be over-calculated and underestimated, respectively. Pedestals, having
1973 a lower core temperature, would decrease the total fusion power. As well, they would
1974 boost bootstrap current due to the quick drop near the plasma’s edge (i.e. they have
1975 a large derivative there).

1976 These improvements could easily be added to the code, because temperature was
1977 addressed as a difficult parameter to handle from the beginning.

1978 **7.4.2 Expanding the Radiation Loss Term**

1979 The next area that would be improved by more sophisticated theory would be the
1980 radiation loss term. From before, it was pointed out that the Bremsstrahlung ra-
1981 diation was the dominant term within the plasma core and, therefore, provided a
1982 first-order approximation. Drawing the radiation losses closer to real world values
1983 would involve adding line radiation and synchrotron radiation. The former of which
1984 would be needed as high-Z impurities become more important.

1985 **7.4.3 Taking Flux Sources Seriously**

1986 The final oversimplification in the model deals with the flux sources involved in a
1987 pulsed reactor – existing at almost every level. First, the derivation of flux bal-
1988 ance started with a simple transformer between a solenoid primary and a plasma
1989 secondary.

1990 After we developed an equation for flux balance, we compared it to ones in the
1991 literature (i.e. PROCESS) to build confidence in the model. To draw this equation
1992 closer to theirs, we then added a PF coil contribution a posteriori. This implicitly
1993 ignored coupling between most of the components. Thus leading to another source
1994 of error for the model. Moreover, this formula for PF coil contribution was much
1995 simpler than ones found in other fusion systems codes.

1996 Even though this model may be extremely simple, it does remarkably well at matching
1997 more sophisticated codes – and does so at a much faster pace. These suggestions were
1998 just ways to account for more realistic physics.

1999 Chapter 8

2000 Concluding Reactor Discussion

2001 The goal of this document was to fairly compare pulsed and steady-state tokamaks
2002 – using a single, comprehensive model. The main conclusion is that both modes of
2003 operation can produce economic reactors, assuming some technological advancement.
2004 The advancement most supported by the results was in magnet technology, as MIT
2005 is currently exploring with high-temperature superconducting (HTS) tape.

2006 Although some skepticism should be allotted to these conclusions, it was shown that
2007 this simple algebraic solver was capable of matching more sophisticated frameworks
2008 with speed and ease. This model may not provide an engineer’s level of rigor for cost
2009 measurements, but does produce empirically-drawn trends applicable to a physics au-
2010 dience. Ultimately, it serves to complement higher dimension codes when researchers
2011 want to investigate new areas of reactor space.

2012 What the results truly show, though, is no economic reactor can be built using existing
2013 technology – regardless of whether it runs as pulsed or steady-state. This is why every
2014 design from the literature exceeds standard values for H and N_G . Some technological
2015 advancement is needed. These may then come from research and development into:

- 2016 • building stronger magnets using HTS tape
- 2017 • discovering reliable regimes of enhanced confinement
- 2018 • producing higher bootstrap fractions with tailored profiles

2019 • optimizing aspect ratio and elongation geometric parameters

2020 As mentioned, using HTS tape to nearly double achievable magnet strengths is one
2021 such advancement capable of making reactors economically viable. To best utilize
2022 this resource, though, HTS tape should only appear in the TF coils for steady-state
2023 machines and in the central solenoid for pulsed ones. This was because the opti-
2024 mum toroidal field strength for pulsed machines was found to be achievable with
2025 conventional low-temperature superconducting (LTS) magnets.

2026 Further, it was shown that past the regime of magnet strengths relevant to HTS, cost
2027 curves undergo considerably diminished returns. As such, HTS technology would be
2028 the final major magnet advancement in the current H-Mode, D-T plasma paradigm.

Appendix A

Cataloging Static Variables

Table A.1: List of Static Variables

Name	Value
is_pulsed	is reactor pulsed or steady-state
H	h factor for ELMy H-mode scaling
Q	Physics Gain (P_F/P_H)
ϵ	inverse aspect ratio
κ_{95}	elongation at 95 flux surface
δ_{95}	triangularity at 95 flux surface
ν_n	parabolic density peaking factor
ν_T	parabolic temperature peaking factor
Z_{eff}	effective charge
f_D	dilution factor
A	average mass number (in amus)
l_i	internal inductance (interchangeable with ρ_m)
ρ_m	normalized radius of current peak (interchangeable with l_i)
N_G	Greenwald density fraction
η_T	thermal efficiency of the reactor
η_{RF}	efficiency of the RF antenna
τ_{FT}	time of flattop of reactor pulse
B_{CS}	strength of magnetic field in central solenoid
$(\beta_N)_{max}$	max allowed normalized beta normal
$(q_*)_{max}$	min allowed safety factor
$(P_W)_{max}$	maximum allowed wall loading power per surface area

2031 Appendix B

2032 Simulating with Fussy.jl

2033 Fussy.jl is a 0-D fusion systems code written using the Julia language. The reason for
2034 choosing Julia over say Matlab and Python was due to metaprogramming concerns
2035 and its tight-knit computational community, respectively. Incorporating the model
2036 used throughout this paper, the code is quick to run and matches more sophisticated
2037 frameworks with high fidelity.

2038 This chapter will be broken down into three steps. The first is getting a user up
2039 and running with the code. Once the user gets to this point, hopefully they will
2040 wonder how the code is structured. This will be the second step. The final step
2041 will be explaining the various functions callable on reactor objects – the atomic data
2042 structure for Fussy.jl.

2043 B.1 Getting the Code to Work

2044 The hardest step of any codebase is getting it up and running. These instructions
2045 should get a user to a point where they are a few internet searches away from a
2046 working copy of Fussy.jl. As an aide, you can view an interactive collection of Fussy.jl
2047 Jupyter notebooks at the following website:

2048 www.fusion.codes

2049 Although `fusion.codes` is a nice tool for viewing this document’s results, it is a little
2050 slow for producing new data – and it also lacks a method for storing it. Therefore,
2051 an advanced user should first download a copy of Julia from:

2052 julialang.org/downloads

2053 Currently the `Fussy.jl` codebase is written using `v0.6`, but should be `v1.0` compatible
2054 by 2019. Using Julia nomenclature, `Fussy.jl` is a Julia package. It can be cloned using
2055 Julia conventions from the following Github repository:

2056 <https://github.com/djseagal/Fussy.jl.git>

2057 Once the `Fussy.jl` package has been cloned into your Julia package library, you should
2058 be able to access it through the Julia REPL or a Jupyter notebook. You can now
2059 reproduce every plot in this text. A quick test to see if your code works is:

2060

```
2061     using Fussy
2062     cur_reactor = Reactor(15)
2063
2064     @assert cur_reactor.T_bar == 15
```

2065 B.2 Sorting out the Codebase

2066 Assuming the user got to this section, the code works and now you want to know
2067 what you can do with it. The place to start is in the `src` folder, again viewable online
2068 at:

2069 git.io/tokamak

2070 Within the `src` folder are several subfolders as well as a few files (e.g. `Fussy.jl` and
2071 `defaults.jl`). In an attempt to not bore the reader, we will be painting with thick
2072 brushstrokes. Further, the `methods` subfolder will be the topic of the next section –
2073 as most involve calls on a reactor object.

2074 **B.2.1 Typing out Structures**

2075 The place to start in any modeling framework is its data structures. These type
2076 definitions allow the building of nested hierarchies of constructed objects. The most
2077 atomic of these is the Reactor struct, but several other ones allow for solving broader
2078 scoped questions (i.e. Scans, Sensitivities, and Samplings.)

2079 **The Reactor Structure**

2080 Reactors are the most atomic data structure in this fusion systems model. They
2081 store all the fields needed to represent a reactor as it exists in reactor space. This
2082 obviously includes its temperature, current, and radius, but also includes derived
2083 quantities, such as the cost-per-watt and bootstrap fraction. They can be initialized,
2084 solved, updated, and honed. Most other data structures are just wrappers to hold
2085 these reactors – they are described next.

2086 **The Scan Structure**

2087 A Scan object is a collection of reactors made from scanning a list of temperatures.
2088 For example, a scan of five temperatures from 5 keV to 25 keV would result in several
2089 arrays of five reactors. Most often, one of these lists would correspond to beta reactors,
2090 one to kink reactors, and one to wall loading reactors. There may then be fewer than
2091 five reactors in a list if some of the reactors are invalid or fundamentally unsolvable.
2092 This is the data structure that produces the various comparison plots in the results.

2093 **The Sensitivity Structure**

2094 Sensitivity studies are how computationalists test the effect of changing a variable
2095 over multiple values – i.e. do a 20% sensitivity around the H factor. Like Scans,
2096 Sensitivities store various lists of reactors, each corresponding to an interesting data
2097 point. These include limit reactors where the beta limit and kink limit are just

2098 satisfied or when the beta limit and wall loading are just satisfied. Additionally, they
2099 include the minimum capital cost reactors and the minimum cost-per-watt ones.

2100 **The Sampling Structure**

2101 The Sampling struct was created to do simple Monte Carlo runs over a reactor's static
2102 values. While sensitivities only allow one variable to change at a time, samplings
2103 randomly assign a list of variables to some neighborhood of possible values. These
2104 are how the scatter plots are made. Succinctly, where sensitivity studies show local
2105 changes to variables, Monte Carlo samplings show global trends in reactor design.

2106 **The Equation Structure**

2107 In order to store the various equations from ?? is the Equation Struct. It stores the γ
2108 exponents for: R_0 , B_0 , and I_P . – as well as the function representing $G(\overline{T})$. Repeated
2109 these are the unknowns in:

$$R_0^{\gamma_R} \cdot B_0^{\gamma_B} \cdot I_P^{\gamma_I} = G(\overline{T}) \quad (??)$$

2110 Concretely, there are 16 objects that use this struct – one for each equation (e.g. for
2111 fusion power, the beta limit, and temperature assignment).

2112 **The Equation Set Structure**

2113 The step up from the Equation struct are the Equation Sets. These collections of
2114 three equations allow R_0 , B_0 , and maybe I_P to be substituted out of the current
2115 balance root-solving equation. This is where ?????????????? come into play.

2116 B.2.2 Referencing Input Decks and Solutions

2117 With more than twenty static variables in the model, the range of tokamak reactors
2118 is basically infinite. To help users build a net of designs to explore reactor space
2119 are seven input decks. These are the ones given in the results: Arc, Act I /II, Demo
2120 Steady/Pulsed, Proteus and Charybdis. Coupled with the non-prototype reactors are
2121 solution reactors that store various quantities from the original papers (e.g. P_F , f_{BS} ,
2122 R_0). These are how the comparison tables were constructed.

2123 B.2.3 Acknowledging Utility Functions

2124 For the uninitiated, utility functions are grab bag functions that do not really belong
2125 in a codebase – but do anyway. This sentiment does not mean they are worthless,
2126 just not fusion related at all. In Fussy.jl, the most notable are a normalized integral
2127 calculator, a filter that includes numeric tolerances, and a robust root solver.

2128 Although since incorporated into the official Roots.jl package, `find_roots` allows
2129 finding an arbitrary number of roots within a bounded range. This was needed
2130 because many roots can be found at various levels of the reactor solving problem –
2131 i.e. for I_P , \bar{T} , η_{CD} , etc.

2132 B.2.4 Mentioning Base Level Files

2133 In addition to subdirectories within the `src` folder are three files: Fussy.jl, abstracts.jl,
2134 and defaults.jl. Fussy.jl is the package’s main file that actually stores the Fussy
2135 module. While, abstracts.jl stores various abstract structures that help clean up
2136 other files.

2137 Finally, defaults.jl stores various default values that are important to the codebase.
2138 For example, this is where the various scaling law exponents are stored. It is also
2139 where the bounding values for the different root solving problems live. These include
2140 minimum and maximum values for: I_P , \bar{T} , η_{CD} .

2141 Now that a majority of the files have been discussed, we can turn to the reactor
2142 methods. These constitute most of the interesting functionality within the codebase.

2143 B.3 Delving into Reactor Methods

2144 The reactor is the most atomic data structure in this model. It therefore makes
2145 sense that it has many instance methods. These include all the coefficients, fluxes,
2146 powers, etc. It also includes methods that solve a reactor, perform a match on some
2147 field's value, or converge η_{CD} to self-consistency. The various subdirectories within
2148 the `src/methods/reactors` folder will now be discussed.

2149 Calculations

2150 The calculation subdirectory of reactor methods are used to set various important
2151 values in the solver. For dynamic variables, these include: \bar{n} , R_0 , B_0 , and I_P . This
2152 folder also includes the calculation of the Bosch-Hale reactivity and the Ehst-Karney
2153 current drive efficiency.

2154 Coefficients and Composites

2155 The coefficients and composites directories correspond to the model's static and dy-
2156 namic coefficients, respectively. For clarity, static coefficients, including K_n and K_{CD} ,
2157 were labeled with a K. Whereas, dynamic coefficients then started with G's – i.e. G_{PB}
2158 and G_V .

2159 Fluxes and Powers

2160 Within flux balance and power balance were around a dozen terms or sub-terms.
2161 Although not directly used in the conservation equations, sub-terms are used to com-
2162 pare the model to ones from the literature. For clarity, fluxes include: Φ_{CS} , Φ_{PF} ,
2163 Φ_{RU} , Φ_{FT} , Φ_{res} , and Φ_{ind} . The powers, then, include: P_F , P_{BR} , P_κ , P_{src} , P_W , etc.

2164 Profiles

2165 The next collection of reactor methods are the various profiles. Most obviously, these
2166 include radial plasma profiles for density, temperature, and current. However, this
2167 folder also includes the magnetic field strength as a function of radius – as was used
2168 within current drive efficiency calculations.

2169 Geometries

2170 Additionally, there are many geometric relations. These include the various tokamak
2171 thicknesses: a, b, c, d – as well as the radius and height of the central solenoid. This
2172 group also includes the volume, perimeter, surface area, and cross-sectional area.
2173 It also includes the many subscripted fields. For example, the elongation (i.e. κ_{95})
2174 includes the following alternative definitions: κ_X , κ_P , and κ_T

2175 Formulas

2176 The final set of reactor methods are formulas that do not really fit anywhere else.
2177 If a method is not related to geometry, power, calculations, etc, it ends up here.
2178 For example, this group includes: β_N , f_{BS} , C_W , and τ_E . Total, there are around 25
2179 formulas – as of the writing of this document.

2180 B.4 Demonstrating Code Usage

2181 Now that the Fussy.jl package has been described in detail, the final step is showing a
2182 simple example that can recreate a figure from the results chapter. This will closely
2183 match the Jupyter notebook available at:

2184 www.git.io/fussy_sensitivity

2185 Our goal will be to make a cost curve for the ARC reactor as a function of H – a so
2186 called sensitivity study plot.

2187 B.4.1 Initializing the Workspace

2188 The first step for any Fussy.jl Jupyter notebook is loading the required packages – i.e.
2189 the Fussy.jl and Plots.jl packages. This can be done using the following commands:

```
2190     addprocs(6)
2191
2192     @everywhere using Fussy
2193     using Plots
```

2194 The Plots.jl package may take a minute to load – similar to Matlab’s initial boot
2195 time. If the kernel raises an error about Plots.jl not being installed, use the following
2196 lines:

```
2197     import Pkg
2198     Pkg.add("Plots")
```

2199 B.4.2 Running a Study

2200 Now that the necessary packages have been loaded, we can move on to actually
2201 running the sensitivity study. We will split this command into two steps to make it
2202 more explicit.

2203 The first step will be making several variables that store: boolean flags, numbers, and
2204 symbols – which are like strings, but prefaced with a colon (:) instead of surrounded
2205 by double quotes (").

```
2206     cur_param = :H
2207     cur_deck = :arc
2208     is_pulsed = false
2209     is_consistent = true
2210     cur_sensitivity = 1.0
```

*The `addprocs` and `@everywhere` commands are to parallelize the code. This is because `addprocs(6)` activates 6 worker processes and `@everywhere Fussy.jl` adds Fussy.jl to the main kernel and worker processes.


```
2211     cur_num_points = 41
```

2212 These six variables almost completely describe a sensitivity study. The first two
2213 saw we are using the Arc reactor deck and running a sensitivity over the H-factor
2214 parameter. Next, the two boolean values refer to the reactor (1) being treated as
2215 pulsed or steady-state and (2) whether to handle η_{CD} self-consistently.* Ergo, what
2216 these two flags do is make sure ARC is being handled as a steady-state reactor with
2217 a self-consistent η_{CD} . The last two variables are then ways to change the sensitivity
2218 of the study (with 1.0 \rightarrow 100%) and the number of reactors it will produce (i.e. 41).
2219 Now all six of these variables can be piped into a call to the **Study** struct to start
2220 running the sensitivity study:

```
2221     cur_study = Study(  
2222         cur_param,  
2223         deck = cur_deck,  
2224         is_pulsed = is_pulsed,  
2225         is_consistent = is_consistent,  
2226         sensitivity = cur_sensitivity,  
2227         num_points = cur_num_points  
2228     )
```

2229 Note here that the equal signs inside the parentheses are called keyword arguments,
2230 which are common to most modern programming languages. After executing the
2231 command, the code will need to run for a few minutes.

2232 B.4.3 Extracting Results

2233 At this point, a user should have a completed sensitivity study they wish to plot.
2234 To make the plot useful, the study data structure first has to be unpacked and its
2235 contents cleaned. This is the goal of this subsection.

2236 First and foremost, a study has four families of reactors within it: beta-wall (i.e.

*Note that, currently, a pulsed reactor cannot be self-consistent in η_{CD} – it therefore causes an error.

2237 "wall"), beta-kink (i.e. "kink"), minimum capital cost (i.e. "W_M"), and minimum
2238 cost-per-watt (i.e. "cost"). Therefore, we will extract these reactor lists into a new
2239 dictionary data structure:

```
2240     cur_dict = Dict()  
2241  
2242     cur_dict["Beta-Wall"] = cur_study.wall_reactors  
2243     cur_dict["Beta-Kink"] = cur_study.kink_reactors  
2244  
2245     cur_dict["Min Cost per Watt"] = cur_study.cost_reactors  
2246     cur_dict["Min Capital Cost"] = cur_study.W_M_reactors
```

2247 Next, we will want to filter out all the invalid reactors that constitute non-physically
2248 realizable ones. These would likely be reactors that could fit in your hand or take up
2249 a whole city block.

```
2250     for (cur_key, cur_value) in cur_dict  
2251         cur_dict[cur_key] = filter(  
2252             cur_reactor -> cur_reactor.is_valid,  
2253             deepcopy(cur_value)  
2254         )  
2255     end
```

2256 B.4.4 Plotting Curves

2257 Our goal is now to turn our unpacked, clean reactor lists into plots – i.e. measuring
2258 costs-per-watt as a function of H. For simplicity, this will lack a lot of the features
2259 shown in the Jupyter notebook from the beginning of the section. Additionally, we
2260 will be doing it in an iterative process made possible by the Plots.jl framework.

2261 The first step is simply making a plot object

```
2262     cur_plot = plot()
```

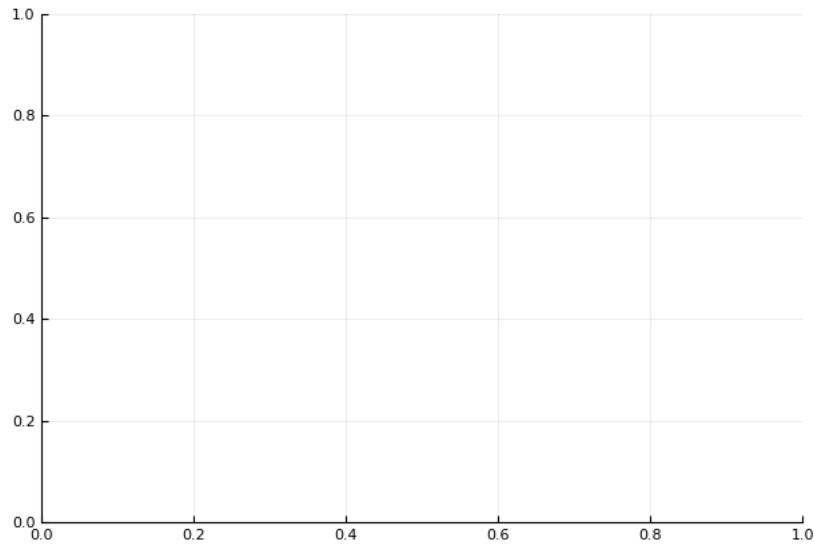


Figure B-1: A Blank Plot

A simple 2-D plot with no labels or data.

2263 After execution, this should produce the plank 2-D plot shown in ??.

2264 Next we will add a simple title and labels for the axes:

```
2265     title!("Arc")
```

```
2266
```

```
2267     xlabel!("H")
```

```
2268     ylabel!("Cost")
```

2269 The exclamation marks ensure this title and the labels are added to the `cur_plot`.

2270 Upon execution, you should see a plot with this information (??).

2271 Now we will loop over the dictionary of reactors and add them one at a time.

```
2272     for (cur_key, cur_value) in cur_dict
```

```
2273         cur_x = map(cur_reactor -> cur_reactor.H, cur_value)
```

```
2274         cur_y = map(cur_reactor -> cur_reactor.cost, cur_value)
```

```
2275         plot!(cur_x, cur_y, label=cur_key)
```

```
2276     end
```

```
2277     plot!()
```

2278 This results in the not very useful plot shown in ??. Note that each label is exactly

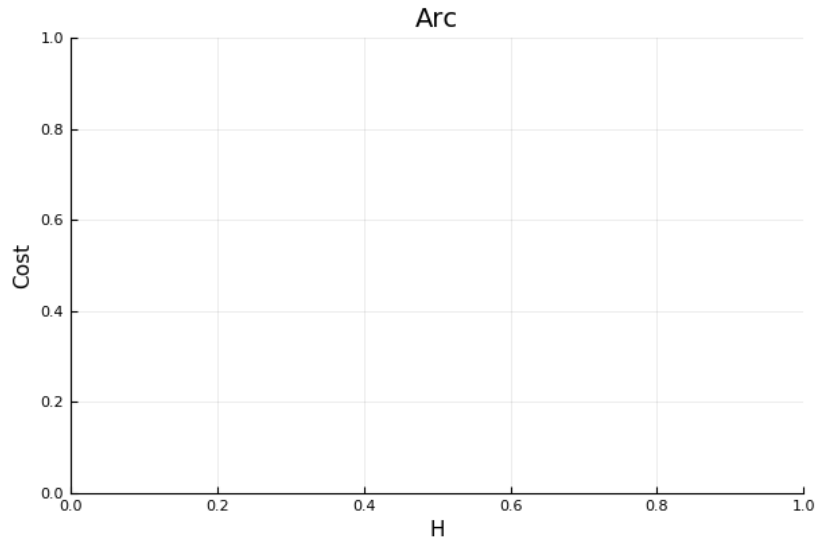


Figure B-2: An Empty Plot

A simple 2-D plot with labels, but no data.

2279 the key assigned to it in `cur_dict`.

2280 The final step is adding proper limits to make what is going on obvious to the reader:

2281 `ylims!(0, 0.03)`

2282 The addition of which can be seen in `??`.

2283 This completes the example. At this point, you should now be able to use every
2284 feature of `Fussy.jl`. Good luck!

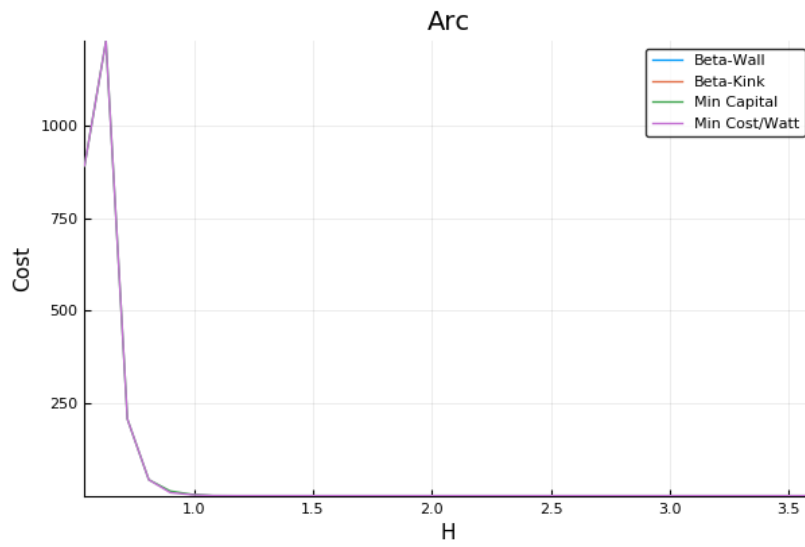


Figure B-3: An Unscaled Plot

A simple 2-D plot with Bad Limits.

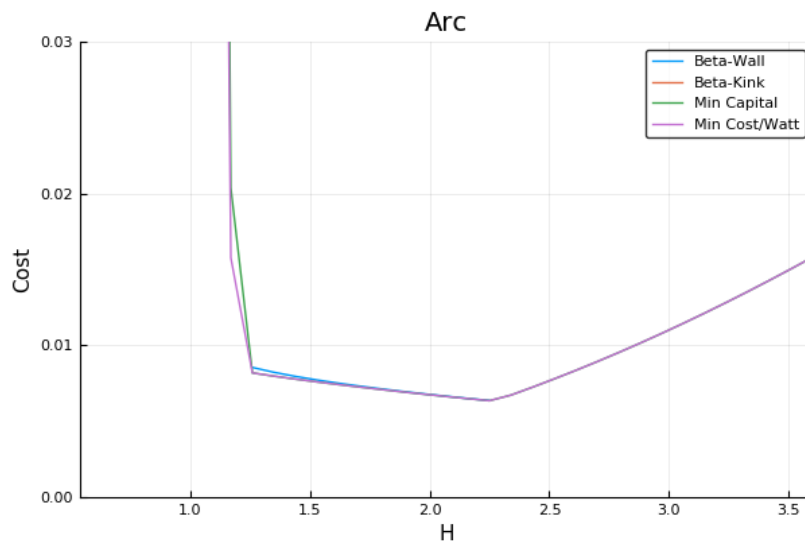


Figure B-4: A Scaled Plot

An example plot showing cost as a function of the H factor.

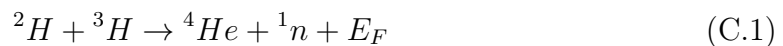
2285 Appendix C

2286 Discussing Fusion Power

2287 In a tokamak reactor, the main source of output power is fusion. Therefore, this
2288 chapter goes over a quick background of fusion power and describes a method for
2289 how to calculate the reactivity term that appears inside it. The particular method
2290 used for this reactivity approximation was done by Bosch and Hale in 1992.²⁹

2291 C.1 Theoretical Background

2292 The natural place to start when introducing fusion energy is the binding energy per
2293 nucleon curve shown in ???. As can be seen, this function reaches a maximum value
2294 around the element Iron (A=56). What this means at a basic level is: elements lighter
2295 than iron can *fuse* into a heavier one (i.e. hydrogens into helium), whereas heavier
2296 elements can *fission* into lighter ones (e.g. uranium into krypton and barium). This
2297 is what differentiates fission (uranium-fueled) reactors from fusion (hydrogen-fueled)
2298 ones. For fusion reactors, the most common reaction in a first-generation tokamak
2299 will be:



2300

$$E_F = 17.6 \text{ MeV} \quad (\text{C.2})$$

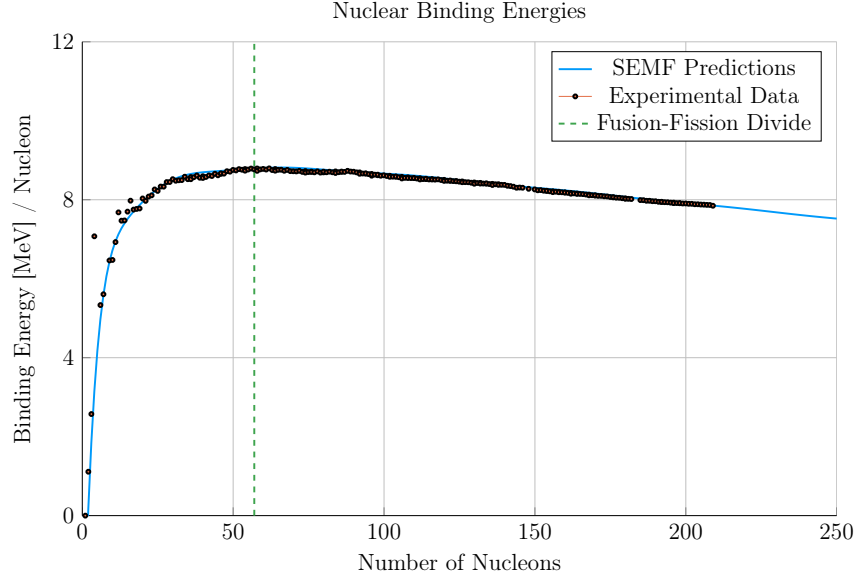


Figure C-1: Comparing Nuclear Fusion and Fission

The binding energy per nucleon is what differentiates nuclear fusion from fission. Nuclei heavier than Iron fission (e.g. Uranium), while light ones – such as Hydrogen – fuse.

2301 What this reaction (shown in ??) describes is two isotopes of hydrogen – i.e. deuterium
 2302 and tritium – fusing into a heavier element, helium, while simultaneously ejecting a
 2303 neutron. The entire energy of the fusion reaction (E_F) is then divided up 80-20
 2304 between the neutron and helium, respectively. Quantitatively, the helium (often
 2305 referred to as an alpha particle) receives 3.5 MeV.

$$P_n = 0.8 \cdot P_F \quad (\text{C.3})$$

2306

$$P_\alpha = 0.2 \cdot P_F \quad (\text{C.4})$$

2307 The final point to make is the main difference between the two fusion products:
 2308 helium (i.e. the alpha particle) and the neutron. First, neutrons lack a charge – they
 2309 are neutral. This means they cannot be confined with magnetic fields. As such, they
 2310 simply move in straight lines until they collide with other particles. As the structure
 2311 of a tokamak is mainly metal, the neutron is much more likely to collide there than the
 2312 gaseous plasma, which is orders of magnitude less dense. Conversely, alpha particles

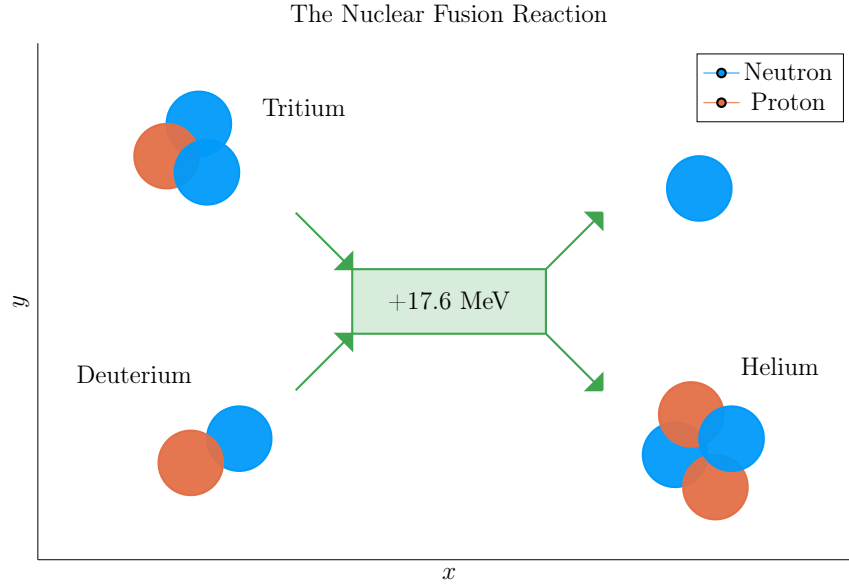


Figure C-2: The D-T Fusion Reaction

In a first generation tokamak reactor, the main source of energy will come from two hydrogen isotopes fusing into a helium particle – and ejecting a 14.1 MeV neutron.

are charged – when stripped of their electrons – and can therefore be kept within the plasma using magnets. What this means practically is that of the 17.6 MeV that comes from every fusion reaction, only 3.5 MeV remains inside the plasma (within the helium particle species).

C.2 Bosch-Hale Reactivity

The formula for fusion power used in this model makes use of a reactivity term – (σv) :

$$P_F = \int E_F n_D n_T \langle \sigma v \rangle d\mathbf{r} \quad (\text{C.5})$$

Summarizing the work of ??, this fusion power volume integral can be reduced to a 0-D form – assuming the geometry prescribed by this model:

$$P_F = K_F \cdot (\bar{n}^2 R_0^3) \cdot (\sigma v) \quad [MW] \quad (\text{C.6})$$

2322

$$\langle \sigma v \rangle = 10^{21} (1 + \nu_n)^2 \int_0^1 (1 - \rho^2)^{2\nu_n} \langle \sigma v \rangle \rho d\rho \quad (\text{C.7})$$

2323

$$K_F = 278.3 (f_D^2 \epsilon^2 \kappa g) \quad (\text{C.8})$$

2324 This reactivity term (or volumetric fusion reaction rate) can then be approximated
2325 by the Bosch-Hale parameterization, with coefficients given in ??^{29,30}

$$\langle \sigma v \rangle = C_1 \cdot \theta \cdot \exp(-3\xi) \cdot \sqrt{\frac{\xi}{m_\mu c^2 T^3}} \quad [\text{m}^3/\text{s}] \quad (\text{C.9})$$

2326

$$\theta = T \cdot \left(1 - \frac{T(C_2 + T(C_4 + TC_6))}{1 + T(C_3 + T(C_5 + TC_7))} \right)^{-1} \quad (\text{C.10})$$

2327

$$\xi = \left(\frac{B_G^2}{4\theta} \right)^{1/3} \quad (\text{C.11})$$

2328 For D-T (Deuterium-Tritium) fuel within a standard fusion temperature regime (i.e.
2329 $T \in [10, 20]$ keV), this can be simplified to:³⁰

$$\langle \sigma v \rangle_{\text{DT}} = 1.1 \times 10^{-24} \cdot T^2 \quad [\text{m}^3/\text{s}] \quad (\text{C.12})$$

2330 In our model, each appearance of T is set to the radial profile defined earlier – as it
2331 appears inside an integral.

2332 Example tabulations for this reactivity are given in ??^{29–31}

Table C.1: Bosch-Hale parametrization coefficients for volumetric reaction rates

	${}^2\text{H}(\text{d,n}){}^3\text{He}$	${}^2\text{H}(\text{d,p}){}^3\text{H}$	${}^3\text{H}(\text{d,n}){}^4\text{He}$	${}^3\text{He}(\text{d,p}){}^4\text{He}$
B_G [keV $^{1/2}$]	31.3970	31.3970	34.3827	68.7508
$m_\mu c^2$ [keV]	937 814	937 814	1 124 656	1 124 572
C_1	5.43360×10^{-12}	5.65718×10^{-12}	1.17302×10^{-9}	5.51036×10^{-10}
C_2	5.85778×10^{-3}	3.41267×10^{-3}	1.51361×10^{-2}	6.41918×10^{-3}
C_3	7.68222×10^{-3}	1.99167×10^{-3}	7.51886×10^{-2}	-2.02896×10^{-3}
C_4	0.0	0.0	4.60643×10^{-3}	-1.91080×10^{-5}
C_5	-2.96400×10^{-6}	1.05060×10^{-5}	1.35000×10^{-2}	1.35776×10^{-4}
C_6	0.0	0.0	-1.06750×10^{-4}	0.0
C_7	0.0	0.0	1.36600×10^{-5}	0.0
Valid range (keV)	$0.2 < T_i < 100$	$0.2 < T_i < 100$	$0.2 < T_i < 100$	$0.5 < T_i < 190$

Table C.2: Tabulated Bosch-Hale reaction rates [m 3 s $^{-1}$]

T (keV)	${}^2\text{H}(\text{d,n}){}^3\text{He}$	${}^2\text{H}(\text{d,p}){}^3\text{H}$	${}^3\text{H}(\text{d,n}){}^4\text{He}$	${}^3\text{He}(\text{d,p}){}^4\text{He}$
1.0	9.933×10^{-29}	1.017×10^{-28}	6.857×10^{-27}	3.057×10^{-32}
1.5	8.284×10^{-28}	8.431×10^{-28}	6.923×10^{-26}	1.317×10^{-30}
2.0	3.110×10^{-27}	3.150×10^{-27}	2.977×10^{-25}	1.399×10^{-29}
3.0	1.602×10^{-26}	1.608×10^{-26}	1.867×10^{-24}	2.676×10^{-28}
4.0	4.447×10^{-26}	4.428×10^{-26}	5.974×10^{-24}	1.710×10^{-27}
5.0	9.128×10^{-26}	9.024×10^{-26}	1.366×10^{-23}	6.377×10^{-27}
8.0	3.457×10^{-25}	3.354×10^{-25}	6.222×10^{-23}	7.504×10^{-26}
10.0	6.023×10^{-25}	5.781×10^{-25}	1.136×10^{-22}	2.126×10^{-25}
12.0	9.175×10^{-25}	8.723×10^{-25}	1.747×10^{-22}	4.715×10^{-25}
15.0	1.481×10^{-24}	1.390×10^{-24}	2.740×10^{-22}	1.175×10^{-24}
20.0	2.603×10^{-24}	2.399×10^{-24}	4.330×10^{-22}	3.482×10^{-24}

Appendix D

Selecting Plasma Profiles

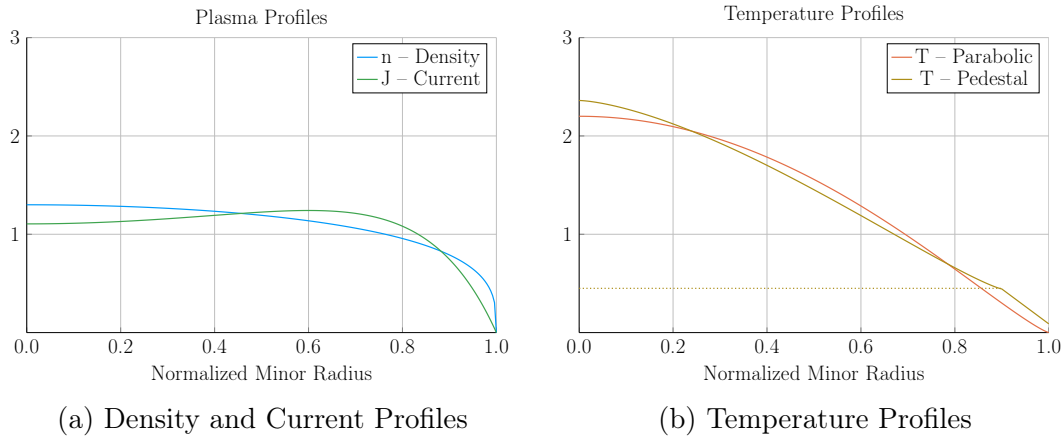


Figure D-1: Radial Plasma Profiles

The three most fundamental properties of a fusion plasma are its temperature, density, and current. These profiles allow the model to reduce from three dimensions to half of one.

D.1 Density — n

The Density is important to us. We use it in the Greenwald density limit, so it should be clean in both line-averaged and volume-averaged forms. Because of its flat profile,

2338 a parabola is a good approximation for H-mode pulses:

$$n(\rho) = \bar{n} \cdot (1 + \nu_n) \cdot (1 - \rho^2)^{\nu_n} \quad (\text{D.1})$$

2339 The line average density is related to \bar{n} through:

$$\hat{n} = \bar{n} \cdot \left(\frac{\pi^{1/2}}{2} \right) \cdot \frac{\Gamma(\nu_n + 2)}{\Gamma(\nu_n + 3/2)} \quad (\text{D.2})$$

2340 The convenience of this function comes from how the volumetric average comes out.

2341 To relate this to the volume integral, we use:

$$\bar{x} = \frac{1}{V} \int x(\rho) dV \quad (\text{D.3})$$

2342 For a normalized radial profile that does not depend on angle,

$$V = \int_0^1 \rho d\rho = 1/2 \quad (\text{D.4})$$

2343 Then, when $x = n$,

$$\bar{n} = 2 \int_0^1 n(\rho) \rho d\rho = \bar{n} \quad (\text{D.5})$$

2344 Additionally, the Greenwald Density limit that we will use throughout,

$$\hat{n} = N_G \cdot \left(\frac{I_M}{\pi a^2} \right) \quad (\text{D.6})$$

2345 can now be written in the following form:

$$\bar{n} = K_n \cdot \left(\frac{I_M}{R_0^2} \right) \quad (\text{D.7})$$

2346

$$K_n = \frac{2 N_G}{\epsilon^2 \pi^{3/2}} \cdot \left(\frac{\Gamma(\nu_n + 3/2)}{\Gamma(\nu_n + 2)} \right) \quad (\text{D.8})$$

2347 D.2 Temperature – T

2348 The Temperature is the swept variable in our model framework. Therefore, it's the
 2349 one we can allow people to be the most cavalier with. Additionally, as temperature
 2350 profiles are highly peaked, their pedestal region is sometimes wrongfully neglected
 2351 with a parabola.

$$T(\rho) = \bar{T} \cdot (1 + \nu_T) \cdot (1 - \rho^2)^{\nu_T} \quad (\text{D.9})$$

2352 Therefore, our model sometimes treats the system as if it had a pedestal region. This
 2353 is mainly for the bootstrap current and fusion power, which were previously known
 2354 to misalign and overshoot, respectively.

$$T(\rho) = \begin{cases} T_{para} , & x \in [0, \rho_{ped}] \\ T_{line} , & x \in (\rho_{ped}, 1] \end{cases} \quad (\text{D.10})$$

2355 Where the piecewise functions are given by,

$$T_{para} = T_{ped} + (T_0 - T_{ped}) \cdot \left(1 - \left(\frac{\rho}{\rho_{ped}} \right)^{\lambda_T} \right)^{\nu_T} \quad (\text{D.11})$$

2356

$$T_{line} = T_{sep} + (T_{ped} - T_{sep}) \cdot \left(\frac{1 - \rho}{1 - \rho_{ped}} \right) \quad (\text{D.12})$$

2357 This temperature profile is related to the volume-averaged temperature through,

$$\bar{T} \cdot V = \int_0^{\rho_{ped}} T_{para}(\rho) \rho d\rho + \int_{\rho_{ped}}^1 T_{line}(\rho) \rho d\rho \quad (\text{D.13})$$

2358 Starting with the second integral,

$$\int_{\rho_{ped}}^1 T_{line}(\rho) \rho d\rho = \frac{1}{3} \cdot (1 - \rho_{ped}) \cdot ((T_{sep} + T_{ped}/2) + \rho_{ped} \cdot (T_{ped} + T_{sep}/2)) \quad (D.14)$$

The first integral can be handled by breaking it into to,

$$\begin{aligned} \int_0^{\rho_{ped}} T_{para}(\rho) \rho d\rho &= T_{ped} \cdot \int_0^{\rho_{ped}} \rho d\rho + \\ &\quad (T_0 - T_{ped}) \cdot \int_0^{\rho_{ped}} \left(1 - \left(\frac{\rho}{\rho_{ped}}\right)^{\lambda_T}\right)^{\nu_T} \cdot \rho d\rho \end{aligned} \quad (D.15)$$

2359 The first sub-integral is then,

$$T_{ped} \cdot \int_0^{\rho_{ped}} \rho d\rho = \frac{T_{ped} \rho_{ped}^2}{2} \quad (D.16)$$

2360 Utilizing the following transformation,

$$u = \frac{\rho}{\rho_{ped}} \quad (D.17)$$

2361

$$d\rho = \rho_{ped} du \quad (D.18)$$

2362

$$u(\rho = \rho_{ped}) = 1 \quad (D.19)$$

2363 The second sub-integral becomes (assuming independence from T_0 and T_{ped}),

$$(T_0 - T_{ped}) \cdot \rho_{ped}^2 \cdot \int_0^1 (1 - u^{\lambda_T})^{\nu_T} \cdot u du \quad (D.20)$$

2364 Where:

$$\int_0^1 (1 - u^{\lambda_T})^{\nu_T} \cdot u \, du = \frac{\Gamma(1 + \nu_T) \Gamma\left(\frac{2}{\lambda_T}\right)}{\lambda_T \cdot \Gamma\left(1 + \nu_T + \frac{2}{\lambda_T}\right)} \quad (\text{D.21})$$

2365 We are now in a position to solve for T_0 in terms of \bar{T} :

$$T_0 = T_{ped} + \frac{\bar{T} - K_{TU}}{K_{TD}} \quad (\text{D.22})$$

2366

$$K_{TU} = T_{ped} \rho_{ped}^2 + \frac{(1 - \rho_{ped})}{3} \cdot ((2T_{sep} + T_{ped}) + \rho_{ped} \cdot (2T_{ped} + T_{sep})) \quad (\text{D.23})$$

2367

$$K_{TD} = \rho_{ped}^2 \cdot \left(\frac{2}{\lambda_T}\right) \cdot \frac{\Gamma(1 + \nu_T) \Gamma\left(\frac{2}{\lambda_T}\right)}{\Gamma\left(1 + \nu_T + \frac{2}{\lambda_T}\right)} \quad (\text{D.24})$$

2368 Which although not pretty, can be plugged into the original equation.

2369 D.3 Pressure – p

2370 The first point to make is that we are not using the same temperature profile for
 2371 the pressure as for the temperature. This is because it would lead to hypergeometric
 2372 functions that are not worth the headache.

2373 As most of the pressure is at the center, we use simple parabolic profile. This leads
 2374 to:

$$\bar{p} = 0.1581 (1 + f_D) \frac{(1 + \nu_n)(1 + \nu_T)}{1 + \nu_n + \nu_T} \bar{n} \bar{T} \quad [atm] \quad (\text{D.25})$$

2375 D.4 Bootstrap Current – f_{BS}

2376 We start with,

$$f_{BS} = \frac{I_{BS}}{I_P} = \frac{2\pi a^2 \kappa}{I_P} \int_0^1 J_B \rho d\rho \quad (D.26)$$

2377 Expanding the previous equation using the following relations,

$$J_B = -4.85 \cdot R_0 \epsilon^{1/2} \cdot \left(\frac{\rho^{1/2} n T}{d\psi/d\rho} \right) \cdot \left(\frac{dn/d\rho}{n} + 0.54 \cdot \frac{dT/d\rho}{T} \right) \quad (D.27)$$

2378

$$\frac{d\psi}{d\rho} = \frac{\mu_0 R_0 I_P}{\pi} \cdot \left(\frac{\kappa}{1 + \kappa^2} \right) \cdot b_p(\rho) \quad (D.28)$$

2379 Yields:

$$f_{BS} = -K_{BS} \int_0^1 (1 - \rho^2)^{\nu_n} \cdot \left(\frac{\rho^{3/2}}{b_p(\rho)} \right) \cdot \left(\frac{T}{n} \cdot \frac{dn}{d\rho} + 0.54 \cdot \frac{dT}{d\rho} \right) d\rho \quad (D.29)$$

2380

$$K_{BS} = K_n \cdot \left(\frac{2\pi^2 \cdot 4.85 \cdot \epsilon^{5/2}}{\mu_0} \right) \cdot (1 + \nu_n) \cdot (1 + \kappa^2) \quad (D.30)$$

2381 Here, b_p comes from:

$$b_p(\rho) = \frac{-e^{\gamma\rho^2}(\gamma\rho^2 - 1 - \gamma) - 1 - \gamma}{\rho(e^\gamma - 1 - \gamma)} \quad (D.31)$$

2382 And the value of γ comes from the the normalized internal inductance:

$$l_i = \frac{4\kappa}{1 + \kappa^2} \int_0^1 b_p^2 \frac{d\rho}{\rho} \quad (D.32)$$

2383 With our profiles,

$$-\left(\frac{T}{n} \cdot \frac{dn}{d\rho} \right) = 2\nu_n \cdot \left(\frac{T \cdot \rho}{1 - \rho^2} \right) \quad (D.33)$$

2384 While treating temperature differently results in,

$$-\left(\frac{dT}{d\rho}\right)_{para} = \left(\frac{T_0 - T_{ped}}{\rho_{ped}^{\lambda_T}}\right) \cdot (\nu_T \lambda_T) \cdot \rho^{\lambda_T-1} \cdot \left(1 - \left(\frac{\rho}{\rho_{ped}}\right)^{\lambda_T}\right)^{\nu_T-1} \quad (D.34)$$

2385

$$-\left(\frac{dT}{d\rho}\right)_{line} = \left(\frac{T_{ped} - T_{sep}}{1 - \rho_{ped}}\right) \quad (D.35)$$

2386 Where we will be using the new symbol definition,

$$\partial T = -\left(\frac{dT}{d\rho}\right) \quad (D.36)$$

Which ultimately allows us to write,

$$f_{BS} = K_{BS} \int_0^1 H_{BS} d\rho \quad (D.37)$$

$$H_{BS} = (1 - \rho^2)^{\nu_n-1} \cdot \left(\frac{\rho^{3/2}}{b_p(\rho)}\right) \cdot \left(2\nu_n \cdot \rho \cdot T + 0.54 \cdot (1 - \rho^2) \cdot \partial T\right) \quad (D.38)$$

2387 Where the values of T are determined through,

$$T_{para} = T_{ped} + (T_0 - T_{ped}) \cdot \left(1 - \left(\frac{\rho}{\rho_{ped}}\right)^{\lambda_T}\right)^{\nu_T} \quad (D.39)$$

2388

$$T_{line} = T_{sep} + (T_{ped} - T_{sep}) \cdot \left(\frac{1 - \rho}{1 - \rho_{ped}}\right) \quad (D.40)$$

2389 And the values of ∂T are:

$$\partial T_{para} = \left(\frac{T_0 - T_{ped}}{\rho_{ped}^{\lambda_T}}\right) \cdot (\nu_T \lambda_T) \cdot \rho^{\lambda_T-1} \cdot \left(1 - \left(\frac{\rho}{\rho_{ped}}\right)^{\lambda_T}\right)^{\nu_T-1} \quad (D.41)$$

2390

$$\partial T_{line} = \left(\frac{T_{ped} - T_{sep}}{1 - \rho_{ped}}\right) \quad (D.42)$$

2391 D.5 Volume Averaged Powers

2392 The first thing to consider in a fusion reactor is power balance. It is what separates
2393 a net power producing reactor from a power-consuming research device.

$$\boxed{P_\alpha + P_H = P_\kappa + P_B} \quad (D.43)$$

2394

$$P_\alpha = \frac{P_F}{5} \quad (D.44)$$

2395

$$P_H = \frac{P_F}{Q} \quad (D.45)$$

2396

$$P_\kappa = \frac{3}{2\tau_E} \int p \, d\mathbf{r} \quad [3D] \quad (D.46)$$

2397

$$P_B = 5.35e3 Z_{eff} \int n_{\bar{n}}^2 \sqrt{T} \, d\mathbf{r} \quad [3D] \quad (D.47)$$

2398 As mentioned before, P_F is handled by (σv) and therefore the lefthand-side uses the
2399 pedestal temperature profiles. However, for the same reasons as discussed earlier, the
2400 righthand-side (P_κ and P_B) need to use the parabolic temperature profiles.

2401 Using the parabolic profiles (for n and T) gives for the Bremsstrahlung radiation,

$$P_B = K_B \cdot \left(R_0^3 \bar{n}^2 \sqrt{\bar{T}} \right) \quad [MW] \quad (D.48)$$

2402

$$K_B = 0.1056 \cdot Z_{eff} \cdot (\epsilon^2 \kappa g) \cdot \frac{(1 + \nu_n)^2 (1 + \nu_T)^{1/2}}{1 + 2\nu_n + 0.5\nu_T} \quad (D.49)$$

2403 And a similar exercise for the thermal conduction losses results in:

$$P_\kappa = K_\kappa \cdot \left(\frac{R_0^3 \bar{n} \bar{T}}{\tau_E} \right) \quad [MW] \quad (D.50)$$

$$K_{\kappa} = 0.4744 \cdot (1 + f_D) \cdot (\epsilon^2 \kappa g) \cdot \frac{(1 + \nu_n)(1 + \nu_T)}{1 + \nu_n + \nu_T} \quad (\text{D.51})$$

Appendix E

Determining Plasma Flux Surfaces

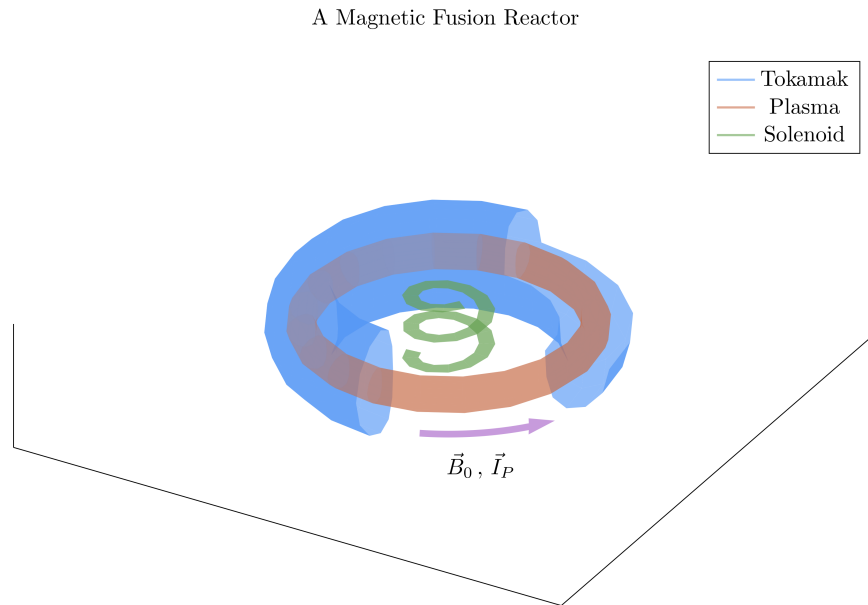


Figure E-1: Cut-Away of Tokamak Reactor

The three main components of a magnetic fusion reactor are: the tokamak structure, the plasma fuel, and the spring-like solenoid at the center.

E.1 Flux Surface Coordinates

We begin with the shape of the outer plasma surface (i.e. the 95% flux surface) written in terms of normalized coordinates x and y as follows – with α being an angle-like

2410 coordinate:

$$R = R_0 + ax(\alpha) \quad (\text{E.1})$$

2411

$$Z = ay(\alpha) \quad (\text{E.2})$$

2412

$$0 \leq \alpha \leq 2\pi \quad (\text{E.3})$$

2413 The surface representation can now be written as:

$$x(\alpha) = c_0 + c_1 \cos(\alpha) + c_2 \cos(2\alpha) + c_3 \cos(3\alpha) \quad (\text{E.4})$$

2414

$$y(\alpha) = \kappa \sin(\alpha) \quad (\text{E.5})$$

2415 The constraints determining c_j – for $j = 1, 2, 3$ – are chosen as:

$$x(0) = 1 \quad (\text{E.6})$$

2416

$$x(\pi) = -1 \quad (\text{E.7})$$

2417

$$x\left(\frac{\pi}{2}\right) = -\delta \quad (\text{E.8})$$

2418

$$x_{\alpha\alpha}(\pi) = 0.3 \cdot (1 - \delta^2) \quad (\text{E.9})$$

2419 The last constraint, which is related to the surface curvature at $\alpha = \pi$, is chosen to
2420 make sure that the surface is always convex. A trial and error empirical fit resulted
2421 in the choice $x_{\alpha\alpha}(\pi) = 0.3 \cdot (1 - \delta^2)$. The constraint relations are easily evaluated and

2422 then solved, leading to values for the c_j ,

$$c_0 = -\frac{\delta}{2} \quad (\text{E.10})$$

2423

$$c_1 = g \quad (\text{E.11})$$

2424

$$c_2 = \frac{\delta}{2} \quad (\text{E.12})$$

2425

$$c_3 = 1 - g \quad (\text{E.13})$$

2426 Here, g is a shaping parameter approximately equal to one:

$$g = \frac{9 - 2\delta - 0.3 \cdot (1 - \delta^2)}{8} \quad (\text{E.14})$$

2427 E.2 Cross-sectional Area and Volume

2428 The plasma cross-sectional area and volume can be evaluated by straightforward
2429 calculations,

$$\begin{aligned} A &= \int \int dR dZ = a^2 \int \int dx dy = a^2 \int_0^{2\pi} x \frac{dy}{d\alpha} d\alpha \\ &= \pi a^2 \kappa g \end{aligned} \quad (\text{E.15})$$

2430

$$\begin{aligned} V &= \int \int \int R dR dZ d\Phi = 2\pi a^2 \int \int R dx dy \\ &= 2\pi a^2 R_0 \int_0^{2\pi} \left(x + \epsilon \frac{x^2}{2} \right) \frac{dy}{d\alpha} d\alpha \approx 2\pi a^2 R_0 \int_0^{2\pi} x \frac{dy}{d\alpha} d\alpha \\ &= 2\pi^2 R_0 a^2 \kappa g \end{aligned} \quad (\text{E.16})$$

2431 The second form of the volume integral makes use of the small inverse aspect ratio

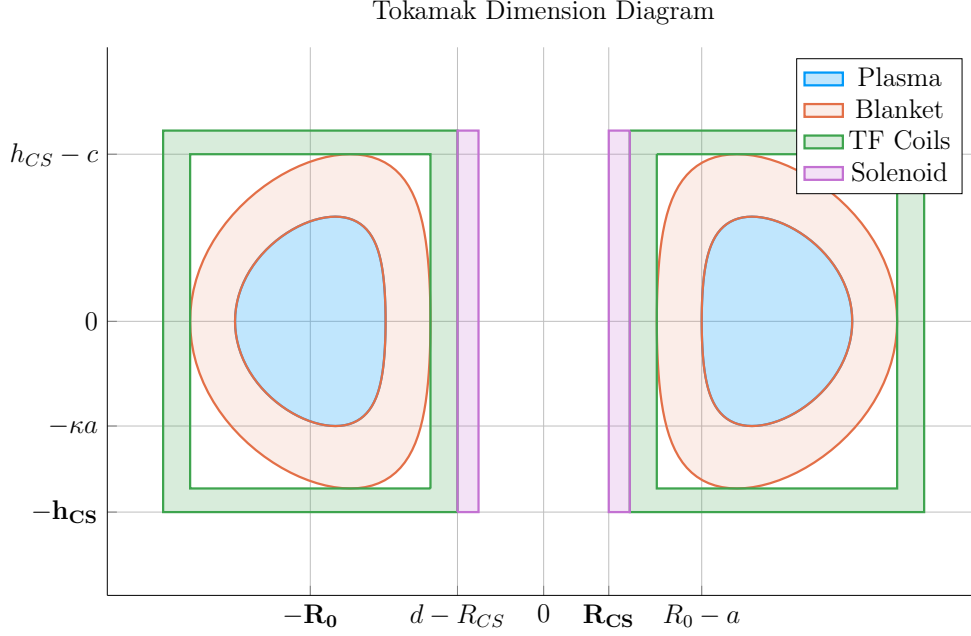


Figure E-2: Dimensions of Tokamak Cross-Section

expansion, $\epsilon \ll 1$, which is a good approximation and used throughout the analysis.

E.3 Surface and Volume Integrals

???? are simple formulas describing the shape of the outer plasma surface. We next modify the model so that it gives a plausible description of the interior flux surfaces as well. The idea is to introduce a normalized flux label, which is radial-like in behavior. This label is denoted by ρ and $\rho \in [0, 1]$ with $\rho = 1$ being the outer plasma surface (i.e. the 95% surface) and $\rho = 0$ being the magnetic axis. Additional trial and error results in the following representation for the flux surfaces,

$$x(\rho, \alpha) = \sigma(1 - \rho^2) + c_0\rho^4 + c_1\rho \cos(\alpha) + c_2\rho^2 \cos(2\alpha) + c_3\rho^3 \cos(3\alpha) \quad (\text{E.17})$$

$$y(\rho, \alpha) = \kappa\rho \sin(\alpha) \quad (\text{E.18})$$

with σ being the shift of the magnetic axis. Usually, $\sigma \sim 0.1$ for a high field tokamak.

2442 Lastly, we note that in the course of the work it will be necessary to integrate functions
 2443 of ρ over the volume and cross-sectional area of the plasma. Specifically we will need
 2444 to evaluate:

$$Q_V = \int \int \int Q(\rho) R dR dZ d\Phi \approx 2\pi R_0 a^2 \int \int Q(\rho) dx dy \quad (\text{E.19})$$

2445

$$Q_A = \int \int Q(\rho) dR dZ = a^2 \int \int Q(\rho) dx dy \quad (\text{E.20})$$

2446 Here, $Q(\rho)$ is an arbitrary function of ρ such as pressure or temperature. In the large
 2447 aspect ratio limit, both integrals require the evaluation of the same quantity:

$$K = \int \int Q(\rho) dx dy \quad (\text{E.21})$$

2448 To evaluate this integral, we need to convert from x, y coordinates to ρ, α coordinates.
 2449 Using the Jacobian of the transformation leads to

$$K = \int \int Q(\rho) (x_\rho y_\alpha - x_\alpha y_\rho) d\rho d\alpha \quad (\text{E.22})$$

2450 Here,

$$\begin{aligned} x_\rho y_\alpha - x_\alpha y_\rho = & \kappa \sin(\alpha) \cdot (c_1 \rho \sin(\alpha) + 2c_2 \rho^2 \sin(2\alpha) + 3c_3 \rho^3 \sin(3\alpha)) \\ & + \kappa \rho \cos(\alpha) \cdot \left[\right. \\ & \quad - 2\rho\sigma + 4\rho^3 c_0 + c_1 \cos(\alpha) \\ & \quad + 2c_2 \rho \cos(2\alpha) + 3c_3 \rho^2 \cos(3\alpha) \\ & \quad \left. \right] \end{aligned} \quad (\text{E.23})$$

2451 Since Q is only a function of ρ , the α integral can be carried out analytically. The
 2452 only term that survives the averaging are the ones containing c_1 . A simple integration

2453 over α then yields the desired results:

$$Q_V = 4\pi^2 R_0 a^2 \kappa g \int_0^1 Q(\rho) \rho d\rho \quad (\text{E.24})$$

2454

$$Q_S = 2\pi a^2 \kappa g \int_0^1 Q(\rho) \rho d\rho \quad (\text{E.25})$$

2455

2456 Appendix F

2457 Expanding on the Bootstrap Current

2458 The bootstrap current fraction – f_{BS} – is an important parameter that enters in
2459 the design of tokamak reactors. It must be calculated with reasonable accuracy to
2460 determine how much external current drive is required. The value of f_{BS} thus has
2461 a strong impact on the overall fusion energy gain. Obtaining reasonable accuracy
2462 requires a moderate amount of analysis, which is presented in a following section.
2463 The results are summarized below.

2464 F.1 Summarized Results

2465 The analysis is based on an expression for the bootstrap current valid for arbitrary
2466 cross section assuming (1) equal temperature electrons and ions $T_e = T_i = T$, (2) large
2467 aspect ratio $\epsilon \ll 1$, and (3) negligible collisionality $\nu_* \rightarrow 0$. Under these assumptions
2468 the bootstrap current $\mathbf{J}_{BS} \approx J_{BS} \mathbf{e}_\phi$ has the form

$$J_{BS} = -3.32 f_T R_0 n T \left(\frac{1}{n} \frac{dn}{d\psi} + 0.054 \frac{1}{T} \frac{dT}{d\psi} \right) \quad (\text{F.1})$$

2469 Here, $f_T \approx 1.46(r/R_0)^{1/2}$ is an approximate expression for the trapped particle frac-
2470 tion and ψ is the poloidal flux.

2471 The analysis next section shows that ?? leads to an expression for the bootstrap
 2472 fraction, assuming for simplicity elliptical flux surfaces, that can be written as:

$$f_{BS} = \frac{I_{BS}}{I} = \frac{2\pi a^2 \kappa}{I} \int_0^1 J_{BS} \rho d\rho = \frac{K_{BS}}{K_n} \frac{\bar{n} \bar{T} R_0^2}{I_P^2} \quad (\text{F.2})$$

2473

$$K_{BS} = 4.879 \cdot K_n \cdot \left(\frac{1 + \kappa^2}{2} \right) \cdot \epsilon^{5/2} \cdot H_{BS} \quad (\text{F.3})$$

2474

$$H_{BS} = (1 + \nu_n)(1 + \nu_T)(\nu_n + 0.054\nu_T) \int_0^1 \frac{\rho^{5/2} (1 - \rho^2)^{\nu_n + \nu_T - 1}}{b_p} d\rho \quad (\text{F.4})$$

2475

$$b_p(\rho) = \frac{-e^{\gamma \rho^2} (\gamma \rho^2 - 1 - \gamma) - 1 - \gamma}{\rho (e^\gamma - 1 - \gamma)} \quad (\text{F.5})$$

2476

$$\bar{J}_\phi(\rho) = -\frac{I}{\pi a^2 \kappa} \left[\frac{\gamma^2 (1 - \rho^2) e^{\gamma \rho^2}}{e^\gamma - 1 - \gamma} \right] \quad (\text{F.6})$$

2477 In this expression b_p is a normalized form of the poloidal magnetic field derived from
 2478 a prescribed model for the *total* flux surface averaged current density profile $\bar{J}_\phi(\rho)$.
 2479 The $\bar{J}_\phi(\rho)$ profile, in analogy with the density and temperature profiles, is not self-
 2480 consistent but is chosen to have a plausible experimental shape characterized by the
 2481 parameter γ . The profile can have either an on-axis ($\gamma < 1$) or off-axis peak ($\gamma > 1$).
 2482 The normalized internal inductance l_i and radial location of the current peak ρ_m are
 2483 related to the value of γ by:

$$l_i = \frac{4\kappa}{1 + \kappa^2} \int_0^1 b_p^2 \rho d\rho \quad (\text{F.7})$$

2484

$$\rho_m = \begin{cases} \left(\frac{\gamma}{\gamma - 1} \right)^{1/2}, & \gamma > 1 \\ 0, & \gamma < 1 \end{cases} \quad (\text{F.8})$$

F.2 Detailed Analysis

The starting point for the analysis is the general expression for the bootstrap current in a tokamak with arbitrary cross section.³² This expression can be simplified by assuming (1) equal temperature electrons and ions $T_e = T_i = T$, (2) large aspect ratio $\epsilon \ll 1$, and (3) negligible collisionality $\nu_* \rightarrow 0$. The bootstrap current $\mathbf{J}_{BS} \approx J_{BS} \mathbf{e}_\phi$ reduces to

$$J_{BS} = -3.32 f_T R_0 n T \left(\frac{1}{n} \frac{dn}{d\psi} + 0.054 \frac{1}{T} \frac{dT}{d\psi} \right) \quad (\text{F.9})$$

Several values of the trapped particle fraction f_T have been given in the literature.³³ For simplicity we use a form valid for large aspect ratio. This is a slightly optimistic value but saves a large amount of detailed calculation. It can be written as,

$$f_T \approx 1.46 (r/R_0)^{1/2} = 1.46 \epsilon^{1/2} \rho^{1/2} \quad (\text{F.10})$$

Here, as in the main text, ρ is a radial-like flux surface label that varies between $0 \leq \rho \leq 1$. In other words $\psi = \psi(\rho)$. Under these assumptions the bootstrap current reduces to:

$$J_{BS} = -4.85 R_0 \epsilon^{1/2} \left(\frac{\rho^{1/2} n T}{d\psi/d\rho} \right) \left(\frac{1}{n} \frac{dn}{d\rho} + 0.054 \frac{1}{T} \frac{dT}{d\rho} \right) \quad (\text{F.11})$$

Since we have specified profiles for $n(\rho)$ and $T(\rho)$ all that remains in order to be able to evaluate $J_{BS}(\rho)$ is to determine $\psi' = d\psi/d\rho$. Keep in mind that at this point, in spite of the approximations that have been made, the expression for $J_{BS}(\rho)$ is still valid for arbitrary cross section.

The analysis that follows shows how to calculate ψ' for an arbitrary cross section including finite aspect ratio. As an example an explicit expression for large aspect ratio, finite elongation ellipse is obtained. Consider the Grad-Shafranov equation for the flux: $\Delta^* \psi = -\mu_0 R J_\psi$. We integrate this equation over the volume of an arbitrary

2505 flux surface making use of Gauss' theorem, which leads to:

$$\int_S \frac{\mathbf{n} \cdot \nabla \psi}{R^2} dS = -\mu_0 \int_V \frac{J_\phi}{R} d\mathbf{r} \quad (\text{F.12})$$

2506 Next, assume that the coordinates of the flux surface can be expressed in terms of ρ
 2507 and an angular-like parameter α with $0 \leq \alpha \leq 2\pi$. In other words, the flux surface
 2508 coordinates can be written as $R = R(\rho, \alpha) = R_0 + ax(\rho, \alpha)$ and $Z = Z(\rho, \alpha) =$
 2509 $ay(\rho, \alpha)$. The functions $R(\rho, \alpha)$ and $Z(\rho, \alpha)$ are assumed to be known. The term on
 2510 the left hand side can be evaluated by noting that

$$dl = d\mathbf{l}t \quad (\text{F.13})$$

2511

$$dl = (R_\alpha^2 + Z_\alpha^2)^{1/2} d\alpha \quad (\text{F.14})$$

2512

$$\mathbf{t} = \frac{R_\alpha \mathbf{e}_R + Z_\alpha \mathbf{e}_Z}{(R_\alpha^2 + Z_\alpha^2)^{1/2}} \quad (\text{F.15})$$

2513

$$\mathbf{n} = \mathbf{e}_\phi \times \mathbf{t} = \frac{Z_\alpha \mathbf{e}_R - R_\alpha \mathbf{e}_Z}{(R_\alpha^2 + Z_\alpha^2)^{1/2}} \quad (\text{F.16})$$

2514

$$dS = R d\phi dl = 2\pi R (R_\alpha^2 + Z_\alpha^2)^{1/2} d\alpha \quad (\text{F.17})$$

2515 It then follows that

$$\mathbf{n} \cdot \nabla \psi = \frac{1}{(R_\alpha^2 + Z_\alpha^2)^{1/2}} \left(Z_\alpha \frac{\partial \psi}{\partial R} - R_\alpha \frac{\partial \psi}{\partial Z} \right) = \frac{1}{(R_\alpha^2 + Z_\alpha^2)^{1/2}} \frac{d\psi}{d\rho} Z_\alpha \rho_R - R_\alpha \rho_Z \quad (\text{F.18})$$

2516 We can rewrite the last term by noting that

$$\begin{aligned} dR &= R_\rho d\rho + R_\alpha d\alpha \quad \rightarrow \quad d\rho = (Z_\alpha dR - R_\alpha dZ) / (R_\rho Z_\alpha - R_\alpha Z_\rho) \\ dZ &= Z_\rho d\rho + Z_\alpha d\alpha \quad \rightarrow \quad d\alpha = (-Z_\rho dR + R_\rho dZ) / (R_\rho Z_\alpha - R_\alpha Z_\rho) \end{aligned} \quad (\text{F.19})$$

2517 from which follows

$$\begin{aligned}\rho_R &= \frac{Z_\alpha}{(R_\rho Z_\alpha - R_\alpha Z_\rho)} \\ \rho_Z &= -\frac{R_\alpha}{(R_\rho Z_\alpha - R_\alpha Z_\rho)}\end{aligned}\tag{F.20}$$

2518 the normal gradient reduces to

$$\mathbf{n} \cdot \nabla \psi = \frac{R_\alpha^2 + Z_\alpha^2}{(R_\rho Z_\alpha - R_\alpha Z_\rho)} \frac{d\psi}{d\rho}\tag{F.21}$$

2519 Using this relation we see that the left hand side of ?? can now be written as:

$$\int_S \frac{\mathbf{n} \cdot \nabla \psi}{R^2} dS = 2\pi \frac{d\psi}{d\rho} \int_0^{2\pi} \frac{R_\alpha^2 + Z_\alpha^2}{(R_\rho Z_\alpha - R_\alpha Z_\rho)} \frac{d\alpha}{R}\tag{F.22}$$

2520 Consider now the right hand side of ?. The critical assumption is that the current
2521 density is approximated by its flux surface averaged value, $J_\phi(\rho, \alpha) \approx \bar{J}_\phi(\rho)$. This is
2522 obviously not self-consistent with the Grad-Shafranov equation. Even so, it should
2523 suffice for present purposes where we only need to evaluate global volume integrals.
2524 Also, in the same spirit as prescribing $n(\rho)$ and $T(\rho)$ we assume that $\bar{J}_\phi(\rho)$ is also
2525 prescribed. Under these assumptions the right hand side of ?? simplifies to:

$$\begin{aligned}-\mu_0 \int_V \frac{J_\phi}{R} d\mathbf{r} &= -2\pi\mu_0 \int_A J_\phi dA \\ &= -2\pi\mu_0 \int_0^\rho d\rho \int_0^{2\pi} J_\phi (R_\rho Z_\alpha - R_\alpha Z_\rho) d\alpha \\ &\approx -2\pi\mu_0 \int_0^\rho d\rho \left[\bar{J}_\phi \int_0^{2\pi} (R_\rho Z_\alpha - R_\alpha Z_\rho) d\alpha \right]\end{aligned}\tag{F.23}$$

2526 Combining the results in ???? leads to the required general expression for $d\psi/d\rho$,

$$\frac{d\psi}{d\rho} \int_0^{2\pi} \frac{R_\alpha^2 + Z_\alpha^2}{(R_\rho Z_\alpha - R_\alpha Z_\rho)} \frac{d\alpha}{R} = -\mu_0 \int_0^\rho d\rho \left[\bar{J}_\omega \int_0^{2\pi} (R_\rho Z_\alpha - R_\alpha Z_\rho) d\alpha \right]\tag{F.24}$$

2527 Next, to help specify a plausible choice for \bar{J}_ϕ it is useful to define the kink safety

2528 factor and the actual local safety factor. The kink safety factor is defined by

$$q_* = \frac{2\pi a^2 B_0}{\mu_0 R_0 I} \left(\frac{1 + \kappa^2}{2} \right) \quad (\text{F.25})$$

2529 where

$$I = \int J_o dA = \int_0^1 d\rho \left[\bar{J}_o \int_0^{2\pi} (R_\rho Z_\alpha - R_\alpha Z_\rho) d\alpha \right] \quad (\text{F.26})$$

2530 This leads to

$$\frac{1}{q_*} = \frac{\mu_0 R_0}{2\pi a^2 B_0} \left(\frac{2}{1 + \kappa^2} \right) \int_0^1 d\rho \left[\bar{J}_\phi \int_0^{2\pi} (R_\rho Z_\alpha - R_\alpha Z_\rho) d\alpha \right] \quad (\text{F.27})$$

2531 Similarly, the local safety factor can be expressed as

$$q(\rho) = \frac{F(\rho)}{2\pi} \int \frac{dl}{RB_p} \quad (\text{F.28})$$

2532 Here, $F(\rho) = RB_o$. Substituting $RB_p = \mathbf{n} \cdot \nabla \psi$ then yields

$$q(\rho) = \frac{F(\rho)}{2\pi \psi'} \int_0^{2\pi} \frac{1}{R} (R_\rho Z_\alpha - R_\alpha Z_\rho) d\alpha \quad (\text{F.29})$$

2533 with $\psi' = d\psi/d\rho$.

2534 For present purposes we can obtain relatively simple analytic expressions for all the
 2535 quantities of interest by assuming the flux surfaces are concentric ellipses, character-
 2536 ized by $R = R_0 + a\rho \cos \alpha$ and $Z = \kappa a\rho \sin \alpha$. We assume low β so that $F(\rho) \approx R_0 B_0$.
 2537 This model accounts for elongation but neglects the effects of triangularity and finite
 2538 aspect ratio. The derivatives in ?????? can now be easily evaluated. Also, after
 2539 some trial and error we chose $\bar{J}_\phi(\rho)$ to be a plausible profile which is peaked off-axis

2540 at $\rho = \rho_m$.

$$\bar{J}_\phi(\rho) = -\frac{I}{\pi a^2 \kappa} \left[\frac{\gamma^2 (1 - \rho^2) e^{\gamma \rho^2}}{e^\gamma - 1 - \gamma} \right] \quad (\text{F.30})$$

2541 Here, $\gamma = 1/(1 - \rho_m^2)$.

2542 These profiles are substituted into ?? after which each of the integrals can be evaluated
2543 analytically. A straightforward calculation yields:

$$\begin{aligned} \rho \frac{d\psi}{d\rho} &= -2\mu_0 R_0 a^2 \left(\frac{\kappa^2}{1 + \kappa^2} \right) \int_0^\rho \bar{J}_\phi \rho d\rho \\ &= \frac{\mu_0 R_0 I}{\pi} \left(\frac{\kappa}{1 + \kappa^2} \right) \frac{(1 + \gamma - \gamma \rho^2) e^{\gamma \rho^2} - 1 - \gamma}{e^\gamma - 1 - \gamma} \end{aligned} \quad (\text{F.31})$$

2544 The safety factors are given by

$$\begin{aligned} \frac{1}{q_*} &= \frac{\psi'(1)}{\kappa a^2 B_0} \\ \frac{q(\rho)}{q_*} &= \frac{\rho \psi'(\rho)}{\psi'(\rho)} \end{aligned} \quad (\text{F.32})$$

2545 ?? is now substituted into the expression for the bootstrap current given by ?. The
2546 resulting expression can then be integrated over the plasma cross section to yield the
2547 bootstrap fraction. A straightforward calculation leads to:

$$f_{BS} = \frac{I_{BS}}{I} = \frac{2\pi a^2 \kappa}{I} \int_0^1 J_{BS} \rho d\rho = \frac{K_{BS}}{K_n} \frac{\bar{n} \bar{T} R_0^2}{I_P^2} \quad (\text{F.33})$$

2548

$$K_{BS} = 4.879 \cdot K_n \cdot \left(\frac{1 + \kappa^2}{2} \right) \cdot \epsilon^{5/2} \cdot H_{BS} \quad (\text{F.34})$$

2549

$$H_{BS} = (1 + \nu_n)(1 + \nu_T)(\nu_n + 0.054\nu_T) \int_0^1 \frac{\rho^{5/2} (1 - \rho^2)^{\nu_n + \nu_T - 1}}{b_p} d\rho \quad (\text{F.35})$$

2550

$$b_p(\rho) = \frac{-e^{\gamma \rho^2} (\gamma \rho^2 - 1 - \gamma) - 1 - \gamma}{\rho (e^\gamma - 1 - \gamma)} \quad (\text{F.36})$$

2551 This is the desired result.

2552 Appendix G

2553 Compending Code Plots

2554 This chapter gives a brief overview of the plots that from using this model on several
2555 reactor prototypes: Charybdis, Proteus, ARC, Demo Pulsed, the two ARIES ACT
2556 reactors. The two types of results this information comes in are: magnet strength
2557 scans and cost sensitivity studies.

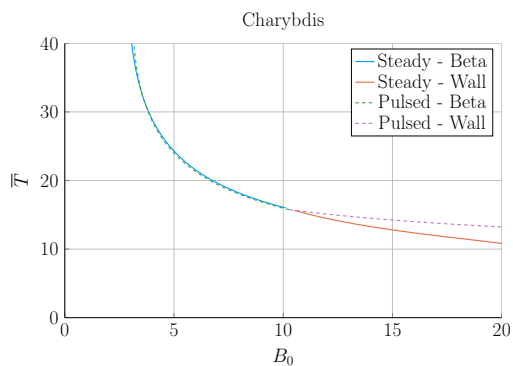
2558 In the former, all static variables are kept constant and only the magnet strength is
2559 allowed to change. The latter then focuses on changing one static variable at a time
2560 and finding several magnet strengths that satisfy certain constraints – i.e. minimum
2561 cost or when two limits are both just marginally satisfied.

2562 G.1 Magnet Strength Scans

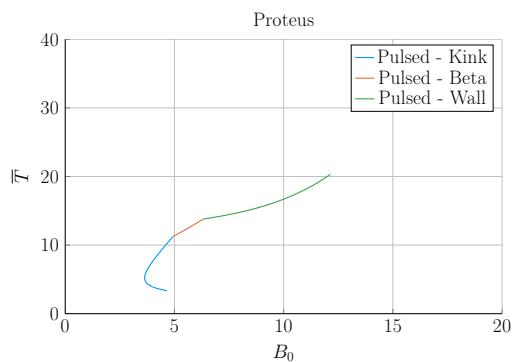
2563 This section includes the following magnet strength scans:

- 2564 1. Plasma Temperature – \overline{T}
- 2565 2. Plasma Density – \overline{n}
- 2566 3. Plasma Current – I_P
- 2567 4. Major Radius – R_0
- 2568 5. Plasma Pressure – \overline{p}
- 2569 6. Confinement Time – τ_E
- 2570 7. Current Drive Efficiency – η_{CD}
- 2571 8. Bootstrap Fraction – f_{BS}
- 2572 9. Magnetic Energy – W_M
- 2573 10. Cost-per-Watt – C_W
- 2574 11. Divertor Head Load – q_{DV}
- 2575 12. Normalized Beta Normal – $(\beta_N)_{norm}$
- 2576 13. Normalized Kink Safety Factor – $(q_{95})_{norm}$
- 2577 14. Normalized Wall Loading – $(P_W)_{norm}$
- 2578 15. Fusion Power – P_F
- 2579 16. Blanket Thickness – b
- 2580 17. TF Coil Thickness – c
- 2581 18. Central Solenoid Thickness – d
- 2582 19. Central Solenoid Height – h_{CS}
- 2583 20. Central Solenoid Inner Radius – R_{CS}

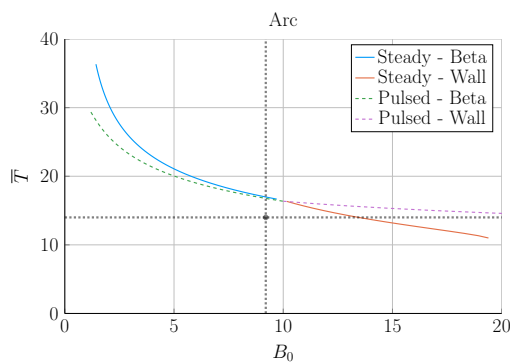
Plasma Temperature – \bar{T}



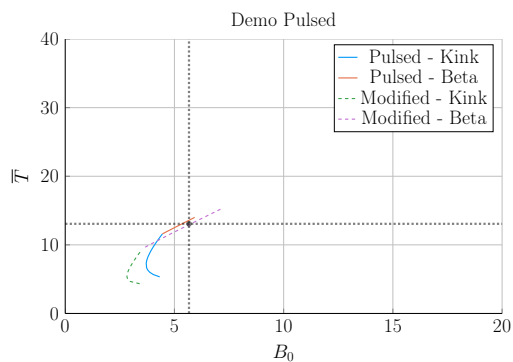
(a) Charybdis



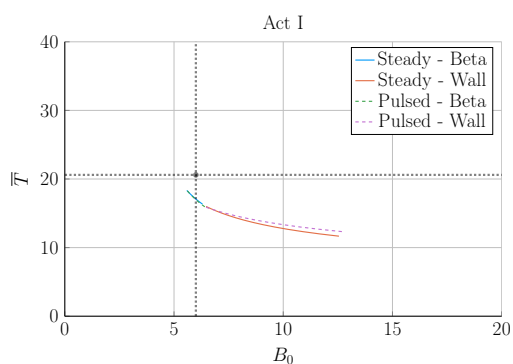
(b) Proteus



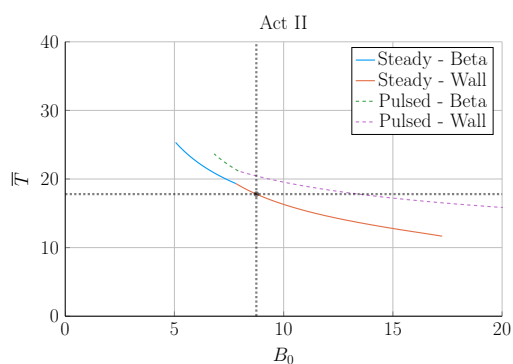
(c) Arc



(d) Demo Pulsed

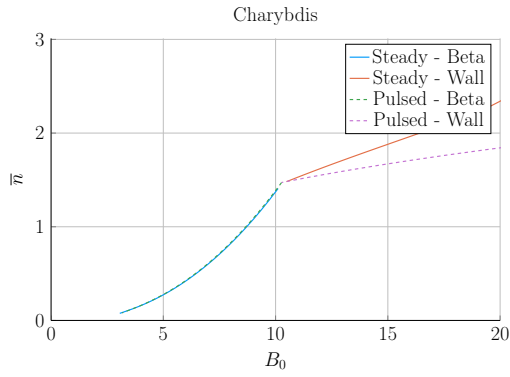


(e) Act I

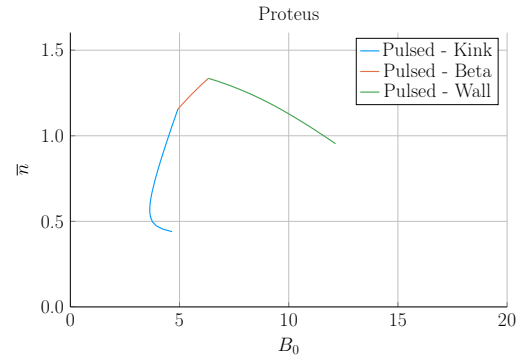


(f) Act II

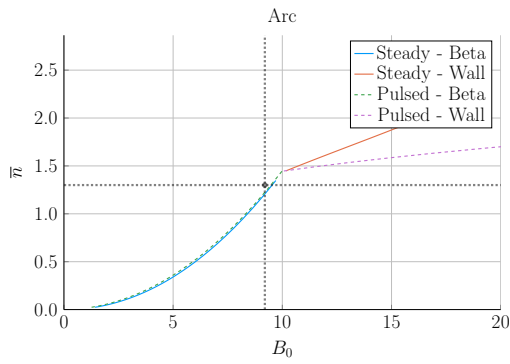
Figure G-1: Magnet Scan: \bar{T} vs B_0



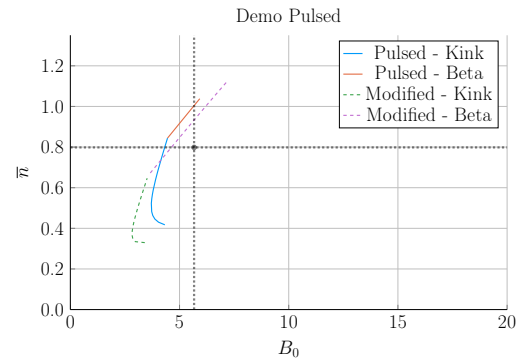
(a) Charybdis



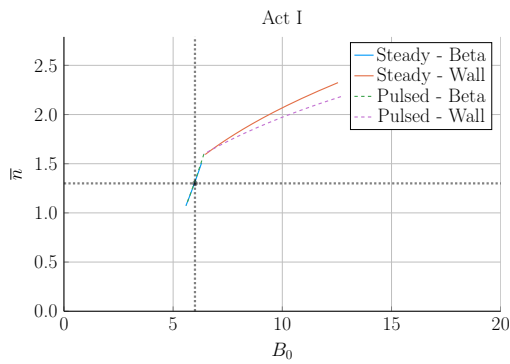
(b) Proteus



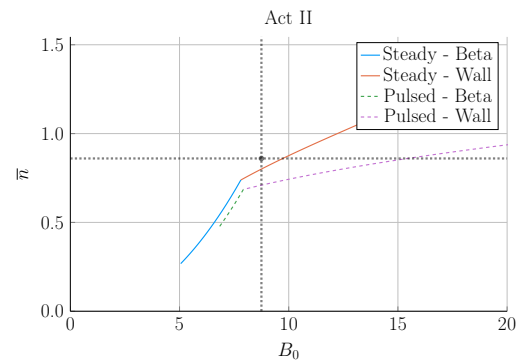
(c) Arc



(d) Demo Pulsed

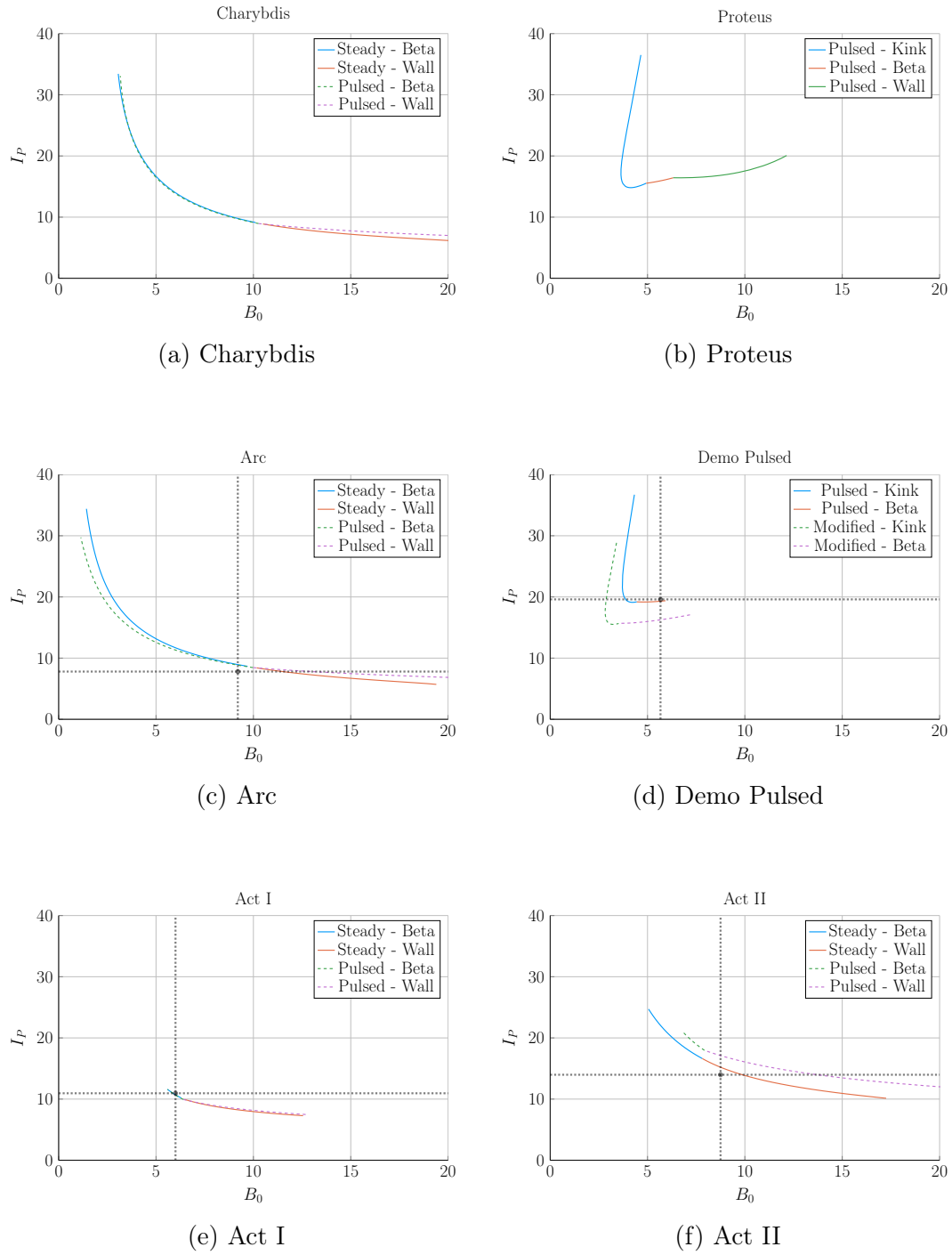


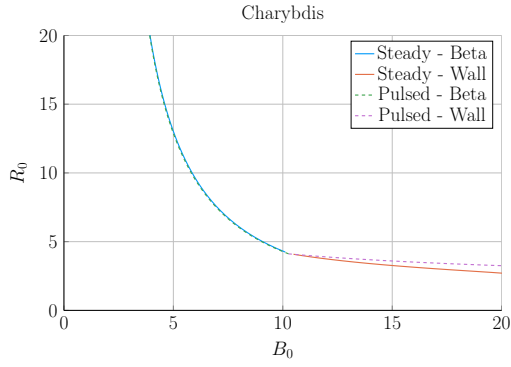
(e) Act I



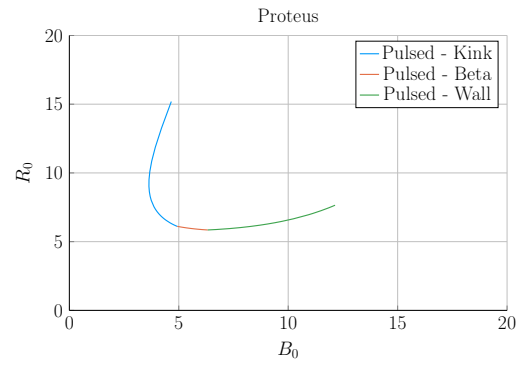
(f) Act II

Figure G-2: Magnet Scan: \bar{n} vs B_0

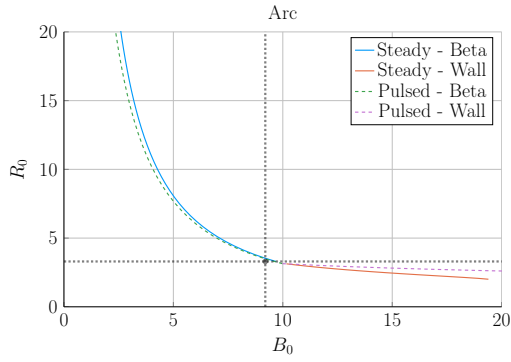
Figure G-3: Magnet Scan: I_P vs B_0

Major Radius – R_0 

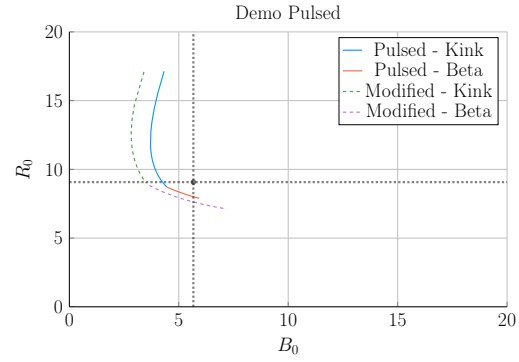
(a) Charybdis



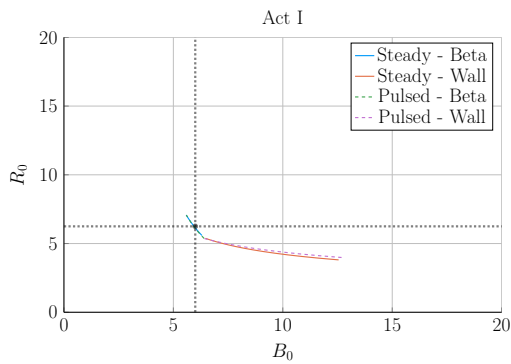
(b) Proteus



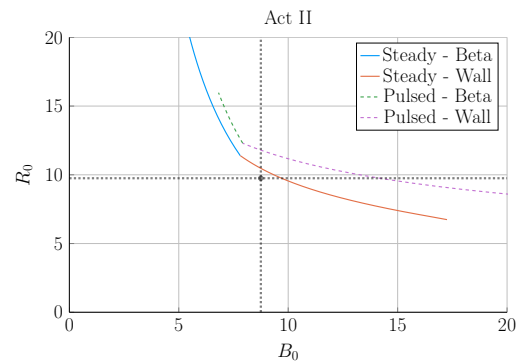
(c) Arc



(d) Demo Pulsed



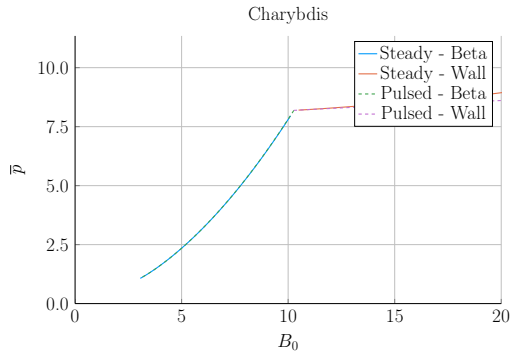
(e) Act I



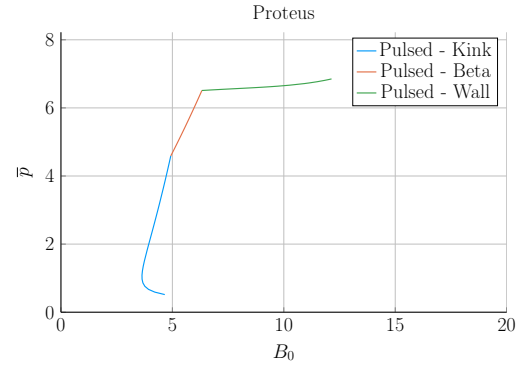
(f) Act II

Figure G-4: Magnet Scan: R_0 vs B_0

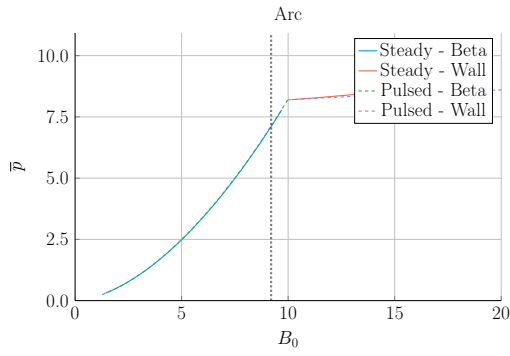
Plasma Pressure – \bar{p}



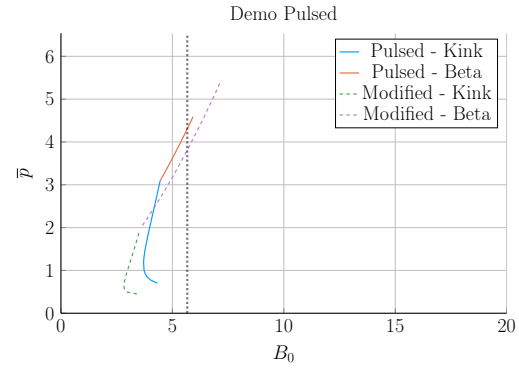
(a) Charybdis



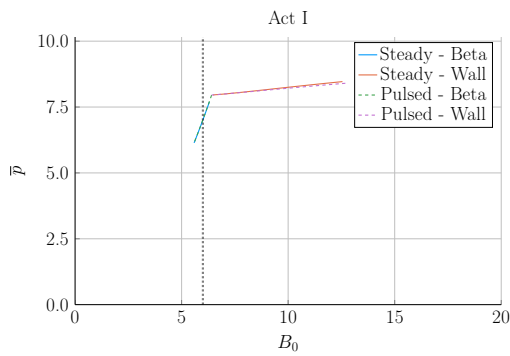
(b) Proteus



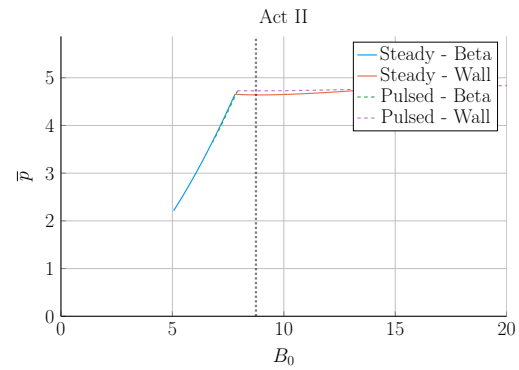
(c) Arc



(d) Demo Pulsed



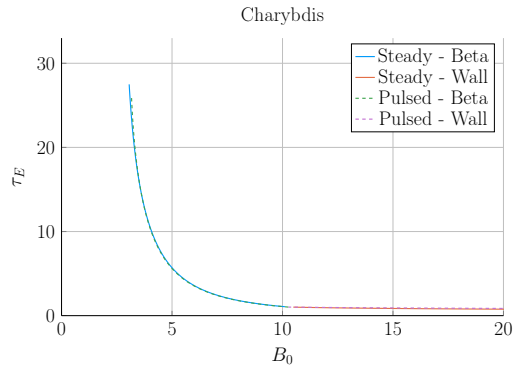
(e) Act I



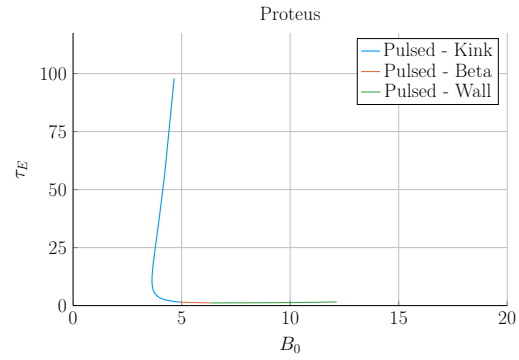
(f) Act II

Figure G-5: Magnet Scan: \bar{p} vs B_0

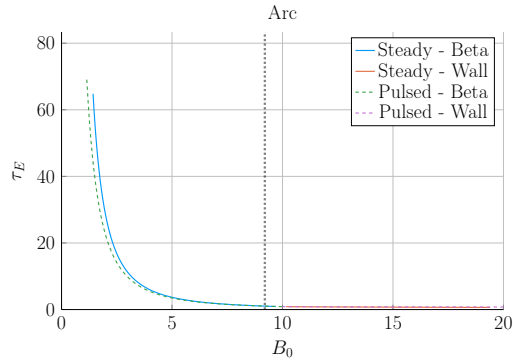
Confinement Time – τ_E



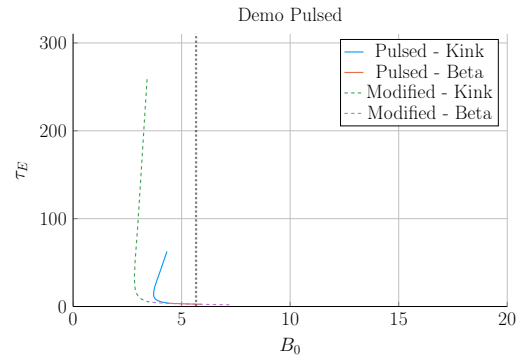
(a) Charybdis



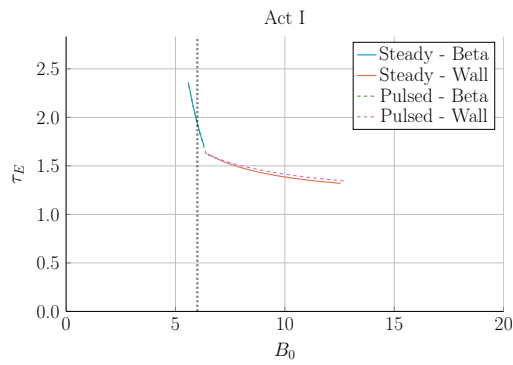
(b) Proteus



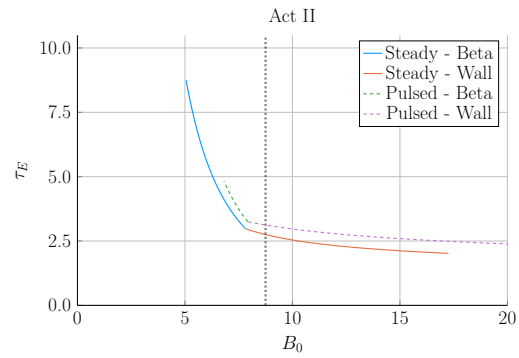
(c) Arc



(d) Demo Pulsed



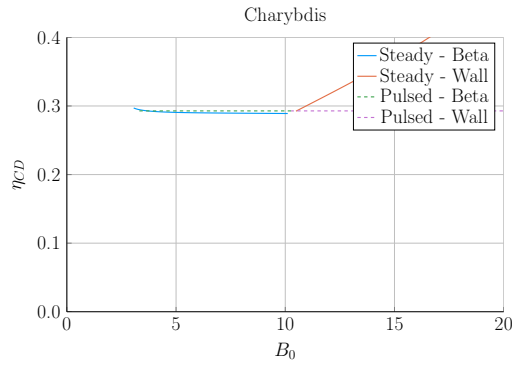
(e) Act I



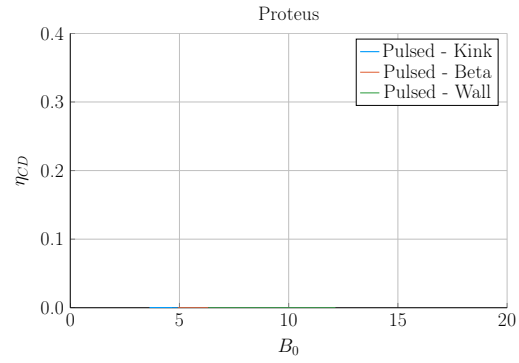
(f) Act II

Figure G-6: Magnet Scan: τ_E vs B_0

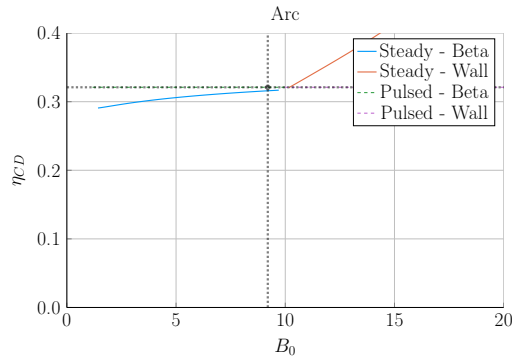
Current Drive Efficiency – η_{CD}



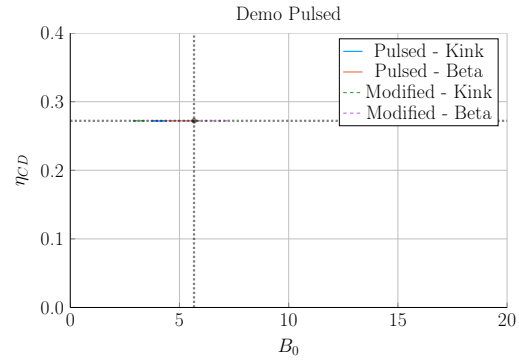
(a) Charybdis



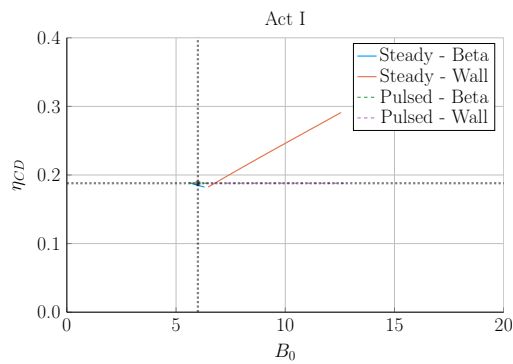
(b) Proteus



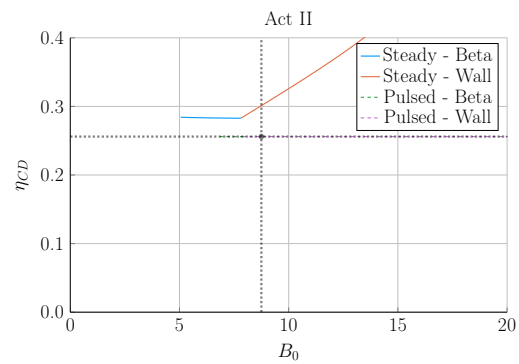
(c) Arc



(d) Demo Pulsed



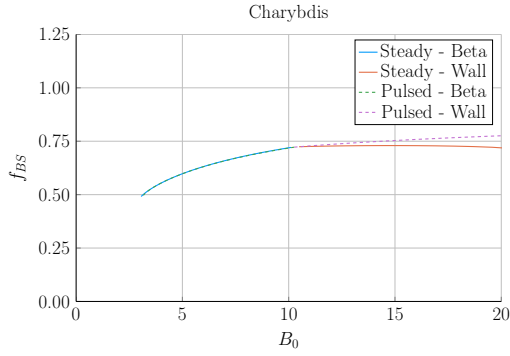
(e) Act I



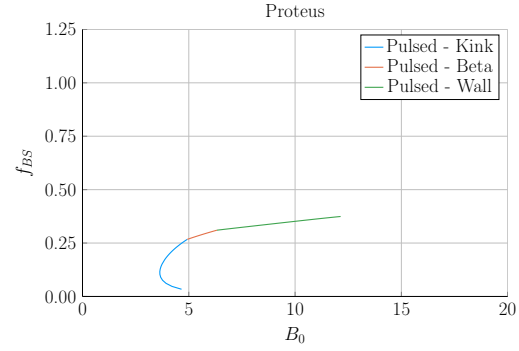
(f) Act II

Figure G-7: Magnet Scan: η_{CD} vs B_0

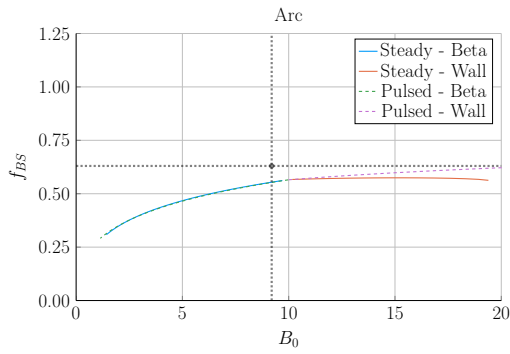
Bootstrap Fraction – f_{BS}



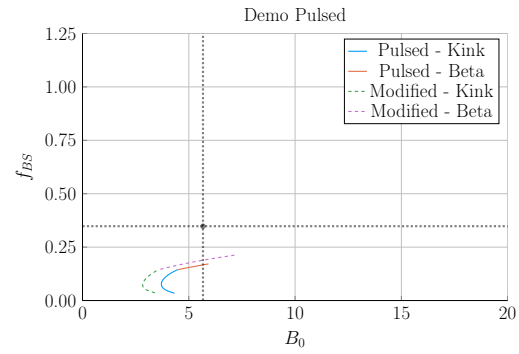
(a) Charybdis



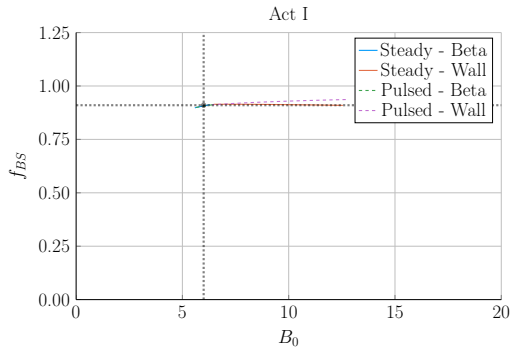
(b) Proteus



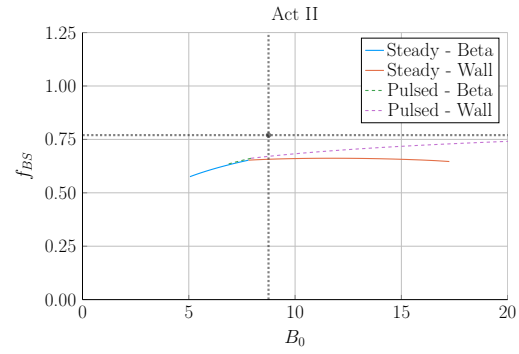
(c) Arc



(d) Demo Pulsed

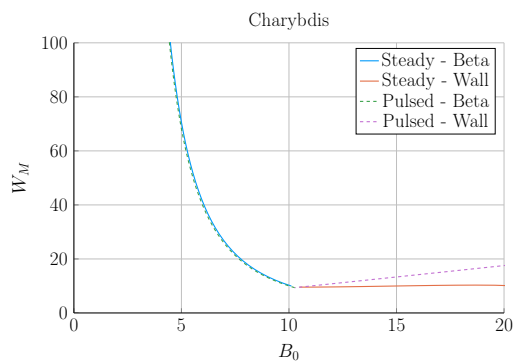


(e) Act I

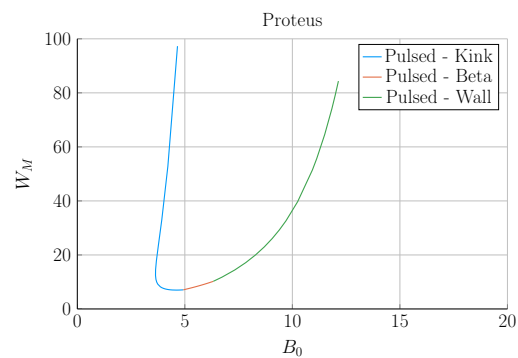


(f) Act II

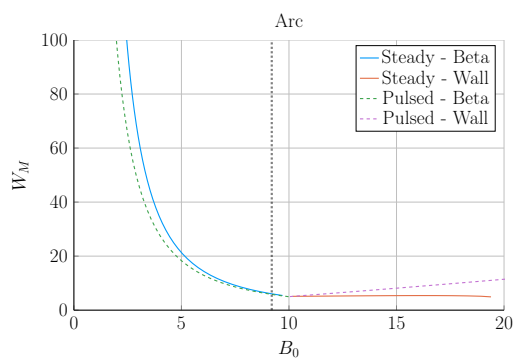
Figure G-8: Magnet Scan: f_{BS} vs B_0

Magnetic Energy – W_M 

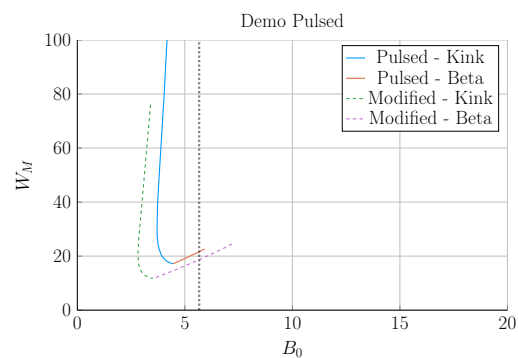
(a) Charybdis



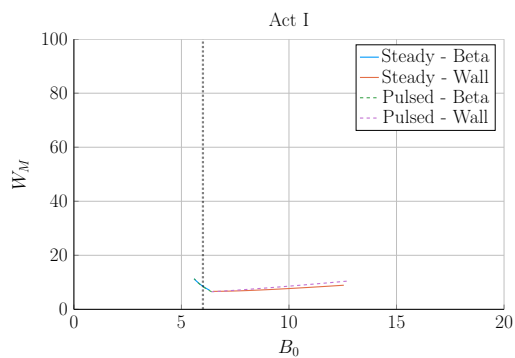
(b) Proteus



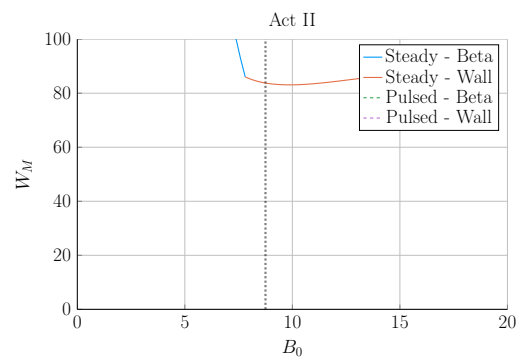
(c) Arc



(d) Demo Pulsed

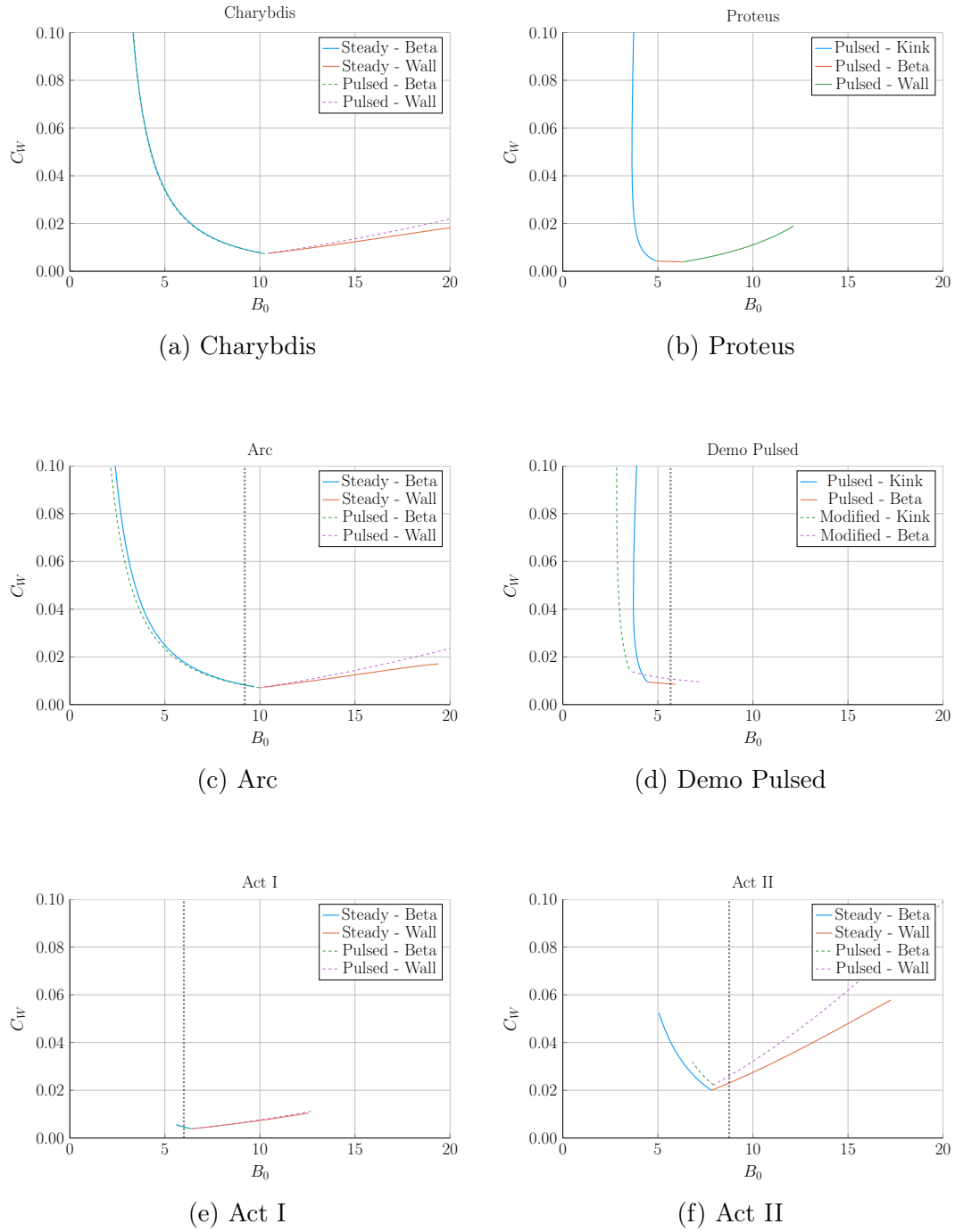


(e) Act I



(f) Act II

Figure G-9: Magnet Scan: W_M vs B_0

Figure G-10: Magnet Scan: C_W vs B_0

Divertor Head Load – q_{DV}

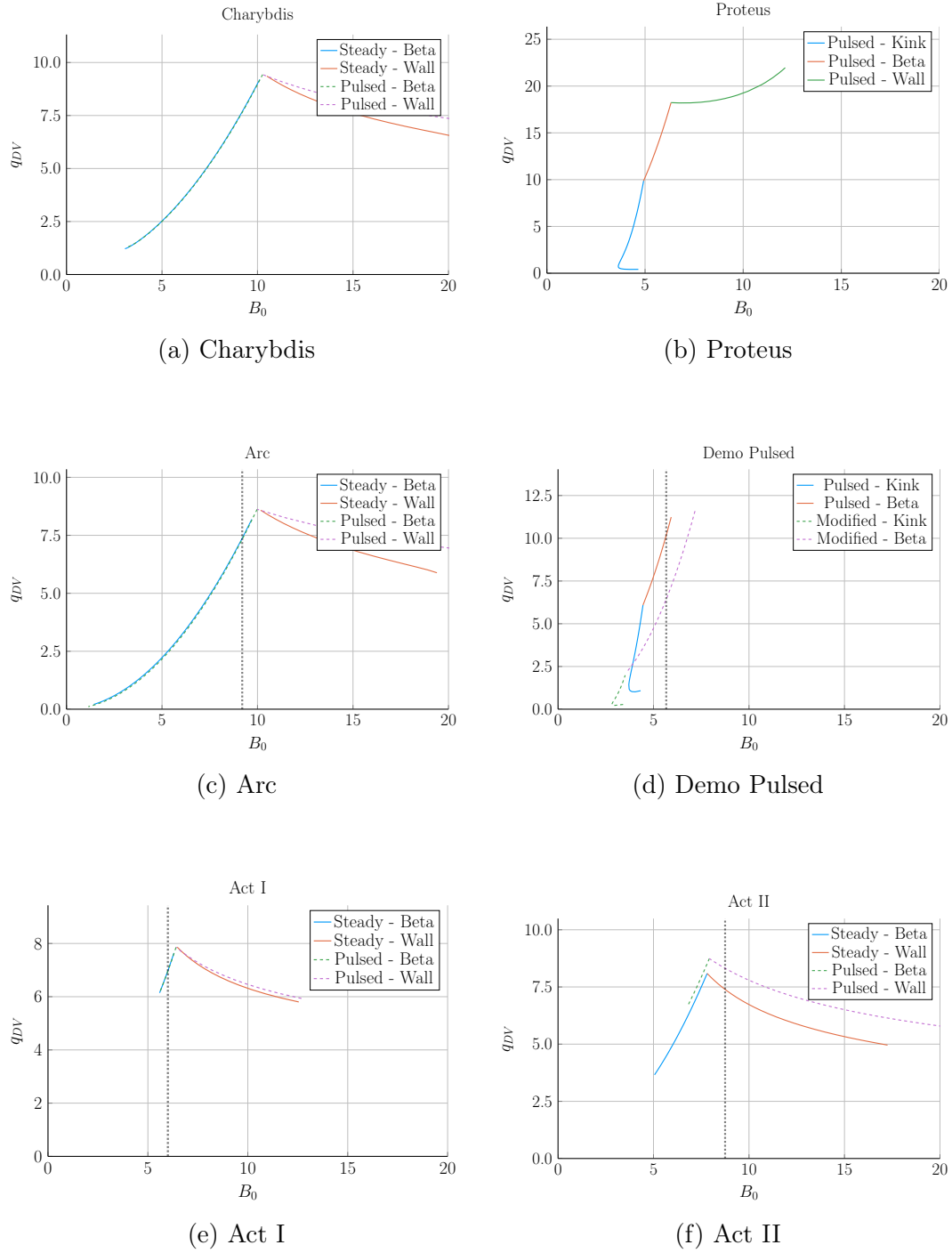


Figure G-11: Magnet Scan: q_{DV} vs B_0

Normalized Beta Normal – $(\beta_N)_{norm}$

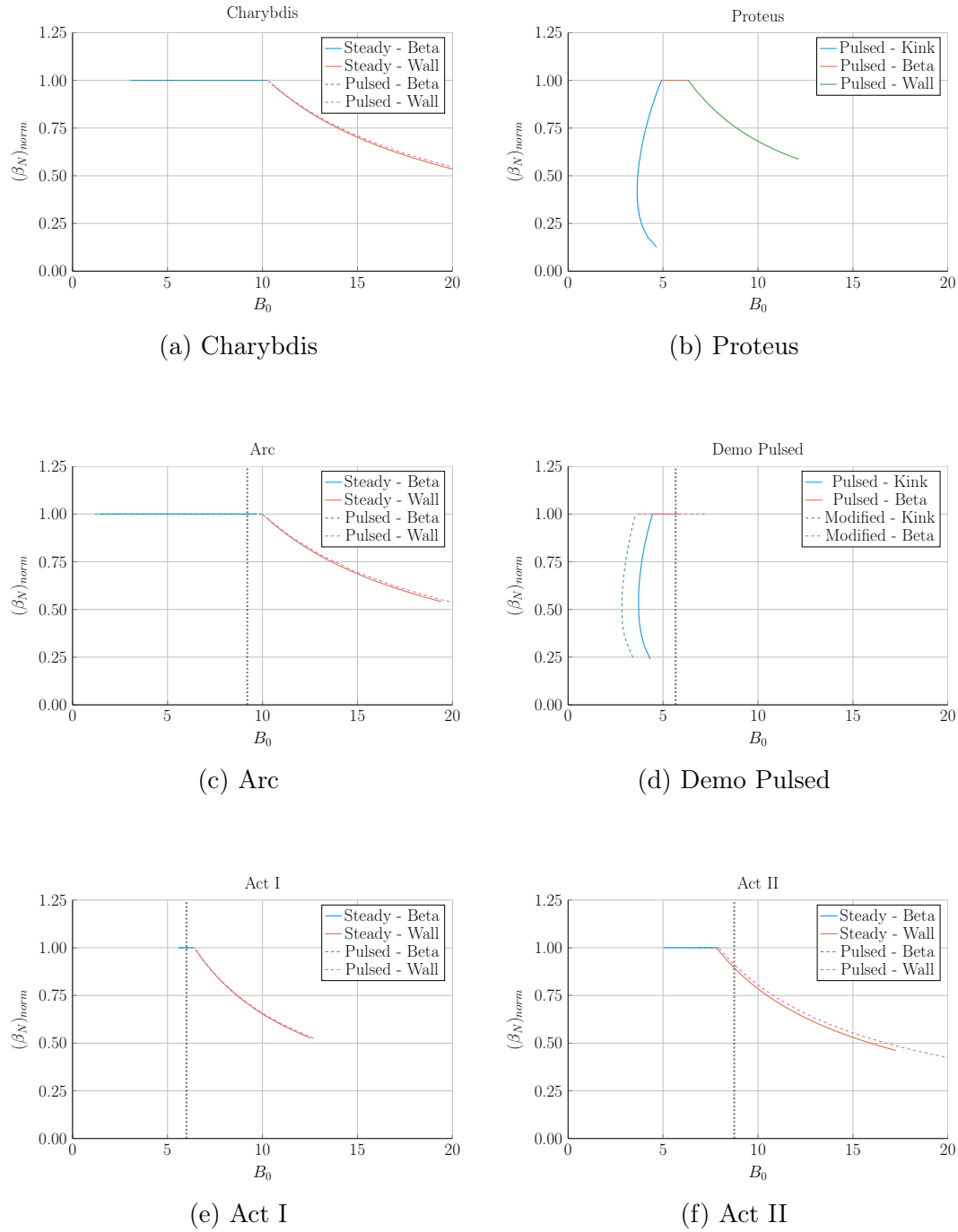


Figure G-12: Magnet Scan: $(\beta_N)_{norm}$ vs B_0

Normalized Kink Safety Factor – $(q_{95})_{norm}$

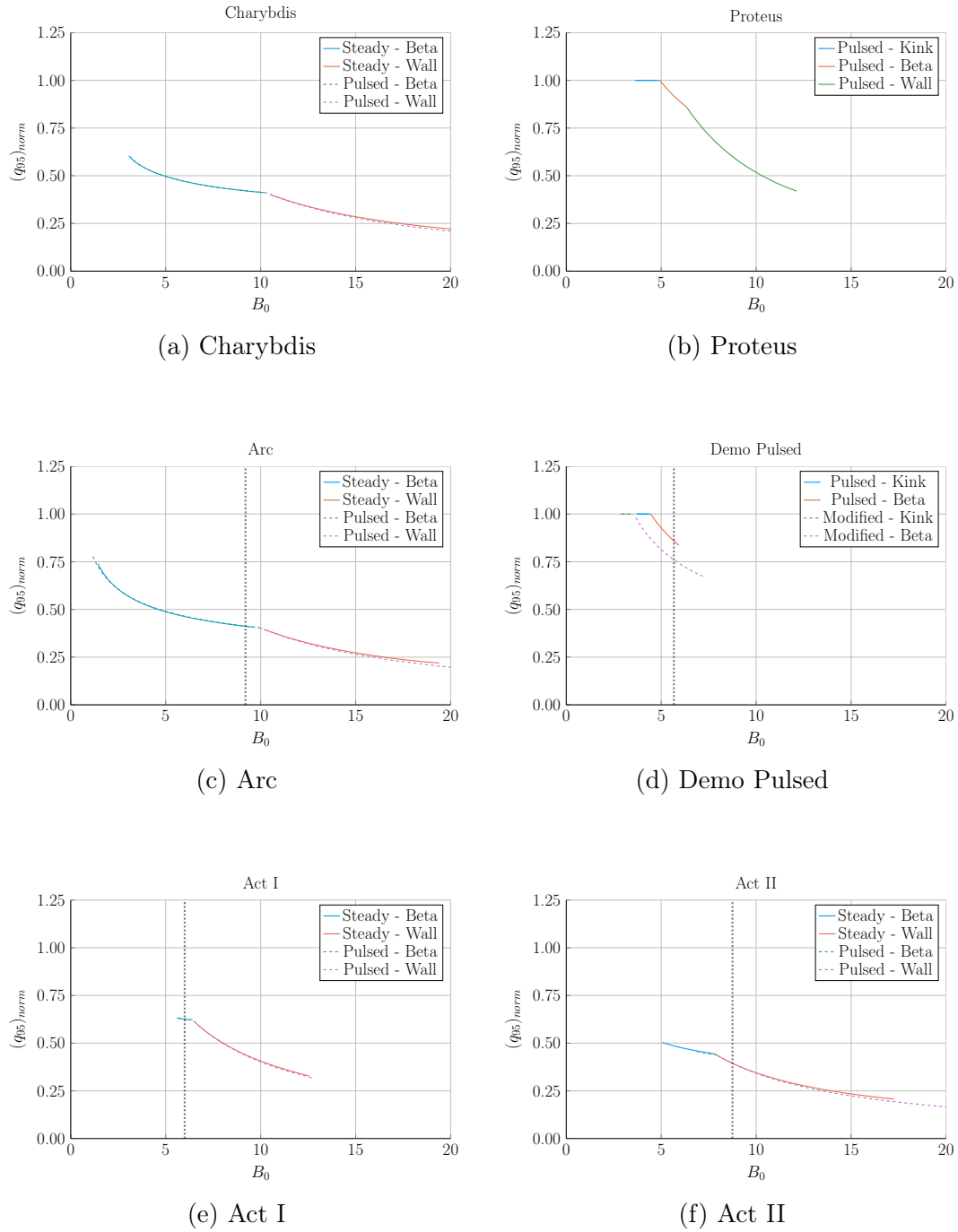


Figure G-13: Magnet Scan: $(q_{95})_{norm}$ vs B_0

Normalized Wall Loading – $(P_W)_{norm}$

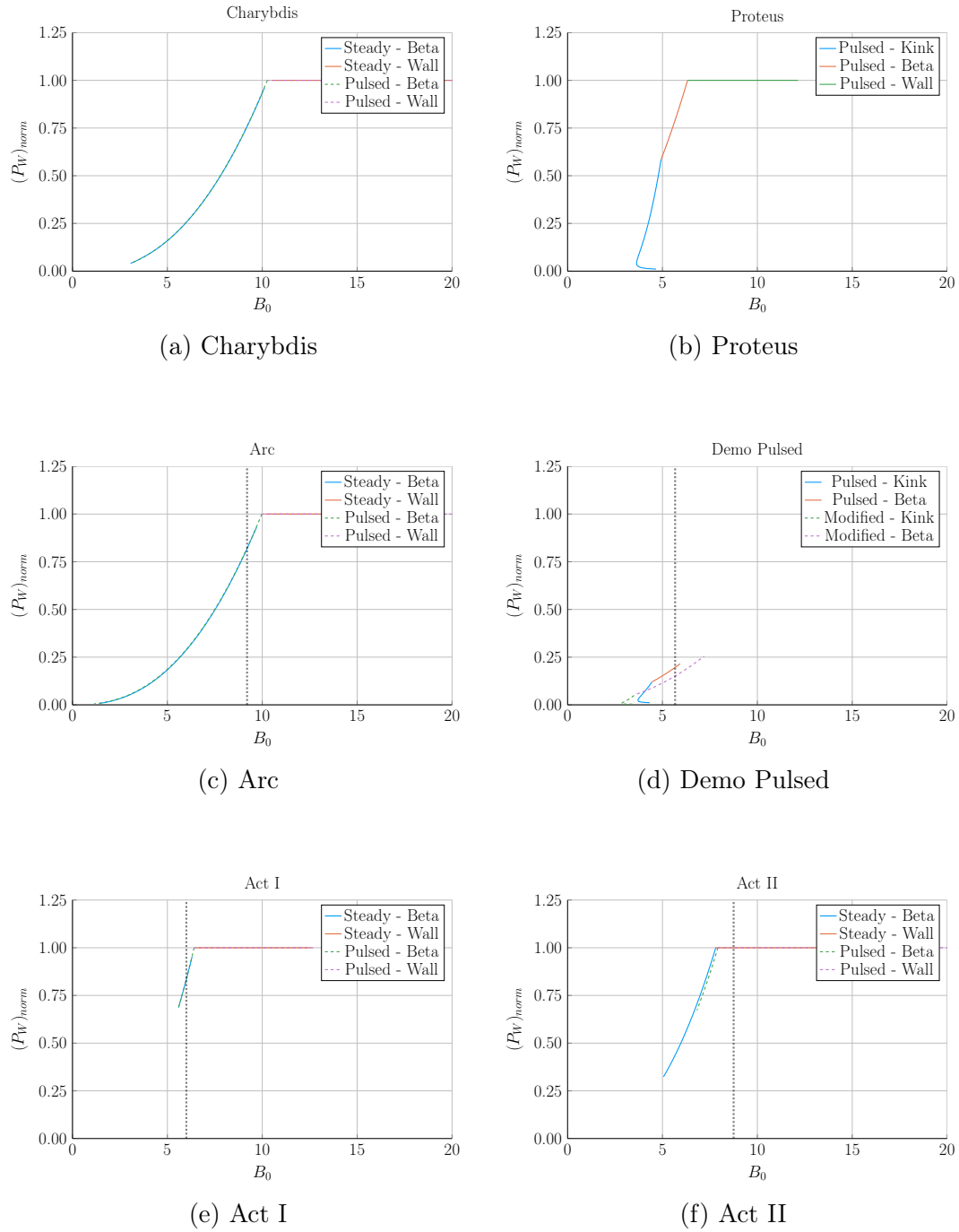
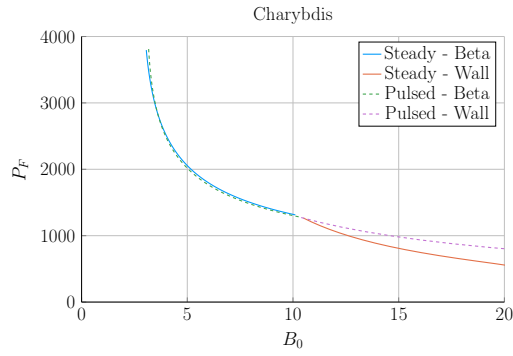
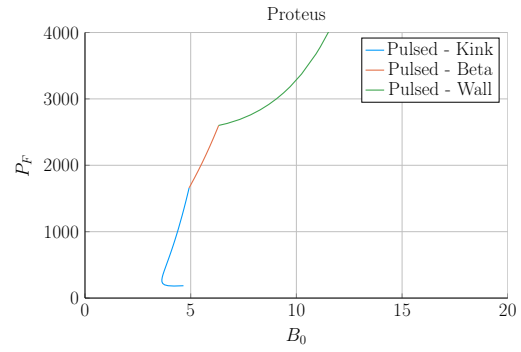


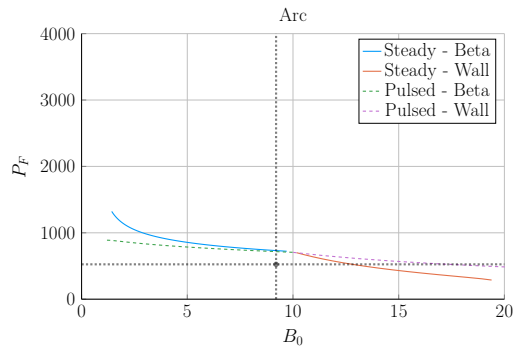
Figure G-14: Magnet Scan: $(P_W)_{norm}$ vs B_0



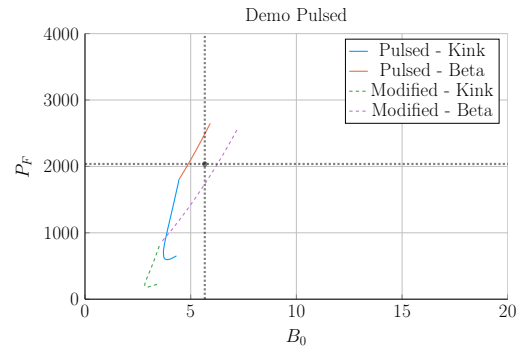
(a) Charybdis



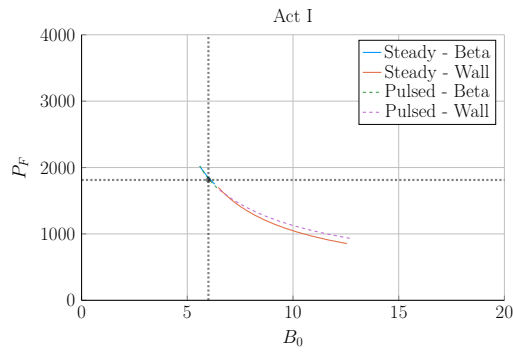
(b) Proteus



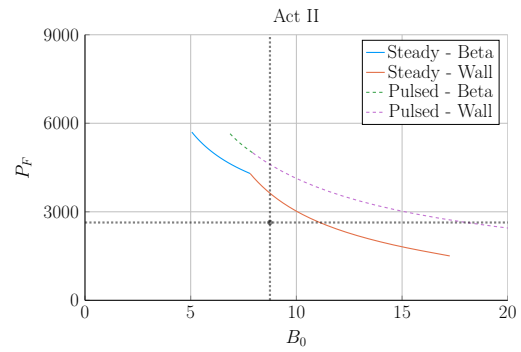
(c) Arc



(d) Demo Pulsed

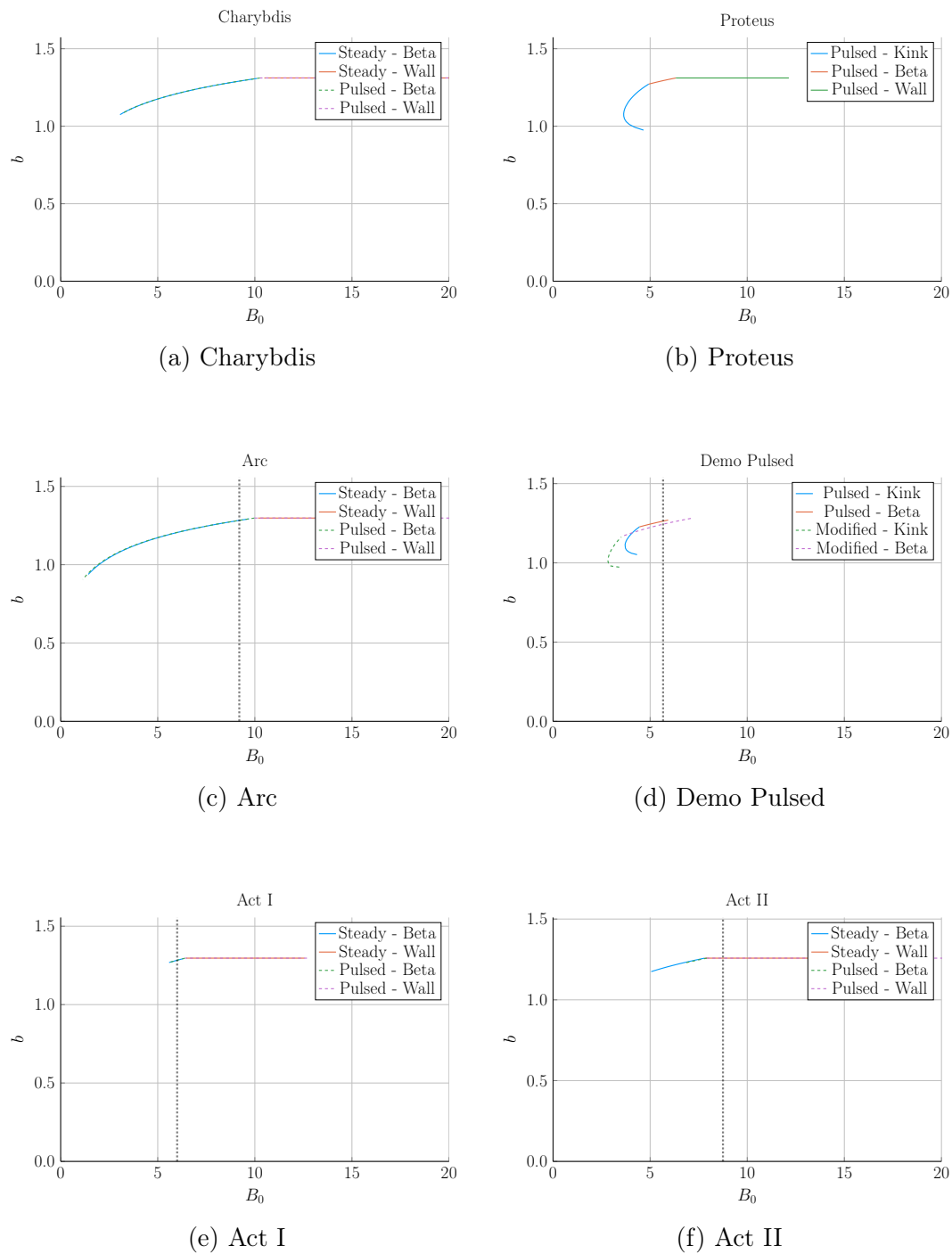


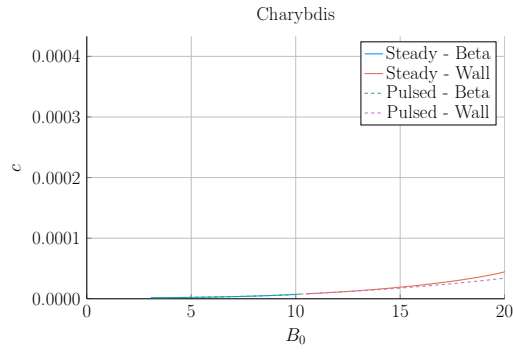
(e) Act I



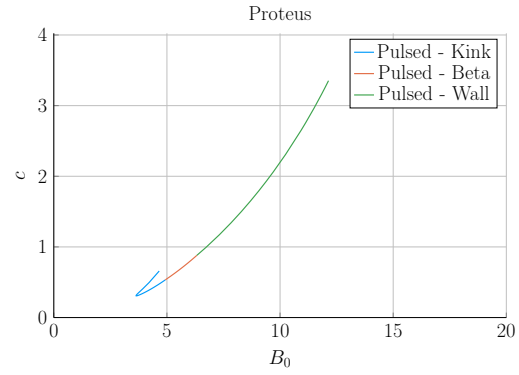
(f) Act II

Figure G-15: Magnet Scan: P_F vs B_0

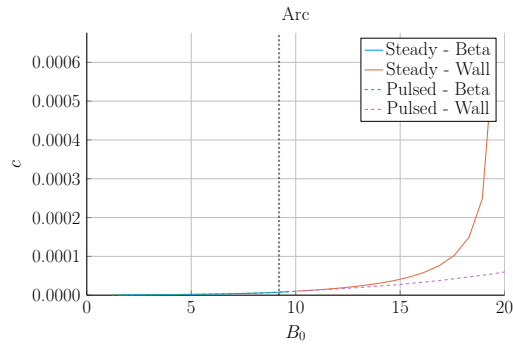
Blanket Thickness – b Figure G-16: Magnet Scan: b vs B_0



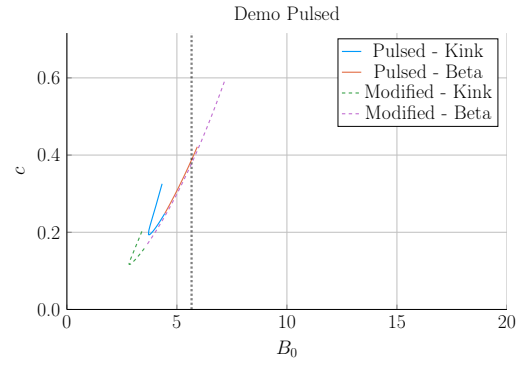
(a) Charybdis



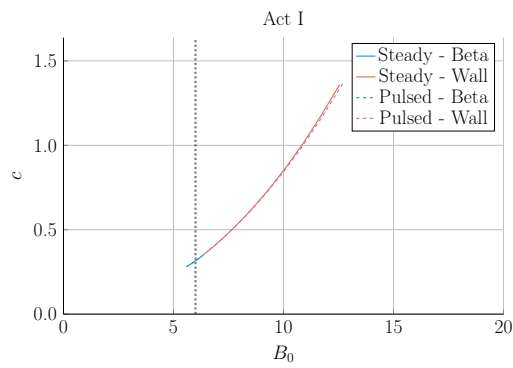
(b) Proteus



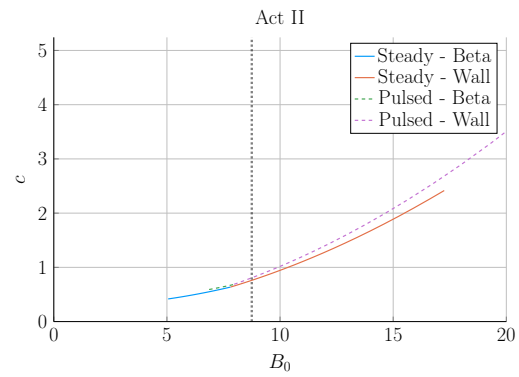
(c) Arc



(d) Demo Pulsed



(e) Act I



(f) Act II

Figure G-17: Magnet Scan: c vs B_0

Central Solenoid Thickness – d

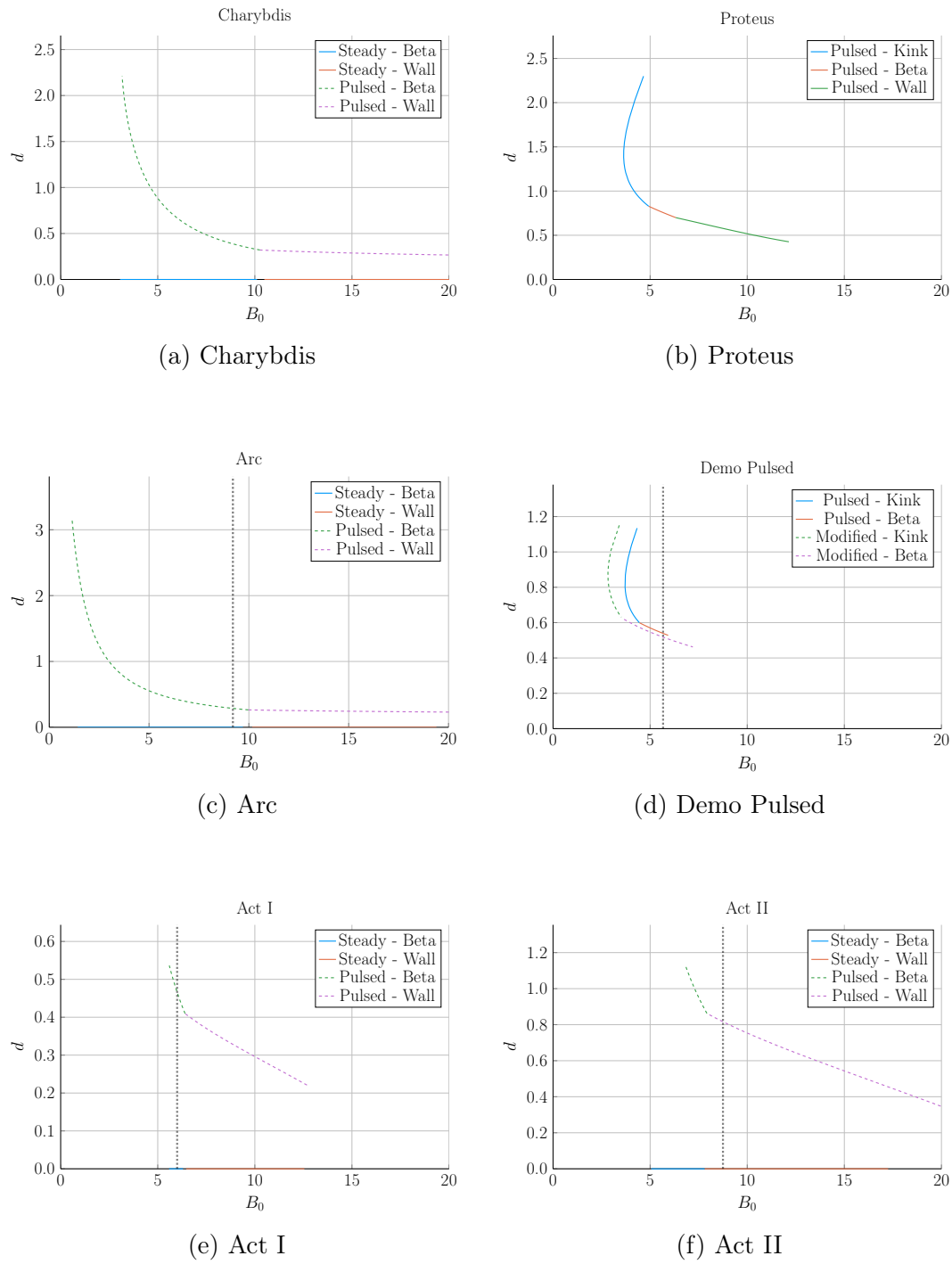
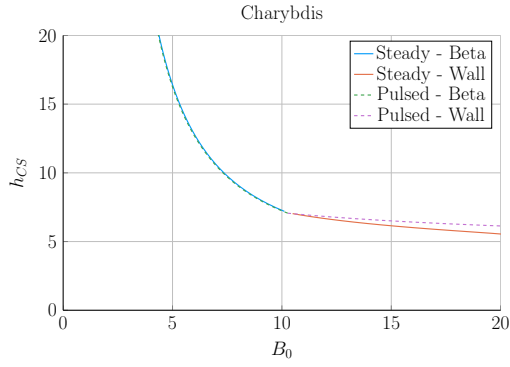
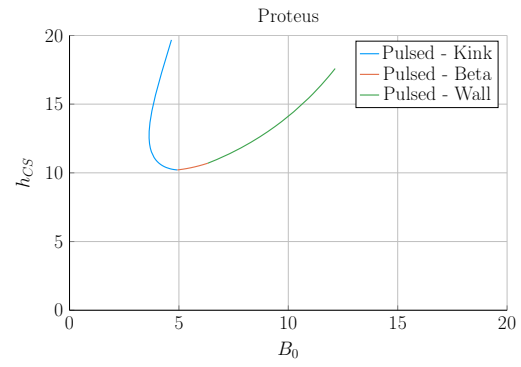


Figure G-18: Magnet Scan: d vs B_0

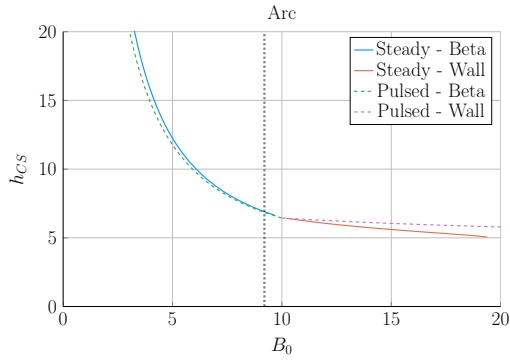
Central Solenoid Height – h_{CS}



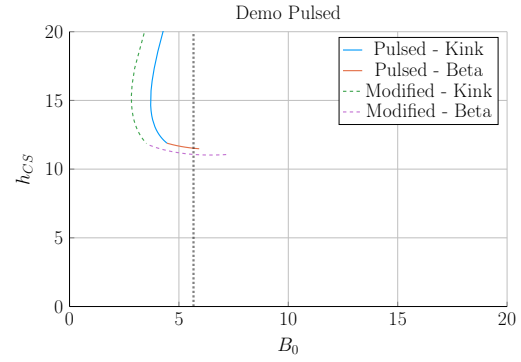
(a) Charybdis



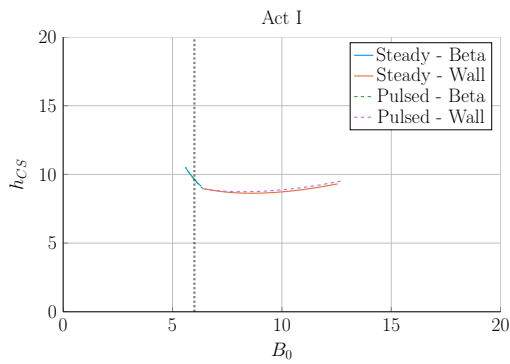
(b) Proteus



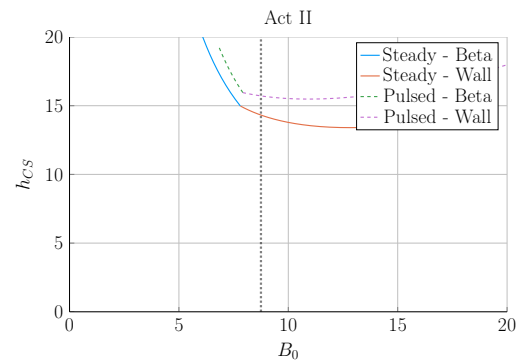
(c) Arc



(d) Demo Pulsed



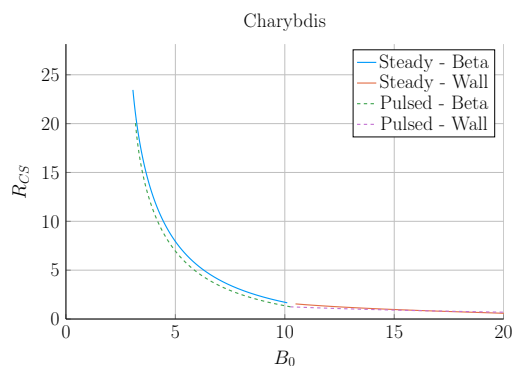
(e) Act I



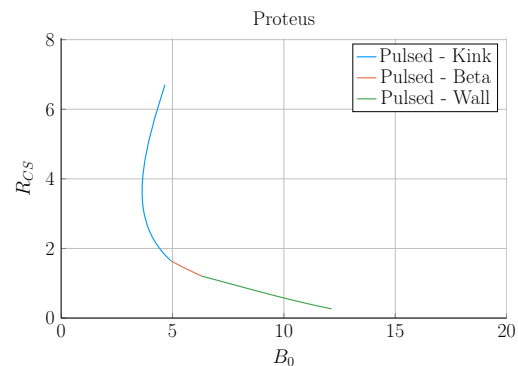
(f) Act II

Figure G-19: Magnet Scan: h_{CS} vs B_0

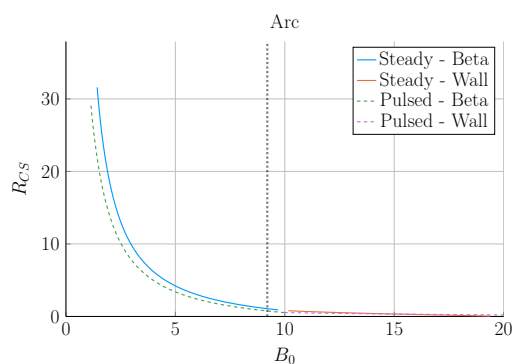
Central Solenoid Inner Radius – R_{CS}



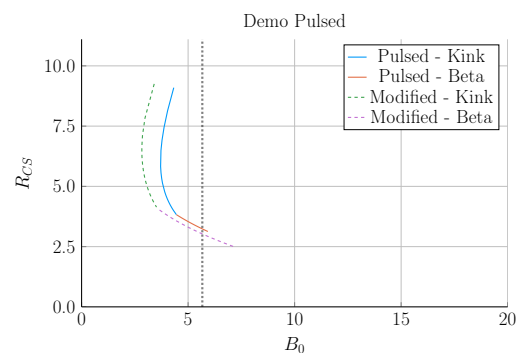
(a) Charybdis



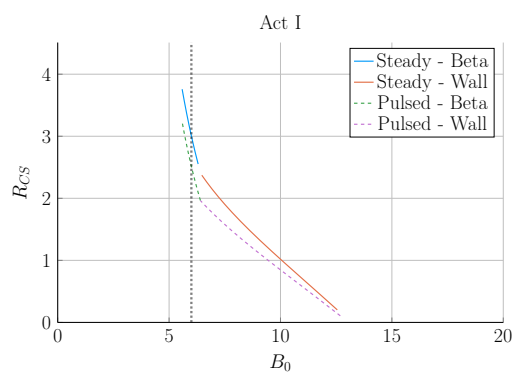
(b) Proteus



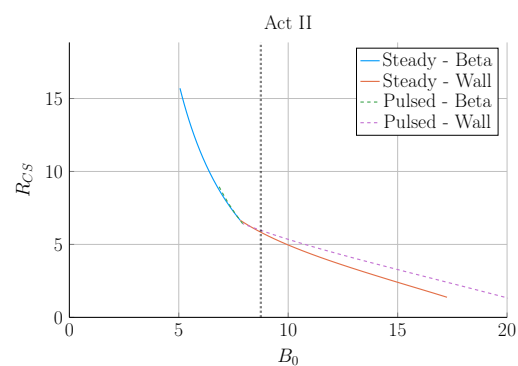
(c) Arc



(d) Demo Pulsed



(e) Act I



(f) Act II

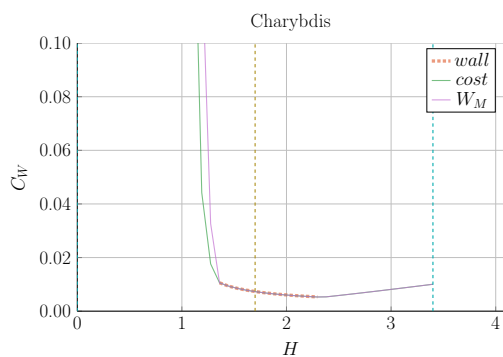
Figure G-20: Magnet Scan: R_{CS} vs B_0

2604 G.2 Cost Sensitivity Studies

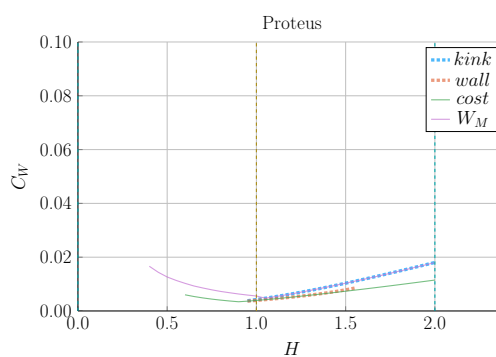
2605 This section includes the following cost sensitivity studies:

- 2606 1. Enhancement Factor – H
- 2607 2. Physics Gain – Q
- 2608 3. Flattop Duration – τ_{FT}
- 2609 4. Greenwald Fraction – N_G
- 2610 5. Dilution Factor – f_D
- 2611 6. Effective Charge – Z_{eff}
- 2612 7. Inverse Aspect Ratio – ϵ
- 2613 8. Elongation – κ_{95}
- 2614 9. Triangularity – δ_{95}
- 2615 10. Density Peaking Factor – ν_n
- 2616 11. Temperature Peaking Factor – ν_T
- 2617 12. Internal Inductance – l_i
- 2618 13. Max Beta Normal – $(\beta_N)_{max}$
- 2619 14. Max Kink Safety Factor – $(q_{95})_{max}$
- 2620 15. Max Wall Loading – $(P_W)_{max}$

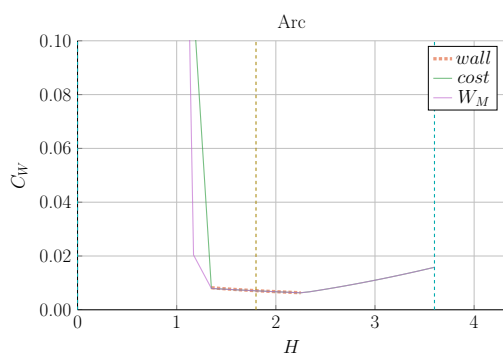
Enhancement Factor – H



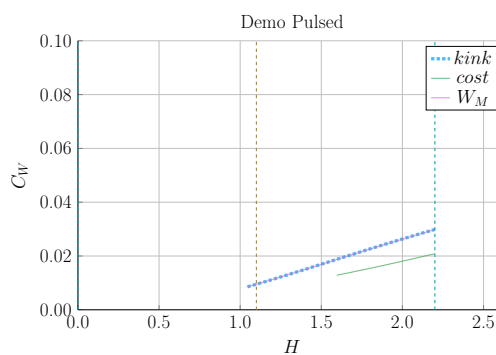
(a) Charybdis



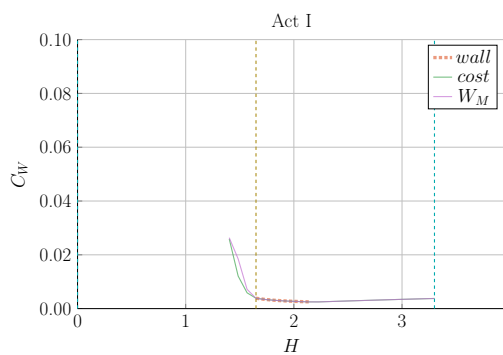
(b) Proteus



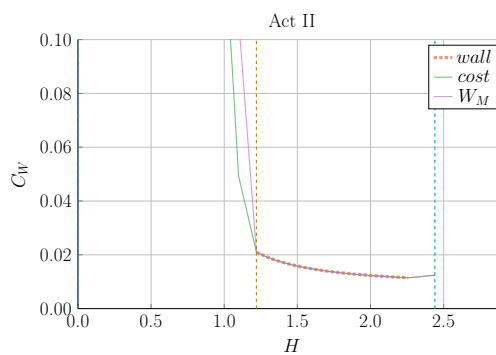
(c) Arc



(d) Demo Pulsed

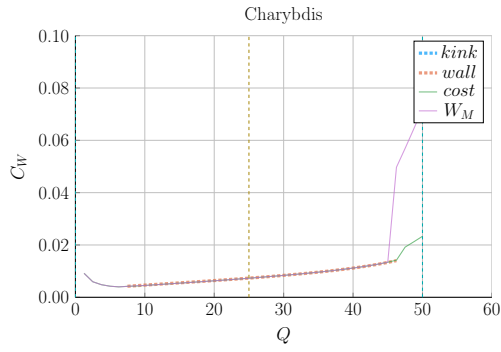


(e) Act I

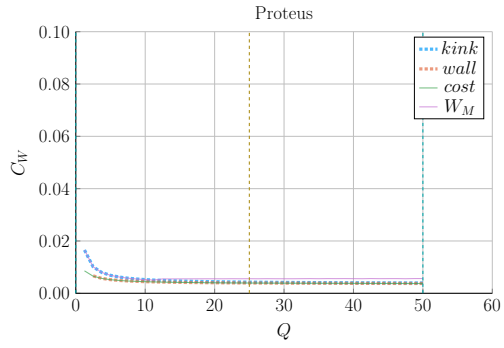


(f) Act II

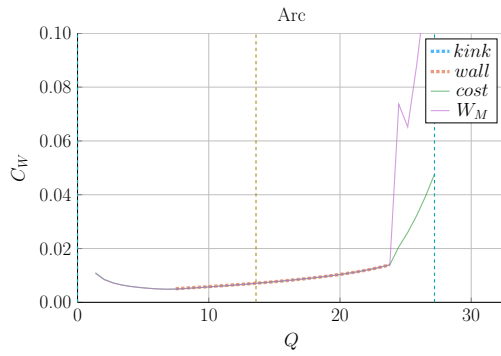
Figure G-21: Cost Sensitivity: H vs. B_0



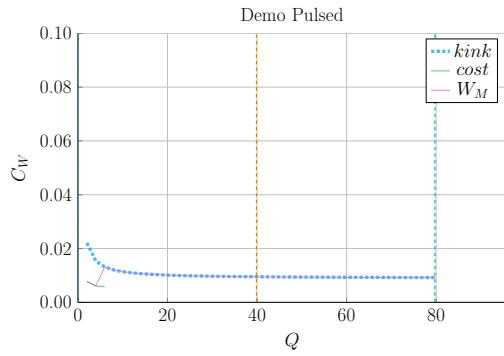
(a) Charybdis



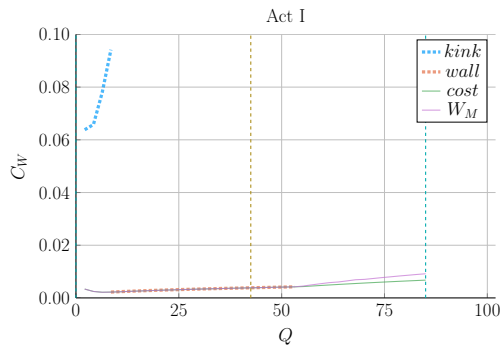
(b) Proteus



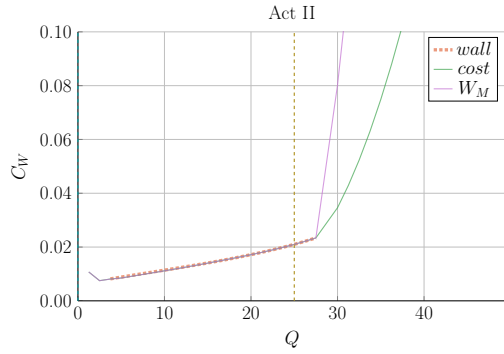
(c) Arc



(d) Demo Pulsed



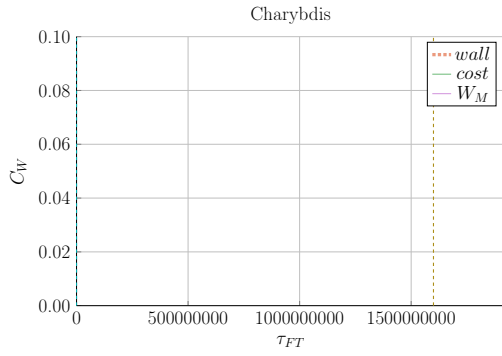
(e) Act I



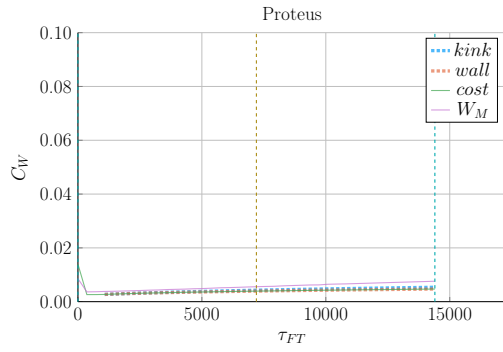
(f) Act II

Figure G-22: Cost Sensitivity: Q vs. B_0

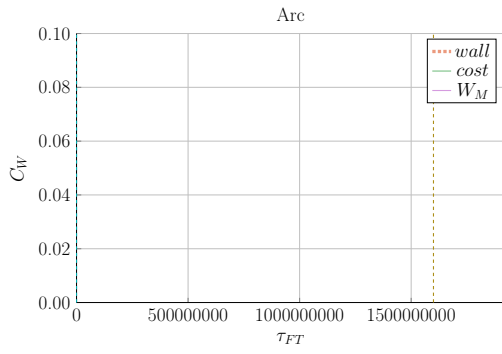
Flattop Duration – τ_{FT}



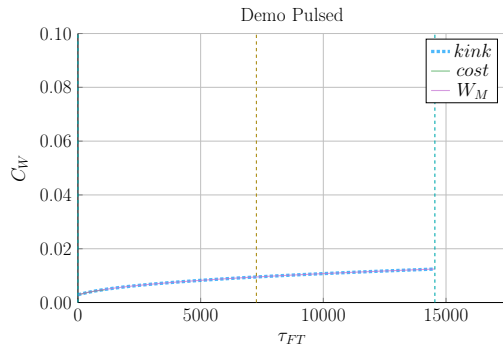
(a) Charybdis



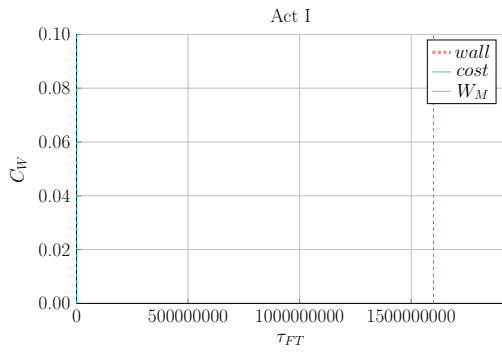
(b) Proteus



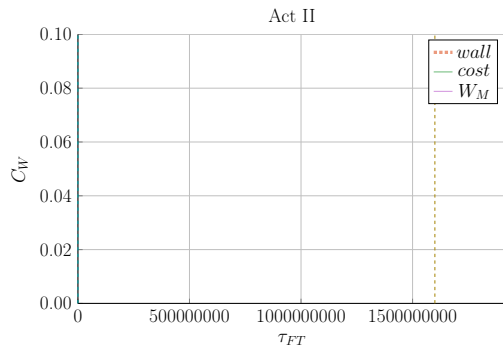
(c) Arc



(d) Demo Pulsed



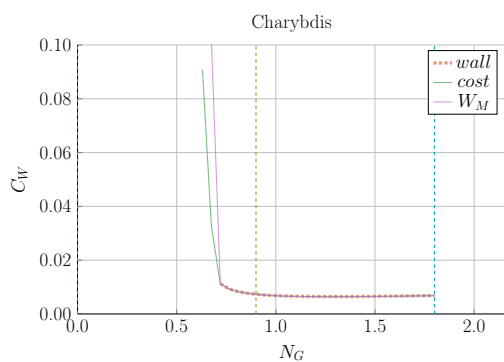
(e) Act I



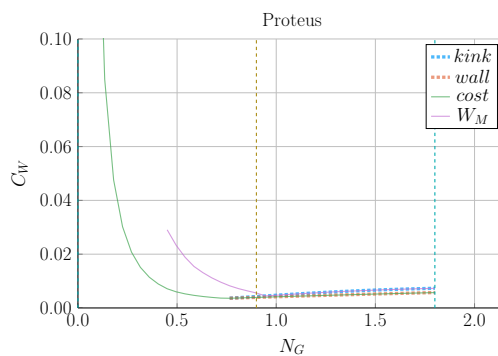
(f) Act II

Figure G-23: Cost Sensitivity: τ_{FT} vs. B_0

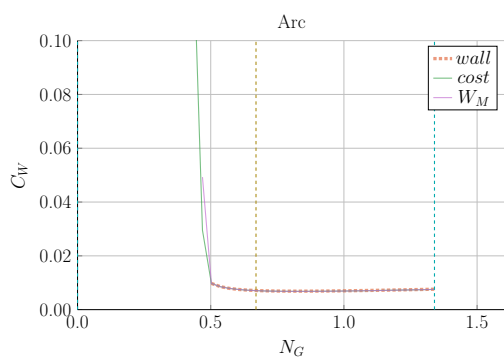
Greenwald Fraction – N_G



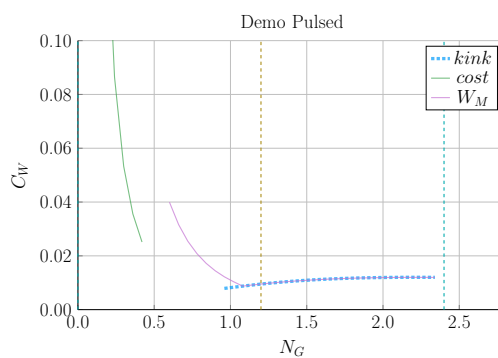
(a) Charybdis



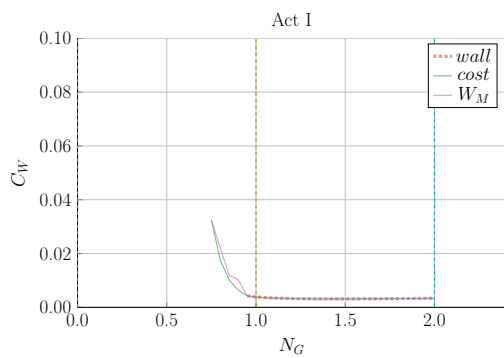
(b) Proteus



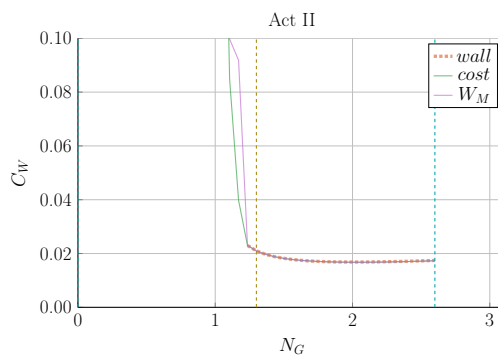
(c) Arc



(d) Demo Pulsed

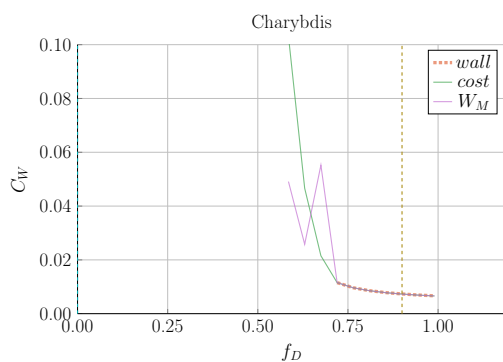


(e) Act I

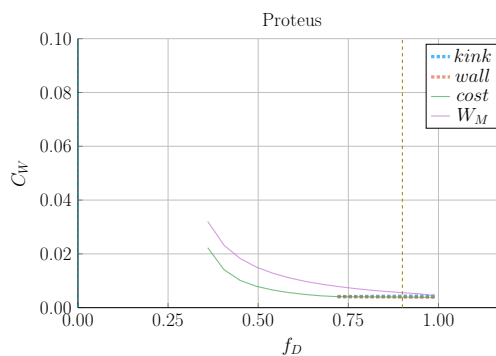


(f) Act II

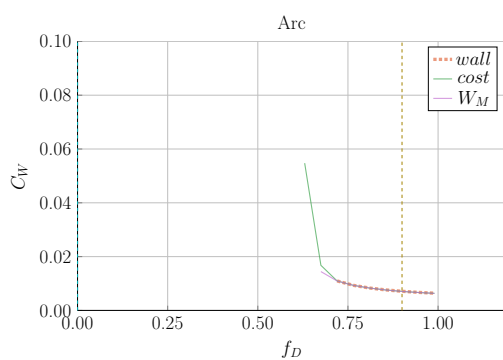
Figure G-24: Cost Sensitivity: N_G vs. B_0

Dilution Factor – f_D 

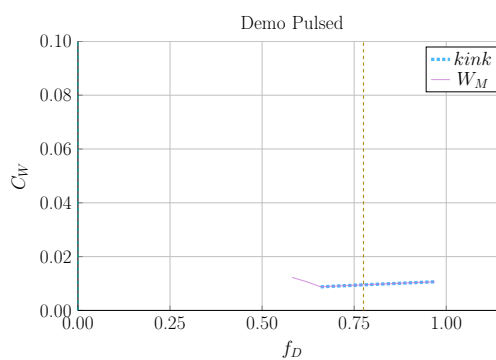
(a) Charybdis



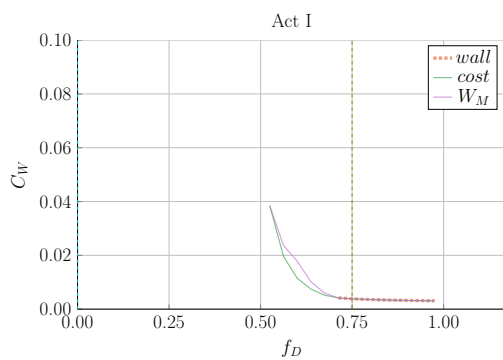
(b) Proteus



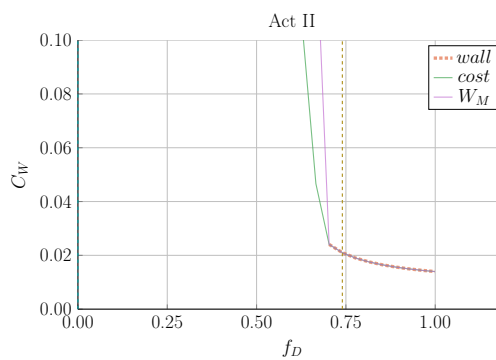
(c) Arc



(d) Demo Pulsed

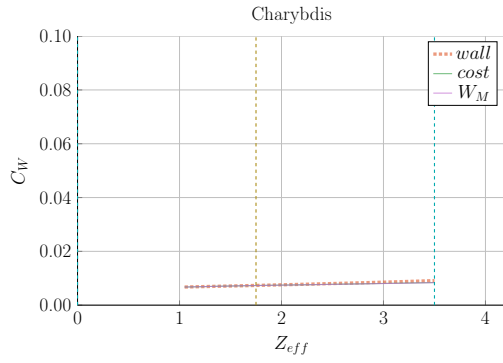


(e) Act I

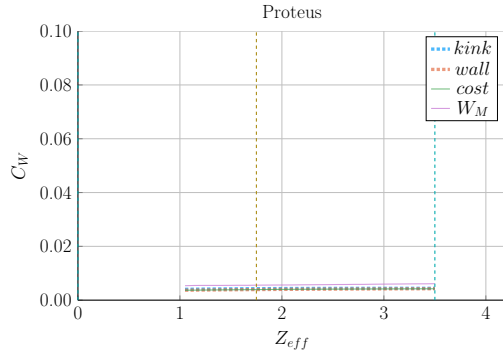


(f) Act II

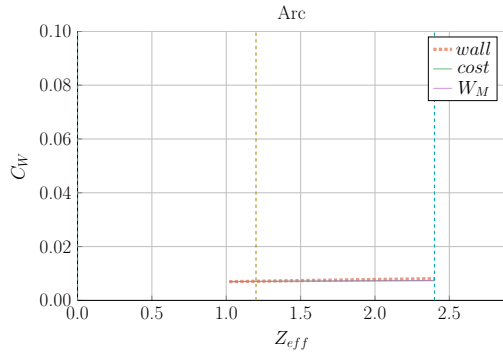
Figure G-25: Cost Sensitivity: f_D vs. B_0



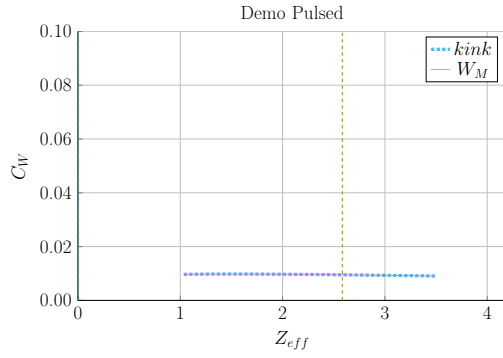
(a) Charybdis



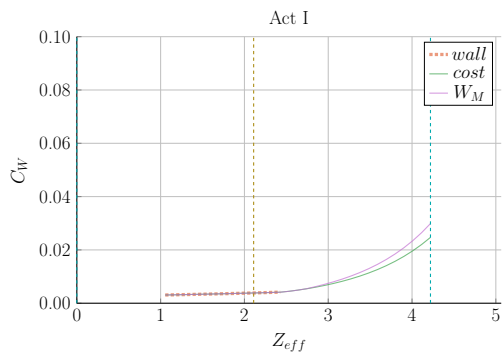
(b) Proteus



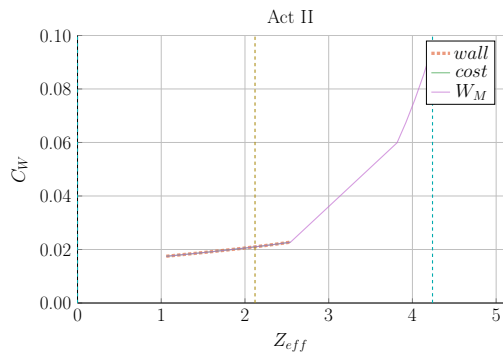
(c) Arc



(d) Demo Pulsed

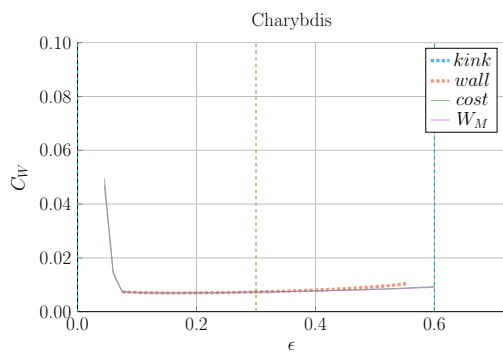


(e) Act I

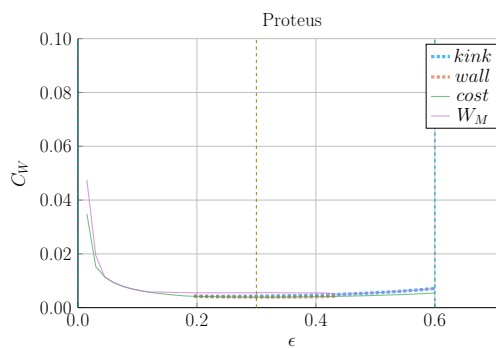


(f) Act II

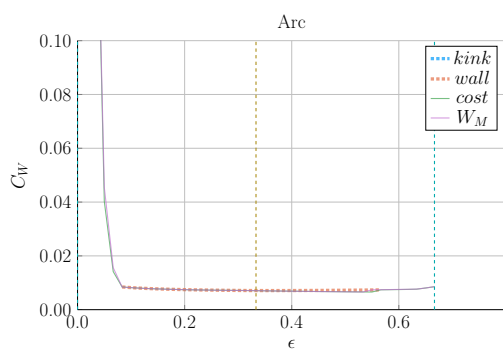
Figure G-26: Cost Sensitivity: Z_{eff} vs. B_0



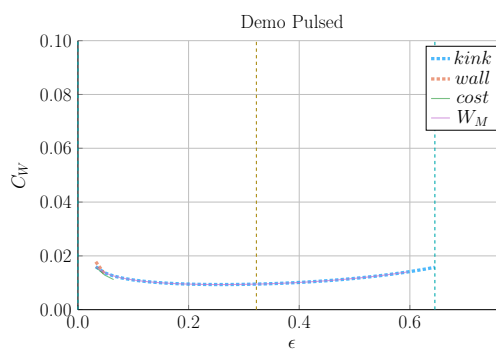
(a) Charybdis



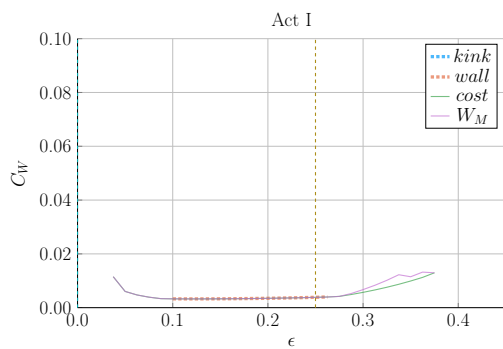
(b) Proteus



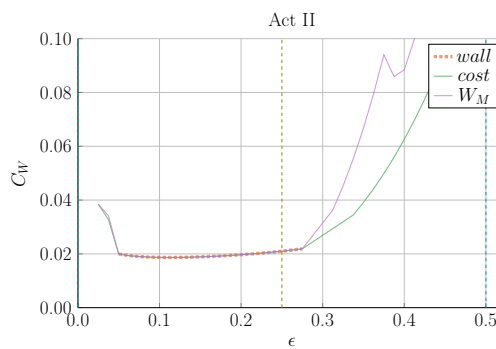
(c) Arc



(d) Demo Pulsed



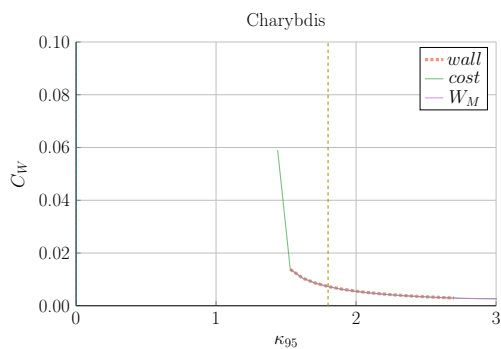
(e) Act I



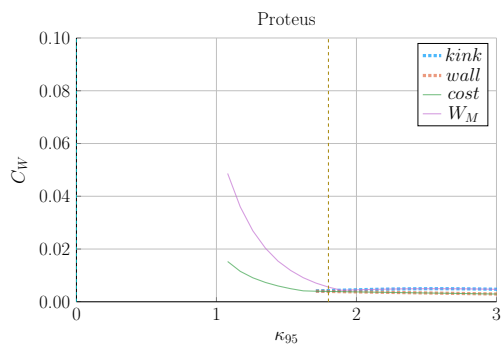
(f) Act II

Figure G-27: Cost Sensitivity: ϵ vs. B_0

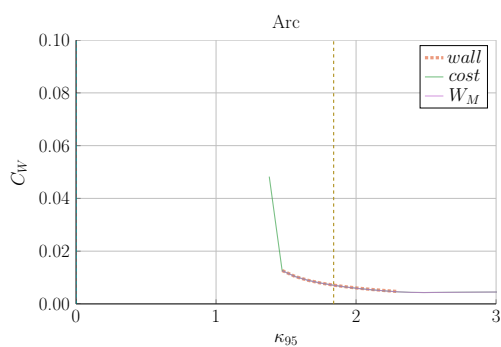
Elongation – κ_{95}



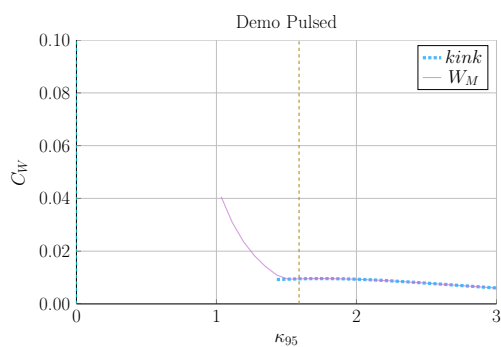
(a) Charybdis



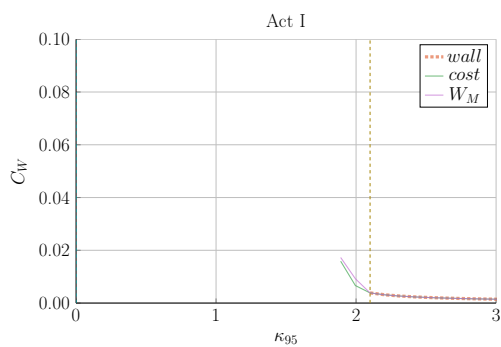
(b) Proteus



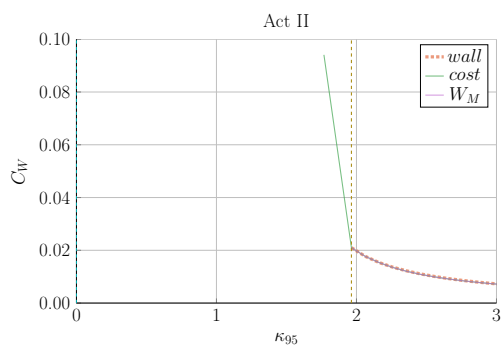
(c) Arc



(d) Demo Pulsed

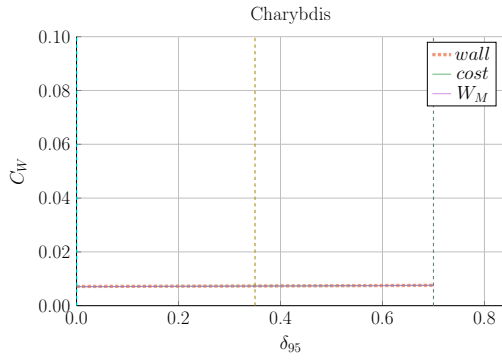


(e) Act I

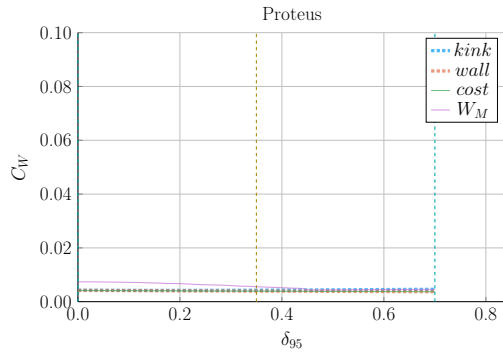


(f) Act II

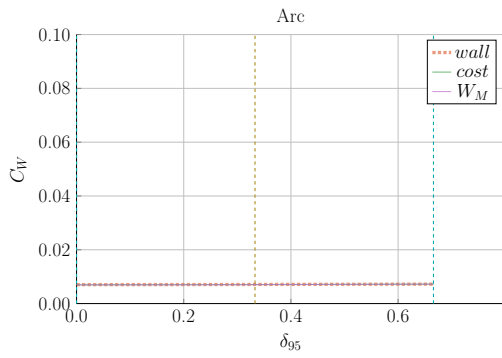
Figure G-28: Cost Sensitivity: κ_{95} vs. B_0



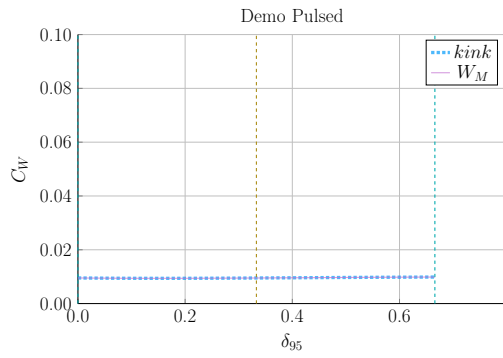
(a) Charybdis



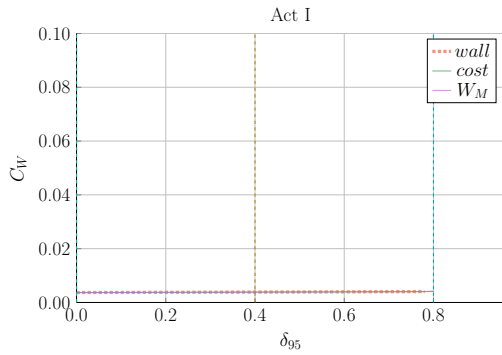
(b) Proteus



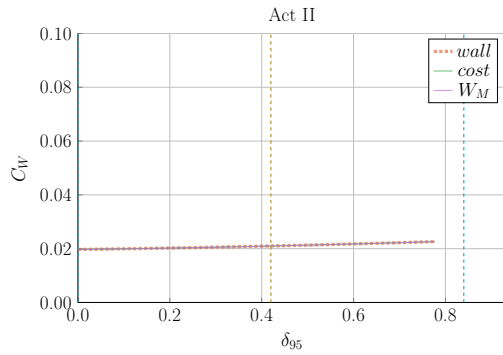
(c) Arc



(d) Demo Pulsed

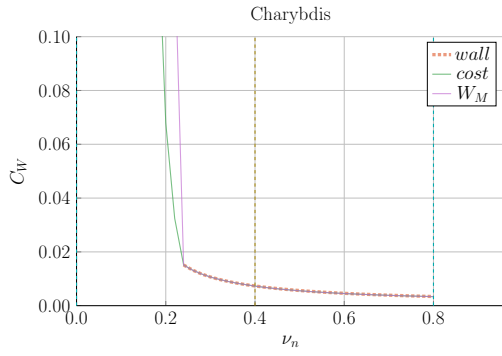


(e) Act I

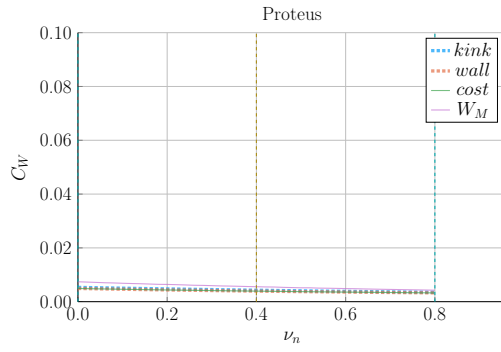


(f) Act II

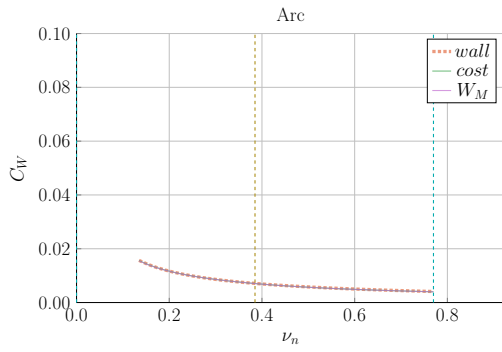
Figure G-29: Cost Sensitivity: δ_{95} vs. B_0



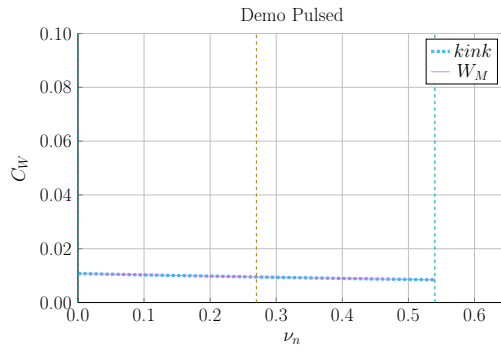
(a) Charybdis



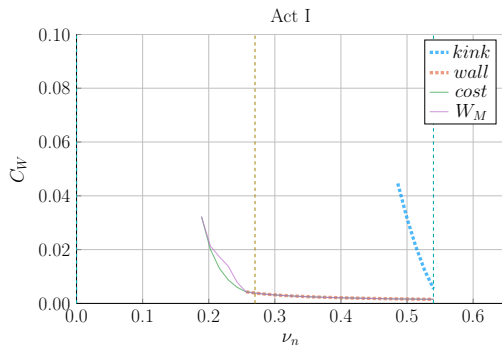
(b) Proteus



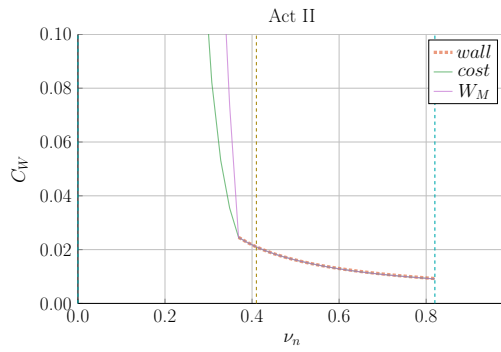
(c) Arc



(d) Demo Pulsed



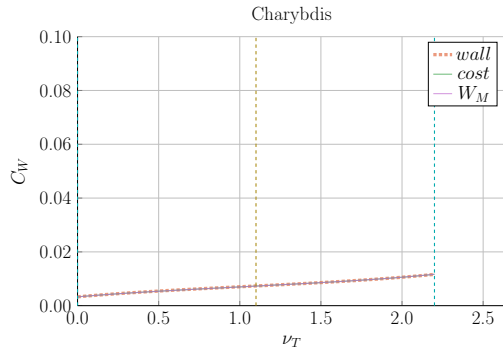
(e) Act I



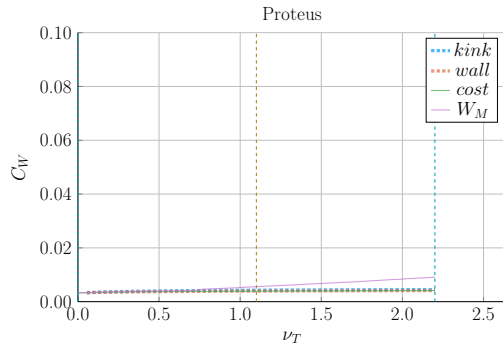
(f) Act II

Figure G-30: Cost Sensitivity: ν_n vs. B_0

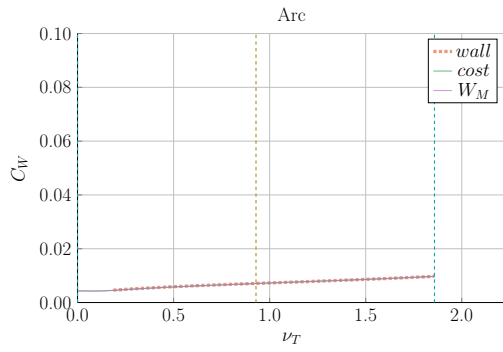
Temperature Peaking Factor – ν_T



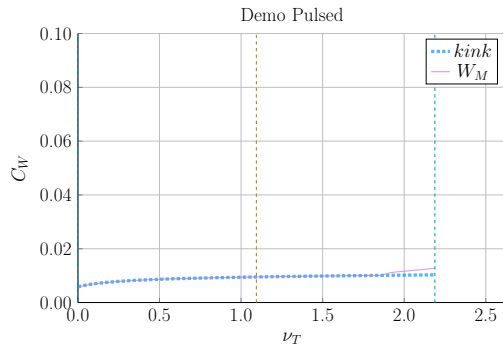
(a) Charybdis



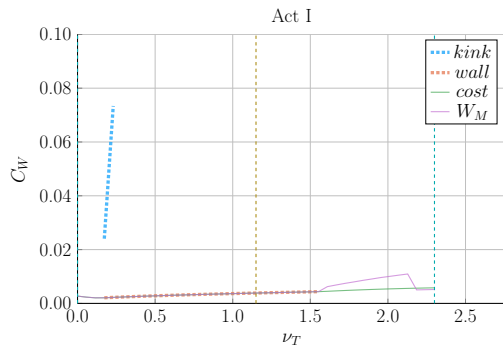
(b) Proteus



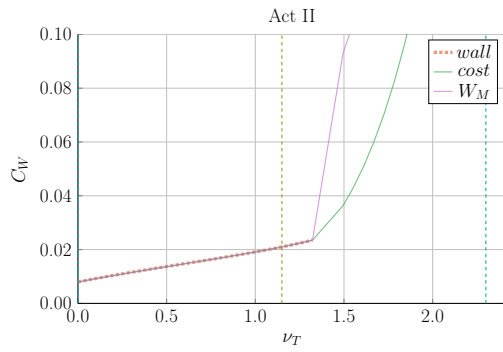
(c) Arc



(d) Demo Pulsed

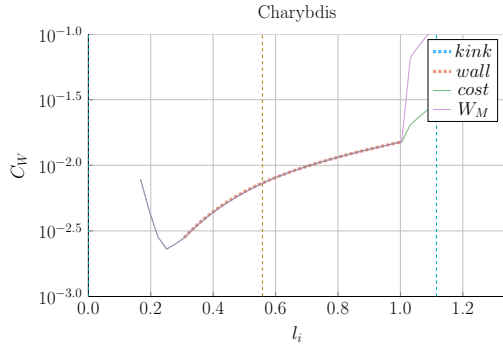


(e) Act I

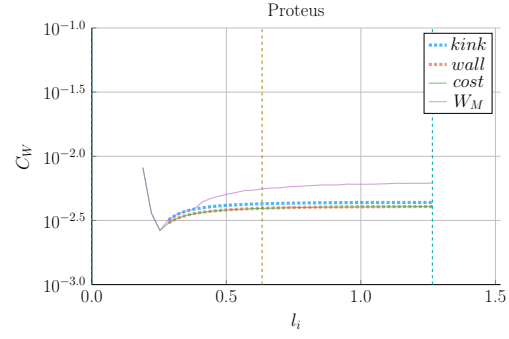


(f) Act II

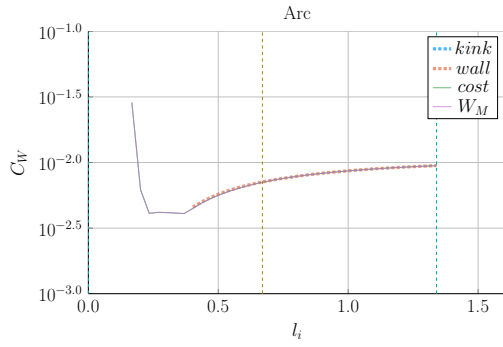
Figure G-31: Cost Sensitivity: ν_T vs. B_0



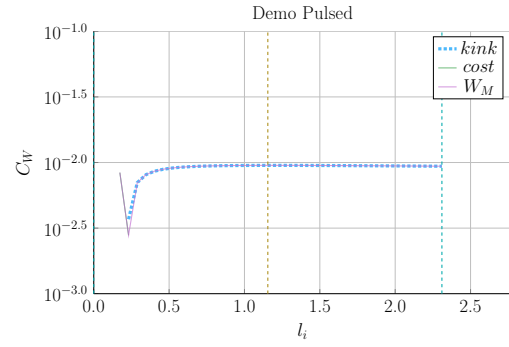
(a) Charybdis



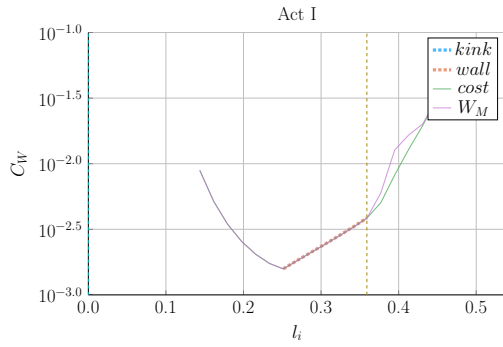
(b) Proteus



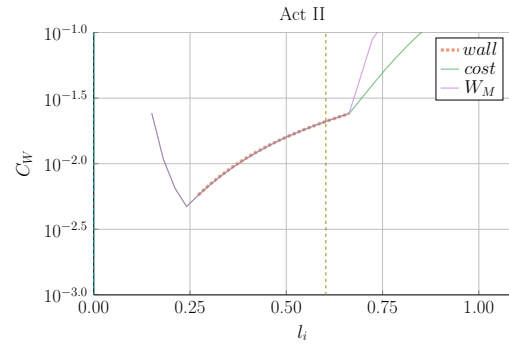
(c) Arc



(d) Demo Pulsed

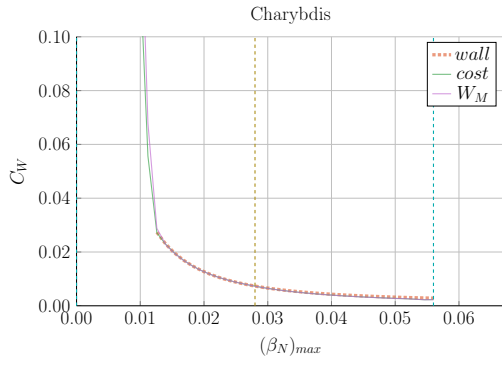


(e) Act I

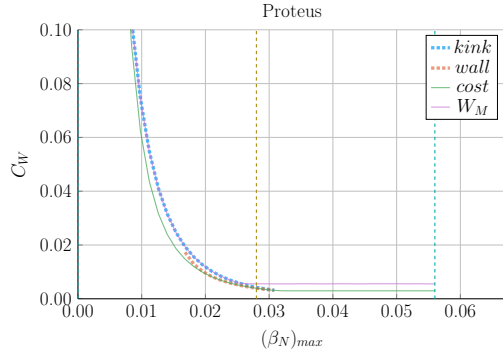


(f) Act II

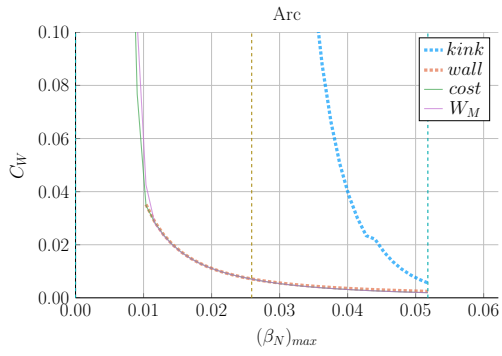
Figure G-32: Cost Sensitivity: l_i vs. B_0



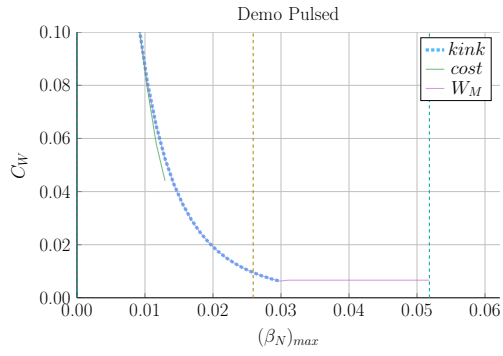
(a) Charybdis



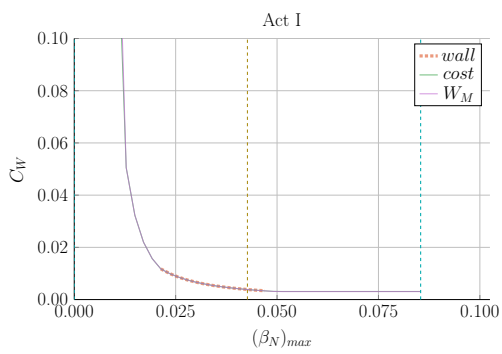
(b) Proteus



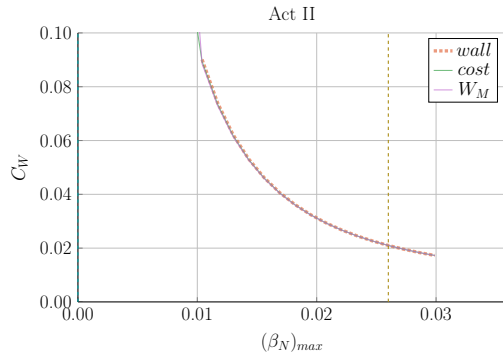
(c) Arc



(d) Demo Pulsed

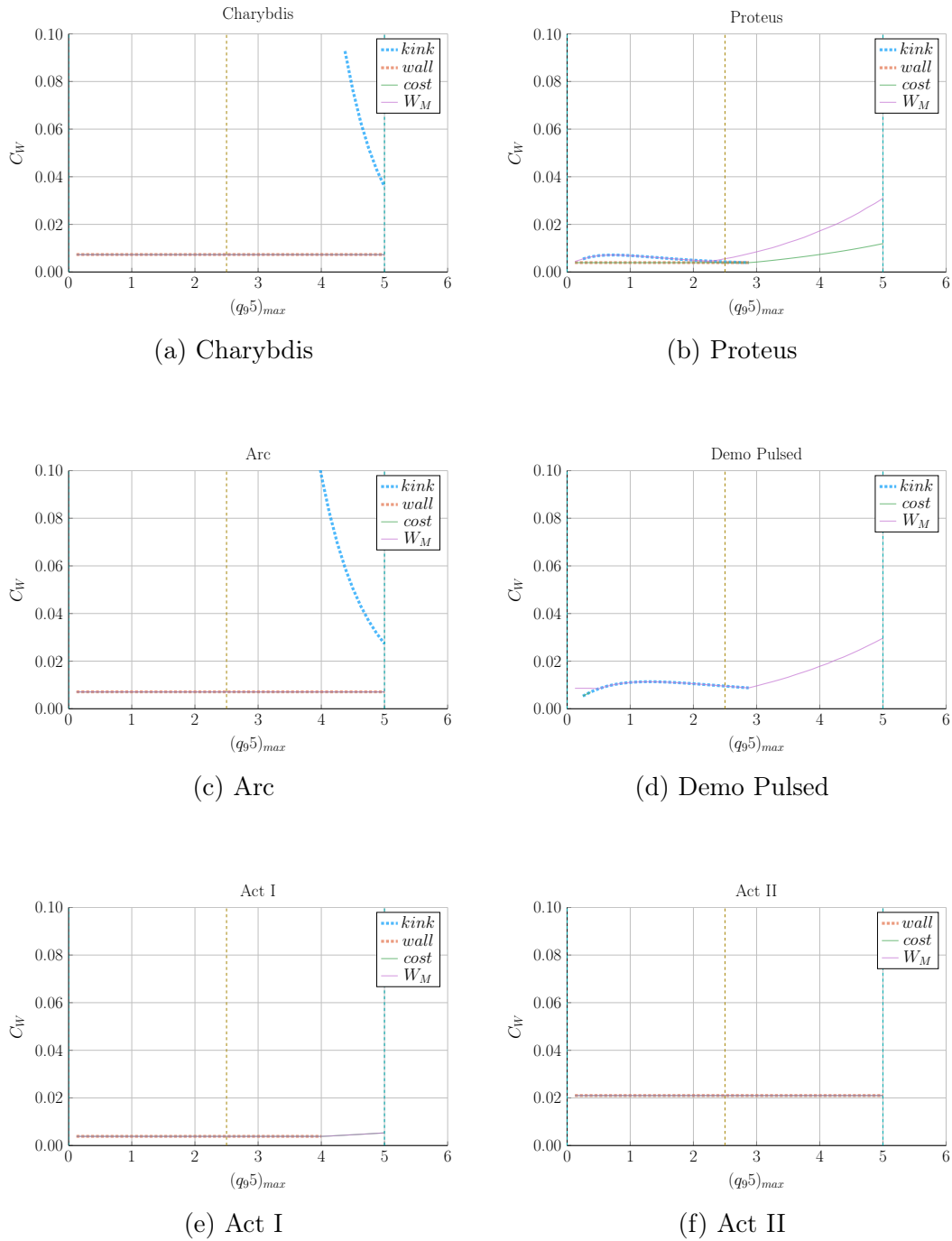


(e) Act I

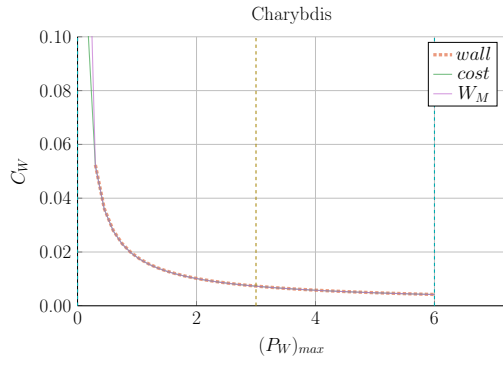


(f) Act II

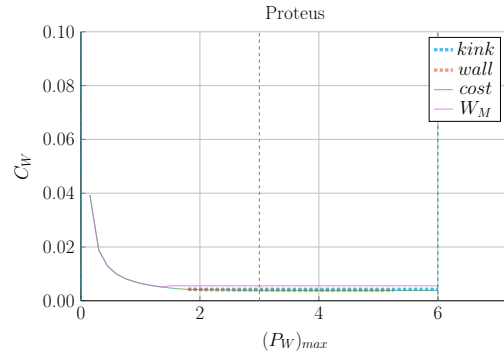
Figure G-33: Cost Sensitivity: $(\beta_N)_{max}$ vs. B_0

Figure G-34: Cost Sensitivity: $(q_{95})_{max}$ vs. B_0

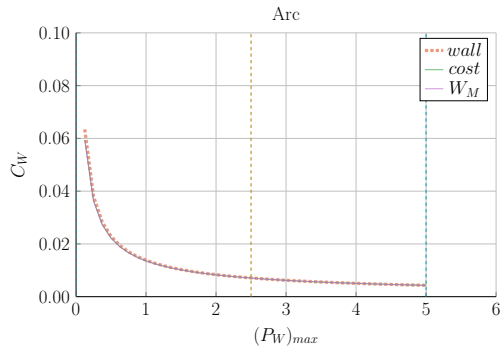
Max Wall Loading – $(P_W)_{max}$



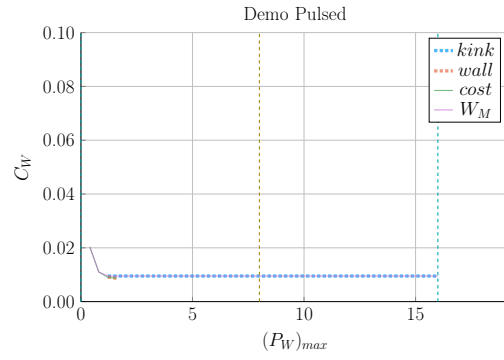
(a) Charybdis



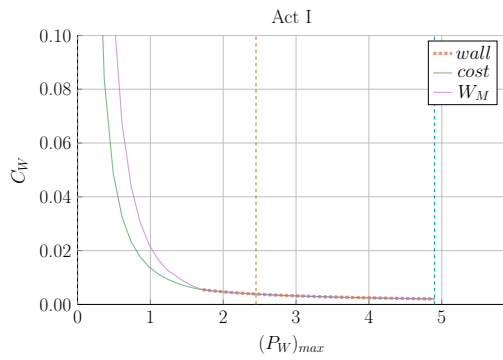
(b) Proteus



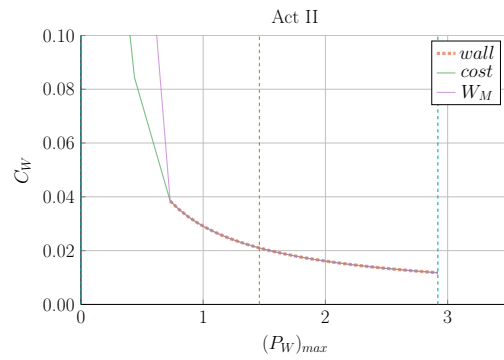
(c) Arc



(d) Demo Pulsed



(e) Act I



(f) Act II

Figure G-35: Cost Sensitivity: $(P_W)_{max}$ vs. B_0

Bibliography

- [1] W Biel, M Beckers, R Kemp, R Wenninger, and H Zohm. Systems code studies on the optimization of design parameters for a pulsed DEMO tokamak reactor, 2016.
- [2] C E Kessel, M S Tillack, F Najmabadi, F M Poli, K Ghanous, N Gorelenkov, X R Wang, D Navai, H H Toudeshki, C Koehly, L El-Guebaly, J P Blanchard, C J Martin, L Mynsburge, P Humrickhouse, M E Rensink, T D Rognlien, M Yoda, S I Abdel-Khalik, M D Hageman, B H Mills, J D Rader, D L Sadowski, P B Snyder, H. St. John, A D Turnbull, L M Waganer, S Malang, and A F Rowcliffe. The ARIES advanced and conservative tokamak power plant study. *Fusion Science and Technology*, 67(1):1–21, 2015.
- [3] GS Lee, J Kim, SM Hwang, Choong-Seock Chang, Hong-Young Chang, MH Cho, BH Choi, K Kim, KW Cho, S Cho, et al. The kstar project: An advanced steady state superconducting tokamak experiment. *Nuclear Fusion*, 40(3Y):575, 2000.
- [4] Jeffrey P Freidberg. *Plasma Physics and Fusion Energy*, volume 1. 2007.
- [5] B. N. Sorbom, J. Ball, T. R. Palmer, F. J. Mangiarotti, J. M. Sierchio, P. Bonoli, C. Kasten, D. A. Sutherland, H. S. Barnard, C. B. Haakonsen, J. Goh, C. Sung, and D. G. Whyte. ARC: A compact, high-field, fusion nuclear science facility and demonstration power plant with demountable magnets. *Fusion Engineering and Design*, 100:378–405, nov 2015.
- [6] M Kovari, R Kemp, H Lux, P Knight, J Morris, and D J Ward. " PROCESS " : A systems code for fusion power plants—Part 1: Physics. *Fusion Engineering and Design*, 89(12):3054–3069, 2014.
- [7] Meszaros et al. Demo I Input File.
- [8] H. Fountain. A dream of clean energy at a very high price. <https://www.nytimes.com/2017/03/27/science/fusion-power-plant-iter-france.html>, 2017. Accessed: 2018-12-6.
- [9] J. Tirone. World’s biggest science experiment seeks more time and money. <https://www.bloomberg.com/news/articles/2016-06-15/world-s-biggest-science-experiment-seeks-more-time-and-money>, 2016. Accessed: 2018-12-6.

- [10] David J. Griffiths. *Introduction to electrodynamics*.
- [11] P J Knight and M D Kovari. A User Guide to the PROCESS Fusion Reactor Systems Code, 2016.
- [12] D C Mcdonald, J G Cordey, K Thomsen, C Angioni, H Weisen, O J W F Kardaun, M Maslov, A Zabolotsky, C Fuchs, L Garzotti, C Giroud, B Kurzan, P Mantica, A G Peeters, and J Stober. Scaling of density peaking in H-mode plasmas based on a combined database of AUG and JET observations. *Nucl. Fusion*, 47:1326–1335, 2018.
- [13] T Onjun, G Bateman, A H Kritz, and G Hammett. Models for the pedestal temperature at the edge of H-mode tokamak plasmas. *Physics of Plasmas*, 9(10), 2002.
- [14] G Saibene, L D Horton, R Sartori, and A E Hubbard. Physics and scaling of the H-mode pedestal The influence of isotope mass, edge magnetic shear and input power on high density ELMy H modes in JET Physics and scaling of the H-mode pedestal. *Control. Fusion*, 42:15–35, 2000.
- [15] Martin Greenwald. Density limits in toroidal plasmas, 2002.
- [16] J Jacquinot,) Jet, S Putvinski,) Jct, G Bosia, Jct), A Fukuyama, U) Okayama, R Hemsworth, Cea Cadarache), S Konovalov, Rrc Kurchatov), W M Nevins, Llnl), F Perkins, K A Rasumova, Rrc-) Kurchatov, F Romanelli, Enea-) Frascati, K Tobita, Jaeri), K Ushigusa, J W Van, U Dam, V Texas), Rrc Vdovin, S Kurchatov), R Zweben, Erm Koch, Kms-) Brussels, J.-G Wégrowe, Cea-) Cadarache, V V Alikaev, B Beaumont, A Bécoulet, S Bern-Abei, Pppl), V P Bhatnagar, Ec Brussels), S Brémond, and M D Carter. Chapter 6: Plasma auxiliary heating and current drive. *ITER Physics Basis Editors Nucl. Fusion*, 39, 1999.
- [17] D A Ehst and C F F Karney. Approximate formula for radiofrequency current drive efficiency with magnetic trapping, 1991.
- [18] Ian H Hutchinson. Principles of plasma diagnostics. *Plasma Physics and Controlled Fusion*, 44(12):2603, 2002.
- [19] Tobias Hartmann, Thomas Hamacher, Hon-Prof rer nat Hartmut Zohm, and Hon-Prof rer nat Sibylle Günter. Development of a Modular Systems Code to Analyse the Implications of Physics Assumptions on the Design of a Demonstration Fusion Power Plant.
- [20] N A Ukan. ITER Physics Design Guidelines at High Aspect Ratio. pages 1–4, 2009.
- [21] J P Freidberg, F J Mangiarotti, and J Minervini. Designing a tokamak fusion reactor - How does plasma physics fit in? *Physics of Plasmas*, 22(7):070901, 2015.

- [22] B Labombard, E Marmor, J Irby, T Rognlien, and M Umansky. ADX: a high field, high power density, advanced divertor and RF tokamak Nuclear Fusion. Technical report, 2017.
- [23] S P Hirshman and G H Neilson. External inductance of an axisymmetric plasma. *Physics of Fluids*, 29(3):790–793, 1986.
- [24] P Libeyre, N Mitchell, D Bessette, Y Gribov, C Jong, and C Lyraud. Detailed design of the ITER central solenoid. *Fusion Engineering and Design*, 84:1188–1191, 2009.
- [25] Jeff P Freidberg, Antoin Cerfon, and Jungpyo Lee. Tokamak elongation: how much is too much? I Theory. *arXiv.org*, pages 1–34, 2015.
- [26] E. J. Doyle, W. A. Houlberg, Y. Kamada, V. Mukhovatov, T. H. Osborne, A. Polevoi, G Bateman, J. W. Connor, J. G. Cordey, T Fujita, X Garbet, T. S. Hahm, L. D. Horton, A. E. Hubbard, F Imbeaux, F Jenko, J. E. Kinsey, Y Kishimoto, J Li, T. C. Luce, Y Martin, M Ossipenko, V Parail, A Peeters, T. L. Rhodes, J. E. Rice, C. M. Roach, V Rozhansky, F Ryter, G Saibene, R Sartori, A. C.C. Sips, J. A. Snipes, M Sugihara, E. J. Synakowski, H Takenaga, T Takizuka, K Thomsen, M. R. Wade, and H. R. Wilson. Chapter 2: Plasma confinement and transport. *Nuclear Fusion*, 47(6):S18–S127, jun 2007.
- [27] H Lux, R Kemp, E Fable, and R Wenninger. Radiation and confinement in 0-D fusion systems codes. Technical report.
- [28] Louis Giannone, J Baldzuhn, R Burhenn, P Grigull, U Stroth, F Wagner, R Brakel, C Fuchs, HJ Hartfuss, K McCormick, et al. Physics of the density limit in the w7-as stellarator. *Plasma physics and controlled fusion*, 42(6):603, 2000.
- [29] H Bosch and G M Hale. Improved formulas for fusion cross-sections and thermal reactivities. 611.
- [30] Zachary S Hartwig and Yuri A Podpaly. Magnetic Fusion Energy Formulary. Technical report, 2014.
- [31] Joseph D Huba. Nrl plasma formulary. Technical report, NAVAL RESEARCH LAB WASHINGTON DC PLASMA PHYSICS DIV, 2006.
- [32] John Wesson and David J Campbell. *Tokamaks*, volume 149. Oxford University Press, 2011.
- [33] C. E. Kessel. Bootstrap current in a tokamak. *Nuclear Fusion*, 34(9):1221–1238, 1994.